1-1-2013

Detailed Characterization of Conventional and Low Temperature Dual Fuel Combustion in Compression Ignition Engines

Andrew C. Polk

Detailed characterization of conventional and low temperature dual fuel combustion in compression ignition engines

By

Andrew C. Polk

A Dissertation
Submitted to the Faculty of
Mississippi State University
in Partial Fulfillment of the Requirements
for the Degree of Doctor of Philosophy
in Mechanical Engineering
in the Department of Mechanical Engineering

Mississippi State, Mississippi

May 2013

Detailed characterization of conventional and low temperature dual fuel combustion in compression ignition engines

By

Andrew C. Polk

Approved:

Sundar R. Krishnan Assistant Professor of Mechanical Engineering (Major Professor)	Kalyan K. Srinivasan Associate Professor and Graduate Coordinator of Mechanical Engineering (Co-Major Professor)
Rogelio Luck Professor of Mechanical Engineering (Committee Member)	D. Keith Walters Associate Professor of Mechanical Engineering (Committee Member)

Sarah A. Rajala
Dean of the Bagley College of Engineering

Name: Andrew C. Polk

Date of Degree: May 10, 2013

Institution: Mississippi State University

Major Field: Mechanical Engineering

Major Professor: Sundar R. Krishnan

Title of Study: Detailed characterization of conventional and low temperature dual fuel combustion in compression ignition engines

Pages in Study: 208

Candidate for Degree of Doctor of Philosophy

The goal of this study is to assess conventional and low temperature dual fuel combustion in light- and heavy-duty multi-cylinder compression ignition engines in terms of combustion characterization, performance, and emissions. First, a light-duty compression ignition engine is converted to a dual fuel engine and instrumented for in-cylinder pressure measurements. The primary fuels, methane and propane, are each introduced into the system by means of fumigation before the turbocharger, ensuring the air-fuel composition is well-mixed. Experiments are performed at 2.5, 5, 7.5, and 10 bar BMEP at an engine speed of 1800 RPM. Heat release analyses reveal that the ignition delay and subsequent combustion processes are dependent on the primary fuel type and concentration, pilot quantity, and loading condition. At low load, diesel-ignited propane yields longer ignition delay periods than diesel-ignited methane, while at high load the reactivity of propane is more pronounced, leading to shorter ignition delays. At high load (BMEP = 10 bar), the rapid heat release associated with diesel-ignited propane appears to occur even before pilot injection, possibly indicating auto-ignition of the propane-air mixture. Next, a modern, heavy-duty compression ignition engine is commissioned with

an open architecture controller and instrumented for in-cylinder pressure measurements. Initial diesel-ignited propane dual fuel experiments (fumigated before the turbocharger) at 1500 RPM reveal that the maximum percent energy substitution (PES) of propane is limited to 86, 60, 33, and 25 percent at 5, 10, 15, and 20 bar BMEP, respectively. Fueling strategy, injection strategy, exhaust gas recirculation (EGR) rate, and intake boost pressure are varied in order to maximize the PES of propane at 10 bar BMEP, which increases from 60 PES to 80 PES of propane. Finally, diesel-ignited propane dual fuel low temperature combustion (LTC) is implemented using early injection timings (50 DBTDC) at 5 bar BMEP. A sweep of injection timings from 10 DBTDC to 50 DBTDC reveals the transition from conventional to low temperature dual fuel combustion, indicated by ultra-low NO_x and smoke emissions. Optimization of the dual fuel LTC concept yields less than 0.02 g/kW-hr NO_x and 0.06 FSN smoke at 93 PES of propane.

ACKNOWLEDGEMENTS

I would like to acknowledge my family, friends, and co-workers for their support and encouragement throughout my educational career. I would especially like to thank my parents for providing me with the means and motivation for education, and my lovely wife, Kristin, for accompanying me on this journey. I would also like to thank my major and co-major professors, Dr. Sundar Krishnan and Dr. Kalyan Srinivasan, for the time, effort, patience, knowledge, wisdom, and friendship they have shared with me. In addition, I would like to thank my committee members, Dr. Keith Walters and Dr. Rogelio Luck, for advising and assisting me throughout my time at Mississippi State University.

I would like to acknowledge the Propane Education & Research Council (PERC), the Sustainable Energy Research Center (SERC), and the Bagley Engineering Graduate Fellowship for financial support. I would also like to thank the teams at PACCAR and Drivven for their technical assistance on the MX10 project.

TABLE OF CONTENTS

LIST OF TABLES

LIST OF FIGURES

NOMENCLATURE

$\phi_{overall}$	Overall equivalence ratio
ϕ_{pilot}	Equivalence ratio based only on the pilot quantity
$\dot{m}_a$	Mass flow of air
$\dot{m}_d$	Mass flow of diesel
$\dot{m}_g$	Mass flow of gaseous fuel
a.u.	Arbitrary units
$dN/dlogD_p$	Normalized particle number concentration
Advance	Occurring earlier in the combustion cycle
AFT	Adiabatic flame temperature
AHRR	Apparent heat release rate
ALPING	Advanced low pilot-ignited natural gas
BDC	Bottom dead center
BMEP	Brake mean effective pressure
$BSNO_x$	Brake-specific oxides of nitrogen
BSCO	Brake-specific carbon monoxide
BSHC	Brake-specific unburned hydrocarbon
BSL	Best straight line

CA10-90	Crank angle duration between 10% and 90% of cumulative heat release
CA50	Crank angle at which 50% of cumulative heat release occurs
CAD	Crank angle degrees
CLD	Chemi-luminescence detection
CO	Carbon monoxide
CO_2	Carbon dioxide
DATDC	Degrees after top dead center
DBTDC	Degrees before top dead center
DCAT	Drivven Combustion Analysis Toolkit
DEF	Diesel exhaust fluid
DPF	Diesel particulate filter
ECM	Engine control module
EPA	United States Environmental Protection Agency
FID	Flame ionization detector
FS	Full Scale
FSO	Full Scale Output
FSL	Flame spread limit
GETDC	Gas exchange top dead center
HCCI	Homogenous charge compression ignition
HRR	Heat release rate
ID	Ignition delay
ID_A	Apparent ignition delay
IMEP	Indicated mean effective pressure

LBV	Laminar burning velocity
LHV	Lower heating value
MON	Motor octane number
MPRR	Maximum pressure rise rate
MPRR-L	Maximum pressure rise rate location
N	Engine Speed
NDIR	Non-dispersive infrared
NO	Nitrogen oxide
NO_x	Oxides of nitrogen
PAH	Poly-aromatic hydrocarbons
PES	Percent energy substitution (of the primary gaseous fuel)
Phi	Equivalence ratio
PM	Particulate Matter
Retard	Occurring later in the combustion cycle
RON	Research octane number
SCR	Selective catalytic reduction
SOC	Start of combustion
SOI	Start of injection of pilot fuel
TDC	Top dead center
THC	Total unburned hydrocarbons

CHAPTER I

INTRODUCTION AND REVIEW OF PAST RESEARCH

The increasing need for improved fuel economy and reduced pollutant emissions from internal combustion engines has refocused attention on combustion strategies that achieve highly efficient, clean combustion over a wide range of engine operating conditions. As of 2010, the United States Environmental Protection Agency (EPA) standards for heavy duty diesel engine exhaust emissions require less than 0.013 g/kW-hr of particulate emissions (PM or soot) and 0.268 g/kW-hr of oxides of nitrogen (NO_x). To meet these standards, engines employing advanced combustion concepts coupled with complex and expensive aftertreament systems have been developed.

Starting in 2007, tightening EPA restrictions on PM emissions caused diesel engine manufacturers to add diesel particulate filters (DPFs) to exhaust aftertreatment. These systems trap solid particles as they pass through a fine mesh. Once a filter becomes clogged it must be regenerated, whereby a fuel jet is ignited at the filter to completely oxidize the trapped particles. These systems reduce overall system efficiency in several ways. First, if the engine is in a vehicle, the additional weight of the system will inhibit performance. Second, the restrictive nature of a filter in the exhaust increases pumping losses and, if turbocharged, reduces the turbine's ability to extract energy from the exhaust, decreasing turbocharger efficiency. Last, the fuel required to "regen" the

filter does not contribute to the engine's power output, therefore is essentially wasted energy.

In 2010, EPA restrictions on NO_x emissions required many diesel engine manufacturers to employ selective catalytic reduction (SCR) systems in order to meet acceptable levels of NO_x. SCR systems inject an aqueous urea solution, or diesel exhaust fluid (DEF), into the exhaust stream where it decomposes into ammonia and carbon dioxide (CO_2). With the catalyst, the ammonia reduces NO_x in the exhaust into water (H_2O) and nitrogen (N_2). The DEF must be carefully injected so that ammonia does not pass through the SCR unreacted, contributing to increased harmful emissions. Due to its complexity, the SCR is typically a bulky system by itself; however, the required reservoir of DEF adds additional weight to the system. The DEF requirement is particularly significant in terms of maintenance cost, since the engine not only requires diesel fuel but DEF as well.

In addition to emissions regulation, energy security and sustainability concerns have driven the search for suitable alternatives (e.g., gaseous alternative fuels [Karim 2003] and biofuels [Sequera *et al.* 2011]) to conventional fossil-derived fuels such as gasoline and diesel. As a result, dual fuel combustion has received renewed interest due to its use of alternative fuels and well-known emissions benefits compared to conventional diesel combustion.

1.1 Review on Some Important Topics

1.1.1 Dec's Conceptual Model of Conventional Diesel Combustion

Before covering more advanced combustion modes, it is important that the modern interpretation of conventional diesel combustion is understood. The most widely

accepted interpretation of conventional diesel combustion is given in [Dec 1997]. In this work, laser sheet imaging and other optical diagnostic techniques are used to summarize and depict the combustion process in a modern diesel engine.

In the absence of wall interactions and swirl, Dec's model first depicts jet development. At the injector, a small region forms containing only liquid fuel while air is entrained and the fuel vaporizes as it travels downstream. A fuel vapor region is formed along the sides of the liquid jet. As the fuel reaches its maximum penetration length, the entrainment of hot air is sufficient to vaporize all fuel. The fuel vapor continues to penetrate into the cylinder and the head vortex region develops, having a relatively evenly distributed fuel and air mixture typically at equivalence ratios[1] ranging from 2 to 4. Chemiluminescence of the head vortex region indicates autoignition, whereupon the premixed burn phase begins, also referred to as the first stage of conventional diesel combustion.

The first part of premixed burn is synonymous with the upturn after the "negative heat release" portion of the heat release curve (due to charge cooling by vaporization of injected liquid diesel fuel). A typical apparent heat release plot is shown in Figure 1.1, where the apparent negative heat release can be observed shortly after the injector begins to open. During this segment of combustion, the fuel at the leading portion of the jet begins to break down in the form of poly-aromatic hydrocarbons (PAH). At this point, soot begins to form at the leading edge of the jet as a result of the fuel-rich premixed burn. The onset of the diffusion flame occurs near the end of the premixed burn. The

[1] Equivalence ratio is defined as the ratio of fuel-to-air mixture to the stoichiometric or chemically correct fuel-to-air mixture. Fuel lean equivalence ratios are denoted by values between 0 and 1, and fuel rich equivalence ratios are denoted by values between 1 and 4, typically.

diffusion flame is defined as the boundary between the fuel-rich jet and the surrounding volume. This thin area is very high in temperature and tends to shorten the liquid penetration length by facilitating vaporization.

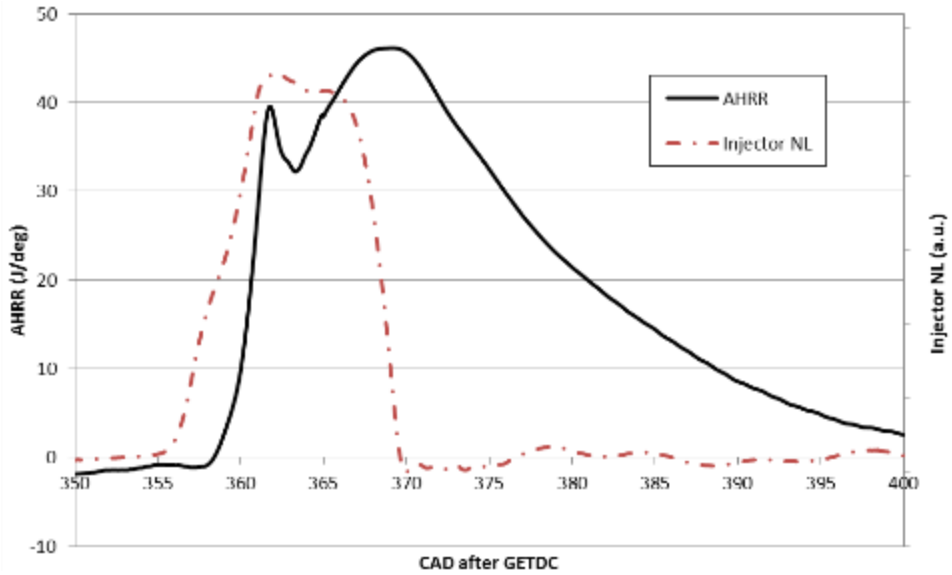

Figure 1.1 Typical heat release for conventional diesel combustion in a 1.9L VW TDI engine

For the last part of premixed burn, the jet continues to penetrate into the cylinder, leading to the mixing controlled phase. Figure 1.2 shows a fully developed flame in the mixing controlled phase, also referred to as the second stage of conventional diesel combustion. As previously indicated, the diffusion flame is a high temperature area on the periphery of the jet; these high temperatures are responsible for both soot oxidation and thermal NO formation. Therefore, the size of the diesel jet will likely be decisive in controlling these phenomena. During mixing controlled combustion, soot is first created outside the fuel-rich (equivalence ratio of 3 to 5) premixed flame. As soot moves down

the jet to the head vortex, particle growth continues, leading to large soot quantities in the head vortex region. A major benefit of dual fuel combustion is the smaller diesel jet required for ignition, therefore reducing NO and soot formation regions in size. Instead, a significant portion of energy comes from the lean, well-mixed air-fuel mixture in the surrounding chamber.

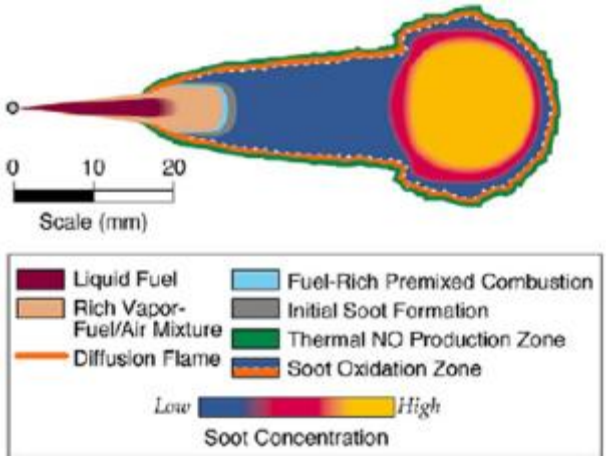

Figure 1.2 Mixing controlled combustion [Dec 1997]

1.1.2 Soot Particle Size

Particulate emissions, while regulated as a whole on a mass basis, vary widely in terms of particle size. This is an important observation in terms of dual fuel combustion because although the PM mass may decrease, the number of particles may increase significantly. As exhaust emissions, different sizes of particles have the potential to affect the environment in different ways. Fine particle concentration, for instance, has shown an association with adverse health conditions [Dockery and Pope 1997]. In addition, particles that are non-toxic in the μm range may be toxic in the nm range.

Therefore, it is important to understand what size particles are produced by a given mode of combustion.

There are primarily two "modes" of particulate formation referenced in diesel particulate literature. The accumulation mode primarily consists of particles in the 0.1-0.3 μm range, a state in which solid carbonaceous material and any material it absorbs resides [Kittelson 1998]. Kittelson states that the nucleation mode comprises particles in the 0.005-0.05 μm range, which usually consists of volatile organic and sulfur compounds formed during exhaust cooling and may contain carbon and metal compounds. However, de Filippo and Maricq [2008] show that not all nanoparticles exist in a volatile state. It is observed that some nanoparticles formed in light-duty engines remain non-volatile to greater than 400 degrees Celsius. According to de Filippo and Maricq, it is not known how two modes of nonvolatile particles can originate simultaneously during diesel combustion, but nonvolatile nanoparticles can be trapped by DPFs with the same efficiency as nucleation mode particles. Regardless of volatility, almost all particulate mass emitted from diesel engines is in the fine particle (accumulation) range and almost all contribution to the particle number arises from the nanoparticle (nucleation) range.

Particle size in engine exhaust is affected by operating conditions and hardware such as aftertreatment systems, etc. Lu *et al.* [2012] indicate that primary particle size decreases with combustion duration but increases with combustion temperature. As opposed to conventional combustion, dual fuel combustion duration is seen to increase at low loads due to the flame propagation combustion mode, likely resulting in smaller particle sizes. In addition, regions with a high local temperature are typically smaller

with dual fuel combustion, likely resulting in smaller particle sizes. In addition to combustion mode effects, increasing engine speed is likely to decrease the particle size and increasing engine load will increase particle size.

1.2 Recent Developments in Dual Fuel Combustion

1.2.1 The Dual Fuel Combustion Concept

A dual fuel engine is a compression ignition engine in which a significant fraction of the fuel chemical energy input arises from a low-cetane fuel (usually gaseous) inducted with the intake air to form a lean premixed fuel-air mixture, which is ignited with timed direct injection of a high-cetane pilot fuel (e.g., diesel) near top dead center (TDC) [Karim 1987]. Dual fuel engines offer the ability to operate on a variety of alternative fuels, while maintaining good fuel conversion efficiencies at high loads and producing low exhaust emissions of NO_x and PM [Stewart *et al.* 2007, Srinivasan *et al.* 2007]. On the other hand, dual fuel combustion can also lead to higher levels of unburned hydrocarbons (THC) and carbon monoxide (CO) emissions and lower fuel conversion efficiencies, especially at low loads.

Some commonly used gaseous fuels in dual fuel engine applications include methane (or natural gas, whose primary component is methane) [Gurgenci and Aminossadati 2009, Papagiannakis and Hountalas 2003, Krishnan *et al.* 2002, Tao *et al.* 1995], propane [Poonia *et al.* 1999, Stewart *et al.* 2007], hydrogen [Bose and Banerjee 2012] and a variety of other low heating value fuels such as producer gas, landfill gas, and biogas [Karim 2003, Ramadhas *et al.* 2008]. In the United States, methane and propane are very attractive for stationary power generation and other off-highway applications because of the existing infrastructure for production and delivery of these

fuels. Moreover, the conversion of existing diesel engines to operate in dual fuel mode requires very little change to the engine hardware; consequently, these engines retain their ability to operate solely on diesel, if necessary.

1.2.2 Performance and Emissions of Dual Fuel Engines

Compared to conventional diesel engines, the typical emissions benefits associated with dual fuel engines include the simultaneous reduction of PM and NO_x emissions. Particulate matter (soot) is reduced because a large part of the fuel energy is released due to combustion of the lean premixed fuel-air mixture, which is nearly devoid of locally-rich premixed regions that are encountered in conventional diesel spray combustion [Weaver and Turner 1994]. This reduces the opportunity for PM formation, and therefore, the overall PM emissions are decreased. Oxides of nitrogen are associated with high local temperatures and the residence times of these high temperature regions. The NO_x emissions have been shown to scale directly with pilot quantity [Karim 1987, Abd Alla *et al.* 2000]. This trend appears to be consistent with Dec's conceptual model of diesel combustion [Dec 1997], which states that NO_x is formed on the periphery of the diesel jet. Since a large part of the fuel energy in dual fuel combustion arises from the lean premixed fuel-air mixture, the pilot diesel sprays are smaller, resulting in smaller regions with high local temperatures, and consequently, NO_x formation is lower.

For part-load operation, however, CO and THC emissions may be higher with dual fuel combustion [Karim *et al.* 1993]. At low load conditions, the gaseous fuel-air mixture is very lean which results in slow combustion rates and low bulk temperatures during combustion. Shoemaker *et al.* [2012] discuss how low bulk temperatures during dual fuel combustion reduce the CO to CO_2 reaction rate, causing increased CO

emissions. Simultaneously, high THC emissions are caused by slow overall burn rates, resulting in bulk quenching of the in-cylinder mixture. Several strategies [Karim 1991, Ishiyama *et al.* 2000] have been explored to improve dual fuel part-load operation, including higher primary fuel concentrations, larger pilot quantities, intake charge heating, partial air throttling, variable pilot injection timing, and primary fuel stratification.

At high loads, fuel conversion efficiencies (FCEs) for dual fuel combustion are similar to typical values for diesel combustion. However, the specific efficiency trends tend to vary with the choice of primary fuel. For example, Gibson *et al.* [2011] showed that diesel-ignited propane combustion yielded higher FCEs than diesel-ignited methane combustion at similar conditions, which was attributed to the higher reactivity and laminar burning velocity (LBV) of propane compared to methane. At low loads, however, FCEs typically decrease with increasing percent energy substitution (PES) from the primary fuel. Several reasons are attributed to this loss in efficiency. Low temperatures and lean fuel-air mixtures lead to incomplete flame propagation and partial oxidation, leaving unutilized fuel energy to be expelled with the exhaust gases. Another reason may be the late combustion phasing (delayed occurrence of the crank angle at which fifty per cent of the cumulative heat release occurs (CA50)). As the bulk of the heat release occurs later in the expansion stroke, less work is transferred to the piston and more energy is expelled with the exhaust gases or lost as heat transfer to the cylinder walls, thus reducing FCEs.

1.2.3 Fuels Used in Dual Fuel Engines

As mentioned previously, a significant amount of research has been performed to understand the performance and emissions characteristics of dual fuel engines utilizing propane and methane as the primary fuels. Methane is one of the most popular primary fuels used in dual fuel applications due to its excellent resistance to knock and relatively high lower heating value (LHV) compared to diesel [Karim 2003]. Propane is also attractive in terms of its energy content but exhibits relatively weaker knock resistance compared to methane. The values of RON, MON, and LHV for these fuels are shown in Table 1.1 [Heywood 1988]. While the increased reactivity of propane results in faster burn rates and potentially higher FCEs, the engine operating range (viable speeds and loads) may be limited by either end-gas knock or premature propane autoignition. Fuel storage in the liquid state is more easily achieved with propane than other gaseous fuels. In order to store natural gas in a liquid state, for example, requires the fuel to be cryogenically stored, which requires both energy and heavy insulation. The operational mixture limits of methane, propane, and hydrogen in both spark ignition engines and compression-ignited dual fuel engines have been investigated by Bade Shrestha and Karim [2006]. From these investigations, it is evident that dual fuel engine operation, especially at low loads, is limited by inconsistent ignition, among other operating variables. Therefore, there is a clear need to perform a detailed characterization of ignition processes in dual fuel engines.

Table 1.1 Fuel Properties

Fuel	Methane	Propane	Diesel
RON	120	112	N/A
MON	120	97	N/A
LHV (MJ/kg)	50	46.4	43.2

1.2.4 Ignition Delay in Dual Fuel Engines

Combustion in dual fuel engines typically occurs after an ignition delay (ID) period. The ID period in dual fuel engines has been studied for several years [Nielson *et al.* 1987, Karim *et al.* 1989, Liu and Karim 1995, Gunea *et al.* 1998, Prakash and Ramesh 1999] but requires further investigation to quantify the effects of specific variables (e.g., overall equivalence ratio, PES, etc.) on the magnitude of the ID period. Understanding the ID period is important as it influences the ensuing combustion process as well as engine performance and emissions. Ignition delay is defined as the period from the start of injection (SOI) of the pilot fuel to the start of combustion (SOC), which must be defined precisely and consistently. The length of ID is primarily governed by the type of primary fuel used, the intake temperature, the pilot injection timing, and the overall equivalence ratio [Karim *et al.* 1989]. A typical trend observed by Liu and Karim [1995] using natural gas as the primary fuel shows that for a given pilot quantity, the ID will increase to a peak as the overall equivalence ratio is increased, decrease to a minimum before the stoichiometric ratio, and then increase again toward misfire as the stoichiometric ratio is approached and surpassed. In any case, it is well known that the ID in dual fuel engines is affected by increasing PES and increasing equivalence ratio.

1.2.5 Dual Fuel Combustion

In addition to ignition delay, understanding the combustion process in dual fuel engines is very important to maximizing the performance and emissions benefits associated with dual fuel combustion. Dual fuel combustion normally occurs in three stages [Karim 2003]: (1) ignition of the pilot fuel, (2) ignition of the fuel-air mixture near the pilot spray, and (3) combustion of the remainder of the primary fuel-air mixture by flame propagation. Together, these phases affect the phasing (CA50) and duration of combustion, which may not be consistent for all operating conditions. Papagiannakis and Hountalas [2004] show that at low loads, combustion duration for dual fuel combustion is longer than the corresponding diesel-only condition, whereas at high loads, it is shorter. It is the author's hypothesis that the combustion phasing and duration will affect performance and emissions of the engine. For instance, a shorter combustion duration phased near TDC will have a higher FCE because more energy is available during the time when it can transfer the most work to the piston. It is likely that this type of combustion will have less CO and THC emissions because the high bulk gas temperatures will facilitate complete fuel oxidation. In turn, a long, delayed combustion process may yield low FCEs and increased THC (quenched flame) or increased CO (incomplete fuel oxidation) emissions due to lower bulk gas temperatures.

1.2.6 Knock in Dual Fuel Engines

One of the limiting factors of dual fuel combustion's range of operation is the phenomenon commonly referred to as "knock." Knock in an internal combustion engine generally refers to undesirable auto-ignition of the fuel air mixture, accompanied by an acoustic ringing or "knocking" sound. Fuels are rated based on resistance to knock using

reference fuels and variable compression ratio engines resulting in RON and MON values. A fuel with a higher octane rating has a higher resistance to knock than a fuel with a lower rating. The RON value is typically the higher of the two octane ratings. The MON value relates more closely to the behavior of the fuel while under load.

The most common form of knock is end-gas knock, where the pressure developed by an oncoming flame front is sufficient to cause auto-ignition of the unburned air-fuel mixture [Heywood 1988]. This type of knock is common during aggressive operation of spark ignition engines, but may also be observed during dual fuel combustion. Ignition of the pilot fuel facilitates ignition of the surrounding air-fuel mixture, which then propagates through the remaining chamber. If the primary fuel's resistance to knock is insufficient, the unburned end gas mixture may auto-ignite, causing knock. Extended end-gas knock operation is highly undesirable as it may cause pitting of the piston or even catastrophic failure of the engine.

The other type of knock, referred to as diesel knock, occurs when the rate of pressure rise is too high [Kubesh and Brehob 1992]. In conventional diesel engines, this occurs with premature injection when conditions will not yet facilitate diesel auto-ignition. The longer ignition delay period allows for a large fraction of the diesel to be premixed, causing an undesirable rate of pressure rise when the fuel eventually burns. Similarly, in HCCI engines at sufficiently high load, a rapid rate of pressure rise can facilitate an acoustic resonance causing the engine to knock [Dec 2009]. In dual fuel engines at high PES and high loads, auto-ignition of the air-fuel mixture is possible even before the diesel pilot, which can cause a rapid rate of pressure rise [Polk *et al.* 2013]. This is caused by high in-cylinder temperatures due to high bulk temperatures at these

loads. In the dual fuel combustion mode, it is possible that diesel knock and end-gas knock could occur in the same cycle. For this reason, knock is often a limiting factor in high load, high PES dual fuel operation, depending on the primary fuel.

1.2.7 Cyclic Combustion Variability in Dual Fuel Combustion

Another limiting factor of dual fuel combustion's range of operation is cyclic variability, often at low load conditions. High concentrations of primary fuel in dual fuel combustion can cause a high coefficient of variation (COV) of indicated mean effective pressure (IMEP). Mean effective pressure refers to an engine size-normalized metric quantifying engine load, and the "indicated" qualifier refers to values calculated from the cylinder, as opposed to at the crank. The IMEP of a combustion cycle is sensitive to metrics such as peak in-cylinder pressures, ignition phasing, combustion phasing, and combustion duration. A low COV of IMEP, therefore, is a good indicator of a consistent combustion process and the engine work output.

One source of variability in dual fuel engines is believed to be the consistency of ignition and combustion phasing [Srinivasan *et al.* 2003]. For injection timings near TDC, Srinivasan *et al.* [2006] states that high COV of IMEP in dual fuel engines operating at low load are likely a result of deteriorating combustion phasing. A retarded ignition phasing (injection near TDC) further retards the combustion phasing, even into the expansion stroke. This is due to the bulk of energy release coming from flame propagation. With flame propagation occurring during the expansion stroke, the flame is susceptible to quenching, resulting in inconsistent combustion phasing.

The use of EGR may further increase the variation of combustion. Lower temperatures and increased diluents will contribute to flame quenching and therefore

inconsistencies in combustion phasing. In addition, partially burned fuel emissions, the quantity of which may vary from cycle to cycle, may be partially recycled through the use EGR. Varying the initial mixture constituents has the potential to further increase variations in both ignition and combustion phasing.

1.3 Recent Developments in Low Temperature Combustion

1.3.1 Concept

A series of advanced combustion strategies, commonly referred to as low temperature combustion (LTC), have received a large amount of attention due to their effectiveness in simultaneously reducing engine-out NO_x and soot emissions [Kamimoto and Bae 1988, Akihama *et al.* 2001, Kook *et al.* 2005, Dec 2009]. Because NO_x emissions are generally formed during combustion when locally high temperatures exceed a certain threshold value (~ 2000 K), one goal of LTC is to reduce local in-cylinder temperatures below this threshold. In addition, locally rich areas must be avoided to prevent the formation of soot. These criteria create a region on an equivalence ratio (normalized air-fuel ratio) versus local temperature plot known as the LTC regime, shown in Figure 1.3. The central idea in LTC is separation of the injection and ignition events (increase ignition delay), which allows for sufficient mixing to reduce local temperatures below the NO_x formation threshold and local equivalence ratios below the soot formation threshold.

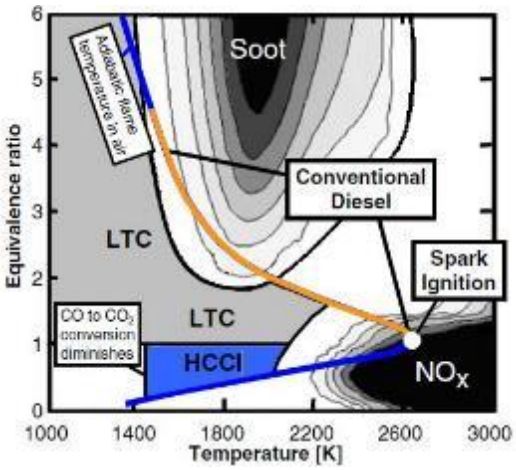

Figure 1.3 LTC equivalence ratio versus temperature [Dec 2009]

1.3.2 LTC Methods

There are several known strategies for limiting combustion to the LTC regime, many of which are reviewed in Dec's advanced compression ignition engine paper [2009]. Early attempts to promote mixing and reduce high local equivalence ratios involved intake-port premixed fuel injection [Ryan and Callahan 1996]. For this method, significant intake heating was required to facilitate adequate evaporation which limited operation due to knock; therefore, compression ratios had to be reduced.

Direct injection techniques were investigated to overcome vaporization issues. Very early direct injection was attempted by Iwabuchi *et al.* [1999] and Akagawa *et al.* [1999]. By injecting during the compression stroke, it was hoped that increased turbulence and density would facilitate mixing. It was found that wall-impingement was an issue with this injection strategy, and "softer," more dispersed injection must be used to prevent impingement and puddling of the injected fuel. However, these unconventional injectors lack the ability to return to conventional diesel combustion at

high loads. Dual injection schemes, as employed by the Toyota "UNIBUS" system [Yanagihara 2001], employ conventional injectors, injecting part of the fuel very early to promote mixing and the remainder of the fuel near TDC, but impingement can still be an issue with this strategy. Narrow included angle injection [Walter and Gatellier 2002] and using dual injectors [Duffy 2004, Sun and Reitz 2008] are additional early injection strategies that have been investigated. Because of diesel's high cetane number, autoignition and end-gas knock can be an issue with early injection techniques. To combat this issue, almost all early injection techniques employ cooled exhaust gas recirculation (EGR) to slow the combustion process and prevent autoignition [Akagawa *et al.* 1999, Walter and Gatellier 2002].

Another approach to LTC injection is to inject fuel late, near cylinder TDC, allowing precise control of ignition and combustion phasing [Kook *et al.* 2005, Ojeda *et al.* 2008]. To facilitate mixing, high fuel injection pressures and injectors with very small nozzle orifices are used, which cause rapid atomization. In addition, strategies such as injecting during the expansion stroke increase the ignition delay [Kimura *et al.* 2001], which allows more time for air-fuel mixing. In addition to late injection, cooled EGR, lowered geometric compression ratios or late IVC closing (to reduce the effective compression ratio) may also be employed to extend the ignition delay and promote mixing.

In addition to injection strategies, large amounts of cooled EGR have been shown to reduce combustion temperatures to the LTC regime, indicated by minimal NO_x and PM emissions. Kook et al [2005] investigated the effect of EGR over a wide range of injection timings, as shown in Figure 1.4. It is shown that NO_x emissions are suppressed

over a range of injection timings before TDC with heavy quantities of simulated EGR (represented by varying intake O_2 concentration), while similar operating conditions with no EGR (21% intake O_2) produced excessive NO_x emissions. Soot reduction using cooled EGR is a complex process due to the competition between soot formation and oxidation processes [Dec 2009]. Akihama *et al.* [2001] shows that smoke can be greatly reduced with a large quantity of cooled EGR; however, as the trend in Figure 1.5 shows, smoke emissions will first increase before decreasing with increasing cooled EGR. Experimentally, PM emissions are often referred to as smoke when not measured gravimetrically. The initial rise in soot emissions and associated reduction in NO_x emissions, when air-fuel ratio is reduced from 40 to 23, is likely the result of reduced combustion temperatures causing incomplete soot oxidation. At air-fuel ratios less than 23, temperatures in fuel rich regions are sufficiently low to suppress soot formation to a greater degree than soot oxidation [Dec 2009]. However, as EGR is further increased to create air-fuel ratios less than 15 (the stoichiometric ratio), CO and THC emissions increase along with a corresponding increase in brake specific fuel consumption (BSFC). At this condition there is not enough air to fully oxidize the CO and THC, lending to their sharp increase.

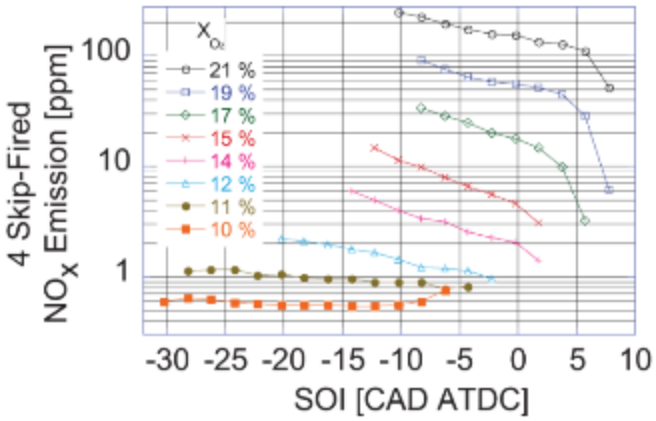

Figure 1.4 NO_x emissions versus SOI for various simulated EGR quantities [Kook *et al.* 2005]

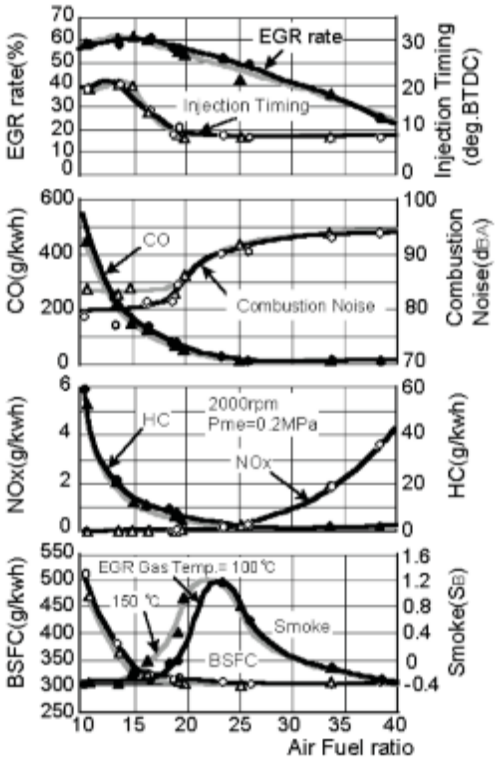

Figure 1.5 The effects of EGR rate over a range of air-fuel ratios for two EGR temperatures at an IMEP of 0.2 MPa [Akihama *et al.* 2001]

1.4 Recent Developments in Dual Fuel LTC

Dual fuel LTC combustion is a relatively new concept which marries the established dual fuel concept with modern, LTC capable engines. Different strategies tend to concentrate on gaining specific advantages (i.e. alternative fuel utilization), but overall dual fuel LTC concepts target high efficiency, low emissions operation. Reactivity controlled compression ignition (RCCI) and advanced low pilot-ignitied natural gas (ALPING) are two concepts utilizing both dual fuel and LTC concepts.

1.4.1 RCCI

The RCCI concept (also called dual fuel HCCI and PCCI) is a relatively recent development which addresses limitations with single fuel homogenous charge compression ignition (HCCI) and premixed charge compression ignition (PCCI) combustion by controlling mixture reactivity using in-cylinder fuel blending of diesel and gasoline. In HCCI combustion, fuel and air are premixed and compression ignited; the mixture is made dilute with the use of EGR which is used to control the phasing of combustion. Volumetric ignition of a homogenous air-fuel mixture facilitates rapid heat release, high efficiency operation, and low NO_x and soot emissions. The HCCI and PCCI combustion modes are very similar in that fuel is injected very early in the cycle; however, the air-fuel mixture in PCCI combustion is stratified in order to control the rate of heat release. Both HCCI and PCCI combustion modes are very efficient due to their volumetric or nearly volumetric heat release but have limited ranges of operation due to rapid rates of pressure rise and relative lack of precise control of combustion phasing. In determining what fuel would be best with these modes of combustion, both diesel and gasoline have been used in PCCI research, each having associated advantages and

disadvantages [Liu *et al.* 2008, Opat *et al.* 2007]. Using port fuel injected (PFI) gasoline and early cycle direct injected diesel, Kokjohn *et al.* [2009] demonstrated that global reactivity (i.e. fuel blending) is capable of controlling HCCI combustion phasing but fuel stratification is needed to control the rate of heat release. Splitter *et al.* [2013] have demonstrated RCCI operation nearing 60 percent thermal efficiency.

1.4.2 ALPING

The ALPING concept was developed using early injection strategies in combination with conventional dual fuel implementation. As with conventional dual fuel combustion, natural gas is fumigated with the intake air forming a lean air-fuel mixture. A very small high-cetane pilot quantity (1-2 percent of the overall fuel energy) is injected very early (e.g. 60 DBTDC) which allows for adequate mixing. Because natural gas is relatively unreactive, low load operation was initially unstable but was improved by heating the intake air, which improved thermal efficiencies significantly [Srinivasan *et al.* 2006]. Using the ALPING concept, Srinivasan *et al.* [2003] demonstrated a 98 percent reduction in NO_x emissions compared to conventional diesel operation. In subsequent research, it was shown that hot EGR was effective in retarding combustion phasing and reduced HC emissions by about 25 percent [Srinivasan *et al.* 2007].

1.5 Objectives

The goal of this dissertation is to implement, optimize, and assess low temperature dual fuel combustion in a compression ignition engine. Propane is chosen as the primary fuel for dual fuel LTC due to its higher reactivity and therefore potentially

higher FCEs as well as its benefits in terms of storage. This goal is achieved by completion of the following objectives:

1. A four-cylinder, 1.9 liter Volkswagen TDI engine is utilized to conduct diesel-ignited propane and diesel-ignited methane combustion experiments and to perform ignition delay and combustion analyses using in-cylinder pressure and energy release measurements. These results are provided to further the understanding of dual fuel combustion and how it affects both the performance and emissions of a light-duty dual fuel engine.
2. A six-cylinder, 12.9 liter heavy-duty PACCAR MX10 engine is commissioned on an open architecture engine controller as a platform for diesel-ignited propane dual fuel LTC. The original equipment (OE) engine control module (ECM) is "reverse engineered," transferring the control logic to a LabVIEW-based Drivven controller, mimicking original engine performance yet allowing complete access to control parameters. This objective is critical in allowing diesel-ignited propane dual fuel combustion to be explored comprehensively on a modern diesel engine platform.
3. The PACCAR engine setup and Drivven system are used to perform baseline diesel-ignited propane dual fuel combustion experiments, implement diesel-ignited propane low temperature combustion on the engine, and finally optimize dual fuel LTC using advanced injection strategies, boost pressure control, and cooled EGR. These results

strengthen the outlook of diesel-ignited propane LTC while bringing to light the challenges to be overcome in its development.

1.6 Organization of the Present Work

This work is organized as a series of sequential experiments and analyses intended to further the understanding of dual fuel combustion and dual fuel LTC. The present chapter outlines the primary objectives and past research on relevant topics. The following chapter defines various equations and metrics used throughout the text. The third chapter outlines the experimental setup of the Volkswagen TDI engine and its instrumentation, including data acquisition (DAQ). This engine setup is used for the experiments performed in chapters four and five. The fourth chapter outlines a detailed investigation of ignition delay for diesel-ignited methane and diesel-ignited propane dual fuel combustion. Ignition delay trends, engine ignition delay trends, and cyclic variability of the start of combustion are examined. Dual fuel combustion is further examined in chapter five, which provides a detailed characterization of the dual fuel combustion process and relates it to performance and emissions metrics. Chapter six outlines the experimental setup of the MX10 12.9L heavy-duty diesel engine, the Drivven open-architecture controller, instrumentation, and DAQ. Two sets of experiments are related in chapter seven. The first corresponds well with the VW experiments, in which only the diesel quantity is changed and other controllable parameters remain un-optimized for dual fuel combustion. The second relates testing designed to optimize both PES and emissions for dual fuel LTC. In chapter eight, conclusions are drawn and summarized from the three primary investigations. Finally, recommendations are given in chapter nine for future experimental research involving the dual fuel LTC concept.

CHAPTER II

DEFINITIONS

2.1 Steady State Calculated Parameters

Relevant engine performance parameters overall equivalence ratio ($\Phi_{overall}$) and percent energy substitution (PES) of the primary gaseous fuel are defined below:

$$PES = \frac{\dot{m}_g LHV_g}{\dot{m}_d LHV_d + \dot{m}_g LHV_g} \times 100\% \tag{2.1}$$

$$\Phi_{overall} = \frac{\left(A/F\right)_{st}}{\left(\frac{\dot{m}_a}{\dot{m}_d + \dot{m}_g}\right)} \tag{2.2}$$

In Equations 2.1 and 2.2, $\dot{m}$ refers to the mass flow rates of diesel (subscript d), gaseous fuel (subscript g), and air (subscript a), and LHV refers to the corresponding lower heating values. The stoichiometric air-fuel ratio $(A/F)_{st}$ is defined as the ratio of the mass of stoichiometric air required for complete oxidation of both the pilot and the primary fuels into CO_2 and H_2O to the mass of fuel. Therefore, $(A/F)_{st}$ was dependent on the primary fuel type (methane or propane) as well as the PES with the corresponding primary fuel.

2.2 In-cylinder Pressure and Apparent Heat Release Rates

Engine position resolved measurements (e.g., in-cylinder pressure) and cylinder volume phasing were ensured by shifting the transient data by an amount determined

while motoring the engine (to avoid crossover in the compression and expansion curves in the motoring log P – log V diagram). An example of this plot is shown in Figure 2.1. In this plot, the isentropic compression and expansion of the cycle should be linear, of a slope equal to the polytropic coefficient (i.e. the specific heat ratio, gamma). A correct phasing will have no "crossover," or loop near TDC, but will have very straight compression and expansion lines. For verification, inspection of the pressure curve should show peak pressure to be about 0.5 CAD before top dead center (this value varies with engine speed and compression ratio). The peak pressure exists shortly before TDC (and not right at TDC) because, in the very small window near TDC, heat transfer out of the cylinder is greater than the added internal energy due to compression, causing an overall decrease in temperature and therefore pressure.

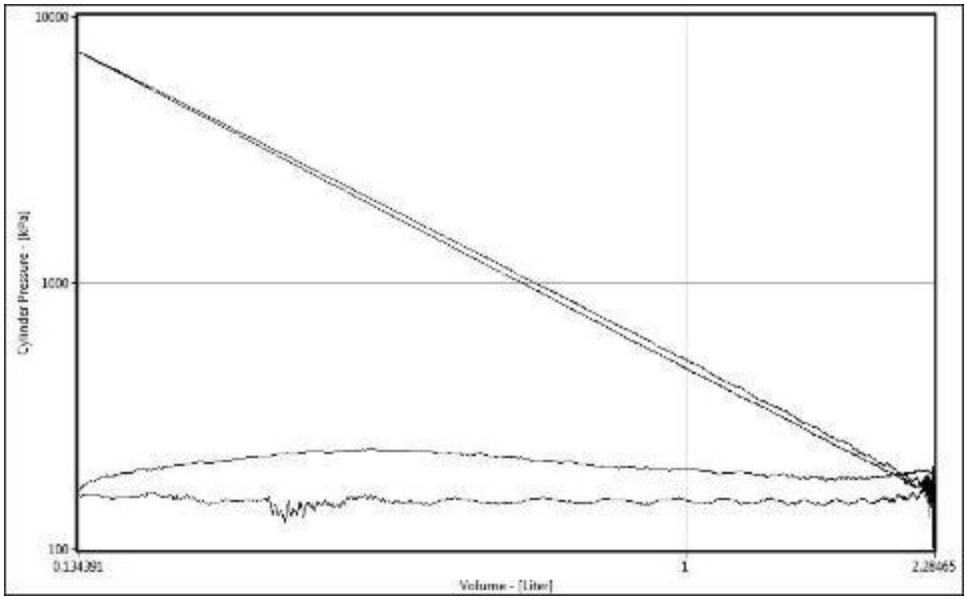

Figure 2.1 Logarithmic pressure versus volume plot of engine motoring

Note: Separation in the gas exchange portion of the plot (lower loop) is due to intake boost conditions. It is speculated that noise in the plot is due to intake and exhaust valve closings.

The pressure data was also scaled by the intake manifold pressure at bottom dead center (BDC) before the compression stroke. In addition to ensemble averaging (i.e., averaging over "n" consecutive cycles), the pressure profiles were smoothed by a "boxcar" style filter, averaging six data points on either side of a given data point to eliminate noise in the pressure data. The apparent heat release rate (AHRR) was then calculated using the following equation [Heywood 1988]:

$$AHRR(\theta) = \frac{\gamma}{\gamma - 1} P \frac{dV}{d\theta} + \frac{1}{\gamma - 1} V \frac{dP}{d\theta} \tag{2.3}$$

The instantaneous volume (V) was calculated from the known compression ratio, bore, stroke, and connecting rod lengths, and the pressure and volume derivatives ($dP/d\theta$ and $dV/d\theta$) were calculated numerically using a fourth-order central difference method. In Chapter 4, the specific heat ratio (γ) was calculated using the correlation:

$$\gamma(T) = 4.5333 \times 10^{-8} T^2 - 1.74 \times 10^{-4} T + 1.464667 \tag{2.4}$$

And in Chapter 5, the specific heat ratio (γ) was calculated using the correlation from Brunt [1998]:

$$\gamma(T) = 1 \times 10^{-8} T^2 - 6 \times 10^{-5} T + 1.338 \tag{2.5}$$

The global in-cylinder temperature was found using the ideal gas equation of state, and the mass trapped in the cylinder was found from the same equation while using the intake manifold temperature, volume, and in-cylinder pressure at intake valve closure (IVC).

In Chapter 7, the specific heat ratio (γ) was given as a constant value, 1.34, because a built-in calculation based on temperature was not available in the Drivven

Combustion Analysis Toolkit (DCAT). In addition, the heat release rates presented in Chapter 7 represent the gross heat release rate, accounting for heat transfer using the correlation from Hohenberg [1979] and a constant wall temperature of 480 degrees Kelvin.

2.3 SOI, SOC, and Ignition Delay

The ignition delay period is defined as the difference between the start of diesel fuel injection (SOI) and the start of combustion (SOC), given in the following equation:

$$ID = SOC - SOI \tag{2.6}$$

In Chapters 4 and 5, the SOI is defined as the crank angle at which injector needle lift reaches 5 percent of the maximum needle lift. The SOC is defined as the crank angle at which the AHRR first becomes positive. These parameters are shown in Figure 2.2. To eliminate confusion caused as a result of noise in the AHRR curves near SOC (leading to AHRR oscillations about zero and inaccuracies in SOC estimation), the last crank angle at which the AHRR curve becomes positive (after any previous oscillations) is taken as the SOC. In Chapter 7, the SOI is defined as "apparent" SOI (ID_A), because injector needle lift was not available. Instead, ID_A is defined as the engine position at which the controller applies voltage to the injector solenoid. Also in Chapter 7, the SOC is defined as CA5, or the location at which 5 percent of the total mass inside the cylinder has burned, which was a metric available in DCAT.

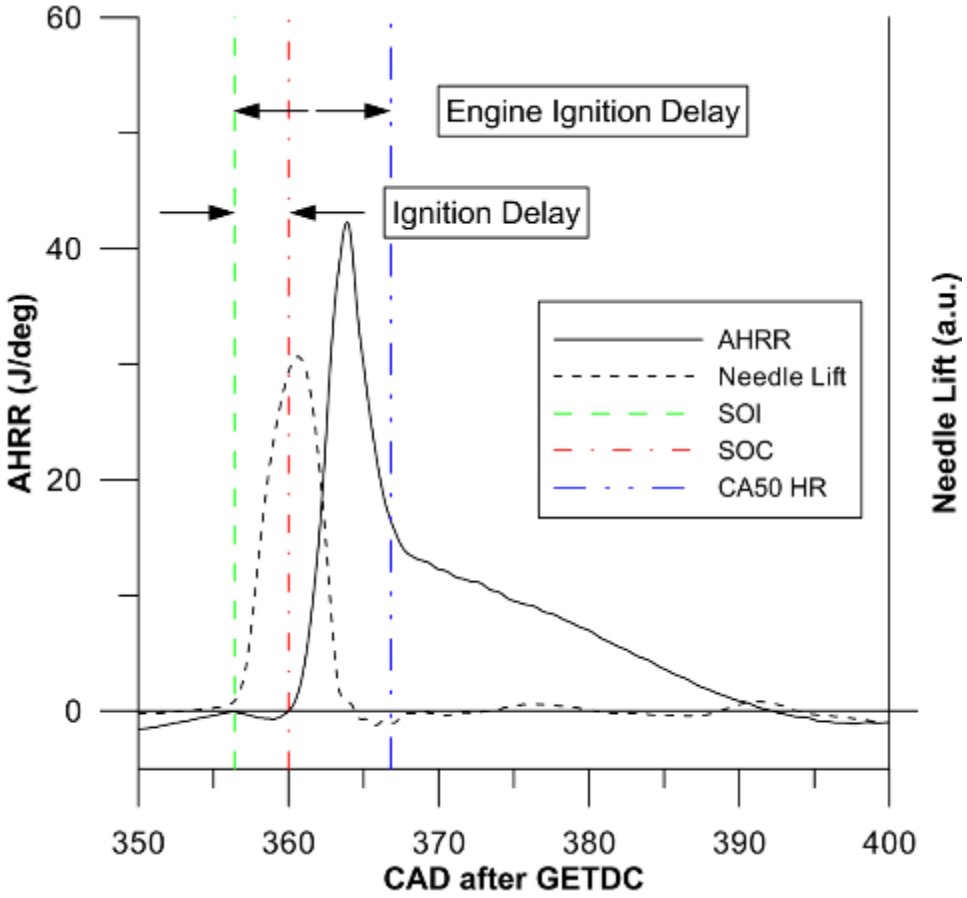

Figure 2.2 Definitions of SOI, SOC, CA50 HR, ignition delay, and EID

2.4 CA50 and CA10-90 Heat Release and Engine Ignition Delay

An important parameter used to quantify the phasing of combustion was the CA50, which was defined as the crank angle at which fifty percent of the cumulative (integrated) heat release occurred. To quantify the overall combustion duration, the CA10-90 was defined as the difference between the crank angle at which 10 percent of cumulative heat release occurred and the crank angle at which 90 percent of cumulative heat release occurred.

Following Kalghatgi *et al.* [2006], the engine ignition delay (EID) was defined as the time elapsed between the SOI and the crank angle at which 50 percent of the cumulative heat release occurred (CA50 HR):

$$EID = CA50 - SOI \tag{2.7}$$

As the EID definition incorporates CA50 HR, EID was computed by numerically integrating the AHRR curve from the SOC until the crank angle (determined as CA50 HR) at which the integral became one-half of the cumulative heat release. For diesel injection near TDC (as in the case of the VW experiments), the diesel fuel autoignited fairly quickly after injection, before it mixed well with the surrounding air. Kalghatgi *et al.* [2006] defined the EID as a metric to identify the level of diesel-air mixing attained at SOC with straight diesel operation. In general, the higher the EID, the better mixed the diesel was with air at SOC. For dual fuel combustion, the EID, in addition to being a measure of pilot diesel spray mixing, also provided some indication of the rate of combustion of both the pilot diesel fuel and the gaseous fuel. Further, the EID also provided an idea of how combustion phasing was affected by dual fueling.

CHAPTER III

EXPERIMENTAL SETUP – VOLKSWAGEN TDI ENGINE

3.1 Test Cell Overview

The first set of experiments in the present work was performed using a Volkswagen 1.9 liter TDI, inline four-cylinder diesel engine in a pre-existing test cell. The controllable parameters in these experiments were the engine speed, diesel fueling rate, intake manifold (boost) pressure, and gaseous fuel flow rate. The engine speed was controlled with a Froude Hoffman AG80 (Imperial) eddy current dynamometer and the engine torque was measured with a calibrated load cell. Diesel fueling rate was controlled using the OE, or "stock," engine control module (ECM) with input from a throttle position sensor, which was activated by dynamometer control software. Intake manifold pressure was controlled by activating a spring return wastegate valve using an I-P (current-to-pressure) transducer, National Instruments hardware, and NI LabVIEW software. Finally, the primary gaseous fuel was metered by a manually controlled needle valve and introduced to the intake air upstream (before) of the turbocharger compressor. Relevant engine details are given in Table 3.1. A schematic of the experimental setup is given in Figure 3.1.

Table 3.1 VW Engine Specifications

Parameter	Value
Engine	Volkswagen TDI
Cylinders	4, inline
Bore	79.5 mm
Stroke	95 mm
Connecting rod length	144.4 mm
Valves per cylinder	4
Nominal compression ratio	19.5:1
Displaced volume	1.9 liters
Injection system	Mechanical
Aspiration	Turbocharged w/ wastegate
EGR	None
Engine Control	OE ECM
Nominal pilot injection timing	4 CAD BTDC

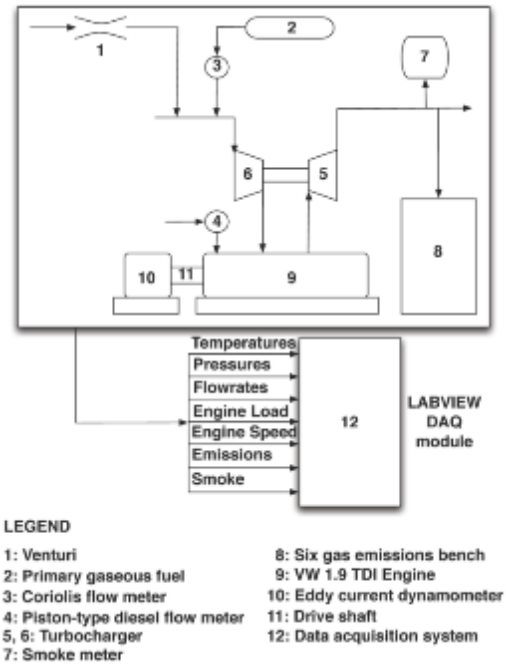

Figure 3.1 Schematic of the Volkswagen experimental setup

3.2 Test Cell Instrumentation

Relevant instrumentation details are given in Table 3.2.

Table 3.2 Instrumentation Specifications

Data Type	Sensor/Instrument	Type	Accuracy
Temperature	Thermocouple	K	Greater: 1.1 °C or 0.4%
Pressure for venturi	Omega PX429	Absolute	0.08% FS BSL
Pressure for venturi	Omega MM Series	Differential	0.08% FS BSL
Pressure for boost	Setra 209	Gauge	0.25% FS
Mass air flow	Flowmaxx	Venturi	
Mass gas. fuel flow	Micro Motion	Coriolis	0.35% of reading
Vol. diesel flow	Max Machinery 213	Piston	0.2% of reading
Smoke	AVL 415S	Filter	0.005 FSN + 3% of reading
NO_x	ESA EGAS 2M	CLD	1% FS
NO	ESA EGAS 2M	CLD	1% FS
THC	ESA EGAS 2M	FID	1% FS
CO-low	ESA EGAS 2M	NDIR	1% FS
CO-high	ESA EGAS 2M	NDIR	1% FS
CO_2	ESA EGAS 2M	NDIR	1% FS
Cylinder Pressure	Kistler 6056A	Piezoelectric	Linearity: 0.3% FSO
Needle Lift	Wolff Controls	Hall Effect	

3.2.1 Steady State Measurements

Engine coolant, pre- and post-turbo air, intake mixture, and post-turbo exhaust temperatures were measured with K-type thermocouples. Typically, these were mounted using 0.25 inch Swagelok compression fittings. The primary gaseous fuel (methane or propane) mass flow rate was measured with an Emerson Micro Motion coriolis mass flowmeter. Intake air mass flow rate was measured with a Flowmaxx venturi flowmeter. Straight intake pipes with lengths of twenty pipe diameters upstream and ten pipe diameters downstream were used to facilitate laminar intake air flow. Diesel volume

flow rate was measured with a Max Machinery Model 213 piston flowmeter. Diesel mass flow rate was then calculated by multiplying by an assumed fuel density of 861.7 kg/m^3. The absolute pressure in the test cell was measured with an Omega PX429 sensor, the differential pressure across the venturi air flowmeter was measured with an Omega MM Series differential pressure transducer, and the intake boost pressure was measured with a Setra 209 pressure transducer. All gaseous exhaust emissions were measured downstream of the turbocharger turbine. Gaseous emissions were routed through an emissions sampling trolley to an integrated emissions bench (EGAS 2M) manufactured by Altech Environnement S.A. (ESA) and smoke was measured with an AVL 415S variable sampling smoke meter. Smoke emissions are given in filter smoke number (FSN) and were sampled after 10 pipe diameters of straight exhaust pipe for laminar flow.

3.2.2 Transient Measurements

Transient measurements such as cylinder pressure require an engine-position based clock for data acquisition. A BEI optical encoder with 0.1 CAD resolution (3600 pulses per revolution) was used for this purpose. A custom crankshaft adapter and a custom encoder bracket were designed and fabricated in-house to facilitate mounting. The bracket was mounted rigidly with the engine (not attached to vibration-isolated mounting points).

In-cylinder pressure was measured using a Kistler 6056A piezoelectric pressure transducer mounted in a Kistler glow plug adapter. A Kistler 5010B charge amplifier with a "medium" time constant setting was used to condition the signal output from the

piezoelectric pressure transducer. Needle lift was measured in a stock injector instrumented with a Wolff needle lift sensor coupled to a signal conditioner.

3.3 Data Acquisition

3.3.1 Hardware

A National Instruments PXI-1050 chassis and PXI-8110 controller were used as the foundation of the DAQ system. An M-Series analog input card (PXI-6229) was used to sample low-speed steady state data (engine speed, load, etc.) and an S-Series analog input card (PXI-6123) was used to sample high-speed transient data (cylinder pressure and injector needle lift). An SCXI expansion chassis and a thermocouple conditioner and amplifier (SCXI-1102B) were used to sample thermocouple temperature data. In addition, the PXI chassis had analog output and power supply capabilities. In an effort to be versatile, the hardware was mounted on a cart for mobility while the software was programmed to accept user inputs for different channel configurations.

3.3.2 Software

The VI, or virtual instrument (LabVIEW program), used for this test cell functioned both to monitor and to record steady state as well as transient combustion data. Steady state data were sampled as analog voltage signals (0 to 10 V) at 100 Hz. Each incoming channel was scaled according to its respective calibration and time averaged at 1 Hz. These data included dynamometer torque and speed as well as engine pressures, temperatures, flow rates, and emissions values. After averaging, these data were distributed to "indicators" in order to be displayed, and also used to process other calculated values such as mass air flow, BMEP, fuel conversion efficiency, and

equivalence ratio, among others. Minimum and maximum thresholds were given to critical values such as oil pressure, coolant temperatures, etc. which would trigger visual indicators in the case of an unsuitable engine operating condition.

The VI also had the ability to record and display transient data such as in-cylinder pressure, injector needle lift, apparent heat release rate, and other calculated transient values. "On-the-fly processing" allowed for close monitoring of critical values such as the maximum pressure rise rate (MPRR) and combustion phasing (CA50).

The recording of engine-position synchronized data was enabled by the use of the BEI optical encoder coupled to the engine crankshaft. The high-resolution signal (3600 pulses per revolution), or A pulse, was used as the sample clock for the analog inputs of cylinder pressure and injector needle lift. The index (1 pulse per revolution), or Z pulse, was used as the trigger which functioned to correctly phase the transient measurements. While the Z pulse was physically located close to engine TDC, software shifting was required for further accuracy because phasing of the pressure signal and cylinder volume is critical for accurate heat release calculations. In order to determine whether the Z pulse for a given engine revolution was for compression or gas exchange, data was sampled for a predetermined number of cycles (in this case 100 cycles) plus one additional cycle. A subset of the data was then taken from the raw array; the length of the subset was determined by the number of cycles recorded and the array index was determined by the phasing and shifting inputs. The phasing input was determined by examining the first cycle of raw data for its peak value and using its location to determine whether or not to shift the array index by 360 degrees. The shifting input was determined by manually entering a value while monitoring a log-log plot of cylinder pressure versus

volume while motoring (spinning but not firing) the engine, as discussed with Figure 2.1. An acceptable shifting input value would locate the peak pressure approximately half a crank angle degree before TDC and yield no "crossover" in the log-log pressure versus volume plot.

After phasing and shifting of the cylinder pressure and the injector needle lift data, the cycles were ensemble averaged, i.e., the values of pressure at 0.1 CAD over successive engine cycles were averaged, then for 0.2 CAD, for 0.3 CAD, and so forth, resulting in a single cycle of pressure data, as follows (where N is the number of cycles):

$$\bar{P}_i = \frac{1}{N}\sum_{j=1}^{N} P_{i,j} \tag{3.1}$$

In addition to ensemble averaging, the data were further smoothed with the use of a "boxcar" filter, or moving average, using M data points before and M data points after a given point, as follows; M = 6 was used in this case:

$$\overline{Filt}_i = \frac{1}{2M+1}\sum_{j=-M}^{M} \bar{P}_{(i+j)} \tag{3.2}$$

As piezoelectric transducers by nature measure only dynamic pressure, the cylinder pressure data was scaled, or "pegged," according to the intake manifold pressure. An engine crank position during which the intake valve is open is chosen (in this case BDC) and "pegged" to the intake manifold pressure, giving the data an absolute reference. The simple equation for pegging is as follows:

$$Ppeg_i = P_i - P_{BDCintake} + P_{man} \tag{3.3}$$

Once shifted, phased, and scaled appropriately, the transient data can then be used for monitoring and further analyses, such as IMEP, MPRR, heat release, and ignition

delay calculations. All transient waveforms and values are recorded alongside the steady state data. The front panel of the latest revision of the VI and an overview of the block diagram are shown in Appendix A.

CHAPTER IV

DUAL FUEL IGNITION DELAY

4.1 Introduction

Defined as the period between the start of ignition (SOI) and the start of combustion (SOC), the ignition delay (ID) period influences the ensuing combustion process as well as engine performance and emissions. The primary objective of this chapter is to characterize dual fuel ID behavior with both propane and methane as primary fuels and over a range of engine operating conditions.

4.2 Objectives

The objectives of this chapter[1] are as follows:

1. Investigate ignition behavior for dual fuel combustion on a stock Volkswagen (VW) 1.9-liter turbocharged direct injection (TDI) engine with the stock electronic control module (ECM) using in-cylinder combustion pressure data.
2. Compare diesel-ignited methane and diesel-ignited propane dual fuel combustion IDs for a range of equivalence ratios and a range of engine loads (BMEPs) and PES at a constant engine speed of 1800 rev/min.

[1] The essence of this chapter was published in the Proceedings of ASME ICEF2011 and has also been accepted for publication in the ASME J Energy Resources Tech [Polk 2011].

3. Quantify ignition delay effects on dual fuel combustion using engine ignition delays (EID) and cyclic variation plots of SOC.

4.3 Experimental Procedure

All experiments were performed at a constant engine speed of 1800 rev/min without any exhaust gas recirculation (EGR). As shown in Tables 4.1 and 4.2, two sets of experiments were performed for both diesel-ignited methane and diesel-ignited propane dual fuel combustion. The first set of experiments focused on understanding the effects of the overall equivalence ratio ($\Phi_{overall}$) on ignition delay behavior for various constant pilot quantity-based equivalence ratios (Φ_{pilot}). For a given pilot quantity (constant Φ_{pilot}), the amount of primary fuel was increased to increase $\Phi_{overall}$ and the ignition delay behavior was recorded. This process was subsequently repeated for other Φ_{pilot} values. In the second set of experiments, dual fuel ignition delays were examined for increasing PES from the gaseous fuels at different brake mean effective pressures (BMEP). For these tests, the BMEP was monitored and maintained at a specified value while both the pilot diesel and primary gaseous fuels were adjusted based on predetermined PES increments within ±1.5 percent. The maximum PES stated in Table 4.2 was dependent on the primary fuel type and the BMEP. If the maximum is not specifically listed for a given condition, then the last stated PES is the maximum for that fuel at that condition.

Table 4.1 Experimental Matrix for $\Phi_{overall}$ Effects at Different (Constant) Φ_{pilot}

← Constant Φ_{pilot} →				
Φ_{pilot}	Increase in $\Phi_{overall}$ with gaseous fuel addition			
	+0.1	+0.2	+0.3	+0.4
0.2	M,P	M,P	M	
0.3	M,P	M,P	M	
0.4	M,P	M,P	M,P	
0.5	M,P	M,P	M,P	M
0.6	M,P	M,P		

M: methane dual fueling, P: propane dual fueling

Table 4.2 Experimental Matrix for PES Effects at Different (Constant) BMEPs

← Constant BMEP →				
BMEP (bar)	Percent Energy Substitution			
	25%	50%	75%	Max
2.5	M,P	M,P	M,P	M,P
5.0	M,P	M		P-47%
7.5	M,P	M,P		
10	M,P	M		P-45%

M: methane dual fueling, P: propane dual fueling

Each set of experiments was performed in the same session to reduce variations in baseline operation and obtain reliable performance and emissions data. In addition, the intake boost pressure was held constant for a given Φ_{pilot} or for a given BMEP. The intake pressure chosen for each condition was based on the nominal boost pressure possible (corresponding to the available exhaust energy) at the baseline diesel operating condition (no gaseous fuel) at the given Φ_{pilot} or BMEP. Engine coolant temperatures and intake charge temperatures were maintained at 85±5°C and 35±5°C, respectively for all experiments.

4.4 Results and Discussion

The ignition delay period in dual fuel engines is dependent on the primary fuel used, pilot quantity, intake charge temperature, and equivalence ratio [Liu and Karim 1995, Gunea *et al.* 1998, Prakash and Ramesh 1999]. In this chapter the ignition delay behavior of two primary fuels, methane and propane, was investigated over a range of pilot quantities and equivalence ratios while intake temperatures were maintained constant (35±5°C). The experimental matrices shown in Tables 4.1 and 4.2 were completed to the extent possible until the onset of engine instability, excessive audible engine noise (perceived knock), or a self-imposed maximum pressure rise rate (MPRR) limit of 15 bar per crank angle degree (CAD) prevented further engine testing. For both propane and methane dual fueling at low BMEPs, the maximum PES of the primary fuel was limited by the onset of misfire or high coefficient of variation of IMEP. At high BMEPs, engine instability limited methane dual fueling whereas extremely high MPRR limited propane dual fueling.

When operating at constant BMEP and varying PES, the pilot quantity was allowed to change with the gaseous fuel substitution, and consequently, the needle lift profile and the maximum needle lift also changed with PES. Therefore, considering the definition used for the SOI (location of 5 percent of the maximum needle lift), if the maximum needle lift changes, the recorded SOI would change even if the actual SOI did not change. A seemingly obvious solution to this problem is to use a constant threshold value for SOI. However, this definition did not work at very high PES (low pilot) where the max needle lift did not even exceed the threshold value. If the threshold was set too low, noise in the needle lift signal yielded a false SOI. Hence, a numerical average was

taken of all SOIs based on the definition of 5 percent of the maximum needle lift, which was then used to arrive at a constant nominal SOI of 4 CAD BTDC.

4.4.1 Ignition in Diesel-Ignited Propane Combustion

4.4.1.1 Equivalence Ratio Effects on Ignition Delay

The ignition delay trends for diesel-ignited propane combustion are shown for different overall equivalence ratios ($\Phi_{overall}$) in Fig. 4.1. In this figure, each curve begins with a baseline pilot-based equivalence ratio (Φ_{pilot}) ranging from 0.2 to 0.6 and each data point after the baseline represents an increasingly higher concentration of propane, leading to an overall equivalence ratio ranging from 0.2 to 0.8 or to the extent possible while maintaining stability at lower Φ_{pilot} values. In this set of experiments, the pilot quantities are held constant for each Φ_{pilot}. Therefore, "the baseline" at each Φ_{pilot} refers to engine operation with diesel alone (no gaseous fuel addition). At lower Φ_{pilot}, the addition of propane tends to increase the ignition delay slightly. Following Liu and Karim [1995], this trend may be attributed to the reduction in in-cylinder temperature due to the displacement of oxygen in the intake air by the fumigated gaseous fuel (propane) and the increased specific heat ratio of the mixture.

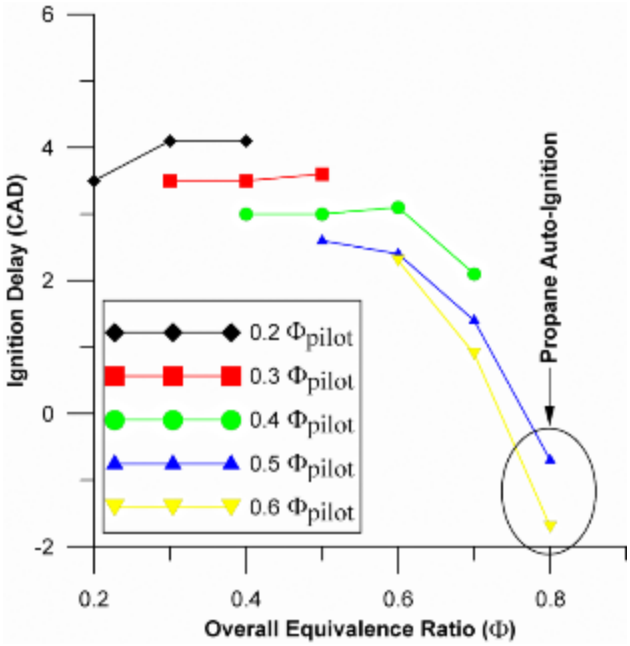

Figure 4.1 Ignition delay vs. overall equivalence ratio for diesel-ignited propane combustion; BMEPs range from 1 bar to 12.9 bar; boost pressure held constant for each Φ_{pilot} value.

Another possible contributing factor to the ignition delay trends is the preignition chemistry. As the propane-air mixture is compressed in the cylinder, it is exposed to increasingly high temperatures over a relatively long period, allowing ample opportunity for low-temperature preignition reactions. With small diesel pilot quantities, these intermediate products of partial oxidation of propane may compete with diesel ignition, thereby extending the ignition delay period [Liu and Karim 1995]. As Φ_{pilot} (and BMEP) is increased, exhaust temperatures increase significantly. Thus, as Φ_{pilot} is increased at constant engine speed, the intake fuel-air mixture will be exposed to higher in-cylinder temperatures due to hotter residual exhaust gases and hotter cylinder wall temperatures. Therefore, it is hypothesized that as pilot quantity and BMEP increase, the extent of partial oxidation in the fuel-air mixture increases, further increasing the pressure and

temperature in the cylinder. As diesel injection occurs at increasingly high in-cylinder temperatures, diesel evaporation, which is controlled by mixing with the hot ambient gases, becomes more rapid and the overall ignition delay period is reduced.

As shown in Fig. 4.1, at relatively high $\Phi_{overall}$ and BMEPs, propane autoignition occurred even before the start of diesel pilot injection. This phenomenon can be observed more closely in Fig. 4.2. The three cases shown in Fig. 4.2 employ relatively large pilot quantities (Φ_{pilot} = 0.5 or 0.6) and $\Phi_{overall}$ = 0.7 or 0.8, all at high BMEPs. In the top left plot (Φ_{pilot} = 0.5, $\Phi_{overall}$ = 0.7), the separation between the needle lift (NL) and the negative AHRR due to diesel evaporation after SOI can be seen clearly. Shown below this plot are the cylinder pressure curve and the AHRR curve showing dual fuel combustion progressing normally. The center plots show that with the same Φ_{pilot} and a slight higher $\Phi_{overall}$ of 0.8, propane begins to autoignite nearly simultaneously with the start of diesel pilot injection, causing a very rapid rise in AHRR and high peak AHRR. The plots in the far-right show that propane clearly autoignites before diesel is injected for Φ_{pilot} = 0.6 and $\Phi_{overall}$ = 0.8, causing more of a staged heat release (with pilot injection not aiding propane heat release until later), which results in a lower peak AHRR. For these conditions where propane autoignites either at or before the SOI, the ambient conditions (high temperatures and high $\Phi_{overall}$) are conducive to preignition reactions in the premixed propane-air mixture to accelerate and release sufficient energy to cause spontaneous ignition. It is important to note that these conditions did not lead to "end-gas knock" that usually follows pilot ignition but premature autoignition of propane even before SOI.

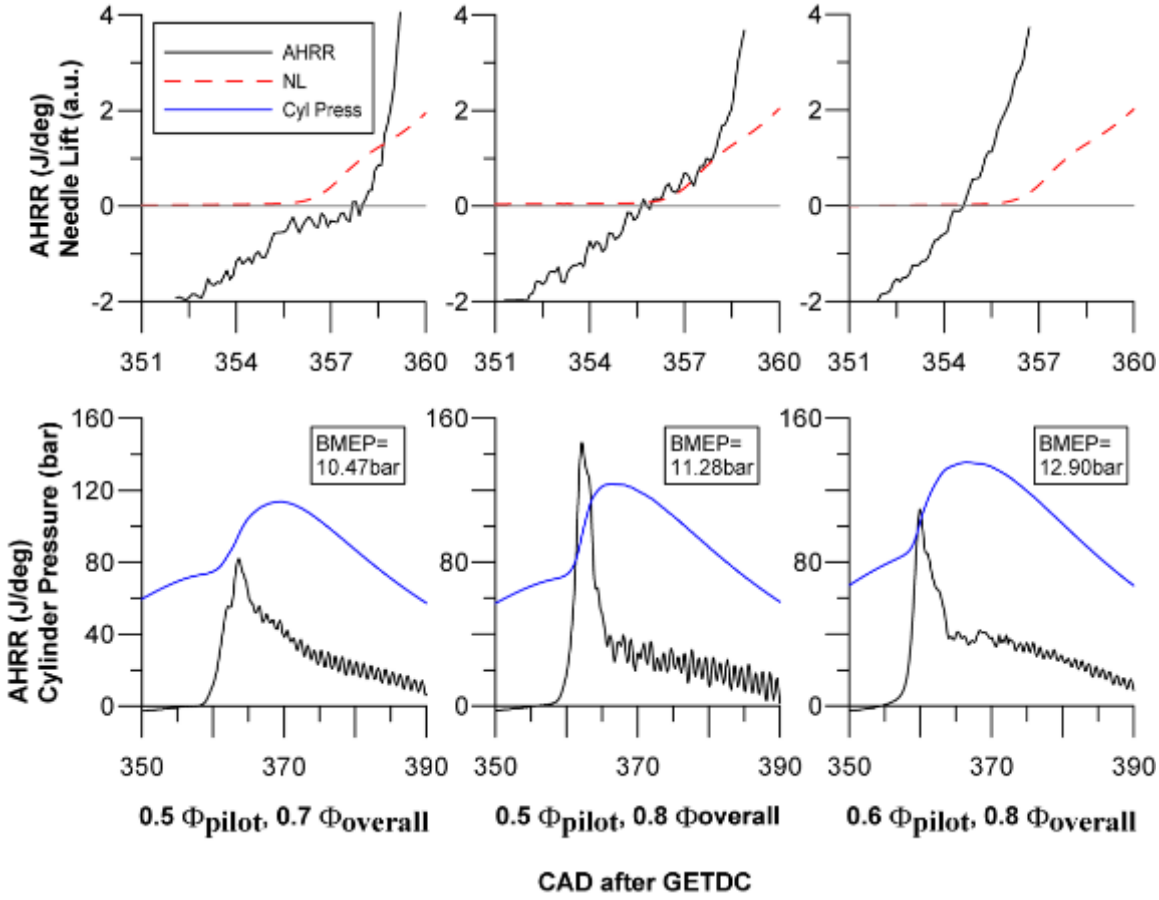

Figure 4.2 Heat release, needle lift, and cylinder pressure profiles for one normal case (no propane autoignition) and two cases with propane autoignition as shown in Fig. 4.2

To examine ignition delay behavior further, Fig. 4.3 shows the cyclic variations in SOC for a constant Φ_{pilot} of 0.5 and various $\Phi_{overall}$ corresponding to Fig. 3. In this figure, the "baseline" is the condition with Φ_{pilot} = 0.5 and no propane substitution, while each subsequent case refers to increasing propane substitution (e.g., +0.1 phi propane corresponds to $\Phi_{overall}$ = 0.6). At $\Phi_{overall}$ of 0.6 and 0.7, as the propane concentration is increased, the average SOC is advanced (ID is shortened) and the variation in SOC increases. Since intake temperature and intake boost pressure were held constant and no

EGR was used, the primary factors influencing ignition behavior were oxygen displacement, residual exhaust gas temperatures, and propane concentration. As $\Phi_{overall}$ (and BMEP) is increased, the in-cylinder temperatures were likely higher causing the SOC to occur earlier but with greater cyclic variability. However, upon reaching the point of propane autoignition ($\Phi_{overall}$ = 0.8), the variation of SOC begins to decrease significantly.

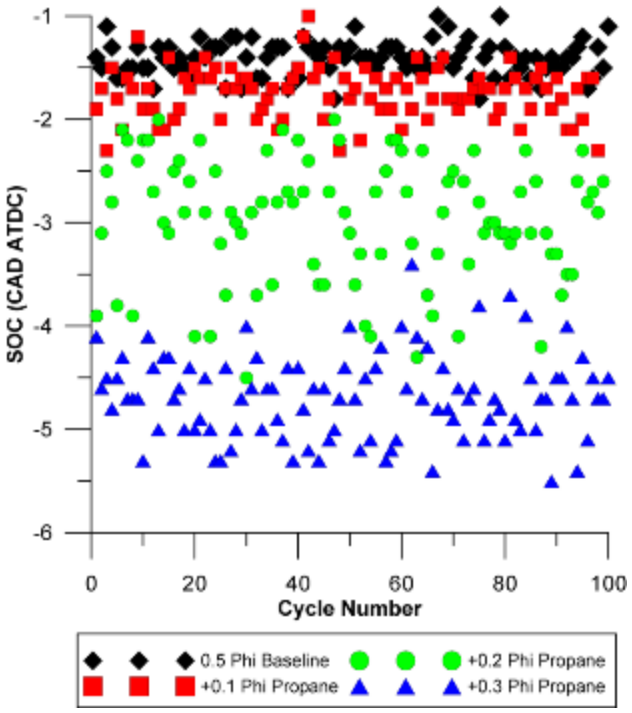

Figure 4.3 Cyclic variations in SOC for Φ_{pilot} = 0.5 and various propane concentrations ($\Phi_{overall}$ =0.6, 0.7, and 0.8) with a constant boost pressure of 1.4 bar and BMEPs ranging from 7.2 to 11.2 bar

standard deviations of SOC were 0.16, 0.25, 0.6, and 0.4 CAD for $\Phi_{overall}$ = 0.5, 0.6, 0.7, 0.8, respectively.

To clarify the effects of $\Phi_{overall}$ on ignition and the ensuing combustion process, engine ignition delay (EID) trends are shown in Fig. 4.4. For dual fuel combustion, the

EID is a measure of the relative phasing of the combustion process (CA50 HR) with respect to the SOI. The EID increases with increasing Φ_{pilot}. For pure diesel operation at different BMEPs (the first data point in various curves), the EID seems to exhibit a linear trend with increasing BMEP. While increasing Φ_{pilot} decreases ID (see Fig. 4.1), it also increases the duration of combustion, thus delaying CA50 HR and increasing the overall EID. For a given Φ_{pilot}, increasing propane concentration enriches the homogeneous fuel-air mixture entering the engine. Due to the fact that a greater fraction of the combustion energy is released more rapidly due to flame propagation at higher propane concentrations, EID is decreased. At lower Φ_{pilot}, the increase in EID is attributed to the initial increase in ignition delays with increasing propane concentrations. By contrast, as Φ_{pilot} is increased, the increased reactivity of propane is more pronounced, leading to a significant decrease in EID even with small increases in propane concentration.

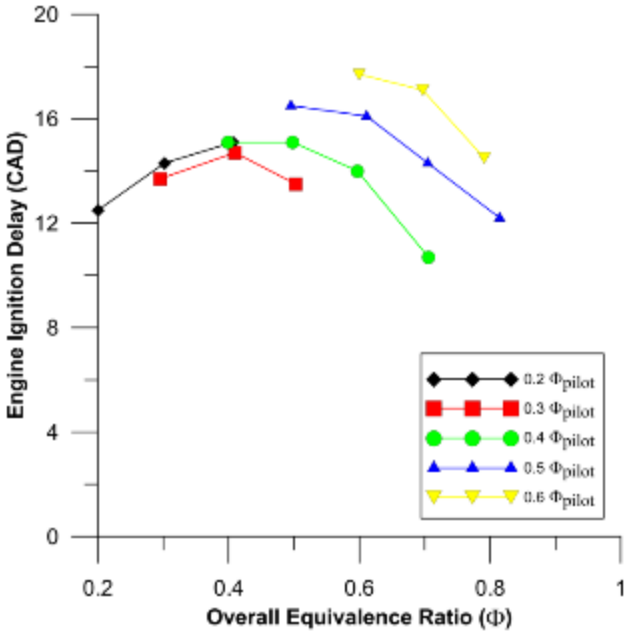

Figure 4.4 Engine ignition delay vs. overall equivalence ratio for diesel-ignited propane combustion; BMEPs ~ 1 bar to 12.9 bar

boost pressure maintained at baseline Φ_{pilot} value.

4.4.1.2 Percent Energy Substitution Effects on Ignition Delay

In Fig. 4.5, the ignition delay behavior of diesel-ignited propane combustion with increasing PES is shown for four different (but constant) BMEPs from 2.5 to 10 bar. These results are fundamentally different from the equivalence ratio effects discussed above because the BMEP is held constant while the pilot quantity (Φ_{pilot}) and primary fuel concentration are allowed to vary as PES is increased. At low BMEPs, propane addition initially increases the ignition delay period. However, as the propane concentration reaches a certain point (e.g., 50% PES at 2.5 bar BMEP), the ignition delay begins to decrease. It should be noted here that the maximum PES possible at 2.5 bar BMEP was about 75 percent while for higher BMEPs, the PES was restricted to about 50 percent due to high MPRR values. At higher BMEPs, while the magnitude of ignition

delay variation is small, the ignition delay either increases (5 bar BMEP), or remains constant (7.5 bar BMEP), or decreases (10 bar BMEP) as PES is increased. For all of these experiments, the boost pressure was maintained at the baseline diesel value (corresponding to 0 percent PES), which was a constant for a given BMEP but increased as BMEP was increased. Since the engine speed was held constant as well, higher BMEPs led to higher exhaust temperatures and higher boost pressures. The higher exhaust temperatures likely were a consequence of higher in-cylinder mixture temperatures that led to shorter ignition delays. Further, the higher boost pressures at higher BMEPs could have reduced the counteracting effects of oxygen displacement and specific heat ratio modifications with increasing PES. The overall result was a net decrease in ignition delays at higher BMEPs.

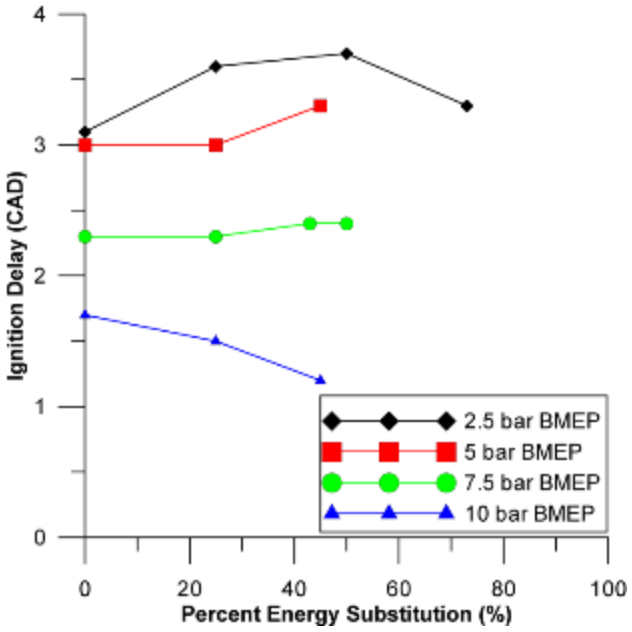

Figure 4.5 Ignition delay vs. PES at BMEPs of 2.5, 5, 7.5, and 10 bar for diesel-ignited propane combustion.

Boost pressure was maintained at 0% PES value for a given BMEP (1.18bar, 1.28 bar, 1.40 bar, and 1.55 bar, respectively).

Figure 4.6 shows the cyclic variations in SOC for different PES at the 2.5 bar BMEP condition shown in Fig. 4.5. In contrast to the trends observed in Fig. 4.3, the differences in SOC behavior with increasing PES are relatively less pronounced. As PES is increased from 0 percent to 25 percent, there is a slight retard in SOC and slightly higher cyclic variations. However, as PES is increased to 50 percent, the cyclic variations in SOC increase substantially. Finally, at 75 percent PES, the average SOC is advanced but the cyclic variations become more significant as the pilot quantity is reduced, leading to more unstable engine operation (the coefficient of variation (COV) of IMEP was 2.9 percent). At 75 percent PES, some cycles experienced more advanced SOC, indicating more pronounced preignition chemical reactions for those cycles. Since the boost pressure was held constant at the baseline value (1.2 bar) corresponding to 0

percent PES, increasing PES increased $\Phi_{overall}$, thus increasing the possibility of preignition reactions in the mixture at higher PES.

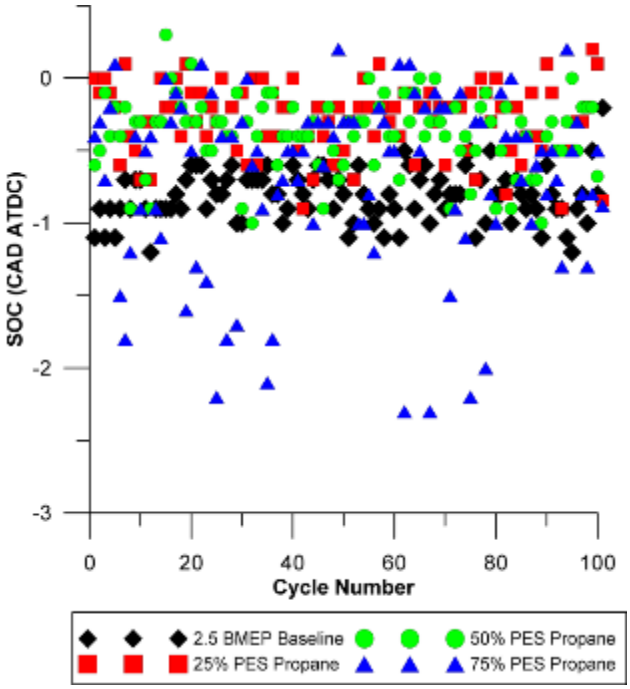

Figure 4.6 Cyclic variations in SOC for 2.5 bar BMEP and various PES of propane with constant boost pressure of 1.2 bar

standard deviations of SOC were 0.17, 0.24, 0.26, and 0.6 CAD for 0, 25, 50, and 73 percent PES, respectively.

4.4.2 Ignition in Diesel-Ignited Methane Combustion

4.4.2.1 Equivalence Ratio Effects on Ignition Delay

Compared to propane, methane is a more stable (less reactive) primary fuel. Therefore, preignition reactions with methane may be relatively weak compared to propane and only the effects of specific heat ratio and oxygen displacement on ignition delay may be significant. As shown in Fig. 4.7, for a given Φ_{pilot}, the ignition delay remains nearly invariant as $\Phi_{overall}$ is increased. At low BMEPs, increasing $\Phi_{overall}$ leads

to a slight increase in ignition delay but at high BMEPs, the changes in ignition delay are relatively small. With constant intake temperatures and methane as the primary fuel, significant ignition delay trends are suppressed with increasing $\Phi_{overall}$, confirming trends reported elsewhere [Karim *et al.* 1989, Liu and Karim 1995]. However, with increasing Φ_{pilot}, the ignition delay tends to decrease significantly. This is due to the fact that the BMEP increases as Φ_{pilot} is increased and residual exhaust gas temperatures and in-cylinder temperatures are higher, thus leading to shorter ignition delays.

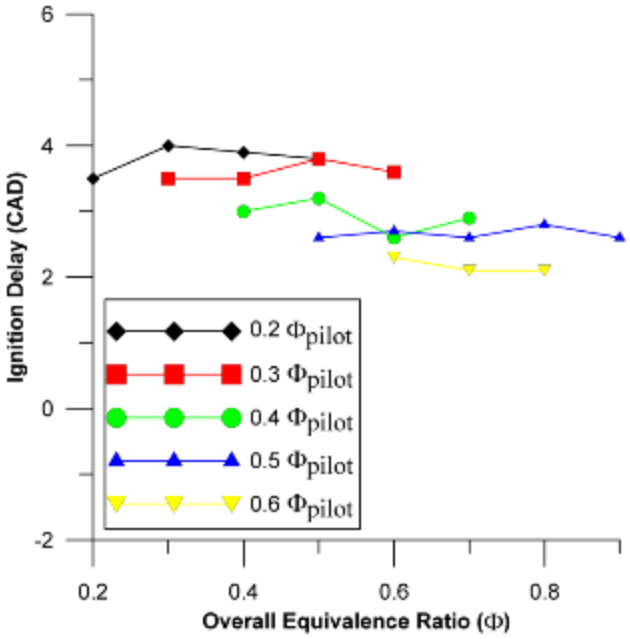

Figure 4.7 Ignition delay vs. overall equivalence ratio for diesel-ignited methane combustion; BMEPs range from 1 bar to 12.9 bar

boost pressure held constant for each Φ_{pilot} value.

Figure 4.8 shows the cyclic variations in SOC for diesel-ignited methane combustion at different $\Phi_{overall}$ with the same legend meanings as in Fig. 4.3. However, these trends are significantly different from the diesel-ignited propane combustion trends

shown in Fig. 4.3. For a constant Φ_{pilot} of 0i.5, the SOC remains relatively invariant with increasing methane concentration. This indicates that, for the equivalence ratio experiments, the injected diesel fuel is the primary contributing factor affecting SOC with very little influence of methane, possibly due to its reduced reactivity compared to propane.

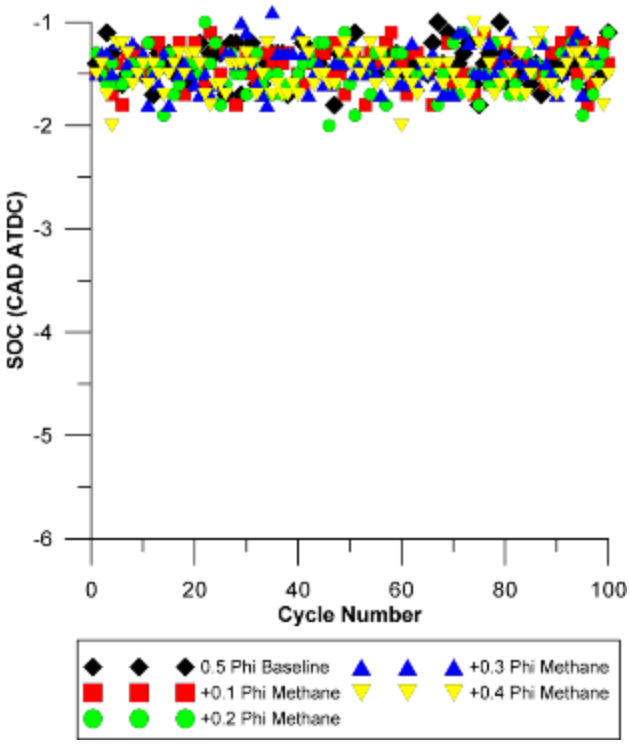

Figure 4.8 Cyclic variations in SOC for $\Phi_{pilot} = 0.5$ and various methane concentrations ($\Phi_{overall} = 0.6$, 0.7, 0.8, and 0.9) with a constant boost pressure of 1.4 bar and BMEPs ranging from 7.2 to 12.2 bar

standard deviations of SOC were 0.17, 0.17, 0.2, 0.19, and 0.19 CAD for $\Phi_{overall}$ of 0.5, 0.6, 0.7, 0.8, and 0.9, respectively.

Again, to understand the effects of overall equivalence ratio on combustion phasing in diesel-ignited methane combustion, engine ignition delay trends are shown in Fig. 4.9. With methane as the primary fuel, the EID trend varies with increasing methane

concentration in a manner that is nearly independent of pilot quantity. These trends are quite different from those observed in Fig. 4.4 for diesel-ignited propane combustion. The EID increases initially with increasing methane concentration, reaches a maximum, and then begins to decrease as methane concentration is further increased. These trends imply that once ignition is achieved with diesel-ignited methane combustion, the phasing of apparent heat release is largely unaffected by the amount of pilot fuel used. A possible hypothesis that may explain these EID trends is that the methane concentration near the pilot spray has a more significant influence on the overall combustion rates than the pilot quantity itself over the range of Φ_{pilot} and $\Phi_{overall}$ investigated here.

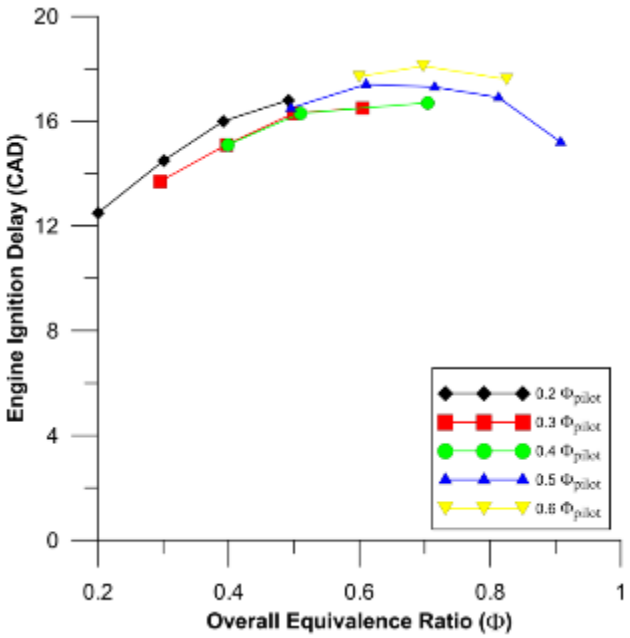

Figure 4.9 Engine ignition delay vs. overall equivalence ratio for diesel-ignited methane combustion; BMEPs ~ 1 bar to 12.9 bar

boost pressure maintained at baseline Φ_{pilot} value.

4.4.2.2 Percent Energy Substitution Effects on Ignition Delay

When methane is used as the primary fuel, its effect on ignition delay is quite evident as PES is increased at constant BMEP and also when BMEP is increased at constant PES (see Fig. 4.10). At lower BMEPs, the diesel quantity is very small; hence a small amount of methane is required to drastically increase the PES. Therefore, ignition delay is increased only slightly at lower BMEPs and PES, consistent with the trends observed in Fig. 4.7. However, at increased concentrations of methane at low BMEPs, the ignition delay tends to decrease as the engine operation becomes more unstable. At higher BMEPs, the amount of methane required to increase the PES also increases, and the ignition delay increase is also more significant. Oxygen displacement and chemical effects are contributors to this ignition delay trend, with the latter likely the more significant factor. In contrast to diesel-ignited propane combustion, the combination of these factors only tend to increase ignition delay when methane is used as the primary fuel, with the exception of high PES at low BMEPs.

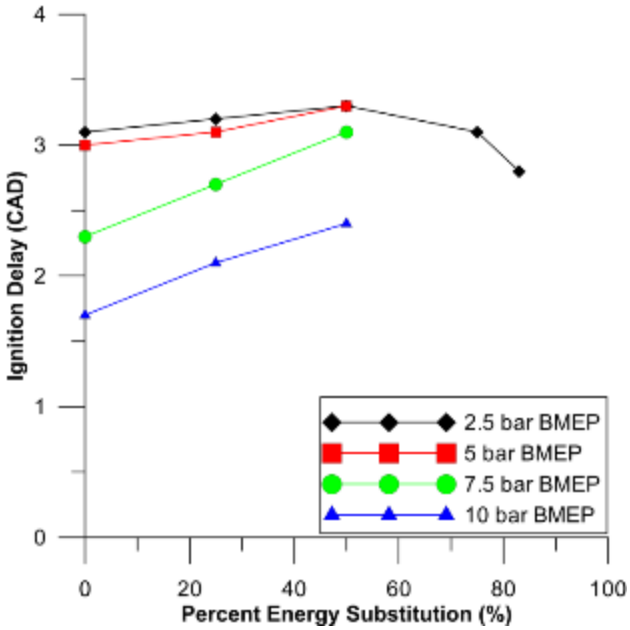

Figure 4.10 Ignition delay vs. PES at BMEPs of 2.5, 5, 7.5, and 10 bar for diesel-ignited methane combustion

Boost pressure was maintained at 0% PES value for a given BMEP (1.18bar, 1.28 bar, 1.40 bar, and 1.55 bar, respectively).

To gain additional insight regarding ID behavior at low BMEPs, the cyclic variations in SOC for diesel-ignited methane combustion at 2.5 bar BMEP is shown in Fig. 4.11. This condition is very similar to the 2.5 bar BMEP case shown in Fig. 4.6 for propane, with the exception that methane allowed the acquisition of one additional set of data for 83 percent PES. At this condition, the two primary fuels (propane and methane) seem to behave very similarly, with methane causing less of an increase in ID at lower PES. As with propane, the variation of SOC increases significantly with increasing PES, especially when engine operation becomes more unstable (COV of IMEP was 5.6 percent) at 83 percent PES. At such high PES, engine instability can be caused due to lower pilot quantities that may have led to inconsistent ignition from one engine cycle to

another. Again, similar to propane, this instability is accompanied by a decrease in average ID.

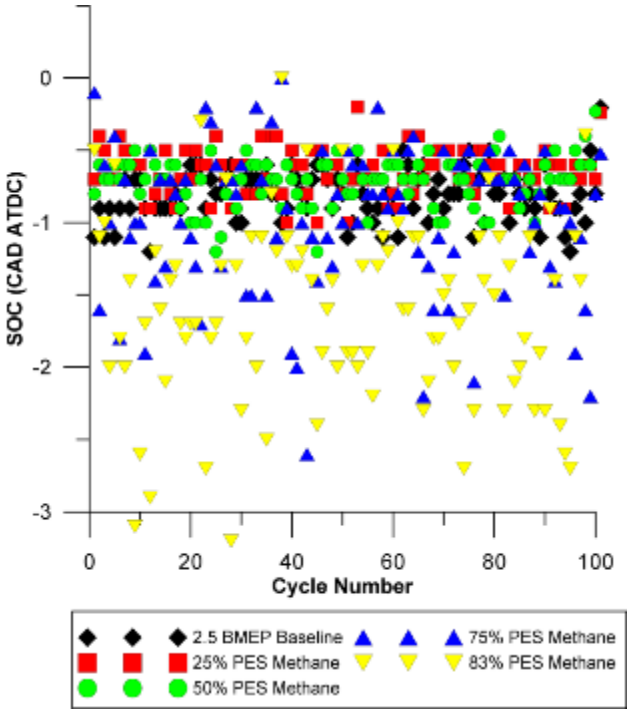

Figure 4.11 Cyclic variations in SOC for 2.5 bar BMEP and various PES of methane with constant boost pressure of 1.2 bar

standard deviations of SOC were 0.17, 0.16, 0.17, 0.51, and 0.63 CAD, respectively for 0, 25, 50, 75, and 83% PES.

4.5 Conclusions

Dual fuel ignition behavior was quantified experimentally for diesel-ignited propane and diesel-ignited methane combustion in a 1.9-liter Volkswagen TDI engine (with the stock ECM and a wastegated turbocharger) at a constant engine speed of 1800 rev/min. Two sets of experiments were performed. First, the effects of fuel-air equivalence ratios based on pilot fuel alone (Φ_{pilot}) and on both pilot and primary fuels ($\Phi_{overall}$) on ignition delay (ID) were investigated. Second, the effects of percent energy

substitution (PES) of the primary gaseous fuel and BMEP on ignition behavior were quantified. The following important conclusions can be drawn from the experimental results presented in this chapter:

1. With constant but large Φ_{pilot} (>0.5), increasing propane concentration (to increase $\Phi_{overall}$) decreased ID. If $\Phi_{overall}$ was sufficiently high (>0.7), spontaneous autoignition (as opposed to end-gas knock) of propane occurred before SOI of diesel pilot. Under similar conditions, increasing methane concentration had little effect on ID.
2. A cycle-by-cycle analysis of diesel-ignited propane combustion showed that for a constant Φ_{pilot}, cyclic variations in SOC increased as $\Phi_{overall}$ was increased. However, SOC variations decreased when in-cylinder conditions facilitated propane autoignition. A similar analysis of diesel-ignited methane combustion revealed very little cyclic SOC variations as $\Phi_{overall}$ was increased.
3. With increasing PES of propane at constant BMEP, different ID trends were obtained at low and high BMEPs. At low BMEPs, ID increased to a maximum and then decreased as engine instability increased. At high BMEPs, increasing PES of propane shortened IDs. By contrast for methane at low BMEPs, increasing PES only increased ID slightly. At higher BMEPs for methane, the increase in ID was more significant with increasing PES.
4. At low BMEPs, increasing PES led to a significant increase in cyclic SOC variations for both propane and methane. As cyclic SOC variations

increased, the average SOC was also advanced, thereby shortening the ID values for both diesel-ignited propane and diesel-ignited methane combustion.

5. The engine ignition delay (EID), the delay between the start of (pilot) injection and the location of 50 percent cumulative heat release, was shown to be a useful metric to understand the influence of ID on dual fuel combustion. For propane at low Φ_{pilot}, the EID increased due to longer IDs and slower combustion rates. As Φ_{pilot} was increased, the higher reactivity of propane led to faster combustion rates and decreased EID significantly even with very small propane additions. For methane, the EID trends were nearly independent of pilot quantity. With increasing methane concentrations, the EID first increased, reached a maximum, and finally decreased. These trends imply that once ignition was achieved with diesel-ignited methane combustion, the ensuing combustion process was largely unaffected by the amount of pilot fuel used, at least for the conditions investigated in this chapter.

CHAPTER V

DUAL FUEL COMBUSTION CHARACTERIZATION

5.1 Introduction

The purpose of this chapter is to characterize the dual fuel combustion mode for diesel-ignited methane and diesel-ignited propane. Two sets of experiments are performed on a light-duty diesel engine and in-cylinder pressure measurements are used to perform a heat release rate analysis. These results are examined in conjunction with performance and engine out emissions data. Combustion phasing and duration are quantified and correlated with NO_x, smoke, CO, and THC emissions trends. Fuel conversion efficiencies are also correlated with combustion phasing and duration.

5.2 Objectives

The objectives of this chapter[1] are as follows:

1. To investigate the effect of pilot quantity, primary fuel concentration, and in-cylinder conditions on dual fuel combustion.
2. To characterize diesel-ignited methane and diesel-ignited propane dual fuel combustion based on in-cylinder pressure and heat release data and to relate dual fuel combustion parameters to performance and emissions results.

[1] The essence of this chapter has been accepted for publication in the Proc. Inst. Mech. Engrs., Part D: Journal of Automobile Engineering [Polk 2013].

5.3 Experimental Procedure

In order to understand the essential combustion characteristics of diesel-ignited methane and diesel-ignited propane combustion, two different sets of experiments were performed. All experiments were performed at a constant engine speed of 1800 rpm. The first set of experiments employed constant pilot quantities and varying concentrations of primary fuel, and therefore the overall equivalence ratio ($\Phi_{overall}$) was allowed to vary, similar to the trends discussed in [Karim 2003]. In these experiments, since the load was also allowed to vary freely, the performance and emissions results quantify the effects of varying the primary fuel equivalence ratio (at constant pilot quantity) on dual fuel combustion behavior. Since load varies while engine speed is held constant, the in-cylinder pressures and temperatures vary widely in a single set of data. To analyze the effects of varying concentrations of primary fuel under similar in-cylinder conditions, the engine load (brake mean effective pressure or BMEP) must be held constant. In the second set of experiments, the BMEP was maintained at a specified value while the pilot and primary fuels were adjusted based on predetermined PES increments within ±1.5 percentage points. Experimental matrices for these two sets of experiments are shown in Tables 5.1 and 5.2 below. The maximum PES stated in Table 5.2 was dependent on the primary fuel type and the BMEP. If the maximum is not specifically listed for a given condition, then the last stated PES is the maximum value possible for that fuel at that condition.

Table 5.1 Experimental Matrix for Overall Equivalence Ratio Effects at Different Pilot Quantities

Constant Pilot Quantity								
Pilot (kg/hr)	$\Phi_{overall}$ 0.2	0.3	0.4	0.5	0.6	0.7	0.8	0.9
1.52	D	M,P	M,P	M				
2.41		D	M,P	M,P	M			
3.49			D	M,P	M,P	M,P		
4.80				D	M,P	M,P	M,P	M
6.30					D	M,P	M,P	

D: diesel-only operation, M: methane dual fueling, P: propane dual fueling

Table 5.2 Experimental Matrix for PES Effects at Different BMEPs

Constant BMEP				
BMEP (bar)	Percent Energy Substitution 25%	50%	75%	Max
2.5	M,P	M,P	M,P	M,P
5.0	M,P	M		P=47%
7.5	M,P	M,P		
10	M,P	M		P=45%

M: methane dual fueling, P: propane dual fueling

Each set of experiments was performed in the same session to reduce variations in baseline operation and obtain reliable performance and emissions data. In addition, the intake boost pressure was held constant for a given pilot quantity or for a given BMEP. The intake pressure chosen for each condition was based on the nominal boost pressure possible (corresponding to the available exhaust energy) at the baseline diesel operating condition (no gaseous fuel). Engine coolant temperatures and intake charge temperatures were maintained at 85±5°C and 35±5°C, respectively for all experiments.

5.4 Results and Discussion

In this section, the combustion, performance, and emissions results for diesel-ignited methane and diesel-ignited propane dual fuel combustion are presented. While interpreting these results, it must be noted that the operating conditions were limited by several factors. At low BMEPs, engine misfire limited the maximum possible primary fuel substitution. At high BMEPs, higher primary fuel concentrations were limited by a self-imposed pressure rise rate limitation of 15 bar/deg. At these conditions, the engine was rapidly approaching knocking conditions, causing considerable audible noise. The maximum possible primary fuel concentrations also varied between the two primary fuels (methane and propane) as well as with pilot quantity.

5.4.1 Constant Pilot Experiments

In this set of experiments, the pilot quantity was held constant while the primary fuel concentration was increased, allowing the overall equivalence ratio and the BMEP to vary. The overall equivalence ratios ($\Phi_{overall}$) ranged from 0.2 to 0.9. For each sweep of primary fuel concentration, a different (but constant) pilot quantity was used. The pilot quantities investigated in these experiments included 1.52 kg/hr, 2.41 kg/hr, 3.49 kg/hr, 4.80 kg/hr, and 6.30 kg/hr, and they correspond to diesel-only equivalence ratios of 0.2, 0.3, 0.4, 0.5, and 0.6, respectively.

5.4.1.1 Heat Release Rate Behavior

Heat release profiles for a combustion process reveal important details about how combustion is progressing, how it is phased, and the duration of combustion. Figure 5.1 shows, for example, the heat release profiles for both diesel-ignited propane and diesel-

ignited methane combustion at the smallest pilot quantity ($\dot{m}$ = 1.52 kg/hr). In addition to the heat release profiles, the measured needle lift profiles for all plots are also shown as insets in Fig. 5.1 to demonstrate the consistency in diesel injection (in both phasing and duration). For the diesel-only condition, the initial peak is primarily associated with premixed combustion and the second peak is predominantly due to mixing-controlled combustion [Dec 1997, Heywood 1988]. As the concentrations of both propane and methane are increased, the initial peak of the AHRR curve is increased, indicating that the amount of gaseous fuel (and its participation in the initial combustion phase) entrained in the pilot spray and immediately surrounding it is increased. The two gaseous fuels behave similarly during this part of combustion. As combustion progresses to the mixing-controlled stage, however, the trends begin to differ between diesel-ignited propane and diesel-ignited methane combustion. As the concentration becomes high enough (e.g., $\Phi_{overall}$ = 0.4), the second stage of heat release, likely associated with flame propagation, increases in magnitude more sharply for propane dual fueling than for methane dual fueling. In this regard, Egolfopoulos *et al.* [2007] show that the lean flammability limit of the gaseous fuel-air mixture under conditions similar to those seen at SOI (unburned mixture temperature and pressure of ~700K and ~50 bar, respectively) are approximately $\Phi_{gaseous}$ = 0.18 for methane and $\Phi_{gaseous}$ = 0.16 for propane, affirming the possibility of flame propagation under all of these conditions. The dissimilar AHRR trends may be the result of different laminar burning velocities (LBV) of the propane-air and methane-air mixtures, which will affect the turbulent burning rates in different ways. The LBV of a mixture is dependent on a number of variables, including adiabatic flame temperature (AFT), molecular structure, and equivalence ratio, among others [Law 2010,

Stone 1999]. In this case, the equivalence ratios are very similar, however the AFT of propane is known to be higher than that of methane and the LBV has been shown to scale with AFT [Heywood 1988, Law 2010]. In addition, Law [2010] shows LBV is also affected by molecular structure, increasing with chemical reactivity even when AFT is kept constant. In summary, propane has a higher LBV, and consequently, the turbulent flame propagation rates are likely higher with diesel-ignited propane combustion compared to diesel-ignited methane combustion. Shown in Fig. 5.2, this expected behavior is confirmed by a shorter combustion duration (defined here as CA10-90) observed for diesel-ignited propane combustion relative to diesel-methane combustion at high gaseous fuel concentrations. These observations help explain the second peak trends in AHRR and are also consistent with the fact that propane is a more reactive fuel than methane.

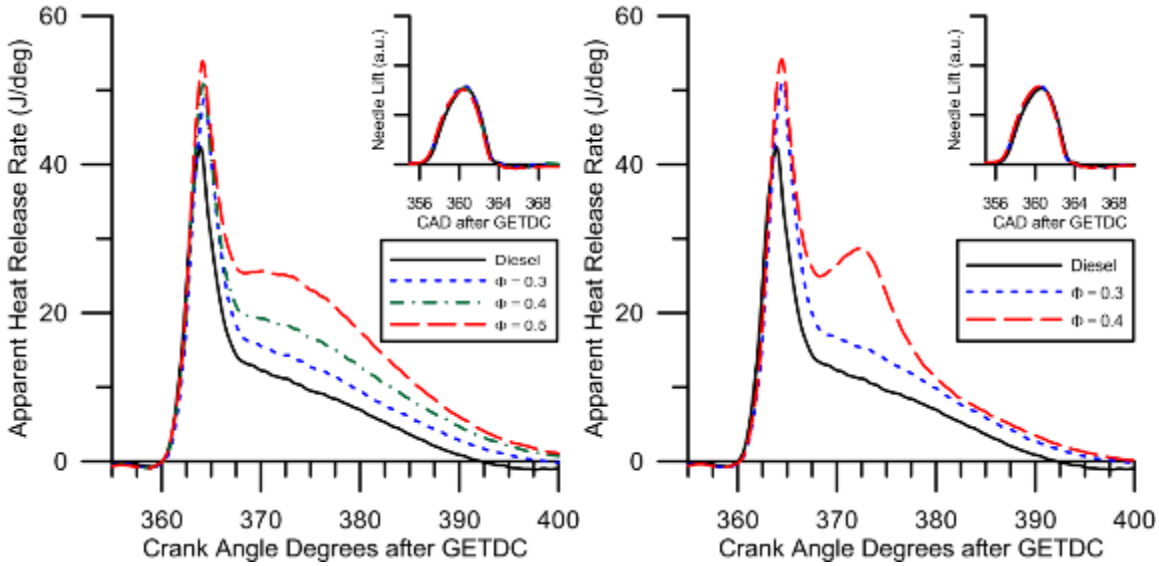

Figure 5.1 Heat release and needle lift profiles for (a) diesel-ignited methane and (b) diesel-ignited propane combustion at a fixed pilot quantity of 1.52 kg/hr

the diesel-only condition represents an equivalence ratio of 0.2.

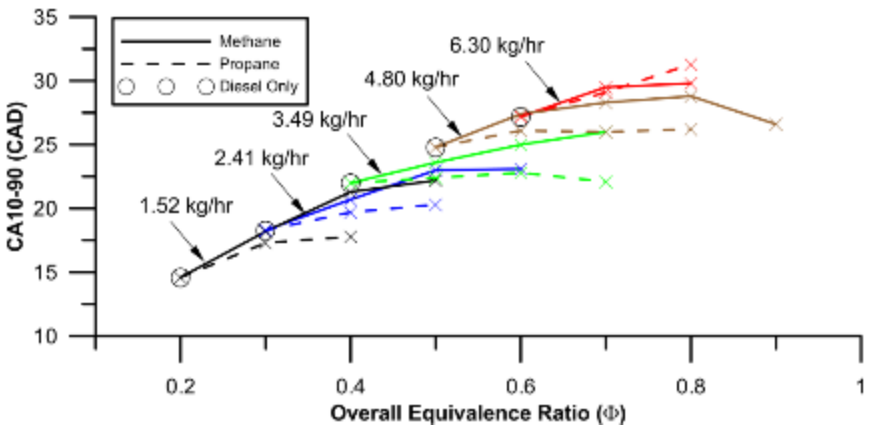

Figure 5.2 CA10-90 for diesel-ignited methane (solid) and diesel-ignited propane (dashed) combustion versus overall equivalence ratio at various fixed pilot quantities.

Increasing the pilot quantity yields significantly different results, as shown in Fig. 5.3 ($\dot{m}$ = 4.80 kg/hr). At this condition, the effects of the gaseous fuel-air mixture on AHRR are far more significant than at the low pilot condition for both fuels. However, these effects differ greatly between diesel-ignited propane and diesel-ignited methane combustion. In diesel-ignited propane combustion, the second stage of heat release quickly dominates combustion as propane concentration is increased. Since BMEP is not held constant in these experiments, as propane concentration is increased, in-cylinder pressures and average in-cylinder temperatures also increase. Cylinder wall and residual gas temperatures rise accordingly, and in turn affect the preignition chemistry of the propane-air mixture, contributing to shorter ignition delay periods. Table 5.3 shows the ignition delay values for baseline diesel, diesel-ignited methane combustion, and diesel-ignited propane combustion at the tested constant-pilot quantities. Polk *et al.* [2011] discuss these ignition delay trends for propane and methane dual fuel combustion in greater detail. Figure 5.4 shows the differences in the early stages of heat release for

increasing propane concentration and increasing methane concentration while employing a large constant-pilot quantity. At relatively higher equivalence ratios, the fact that propane autoignites even before diesel injection (and ignition) begins is clearly evident from the positive AHRR values that precede the injector needle opening for $\Phi_{overall} = 0.8$ as shown in Fig 5.4(b). At the highest propane concentration ($\Phi_{overall} = 0.8$), combustion of the propane-air mixture occurs nearly simultaneously with combustion of the diesel jet, causing an extremely high peak in heat release rate (see Fig. 5.3(b)). In diesel-ignited methane combustion, with the exception of the highest concentration ($\Phi_{overall} = 0.9$), the AHRR profile remains similar to that of straight diesel combustion except with an increasing amount of heat release occurring due to flame propagation. This delays the CA50 since an increasing percentage of heat release occurs later in the combustion process. At the highest methane concentration (and coincidentally the highest overall equivalence ratio of all conditions tested), the heat release profile is changed greatly. At this condition, it is possible that the methane-air mixture is approaching conditions conducive for end-gas knock, leading to the rapid increase in apparent heat release rate as well as the advancement in CA50.

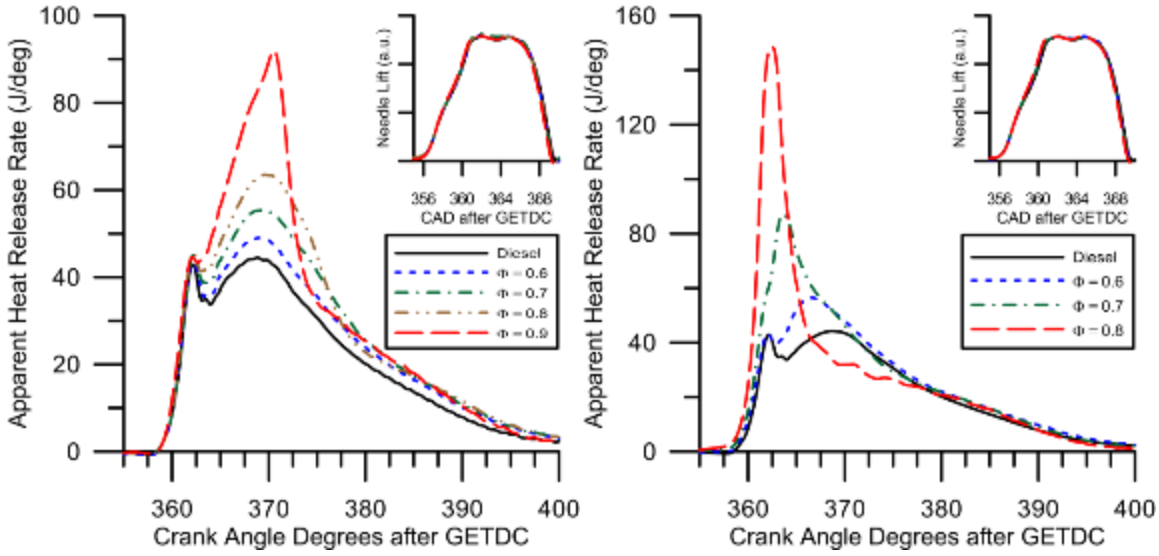

Figure 5.3 Heat release and needle lift profiles for (a) diesel-ignited methane and (b) diesel-ignited propane combustion at a fixed pilot quantity of 4.80 kg/hr

the diesel-only condition represents an equivalence ratio of 0.5.

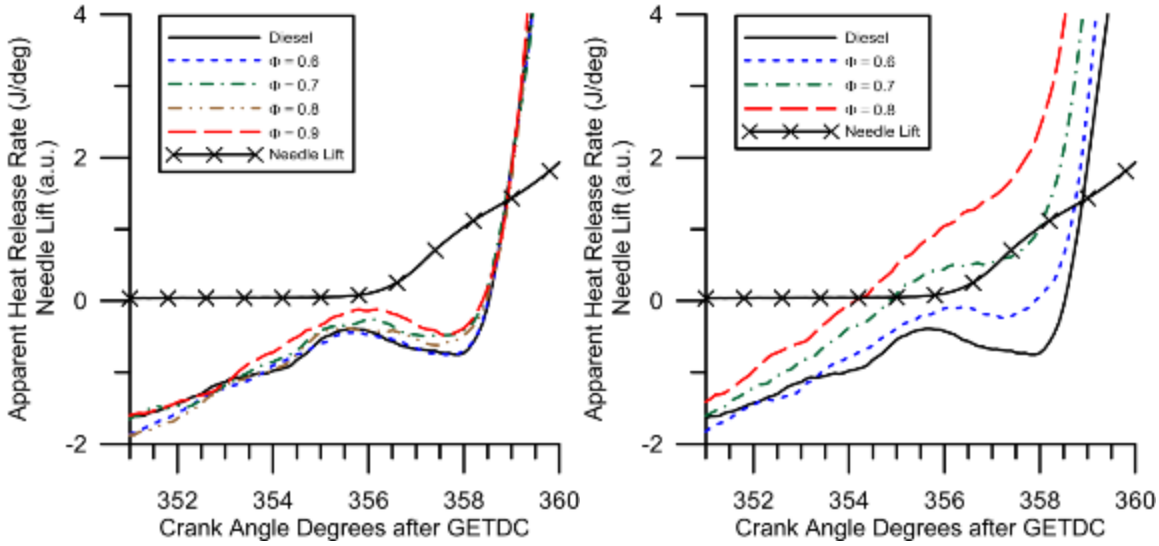

Figure 5.4 A close-up view of heat release and needle lift profiles for (a) diesel-ignited methane and (b) diesel-ignited propane combustion at a fixed pilot quantity of 4.80 kg/hr

the diesel-only condition represents an equivalence ratio of 0.5.

The CA50 trends for both diesel-ignited methane and diesel-ignited propane combustion are shown in Figure 5.5. Initially, CA50 tends to retard as overall equivalence ratio is increased. In diesel-only combustion (shown as open circles), this trend is practically linear. For more diesel fuel to be added, the injection event must have a longer duration, causing fuel to enter the combustion chamber even after the start of combustion, thus delaying the overall combustion phasing (CA50). With dual fuel combustion, however, the CA50 trend indicates a maximum phasing retard for a given pilot quantity and then begins to advance as overall equivalence ratio is further increased. Since all of the air-fuel mixture is present at the start of combustion, there is no additional delay as a result of late injection. However, CA50 does retard at low overall equivalence ratios as gaseous fuel concentration is increased. This may be explained from the fact that more of the combustion energy release arises from flame propagation as evident from the higher second peaks in AHRR as gaseous fuel concentration is increased at low overall equivalence ratios. The subsequent advancement of CA50 with increasing gaseous fuel concentration is due to a shift from a "conventional two-peak" AHRR profile to a "single early peak" AHRR profile, and therefore, a departure from the classical interpretation of dual fuel combustion [Karim 2003]. This effect is much more pronounced with diesel-ignited propane combustion relative to diesel-ignited methane combustion, likely due to differences in preignition chemistry and LBV as discussed previously.

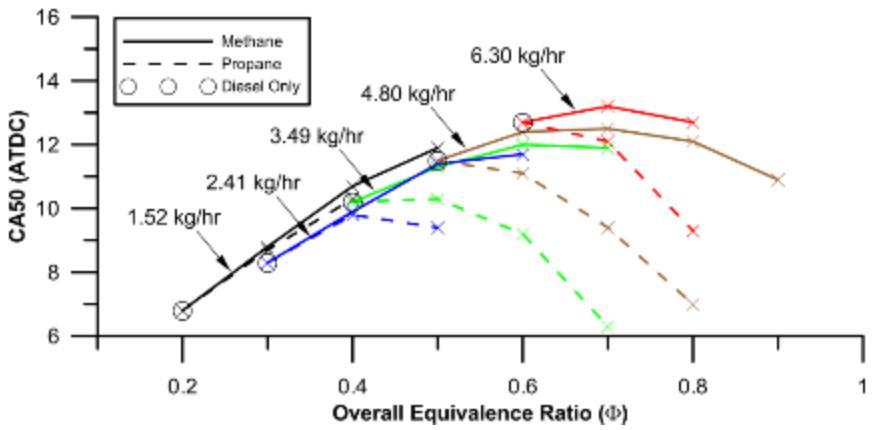

Figure 5.5 CA50 for diesel-ignited methane (solid) and diesel-ignited propane (dashed) combustion versus overall equivalence ratio at various fixed pilot quantities.

5.4.1.2 Emissions and Performance

The NO_x and smoke emissions for all tested constant pilot conditions are shown in Fig. 5.6. For almost all conditions, it is observed that as gaseous fuel concentration is increased, brake-specific NO_x ($BSNO_x$) emissions decreased or remained constant. This trend is primarily driven by the increasing power of the engine at high BMEP conditions. Oxides of nitrogen have been shown to scale with pilot quantity for dual fuel combustion [Karim 1987, Abd Alla 2000]. Therefore, it would be expected that for a given overall equivalence ratio, $BSNO_x$ would decrease with decreasing pilot quantity. However, though the volumetric NO_x concentration in parts per million (ppm) does decrease for smaller pilot quantities at similar overall equivalence ratios, for each given overall equivalence ratio $BSNO_x$ appears to be relatively insensitive to pilot quantity. Compared to methane, propane tends to have slightly higher $BSNO_x$, especially at higher gaseous fuel concentrations and larger pilot quantities. This can be attributed to a more advanced combustion phasing, indicated by CA50 shown in Fig. 5.4. Smoke increases with

increasing primary fuel concentration at constant pilot quantity. This behavior can be explained by invoking Dec's conceptual model of diesel combustion [Dec 1997], which states that soot is primarily formed in the head vortex region and the rich premixed regions of diesel sprays. A possible explanation is that as the primary fuel concentration is increased for a given constant pilot quantity, more fuel is entrained in and around the pilot spray, increasing the size of the head vortex region and enriching the fuel-air mixture therein, and therefore increasing smoke emissions. However, if the pilot spray is very small, as with the smallest pilot quantity shown in Fig. 5.6(b), then the diesel pilot only acts to intiate flame propagation of the lean fuel-air mixture, preventing an increase of smoke emissions. An apparent inconsistency in the smoke trends can be seen at the 6.30 kg/hr pilot quantity. Instead of following the increasing trend with pilot quantity, the smoke for this condition is less than that of the 4.80 kg/hr pilot quantity. This can be explained by the linear trend of the baseline diesel condition and the rapid increase in smoke emissions with overall equivalence ratio. As evident in Fig. 5.6(b), the maximum possible equivalence ratio with the 6.30 kg/hr pilot quantity was lower than the corresponding maximum for the 4.80 kg/hr pilot quantity. Given a high enough overall equivalence ratio, the 6.30 kg/hr condition would likely surpass the 4.80 kg/hr condition in smoke emissions.

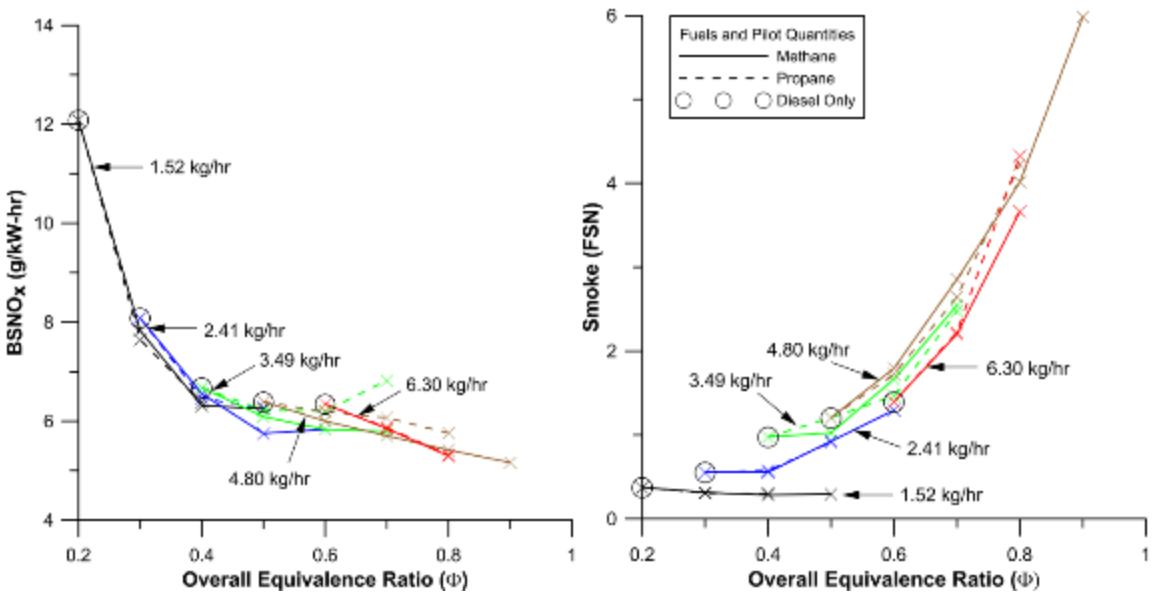

Figure 5.6 (a) Brake specific NO_x and (b) smoke emissions for diesel-ignited methane (solid) and diesel-ignited propane (dashed) combustion versus overall equivalence ratio at various fixed pilot quantities.

In addition to NO_x and smoke emissions, CO and THC emissions are also of concern when examining dual fuel combustion. High CO emissions are typically associated with incomplete bulk oxidation of fuel (since CO is an intermediate major species of combustion) and increased THC may be attributed to incomplete flame propagation, i.e., the flame initiated by the ignited pilot spray cannot spread far enough or fast enough to burn all of the gaseous fuel-air mixture despite the presence of excess oxygen [Karim 1991]. Also, increased THC may be attributed to the fuel-air mixture trapped in crevices around the combustion chamber that may be left unburned at the end of the combustion process. When the equivalence ratio associated with the gaseous fuel is below a certain flame spread limit (FSL), CO and THC emissions are increased and these effects are accompanied by an increase in specific energy consumption. Badr *et al.*

[1999] showed that the FSL decreases as the pilot quantity increases; therefore, for a given concentration of primary fuel, CO and THC emissions should decrease as pilot quantity increases. This behavior is observed in Fig. 5.7, with the exception of CO emissions for diesel-ignited methane combustion at very high overall equivalence ratios. The increase in CO for diesel-ignited methane combustion at 4.80 and 6.30 kg/hr pilot quantities may be attributed to the majority of combustion happening later in the combustion process, where the global temperatures are lower and may be insufficient for CO to fully oxidize before the expansion process is complete.

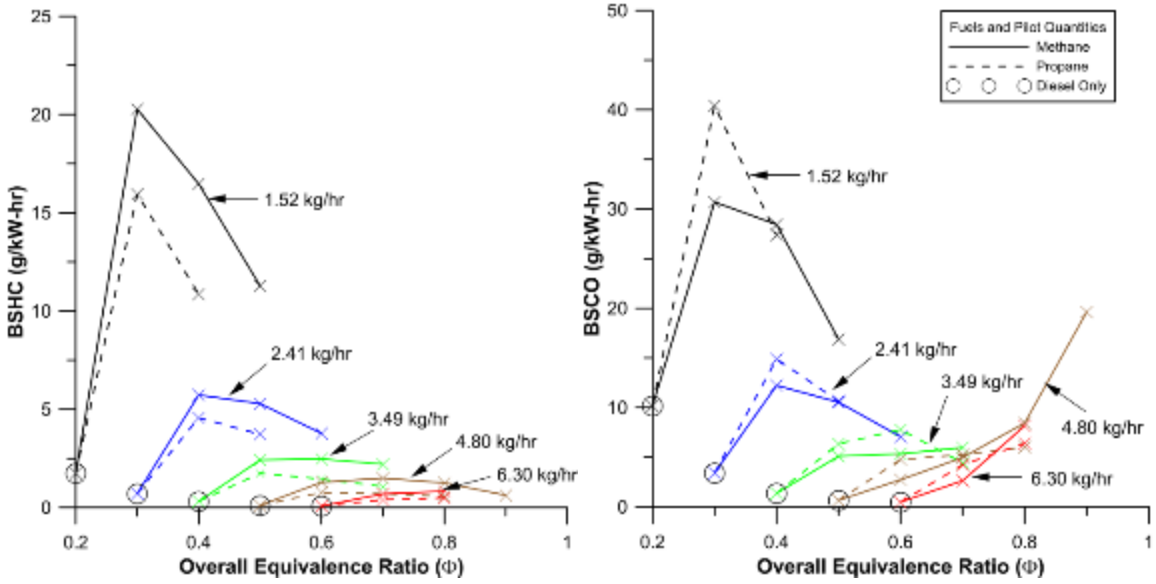

Figure 5.7 (a) Brake-specific HC emissions and (b) brake-specific CO emissions for diesel-ignited methane (solid) and diesel-ignited propane (dashed) combustion versus overall equivalence ratio at various fixed pilot quantities.

Comparing the CO and THC emissions of diesel-ignited methane and diesel-ignited propane combustion, it can be seen for all pilot quantities that, in general,

methane produces more THC emissions and propane produces more CO emissions. This trend is explained in depth by Shoemaker *et al.* [2012], where it is shown that a competition exists between CO and THC in terms of which species gets oxidized preferentially. With diesel-ignited methane combustion, CO oxidation is preferred due to slower burn rates, leaving excess THC emissions, while with diesel-ignited propane combustion, HC consumption is preferred due to faster flame propagation, leaving more CO emissions. In other words, under similar conditions, more propane will undergo partial oxidation than methane. In addition, the advanced combustion phasing of diesel-ignited propane combustion allows for higher temperatures during the combustion process, leaving more opportunity for partial oxidation to occur.

Figure 5.8 shows that the fuel conversion efficiency (FCE) increases as the pilot quantity and the overall equivalence ratio are increased. As pilot quantity is increased, boost pressure is also increased (as dictated by the diesel baseline operating conditions), allowing an increased overall fueling rate for a given equivalence ratio. Similarly, an increase in overall equivalence ratio corresponds to an increase in the overall fueling rate, leading to an increase in CA10-90. A higher CA10-90 at a sufficiently advanced CA50 leads to more energy tranfer to the pistons for a given amount of fuel, increasing the FCE. When comparing diesel-ignited methane and diesel-ignited propane combustion, it is clear that at all concentrations the latter yields higher FCEs than the former. This can likely be attributed to the advanced phasing of CA50 due to the higher LBV and turbulent burn rates associated with propane.

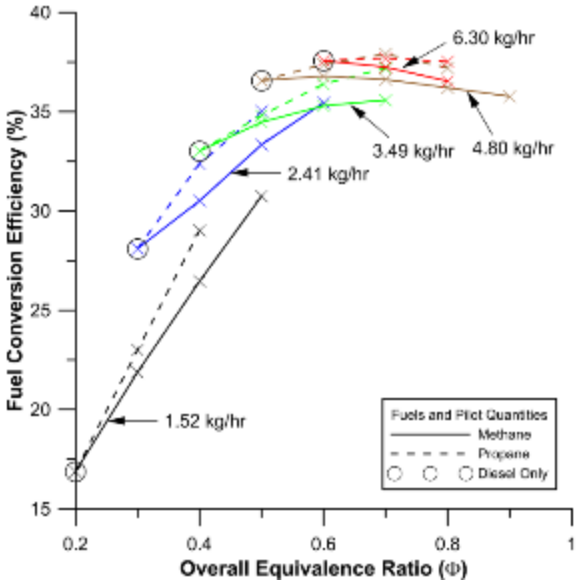

Figure 5.8 Fuel conversion efficiency (FCE) for diesel-ignited methane (solid) and diesel-ignited propane (dashed) combustion versus overall equivalence ratio at various fixed pilot quantities.

5.4.2 Constant BMEP Experiments

In this set of experiments, the load (BMEP) was held constant as the pilot quantity and primary fuel concentration were varied to observe the effects of varying primary fuel concentration under similar in-cylinder conditions (wall temperature, residual gas temperature and concentrations, etc.). The engine load was held to four constant BMEP values of 2.5, 5, 7.5, and 10 bar. The overall percent energy substitution (PES) of the gaseous fuels ranged from 0-83 percent, but was generally limited to approximately 50 percent due to misfire at low loads and knock (autoignition) at high loads. Intake boost pressures, which varied across BMEPs (but remained constant for a given BMEP), were determined based on diesel-only conditions.

It must also be noted that the mass flow of gaseous fuel required to achieve a certain level of PES changes for different BMEPs. For example, very little gaseous fuel is required to alter the PES a great amount at low BMEPs and a significant quantity is required at high BMEPs to reach the same level of PES. Therefore, the fueling rates corresponding to a given PES are not the same at different BMEPs.

5.4.2.1 Heat Release Rate Behavior

The apparent heat release rate profiles for both diesel-ignited propane and diesel-ignited methane combustion for 2.5 bar BMEP are shown in Fig. 5.9. In addition, the needle lift profiles are also shown in the inset plots to indicate the consistency achieved in pilot injection timing and the variations observed in pilot injection duration as PES is varied. It is clear from the AHRR profiles of diesel-ignited methane combustion at 2.5 bar BMEP that the character of combustion changes significantly from straight diesel combustion to high-PES dual fuel combustion. The initial heat release rate peak is decreased as the pilot quantity is decreased and the magnitude of energy release in the second heat release phase is gradually increased. This results in the retardation of CA50 and increases CA10-90, as shown in Figs. 5.10 and 5.11, respectively.

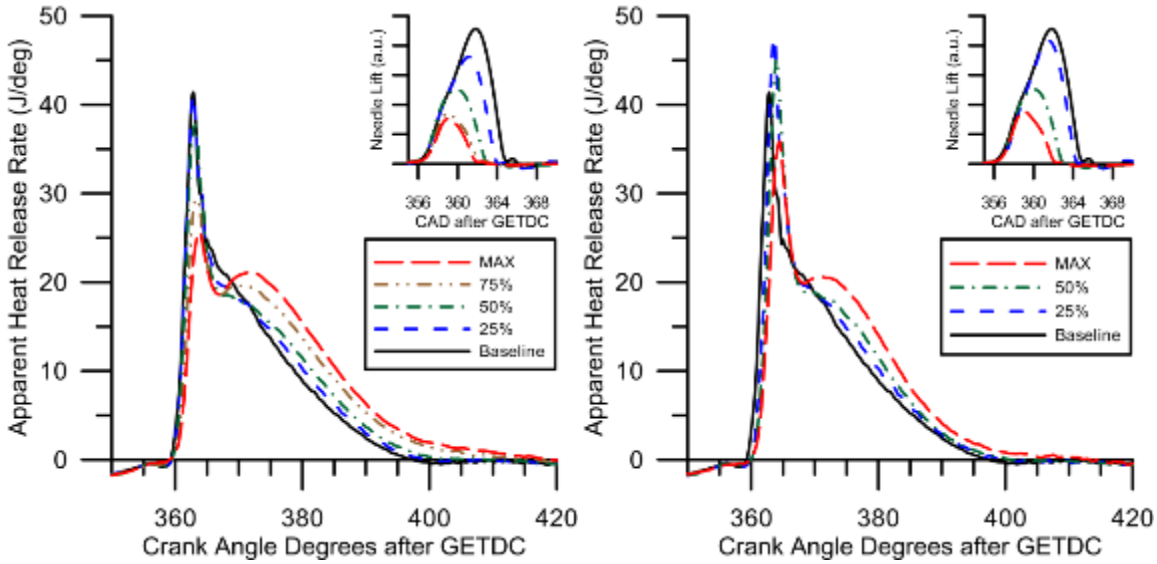

Figure 5.9 Heat release and needle lift profiles for (a) diesel-ignited methane and (b) diesel-ignited propane combustion at a fixed BMEP of 2.5 bar

PES ranges from 0-83%

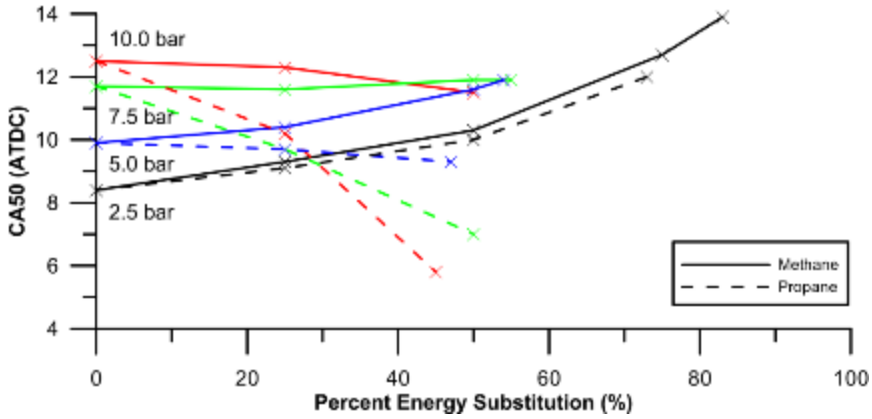

Figure 5.10 CA50 for diesel-ignited methane (solid) and diesel-ignited propane (dashed) combustion versus PES at various fixed BMEPs.

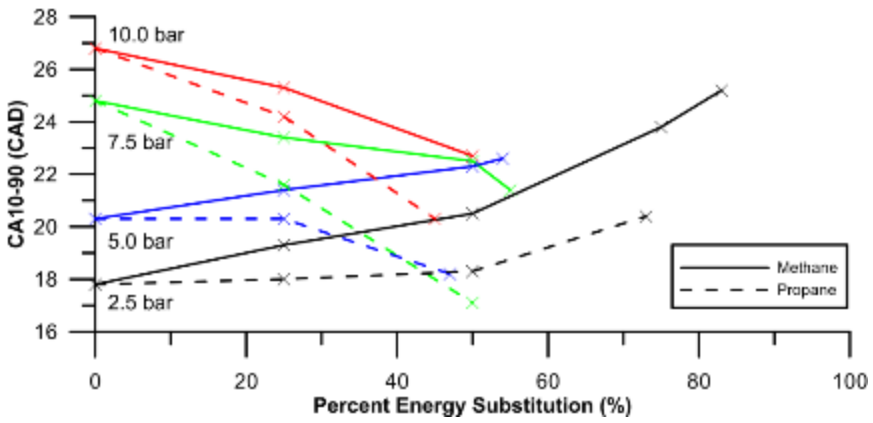

Figure 5.11 CA10-90 for diesel-ignited methane (solid) and diesel-ignited propane (dashed) combustion versus PES at various fixed BMEPs.

The effects of increased PES on both diesel-ignited methane and diesel-ignited propane combustion are clearly evident, though somewhat different. When the pilot quantity is decreased with increasing PES, the initial heat release peak actually increases slightly before decreasing for diesel-ignited propane combustion. As propane concentration is increased, changes in the effective specific heat of the in-cylinder mixture and the displacement of oxygen (due to the presence of propane in the intake) increase the ignition delay period, as shown in Fig. 5.12. These effects are more pronounced with propane at this condition than they are with methane. This allows for the formation of a larger diesel jet and a larger quantity of propane-air mixture to be entrained within the diesel jet before ignition, resulting in a higher initial heat release rate peak for diesel-ignited propane combustion compared to straight diesel fueling up to a PES of 50 percent. A further increase in PES leads to a decrease in the initial heat release rate peak and a shift to higher heat release in the second heat release phase associated with flame propagation.

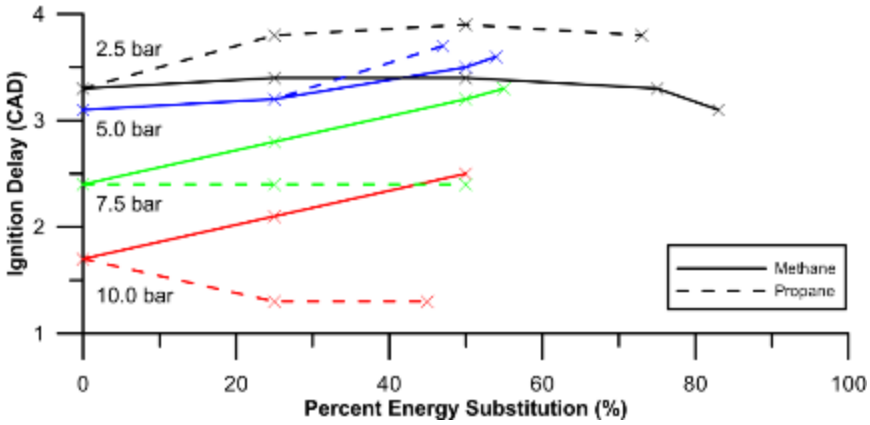

Figure 5.12 Ignition Delay for diesel-ignited methane (solid) and diesel-ignited propane (dashed) combustion versus PES at various fixed BMEPs.

At a BMEP of 10 bar, the change in combustion characteristics with increasing PES is much more pronounced for diesel-ignited propane than for diesel-ignited methane combustion. As shown in Fig. 5.13, the large pilot quantities used for this condition dominate the AHRR profile for diesel-ignited methane combustion. At this condition, the high fueling rates of methane necessary to increase the PES cause an increase in ignition delay (likely due to oxygen displacement and chemical effects) [Liu and Karim 1995]. This behavior is similar to that of diesel-ignited propane combustion at low BMEPs. The initial peak is therefore increased as an increasing concentration of methane is entrained in the pilot spray over an extended ignition delay period but the ensuing combustion process is very similar for 0, 25, and 50 percent PES, indicating that the phasing of diesel and diesel-ignited methane combustion are very similar at this BMEP. However, for diesel-ignited propane combustion, as the PES is varied from 0 to 50 percent the AHRR curve transforms from a typical two-peak profile to a single peak profile. At this BMEP, the ignition of the propane-air mixture occurs very rapidly, with an ignition delay of 1.3

CAD, the lowest of all cases examined in this set of experiments. The preignition chemistry is dictated by the accumulation of radicals [Law 2010], which appears to occur more rapidly with diesel-ignited propane combustion than with diesel-ignited methane combustion. High in-cylinder pressures and temperatures initiate radical accumulation in the propane-air mixture and, combined with the increased reactivity of propane, shorten the ignition delay period. This behavior is a reversal of the ignition delay behavior of propane at low BMEP, indicating there are competing effects determining the duration of ignition delay. Upon diesel injection, the combustion of the propane-air mixture is very rapid, occurring nearly simultaneously with the combustion of the diesel pilot, quantified by the advanced CA50 and shorter CA10-90 shown in Figs. 5.10 and 5.11, respectively. The rapidity of the combustion can be attributed to propane's relatively high LBV, which enhances the turbulent combustion rates. As a direct consequence of the rapidity of propane combustion, the peak heat release rate is increased substantially for the maximum propane PES compared to 25 percent PES. This behavior indicates that volumetric autoignition of propane may likely outweigh any localized flame propagation under these conditions, implying a divergence from the typical three-phase interpretation of dual fuel combustion, as indicated in the constant pilot quantity experiments.

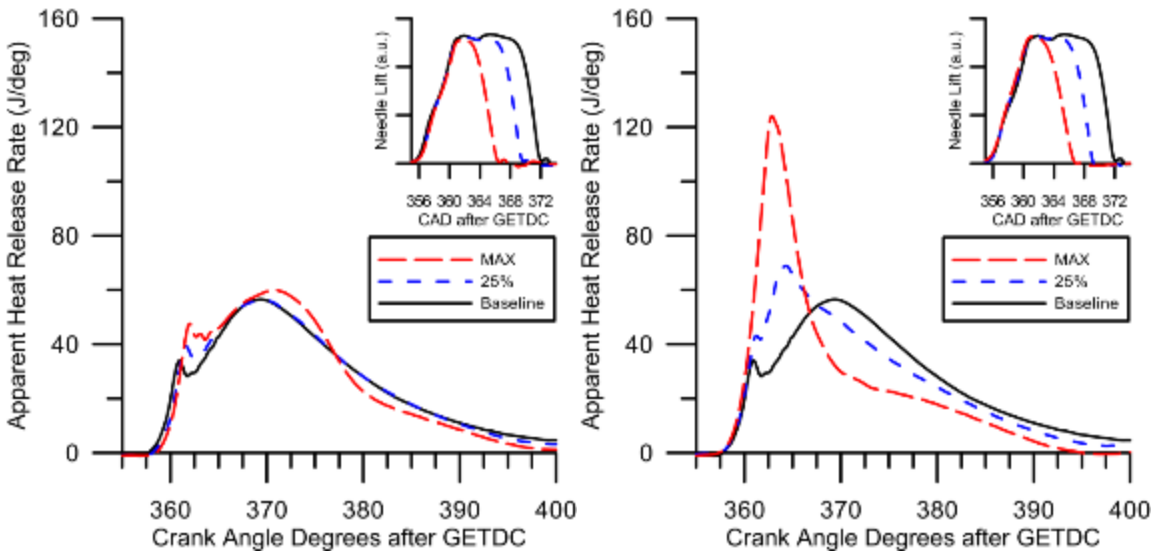

Figure 5.13 Heat release and needle lift profiles for (a) diesel-ignited methane and (b) diesel-ignited propane combustion at a fixed BMEP of 10 bar

PES ranges from 0-50%

5.4.2.2 Emissions and Performance

The emissions trends for $BSNO_x$ and smoke versus PES are shown in Fig. 5.14. At low BMEPs, $BSNO_x$ decreases simultaneously with smoke emissions as PES is increased. This is consistent with the concept that NO_x scales directly with pilot quantity in dual fuel engines because larger pilot sprays lead to larger regions with high local temperatures that foster NO_x formation. However, at higher BMEPs, this trend is reversed for many instances of diesel-ignited propane combustion. Brake-specific NO_x emissions are increased significantly by the advanced CA50 phasing and rapid combustion of the propane-air mixture in these cases. These conditions are associated with very high local in-cylinder temperatures and pressures, which facilitate NO_x formation. In addition, the maximum PES possible at high BMEPs was lower; therefore, the contribution to NO_x formation from the relatively larger diffusion flame area around

the pilot spray was likely higher. For both fuels at all BMEP conditions, smoke emissions decrease with increasing PES. As PES is increased, the pilot size is reduced and a greater fraction of the AHRR arises from the lean premixed gaseous fuel-air mixture instead of the pilot spray. As a result, there are fewer fuel-rich areas for particulate matter to be created, and therefore smoke emissions are reduced. In comparing the two fuels, diesel-ignited propane combustion tends to produce less smoke than diesel-ignited methane combustion. This is most noticeable at the highest BMEPs, where the combustion behaviors of the two fuels are significantly different. The present author hypothesizes that, at these conditions, diesel-ignited propane combustion produces less smoke than diesel-ignited methane combustion because the higher pressures and global temperatures caused by rapid combustion of the lean propane-air mixture allow any soot produced in the diesel head vortex region to be oxidized to a greater extent.

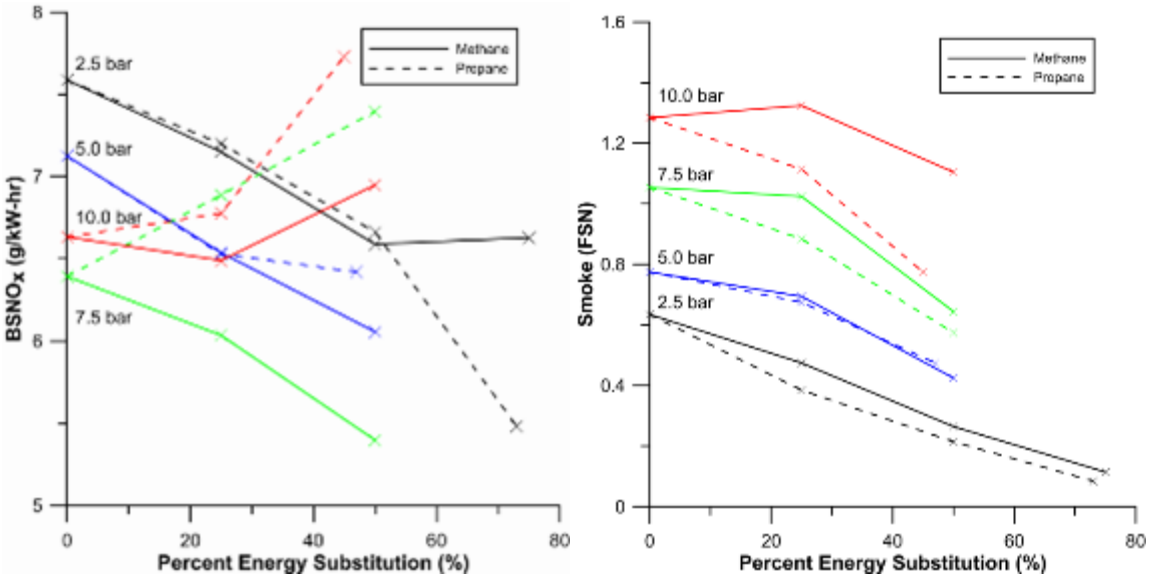

Figure 5.14 (a) Brake-specific NO_x and (b) smoke emissions for diesel-ignited methane (solid) and diesel-ignited propane (dashed) combustion versus PES at various fixed BMEPs

Figure 5.15 shows the CO and THC emissions trends versus PES at constant BMEP for diesel-ignited methane and diesel-ignited propane combustion. At low BMEPs, CO and THC emissions increase steeply with increasing PES, as is typical of dual fuel combustion. This is attributed to low bulk gas temperatures and incomplete oxidation (partially burned fuel, resulting in intermediate stable species such as CO), as well as incomplete flame propagation (unburned fuel). As BMEP is increased, the in-cylinder temperatures are increased and CO and THC emissions are dramatically reduced. As seen in the constant pilot quantity experiments, when comparing the emissions of the two fuels, diesel-ignited methane combustion yields a higher concentration of THC and diesel-ignited propane combustion yields a higher concentration of CO. During combustion, these emissions species must compete for oxidation, as discussed in [Shoemaker 2012], and the differences in primary fuel chemistry regulate the outcome. Propane, being a more reactive fuel, begins to undergo partial oxidation more quickly than methane. Therefore, under similar conditions diesel-ignited propane combustion will yield lower unburned THC emissions and more CO emissions compared to diesel-ignited methane combustion. This is consistent with the AHRR curves which show that the initial heat release is much larger with diesel-ignited propane combustion, allowing more fuel to be wholly or partially burnt quickly after the start of combustion, while in-cylinder pressures and temperatures are still relatively high. Moreover, at high BMEPs and high PES, diesel-ignited propane combustion (with early, single-peak AHRR profiles) proves to be an exception to classical dual fuel combustion (with two-peak AHRR profiles), yielding both lower THC and CO emissions than diesel-ignited methane combustion, likely as a result of its early, rapid heat release.

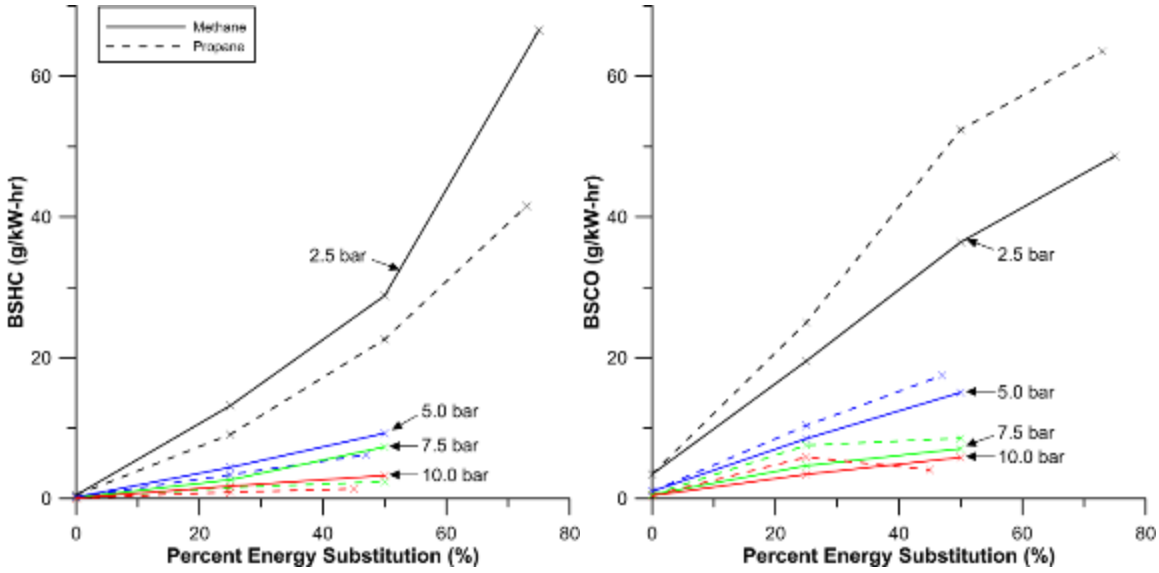

Figure 5.15 (a) Brake-specific HC and (b) brake-specific CO emissions for diesel-ignited methane (solid) and diesel-ignited propane (dashed) combustion versus PES at various fixed BMEPs

Fuel conversion efficiency (FCE) trends for increasing PES at constant BMEPs (but different values) are shown in Fig. 5.16. At BMEP = 2.5 bar (baseline diesel FCE of 27.1 percent), the FCE decreases as PES is increased. At these conditions, the combustion is phased later in the expansion stroke and occurs at a slower rate, as indicated by the retarded CA50 and increased CA10-90. In addition, low bulk gas temperatures at these conditions lead to increased CO and THC emissions, which are in turn expelled in the exhaust as unconverted fuel, reducing FCE to 16.4 percent at 83 percent PES of methane and 20.8 percent FCE at 73 percent PES of propane. At BMEP = 10 bar (baseline diesel FCE of 38 percent), CA50 is relatively invariant with increasing PES for diesel-ignited methane combustion and advanced for diesel-ignited propane combustion and CA10-90 decreased with increasing PES in both cases. This leads to higher in-cylinder pressures earlier in the expansion stroke. In addition, higher bulk gas

temperatures reduce CO and THC emissions. For diesel-ignited methane combustion at high BMEPs, FCE decreases slightly to 37.1 percent as PES is increased to 51 percent. For diesel-ignited propane combustion at high BMEPs, FCE is shown to increase to 39 percent as PES is increased to 46 percent. Compared to diesel-ignited methane combustion, diesel-ignited propane combustion is observed to have better FCEs over the range of conditions examined in this chapter. This may be attributed to propane's increased reactivity, advanced combustion phasing (CA50), and faster combustion rates relative to methane.

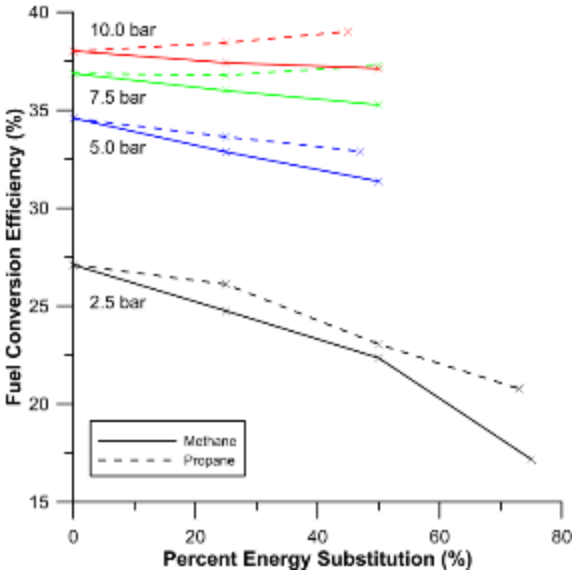

Figure 5.16 Fuel conversion efficiency (FCE) for diesel-ignited methane (solid) and diesel-ignited propane (dashed) combustion versus PES at various fixed BMEPs

5.5 Conclusions

Dual fuel combustion was characterized experimentally with two sets of experiments each for diesel-ignited propane and diesel-ignited methane operation in a

1.9-liter Volkswagen TDI engine (with the stock ECM and a wastegated turbocharger) at a constant speed of 1800 rpm. The first set of experiments utilized several fixed diesel pilot quantities and varied propane and methane concentrations (and consequently overall fuel-air equivalence ratios and BMEPs). The second set of experiments was performed with fixed BMEPs and varying percent energy substitution (PES) of the gaseous fuels. Analysis of the results obtained led to the following important conclusions:

1. With a small fixed pilot quantity ($\dot{m}_d$ = 1.52 kg/hr) and varying overall equivalence ratios, diesel-ignited propane and diesel-ignited methane combustion behave similarly, although the former exhibits slightly faster combustion, likely due to propane's higher laminar burning velocity (LBV). With a larger fixed pilot quantity ($\dot{m}_d$ = 4.80 kg/hr), propane or methane addition causes significant (but different) changes to the combustion process. As propane concentration is increased, CA50 is significantly advanced and the peak AHRR increased, again likely due to propane's relatively high reactivity (rapid radical accumulation) and higher LBV compared to methane. As methane concentration is increased, the AHRR increased primarily during the latter part of combustion (flame propagation), resulting in a retarded or constant CA50. At the highest methane concentration ($\Phi_{overall}$ = 0.9), CA50 is advanced and the peak AHRR is greatly increased, possibly indicating that dual fuel combustion is approaching conditions conducive for knock.
2. For almost all fixed pilot conditions, as gaseous fuel concentration is increased, brake-specific NO_x emissions decrease or remain constant,

while smoke emissions increase. The CO and THC emissions increase with increasing primary fuel concentration at low loads, and decrease as pilot quantity increased. Overall, diesel-ignited propane combustion yields higher CO emissions, lower THC emissions, and slightly higher fuel conversion efficiencies (FCE) than diesel-ignited methane combustion. This is attributed to propane's higher reactivity and LBV, and therefore, more advanced combustion phasing and higher global temperatures.

3. As PES is increased at a constant low BMEP condition, the first peak of the apparent heat release rate (AHRR) generally decreases while the second AHRR peak associated with flame propagation increases. With a high fixed BMEP, the behavior of the two fuels varies significantly. Diesel-ignited methane combustion shows a significant increase in ignition delay and fairly consistent AHRR profiles for different PES. The increase in ignition delay is attributed to oxygen displacement and chemical effects present with the high methane fueling rates needed to achieve the given PES at high BMEPs. For diesel-ignited propane combustion, the ignition delay decreases leading to very rapid combustion at high PES, thereby transforming the combustion from the two-peak profile typical of dual fuel combustion to a single early AHRR peak of substantially higher magnitude. The large amount of propane needed to achieve the given PES at high load allows the propane-air mixture to be rich enough to approach auto-ignition conditions.

4. Both the high-BMEP/high PES and large-pilot/high equivalence ratio behaviors of diesel-ignited propane combustion indicate a departure from the classical three-phase interpretation of dual fuel combustion. Rather, it appears that distributed auto-ignition may outweigh localized flame propagation under these specific conditions, in which combustion resembles a "diesel-regulated HCCI-like" process.
5. For low fixed BMEP conditions, the NO_x emissions decrease simultaneously with smoke emissions as PES is increased (and the pilot quantity is reduced). The NO_x emissions decrease because there are likely fewer locally high temperature regions, and smoke emissions decrease because there are fewer locally fuel-rich regions. At high BMEP conditions, this trend is reversed for diesel-ignited propane combustion, where rapid, advanced combustion cause high global and likely high local temperatures, which facilitate NO_x formation. The CO and THC emissions increase with increasing PES, most noticeably at low BMEPs. Fuel conversion efficiency decreases at low BMEPs with increasing PES, but is maintained at baseline diesel values or even increases at high BMEPs. In general, diesel-ignited propane combustion yields higher CO, lower THC, and higher FCE than diesel-ignited methane combustion over the range of PES examined (at constant BMEP).
6. The phasing and the duration of dual fuel combustion were affected by pilot quantity, in-cylinder conditions, and primary fuel concentration. It is inferred that pilot quantity affects in-cylinder conditions by influencing

the residual gas temperatures and cylinder wall temperatures. In turn, this affects the phasing and duration of combustion, most noticeably with diesel-ignited propane combustion. Earlier phasing of diesel-ignited propane combustion leads to higher FCEs, shorter combustion durations (faster burn rates), and lower THC emissions. Increasing primary fuel concentration has different effects at different BMEPs, but always decreases smoke while at a given constant BMEP. At high BMEPs, increased propane concentration leads to a significant change in dual fuel combustion character, exhibiting an advanced, rapid heat release. This behavior leads to higher FCEs compared to the baseline diesel values and lower smoke emissions. Further investigation of diesel-ignited propane combustion is needed to fully understand the potential of this significantly different dual fuel combustion behavior.

CHAPTER VI

EXPERIMENTAL SETUP – MX10 ENGINE

6.1 Test Cell Setup

The second set of experiments in the present work was performed on a MX10 heavy duty diesel engine. To run the experiments, an appropriate test cell had to be designed and implemented. Relevant engine details are given in Table 6.1. An overview of the heavy duty test cell is shown in Figure 6.1.

Table 6.1 MX10 Engine Specifications

Parameter	Value
Engine	MX10
Cylinders	6, inline
Bore	130 mm
Stroke	162 mm
Connecting rod length	262 mm
Valves per cylinder	4
Nominal compression ratio	17:1
Displaced volume	12.9 liters
Injection system	Solenoid direct injection w/ electronic unit pumps (EUPs)
Aspiration	Turbocharged w/ variable nozzle turbocharger (VNT)
EGR	Cooled
Engine Control	Original equipment engine control module (OE ECM) or Drivven

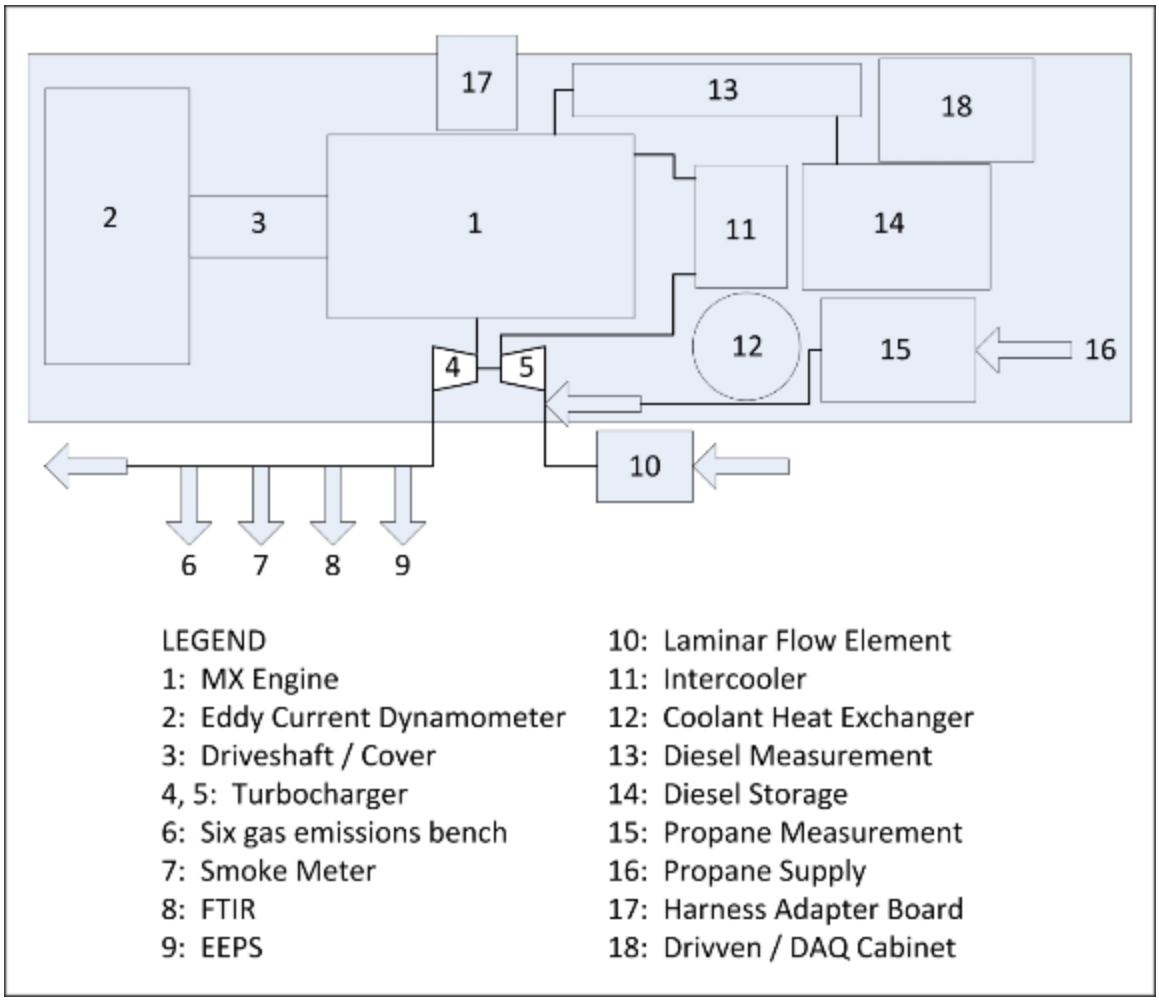

Figure 6.1 MX10 test cell overview

The foundation of the heavy duty test cell is a 6 foot wide by 18 foot long Bay Cast Technologies bed plate. The first piece of equipment mounted to the bedplate was the eddy current dynamometer, a Froude Hofmann AG500 (500 kW), which was positioned at the correct height using a dynamometer riser manufactured by Application Engineering, Inc. As an eddy current dynamometer, or "dyno," dissipates the energy it absorbs as heat, it must be cooled. Facility process water was plumbed to the dynamometer for this purpose; a schematic is shown in Appendix B. Appropriate

electrical and thermocouple connections were made and the dynamometer was later commissioned once there was a load source (MX10 engine) coupled to it.

The engine was hoisted with a gantry crane and mounted on Bay Cast Technologies "elephant feet" style mounts. As the mounts were generic and not specific to the engine, adapters were required to complete its mounting. A thick piece of "L Angle" A36 structural steel was used to span the front two "elephant feet" mounts and secure the front engine mount. One inch thick neoprene rubber of 70A durometer hardness was used between the structural steel crossbar and the "elephant feet" mounts for vibration isolation. Another Bay Cast Technologies product, the moon universal joint, which resembles a ball and socket joint, was used to couple each of the rear engine mounts to the rear elephant feet. As with the front engine mounts, the same thick rubber was used for vibration isolation. A rear engine mount can be seen behind the driveshaft in Figure 6.2.

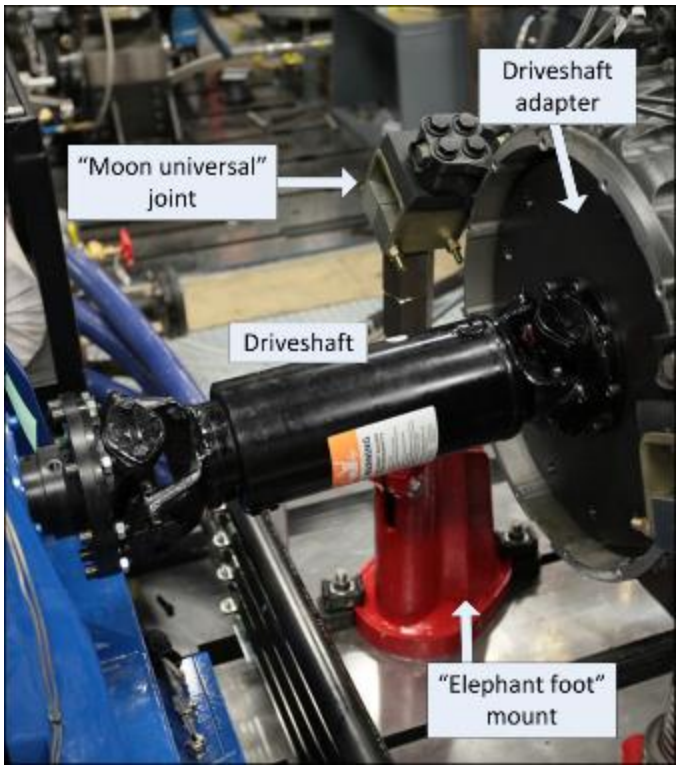

Figure 6.2 MX10 driveshaft, flywheel adapter, and rear engine mount

The engine was coupled to the dynamometer using a driveshaft specified with the help of Joint Clutch and Gear, Inc. (JCGI). This required the use of a custom flywheel adapter for two reasons: (1) to adapt the different fastener hole patterns and (2) to add approximately 1 kg-m2 of rotational inertia to the engine (required by the specified driveshaft). The adapter was designed and machined from one inch thick steel. The driveshaft and adapter are shown in Figure 6.2 and an engineering drawing for the adapter is provided in Appendix B. After mounting the adapter and driveshaft, a robust driveshaft guard was fabricated for safety.

A preliminary fuel system was specified to supply, but not measure, filtered diesel flow to the engine. The 55 gallon fuel tank was designed and submitted to the Anel

Corporation for manufacturing. An AirDog Class 8 Fuel Preparator pump/filter combination unit was used to supply fuel to the engine. In addition to filtering solid particles, the filter also removes any water or gaseous bubbles from the fuel supply.

The thermal management systems used included a large shell and tube heat exchanger for engine coolant conditioning, a water-to-air intercooler for intake air temperature control, and a small shell and tube heat exchanger for fuel temperature control. Engine coolant and fuel temperatures were controlled using Automation Direct PID controllers coupled with Johnson controls three-way mixing valves. Intake air temperature was maintained at a set value with a PID controlled two-way globe valve. Engine coolant was supplied to the then engine at 65±5 degrees Celsius while coolant temperature out of the engine was maintained at 85±5 degrees Celsius. Post-intercooler air temperatures were maintained at 25±5 degrees Celsius. Schematics of the coolant and intake air temperature control systems are shown in Figures 6.3 and 6.4, respectively.

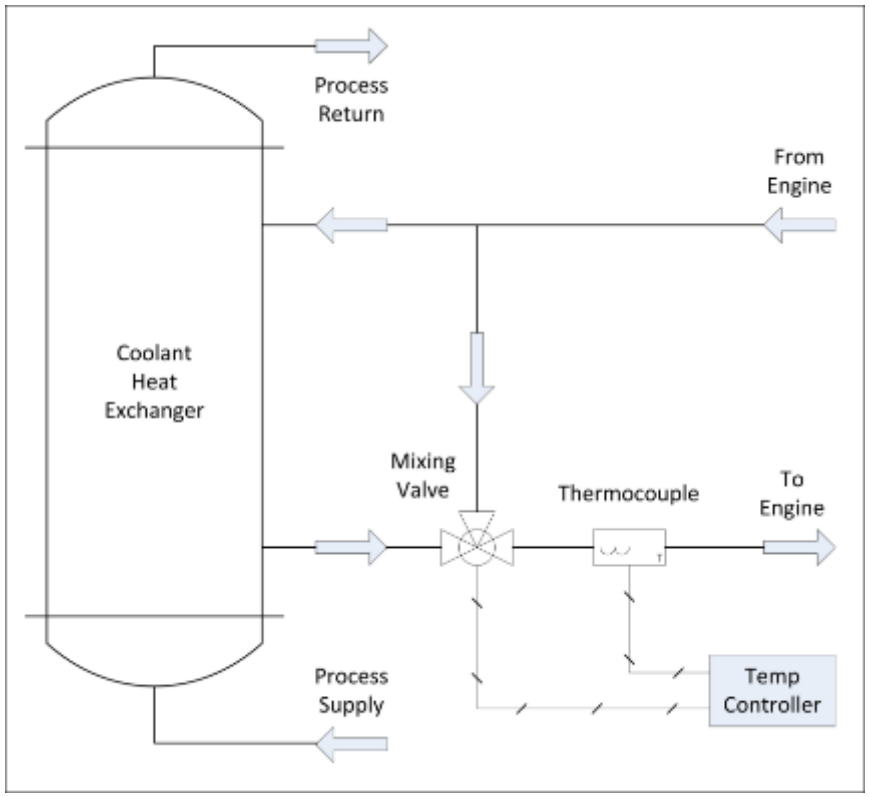

Figure 6.3 Engine coolant temperature control schematic

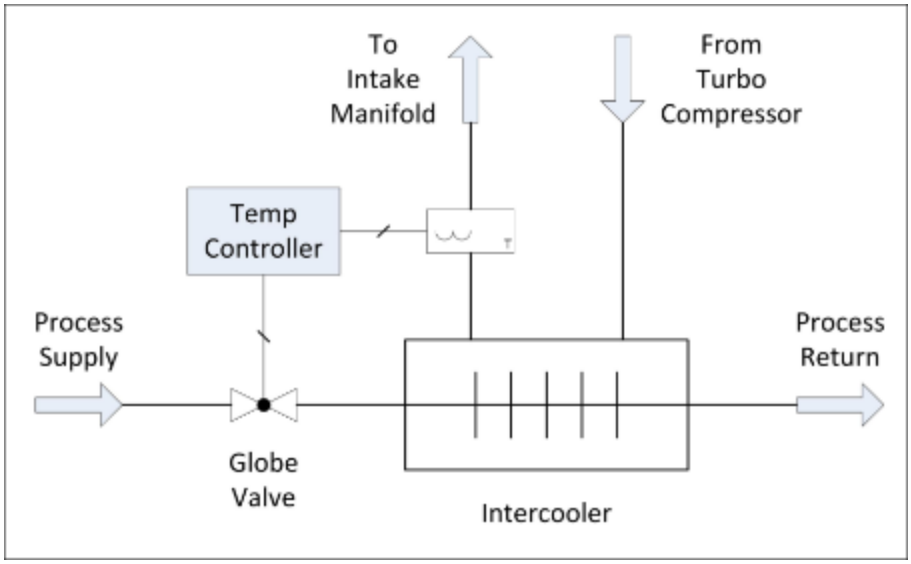

Figure 6.4 Intake air temperature control schematic

The engine wiring harness was wired such that an adapter board (specially designed by Drivven for this engine) could be used, allowing either the original equipment (OE) engine control module (ECM) or Drivven controller to control the engine, depending on which input was connected. Shown in Figure 6.5, the adapter board had three banks of connectors. The top row of connectors was the output, which led to the engine wiring harness and therefore the various sensors, control, and communication modules on the engine. The middle and bottom rows of connectors were identical, receiving input from either the OE ECM or the Drivven controller. These inputs were never connected simultaneously (prevented interference from pull-up resistors in sensors, power sources, etc.); however, the extra set of plugs provided easy access for sampling the various signals of the engine for debugging or "reverse engineering" purposes.

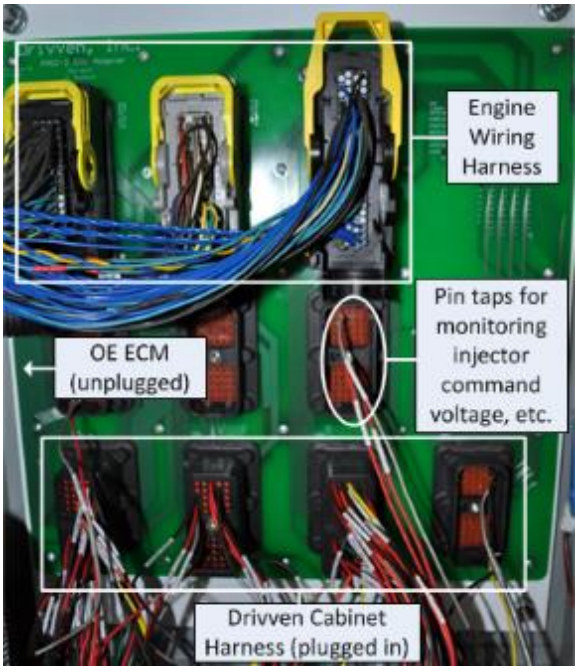

Figure 6.5 Engine harness, Drivven harness, and OE ECM harness adapter board

For the OE ECM to function properly it had to run as if it was in a vehicle; therefore, several signals had to be simulated. Pedal position (voltage) was supplied by the dynamometer controller while a custom idle validation circuit closed a switch at approximately 10 percent pedal position. The idle validation circuit is required by the OE ECM as a safety check for pedal position. The ECM was non-standard, and therefore aftertreatment system simulation was not required. The vehicle controller area network (CAN) signals were simulated using an NI compact Real-Time I/O (cRIO) two port CAN module (NI 9853) in conjunction with a field programmable gate array (FPGA) controller and LabVIEW Real-Time software. The CAN protocol was implemented in the open LabVIEW environment using the SAE J1939 standard. The resulting front panel and block diagram of the CAN interface VI is shown in Appendix C. With the CAN system in place, CCVS, EBC1, EBC2, PTO, CM1, AIR1, and HRW signals could be simulated to prevent the ECM from generating new faults. In addition, existing faults could be viewed for debugging purposes.

Intake and exhaust streams were oriented vertically, as shown in Figure 6.6, due to the required laminar sections for air flow rate measurement in the intake and smoke measurement in the exhaust. The exhaust stream had to be vented directly through the roof because the high exhaust flow rates of the MX10 engine exceeded the capabilities of the existing exhaust ventilation system.

Figure 6.6 Intake and exhaust plumbing with vertical orientation

Upon completion of the test cell setup, the engine and the dynamometer were run over the entire speed-load operating range, ensuring both engine and dynamometer would operate at full capacity and that all engineered subsystems performed adequately. The "lug curve," or full load output over the engine's operating range is shown in Figure 6.7. One subsystem that lacked the necessary robustness for full load operation was the charge air system. The charge air routing pipes at first consisted of separate sections joined with straight and elbow silicone couplers. To withstand the significant boost

pressures and forces in the charge air system, the intake charge air plumbing had to be welded together, using as few silicone couplers as possible, as shown in Figure 6.8.

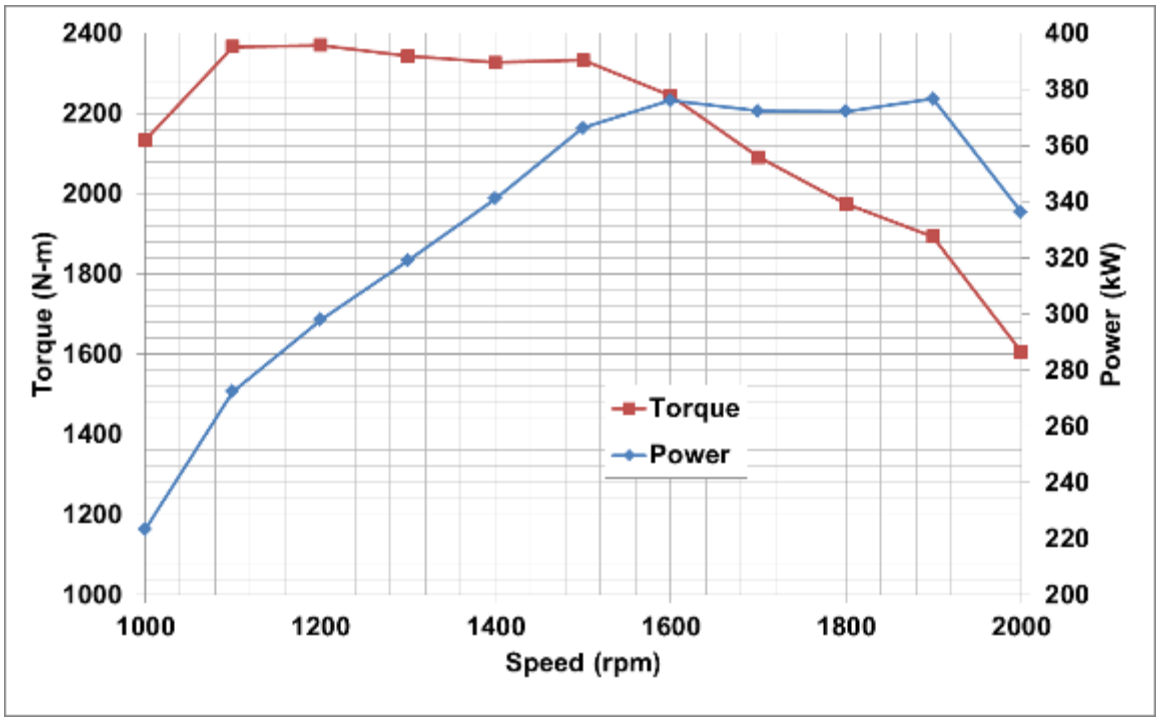

Figure 6.7 MSU generated OE ECM Lug Curve

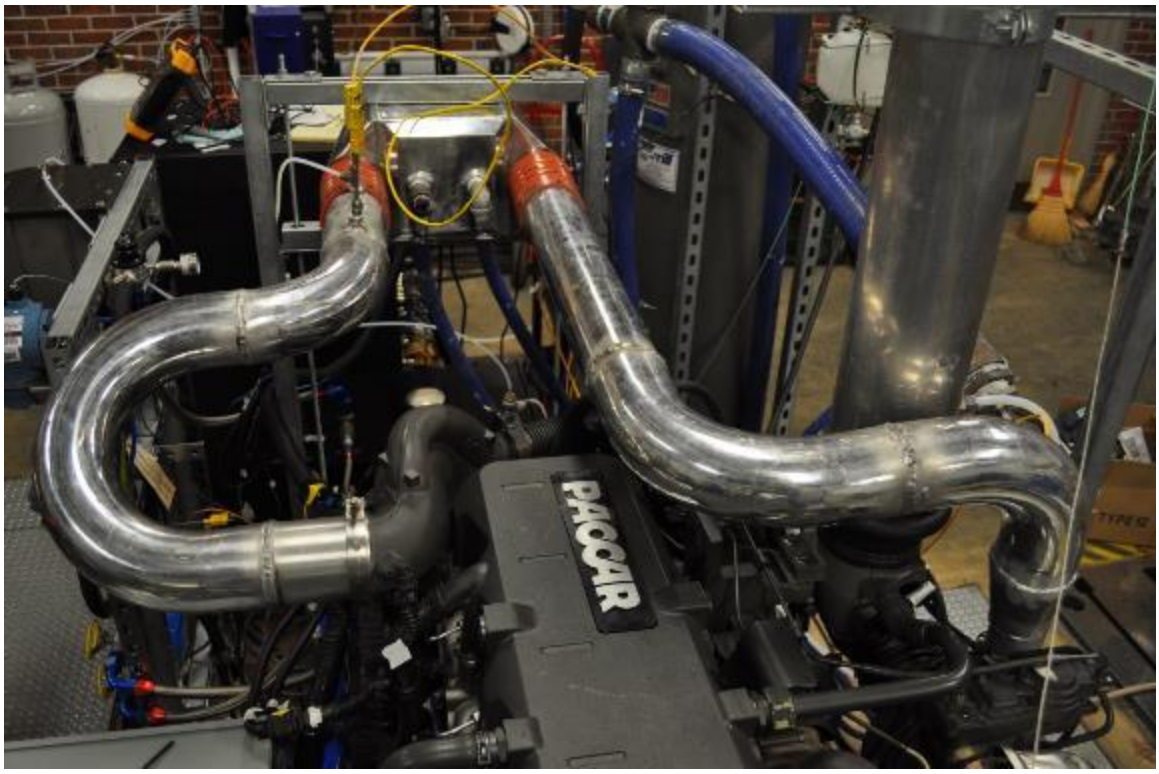

Figure 6.8 Intake charge air plumbing

The propane injection system used consists of six injectors, two rails, a filter, a pressure regulator, and an emergency shutoff solenoid. The injectors and filter were obtained from a G-Volution propane injection kit. The pressure regulator and fuel shutoff solenoid were specified for LPG operation up to 50 psig. Propane storage consisted of three 100 lb. propane cylinders connected in parallel. Each cylinder had a high pressure regulator (up to 150 psi) and a flash arrestor. A schematic of the propane system is shown in Figure 6.9. The propane was fumigated into the intake air before the turbocharger and the fuel stream was directed in the downstream direction.

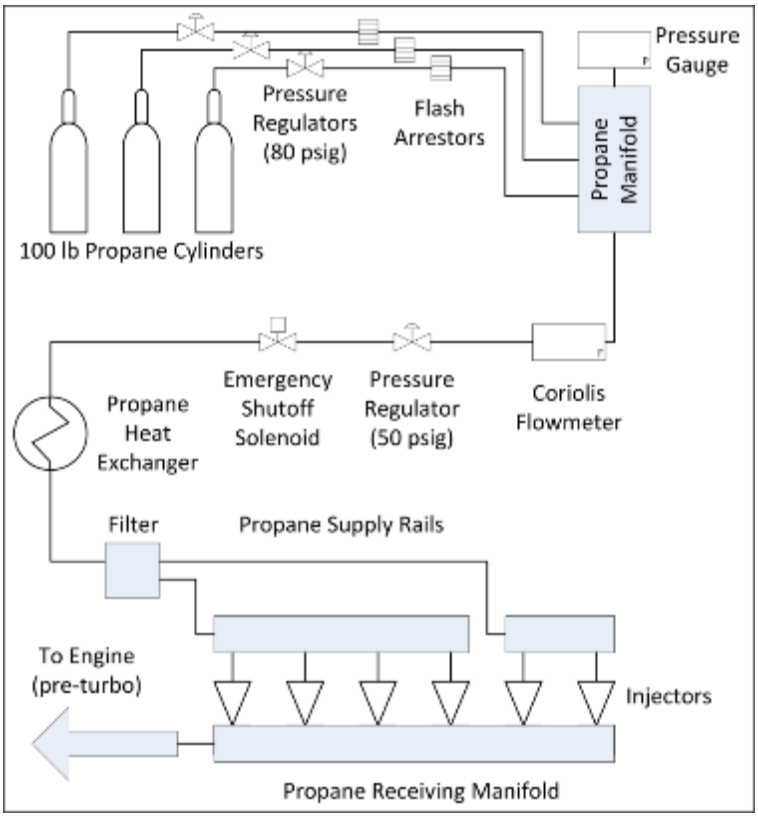

Figure 6.9 Propane injection and storage systems

6.2 Drivven Controller Hardware

The next step for the MX10 engine was to transition to an open-architecture, LabVIEW-based engine controller manufactured by Drivven, Inc. The system primarily consists of several National Instruments (NI) compact reconfigurable input / output (cRIO) expansion chassis and specialized Drivven input and output modules. All of the cRIO expansion chassis communicate with an NI PXI system using an FPGA interface. This allows for very rapid and robust control of multiple engine parameters in real-time. A schematic of the Drivven cabinets containing cRIO expansion chassis, cRIO modules, voltage rails, and relays, and a signal conditioner is shown in Figure 6.10.

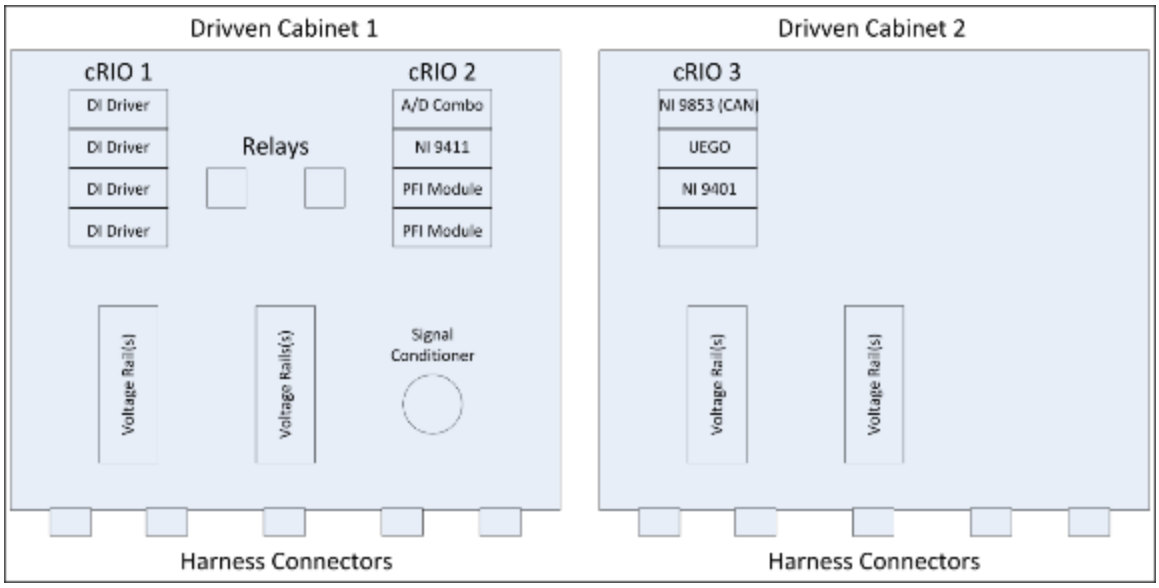

Figure 6.10 Drivven cabinets

The cRIO modules each interface with a cRIO expansion chassis, which in turn interfaces with a field programmable gate array (FPGA) controller, or target, in the PXI chassis. As there are a finite number of logic gates on a given FPGA circuit, the large quantity of logic required for this application caused the FPGA chassis to be split between two separate FPGA targets: (1) modules that required engine synchronous input and output (I/O) and (2) modules that did not require engine synchronous I/O (asynchronous). The synchronous FPGA target is an NI 7853R FPGA card, utilizing a Virtex V series FPGA integrated circuit. The smaller NI 7813R FPGA card is used for asynchronous control and utilizes Virtex II series FPGA hardware. The synchronous target interfaces with the following modules: four three-channel Drivven direct injection (DI) drivers which control six solenoid injectors and six electronic unit pumps, two Drivven port fuel injection (PFI) drivers which control the main power relay (MPR),

EGR valve, and six propane fuel injectors, a Drivven AD Combo module which receives and conditions analog input from the engine sensors, and an NI 9401 module which receives the encoder signals. The asynchronous target interfaces with a Drivven O_2 sensor (UEGO) module which controls closed loop fueling (not used), an NI 9853 CAN module for CAN communication, and an NI 9411 digital input/output (DIO) module for debugging engine timing signals (when needed).

6.3 Drivven Controller Software

The LabVIEW software for the DRIVVEN system requires several "levels" of code. The base of the system exists at the FPGA level, where the software interacts with the cRIO expansion chassis modules and current engine crankshaft position is calculated at approximately 40 MHz. The primary functionality of the system exists on the Real-Time level, where inputs are read from the FPGA level, new control parameters calculated, and outputs are written to the FPGA level at approximately 100 Hz. Finally, the top-most level is the CalVIEW user interface, which allows user interaction with the Real-Time level without adding unnecessary code.

6.3.1 FPGA

At the FPGA (field programmable gate array) level, tasks such as engine position tracking, fuel injection, and CAN I/O are performed. These tasks are time-sensitive and must be extremely reliable. The FPGA environment is suitable for these types of tasks because of its embedded nature. All FPGA code must be compiled after which it is deployed onto a FPGA target; that is, an integrated circuit designed to implement user designated logic or code. All FPGA code deployed onto the target can operate very

rapidly. The code implemented in the engine-synchronous target operates at 40 MHz, and most timing related tasks are discretized into 40 MHz clock ticks. Other tasks, such as CAN I/O happen as quickly as the FPGA target can operate the logic.

6.3.1.1 Engine Synchronous FPGA

There are four major parts of the engine synchronous FPGA code, shown in Appendix D:

1. Engine position tracking (EPT) subVI – tracks the position of the engine based on Boolean signals from Hall effect or variable reluctance (VR) sensor inputs (crank and cam inputs) and provides a cluster of data including current position in ticks as well as a "Fuel/Spark Supervisor" signal, which is used to communicate engine position to other engine-synchronous device drivers on the FPGA level.
2. Direct injection (DI) driver subVIs – fires the injector and electronic unit pump solenoids at a specified engine position for a given duration with a calibrated current profile; the device driver interfaces with the EPT "Fuel Spark Supervisor" for an engine position input.
3. Port fuel injection (PFI) driver subVIs – may be configured as either synchronous or asynchronous (in this case, asynchronous since fuel is fumigated before the intake); the primary inputs are frequency, duration, and current profile.
4. Drivven Combustion Analysis Toolkit (DCAT) – this portion of the FPGA code uses the optical crank encoder inputs through the NI 9401 cRIO

module to track engine position and communicates with the high speed DAQ cards (S-Series) through the PXI triggers on the PXI backplane

6.3.1.2 Asynchronous FPGA

Because the UEGO and 9411 modules are not currently used, only the CAN I/O is required in the asynchronous FPGA code. CAN communication is required using the Drivven controller in order to communicate with the humidity sensor and turbocharger VNT actuator on the secondary engine CAN network. The following portions of the FPGA code are shown in Appendix D:

1. CAN input – reads the incoming CAN messages and places them into a First In, First Out (FIFO) style queue.
2. CAN output – removes CAN messages from the outgoing FIFO, formats the bits appropriately, and writes the messages to the CAN bus.

6.3.2 Real-Time and Control Logic

Most control logic exists at the Real-Time (RT) level. The four functions of the RT code are: (1) engine control, (2) CAN communication, (3) analog outputs, and (4) data acquisition. Unlike the FPGA level, the RT level offers more flexibility in terms of code size, structure, and allows quick editing as it does not need to be compiled; however, it gains these advantages at the expense of timing and reliability. Whereas the engine synchronous FPGA code operates at 40 MHz, the engine control portion of the RT code only operates at approximately 100 Hz, or a period of about 10 milliseconds, and tends to vary slightly from loop to loop.

The engine control portion of the RT code is split into three primary sections, split using a flat sequence structure (which ensures that operations are performed in sequential order), as shown in Appendix D:

1. Read Inputs – Reads and processes inputs from the FPGA level; this includes analog sensor info, engine speed, module status, and fault detection.
2. Control Algorithms – Processes new control values based on new data input from step one; this includes torque command, fueling rate, EGR rate, and VNT actuation.
3. Write Outputs – Process and writes new outputs to the FPGA level based on new data from step two; these include injector and pump timing and duration as well as PFI and relay ("LowSide") control.

In addition to these primary functions, the RT level also handles the bulk of the CAN communication and the SAE J1939 protocol. These functions exist in a separate subVI (a subroutine in LabVIEW) which operates in parallel with the aforementioned sequence structure. Other PXI hardware (analog output, power supply) are also controlled at the RT level, each of which has a separate subVI for its tasks. The last major piece of logic at the RT level is the Drivven Combustion Analysis Toolkit (DCAT), a data acquisition related feature to be discussed in a later section.

6.3.2.1 Torque Command

The torque command subVI calculates a "desired BMEP" based on engine speed and pedal position in percent. Based on engine speed and pedal position, a lookup table interpolates for a desired BMEP. The output of this subVI is used, along with engine

speed, in almost every other control subVI as lookup table inputs. Before outputting the BMEP value, a manual override selector allows the user to set a desired BMEP manually in the user interface.

6.3.2.2 Diesel Injector and Pump Control

Diesel solenoid injection and electronic unit pump (EUP) control are operated solely in "open loop" mode; that is, there are no feedback-based engine sensors, i.e., an oxygen sensor in the exhaust stream. This subVI uses the desired BMEP value from the aforementioned Torque Command subVI and the engine speed as inputs to two-dimensional lookup tables containing values such as the start of injection solenoid activation (SOI), injection duration, start of pump solenoid activation (SOP), pump duration, and up to four additional injector and pump actions (two pre- and two post-injections). As with the Torque Command VI and all other control subVIs, there are limits for the various control variables as well as manual overrides. The manual controls were the primary method of controlling pilot quantity during dual fuel operation.

Before operation, the DI modules must be calibrated to a known current profile. Using the correct current profiles for the injectors and pumps are critical for correct operation. The basic theory of operation requires that a high, or "peak," voltage (50 V) be applied to the solenoid to open the injector or pump. After a peak time (usually in milliseconds), or a peak current is reached, the voltage drops to battery voltage (12V), switching ON and OFF to dither the current at its "hold" value (about 10 A) in order to keep the solenoid open for its duration.

6.3.2.3 Engine CAN Bus and VNT Control

The two devices on the secondary engine CAN (E-CAN) bus are the turbocharger VNT actuator and the humidity sensor. This CAN bus follows the SAE J1939 protocol but uses proprietary identifiers for turbocharger communications. Data written to the turbocharger include the actuator state and the actuator position requested. The turbocharger VNT actuator is controlled on a percent basis, from 0 to 100 percent in 0.1 percent steps. The VNT actuator position is calculated based on a feed-forward lookup table using engine speed and desired BMEP. Data received from the turbocharger includes actuator state, position, error state, and temperature. Data such as relative humidity, intake air temperature (IAT), and intake air pressure are read from the humidity sensor CAN data.

6.3.2.4 EGR Valve Control

The EGR valve is controlled using two LowSide driver channels on the first PFI module and pulse width modulation (PWM) to control current through the EGR valve actuator. The two channels act in unison to provide the necessary electrical current to the valve without saturating either channel. The frequency and duty cycle (percent ON time) of the EGR signal varies in order to maintain a constant ON duration of 10 ms. Position feedback via a 0.5 to 4.5 V signal allows precise PID control of this variable.

6.3.2.5 Propane Injector Control

Since propane will be fumigated before the turbocharger, engine synchronous control is not necessary for this setup. The PFI injector current profile is similar to the DI control, requiring both peak (4 A) and hold (1.5 A) current values, however an engine

position is not required. Similar to PWM operation, the propane fuel injectors operate at a given frequency, which in this case is proportional to engine speed. Injection duration is controlled manually via the user interface.

6.3.3 User Interface

The CalVIEW interface allows interaction with the RT level without adding additional code, which could potentially inhibit performance of the RT target. CalPoint controls and indicators, placed at the RT level, communicate directly with controls and indicators in the Host VI. The user interface for the engine controller is shown in Figure 6.11. Despite the somewhat complex front panel, the block diagram for the Host VI is very simple, requiring little code other than plots, etc.

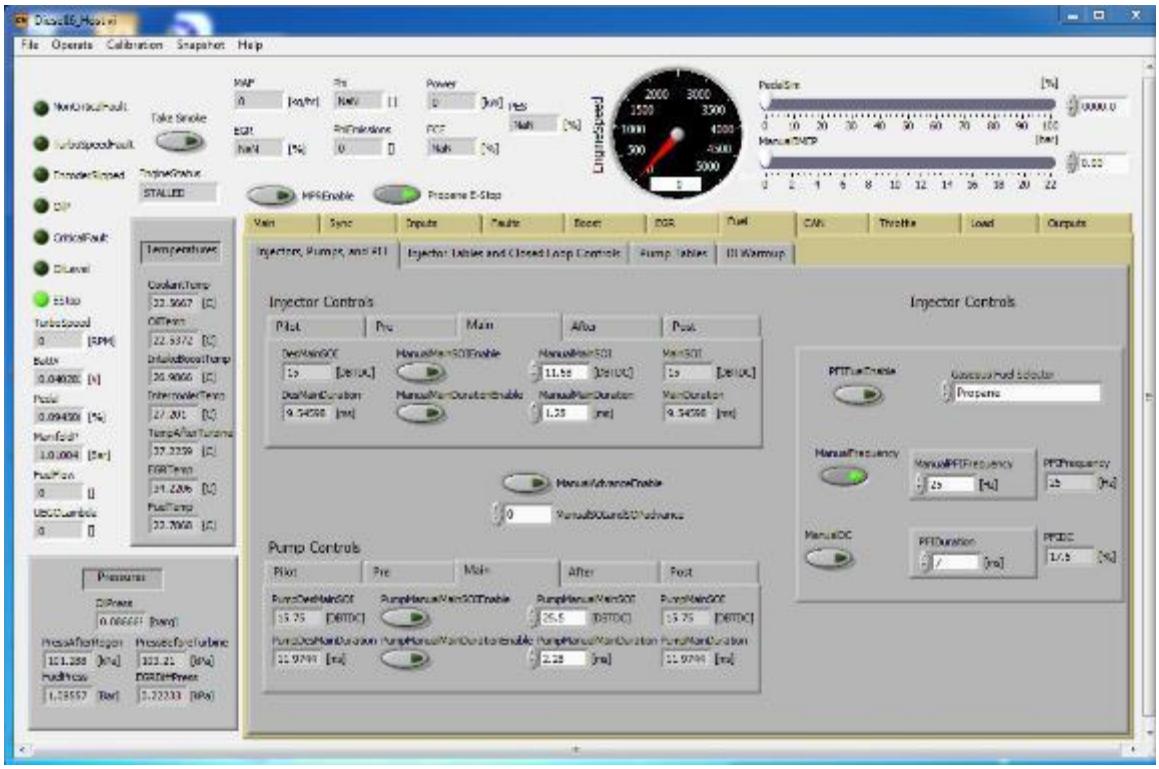

Figure 6.11 CalVIEW – Engine control user interface

6.3.4 Calibration

Before operating the MX10 engine on the Drivven controller, the various control parameters had to be mapped from the OE ECM during operation. A test matrix ranging from 600 to 2000 RPM engine speed in 100 RPM increments and 0 to 22 bar BMEP in 2 bar increments was completed. Values of injector solenoid timing and duration, pump solenoid timing and duration, boost pressures, VNT actuator position, and EGR valve position were recorded and arranged into two-dimensional speed versus load tables. The minimum pedal position required to operate the engine at each speed was found and was given the "0 BMEP" designation. Any pedal position below this threshold while at the given speed would return a "negative BMEP," corresponding to a lower operating point, which allowed engine speed to decrease. Speeds lower than 600 RPM (during engine cranking) were not able to be mapped; therefore, tables were created by trial and error. The phasing of the SOI and SOP were kept constant on a time basis rather than on engine position (crank angle basis) throughout cranking.

After the Drivven system was calibrated, a maximum load sweep was completed from 1000 to 2000 rpm. As shown in Figure 6.12, the variation between the maximum load for the Drivven controller and data provided from the manufacturer was less than 3 percent from 1100 to 2000 rpm.

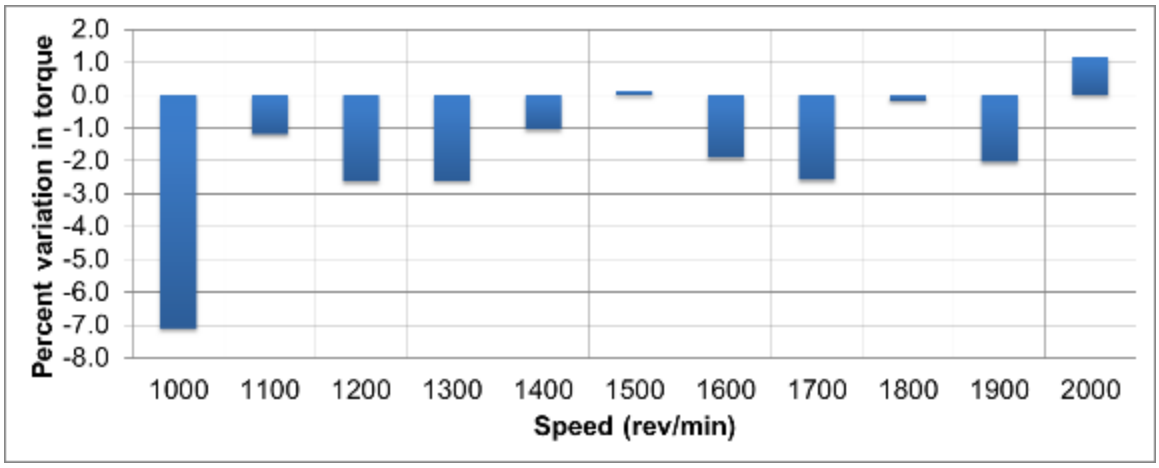

Figure 6.12 Percent variation in lug torque between Drivven and manufacturer data

6.4 Test Cell Instrumentation

The test cell instrumentation for the MX10 engine test cell is similar to that of the Volkswagen engine test cell in many aspects. Relevant instrumentation details are given in Table 6.2.

Table 6.2 Instrumentation Specifications

Data Type	Sensor/Instrument	Type	Accuracy
Temperature	Thermocouple	K	Greater: 1.1 °C or 0.4%
Pressure for LFE	Omega MM	Absolute	0.08% FS BSL (30 psia)
Pressure for LFE	Omega MM	Differential	0.03% FS BSL (10 inH_2O)
Pressure for boost	Omega MM	Gauge	0.25% FS BSL (50 psig)
Mass air flow	Meriam MC2-6	Laminar Flow Element (LFE)	
Mass propane flow	Micro Motion	Coriolis	0.35% of reading
Mass diesel flow	Micro Motion	Coriolis	0.05% of reading
Smoke	AVL 415S	Filter	0.005 FSN + 3% of reading
NO_x	ESA EGAS 2M	CLD	1% FS
NO	ESA EGAS 2M	CLD	1% FS
THC	ESA EGAS 2M	FID	1% FS
CO-low	ESA EGAS 2M	NDIR	1% FS
CO-high	ESA EGAS 2M	NDIR	1% FS
CO_2	ESA EGAS 2M	NDIR	1% FS
Cylinder pressure	Kistler 6125C	Piezoelectric	Lin: 0.4% FSO
Fuel pressure	Kistler 4067C3000	Piezoresistive	EP Lin: 0.5% FSO

6.4.1 Steady State Instrumentation

Engine coolant, dynamometer, post-intercooler, intake mixture, fuel, and post-turbo exhaust temperatures were measured with K-type thermocouples. Typically, these were mounted using 0.25 inch Swagelok compression fittings.

Diesel volume flow rate was measured with an Emerson Micro Motion coriolis mass flowmeter (Model: CMF025M319N2BAEZZZ). To facilitate accurate fuel measurement with one flow meter and to allow fuel return simultaneously, a "diesel level tank" manufactured by Application Engineering, Inc. was used. The level tank functions by regulating flow from the flowmeter using a float device; as mass exits the system, i.e.

consumed in the engine, fuel is supplied to the system at the same rate. Fuel was supplied to the level tank by an Airdog Class 8 Fuel Preparator pump/filter combination unit, which removes gaseous bubbles and water from the fuel in addition to solid contaminants. A typical bypass style fuel pressure regulator was used to regulate pressure at the inlet of the level tank to a maximum of 6 psig. Fuel temperature was conditioned using a shell-and-tube heat exchanger, three-way mixing valve, and a temperature controller. Fuel temperature was maintained at 40±1°C. A schematic of the fuel system is shown in Figure 6.13. Intake air mass flow rate was measured with a Meriam MC2-6 Laminar Flow Element. Straight six inch intake piping with the lengths of ten pipe diameters upstream and five pipe diameters downstream was used to facilitate laminar intake air flow. The primary gaseous fuel (propane) mass flow rate was also measured with an Emerson Micro Motion coriolis mass flowmeter (Model: CMF025M319N2BAEZZZ).

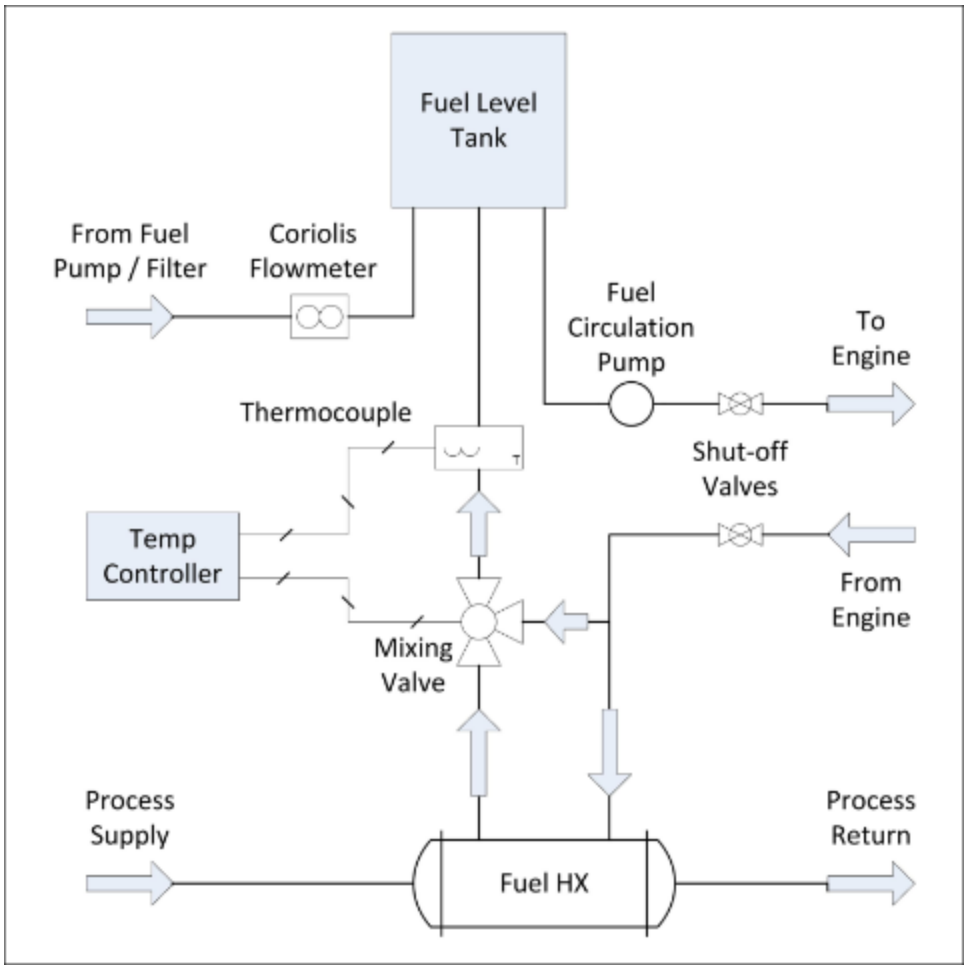

Figure 6.13 Diesel measurement and conditioning system

Pressures in the test cell were measured with Omega MM Series custom pressure transducers. The absolute pressure transducer (for LFE flow) had a 0-30 psia range, differential pressure (for LFE flow) had 0-10 in-H2O range, and the remaining gauge pressure transducers (for boost, exhaust, fuel, coolant, propane, and oil) had ranges of either 0-50 psig or 0-150 psig. Pressure transducer accuracies and other details are given in Table 6.2.

All gaseous exhaust emissions were measured downstream of the turbocharger turbine. Gaseous emissions were routed through an emissions sampling trolley to an integrated six-gas emissions bench (EGAS 2M) manufactured by Altech Environnement S.A. and smoke was measured with an AVL 415S variable sampling smoke meter. The emissions bench provides measurements for total hydrocarbons (THC), oxides of nitrogen (NO, NO_x), carbon dioxide in the exhaust and intake mixture (CO_2, CO_2-EGR), carbon monoxide (CO), oxygen (O_2), and ammonia (NH_3). Smoke emissions are given in filter smoke number (FSN) and were sampled after 10 pipe diameters of straight exhaust pipe for laminar flow. Particulate size distribution was measured with a TSI Engine Exhaust Particle Sizer (EEPS). Exhaust emissions were sampled with a thermal dilutor at a factor of 1:261 and then passed through the EEPS. Emissions speciation was achieved with an AVL Fourier Transform Infra-red (FTIR) SESAM i60 FT. This device uses FTIR spectroscopy to measure pre-calibrated gas components of diesel exhaust, including those measured by the six-gas emissions bench as well as formaldehyde, acetaldehyde, formic acid, sulfur dioxide, methane, propane, and other various hydrocarbons.

6.4.2 Transient Instrumentation

Transient measurements such as cylinder pressure require an engine-position based clock for data acquisition. A BEI optical encoder with 0.1 CAD resolution (3600 pulses per revolution) was used for this purpose. A custom crankshaft adapter and custom encoder bracket were designed and fabricated in-house to facilitate mounting. Engineering drawings with dimensions are shown in Appendix B. The bracket, shown in Figure 6.14, was mounted rigidly with the engine (not attached to the vibration-isolated mounting points).

Figure 6.14 Encoder bracket, crankshaft adapter, and coupler

In-cylinder pressure for cylinder 6 was measured using a Kistler 6125C piezoelectric pressure transducer mounted slightly recessed from the surface of the cylinder head in a Kistler sleeve adapter (neither flush mounted nor having a long or narrow measuring bore). A Kistler 5010B charge amplifier with a "short" time constant setting was used to condition the signal output from the piezoelectric pressure transducer. Fuel line pressure for cylinder 6 was measured using a Kistler 4067C3000 piezoresistive sensor and a Kistler 4618A0 amplifier conditioned the signal. To sample the fuel pressure signal, a Kistler 6533A11 clamp-on fuel line adapter was used. An example of the fuel pressure signal is shown in Figure 6.14. Injector needle lift was unavailable;

therefore, the injector command voltage was sampled for "apparent SOI," also shown in Figure 6.15.

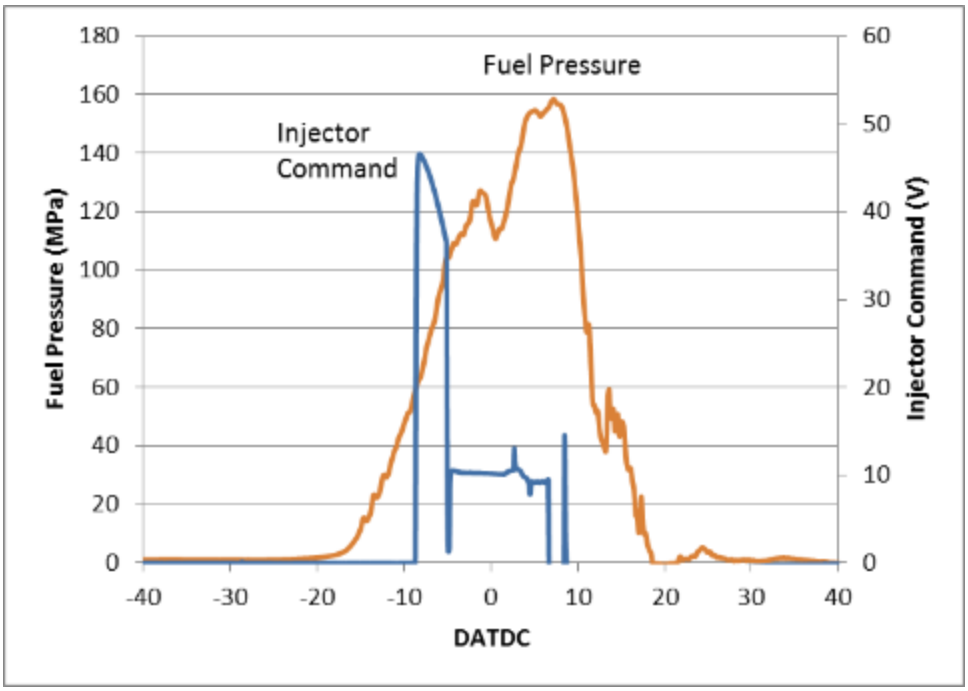

Figure 6.15 Example fuel pressure and injector command signal at 10 bar BMEP

6.5 Data Acquisition with DCAT

The data acquisition software used for both steady state and transient combustion data was the Drivven Combustion Analysis Toolkit (DCAT). The DCAT is comprehensive combustion analysis software presented as an example VI composed of many subVIs, many of which are password protected. While some portions of DCAT are not alterable, the code is arranged such that the user can access almost any data recorded or processed by DCAT and use it however he or she may wish. This offers considerable flexibility and allows direct integration with the engine control portions of the code.

To use DCAT, the PXI hardware must be configured in a specific arrangement. The method used to communicate hardware triggers from the FPGA to the S-Series hardware has two requirements. The first is that the FPGA controller hosting the DCAT FPGA code must be installed in the first PXI slot after the controller. The second is that jumpers must be installed in the S-Series hardware, connecting digital ports to programmable function interface ports for communication and triggering. There are many setup options for DCAT, including engine geometry, filters, and heat transfer correlations. The numerous settings are outlined in Appendix E. The Drivven DCAT manual, incorporated into the DCAT user interface, further details the hardware setup and software configuration options.

Steady state data, referred to as "medium speed" channels in DCAT, were sampled at a rate of 1 kHz. These channels included dyno speed and load, pressures, temperatures, flow rates, and emissions. As data are recorded, DCAT associates the incoming medium speed data with the cycle during which they were recorded and then averages all the samples recorded during a given cycle, leaving cycle-resolved medium speed data. In addition to the individual measurements, DCAT also calculates statistical data such as the mean, standard deviation, and coefficient of variation (COV) of every signal.

The time averaged value of select channels from the medium speed data are collected and used to process additional calculated channels such as mass air flow, BMEP, fuel conversion efficiency, percent energy substitution (PES), equivalence ratio, and brake-specific emissions (following the SAE J1003 recommended practice). The calculated channels are then reinserted into the DCAT interface as "slow speed" channels

at a rate of 1 Hz. In this manner, all data are recorded in a consolidated location. In addition, DCAT records all CalPoint values without DCAT association (controls, indicators, etc.).

CHAPTER VII

CONVENTIONAL AND LOW TEMPERATURE DUAL FUEL COMBUSTION IN MX10 ENGINE

7.1 Introduction

The purpose of this chapter is to investigate and to optimize conventional and low temperature dual fuel combustion (LTC) using diesel-ignited propane in a heavy-duty diesel engine. The dual fuel combustion mode will first be characterized using stock engine control parameters over a range of engine loads and primary fuel concentrations. This test relates to previous experiments on the VW TDI engine, allowing some comparison. In addition, this test extends the dual fuel combustion characterization to higher BMEP conditions that were not achievable with the VW TDI engine and introduces EGR as a variable (not present on the VW TDI). Fueling strategies, injection strategies, EGR rates, and intake boost pressures will be used to optimize the dual fuel combustion mode for maximum percent energy substitution (PES) of propane and minimum NO_x and smoke emissions. Next, injection strategies for LTC (e.g., very early injection) will be used to separate the injection and combustion events to promote mixing and simultaneously decrease NO_x and smoke emissions, as in ALPING LTC combustion [Srinivasan 2003]. Injection timing, fueling strategy, turbocharger VNT actuation, and EGR rate control will be used to optimize the combustion process, i.e., to increase fuel conversion efficiency, to reduce emissions, or to extend operation by reducing cyclic

combustion variability. Other emissions, such as unburned hydrocarbons and carbon monoxide (often observed with dual fuel combustion) will be minimized, if possible.

7.2 Objectives

The objectives of this work are as follows:

1. Investigate conventional diesel-ignited propane dual fuel combustion on a modern, heavy-duty diesel engine.
2. Implement and assess dual fuel LTC combustion in a multi-cylinder heavy-duty diesel engine by optimizing the injection strategy, fueling strategy, EGR rate, and intake boost pressure.

7.3 Results and Discussion

Two sets of steady state, diesel-ignited propane dual fuel experiments were performed using the heavy duty MX10 diesel engine. Engine speed was maintained at 1500 rpm for all experiments.

7.3.1 Conventional Dual Fuel Constant BMEP Experiments

In the first set of dual fuel tests, engine load was maintained at four constant BMEP conditions: 5 bar, 10 bar, 15 bar, and 20 bar. Stock control parameters were used for injection timing, pump timing, EGR valve position, and VNT actuator position and were based on the "diesel-only" condition at each load point. At each engine load, the diesel pilot injection duration and primary fuel (propane) flowrate were adjusted to achieve various primary fuel concentrations within ±1 percentage points, ranging from diesel-only conditions to the maximum achievable PES of propane in increments of 10 percent. The experimental matrix for this set of tests is shown in Table 7.1 and ranges of

P_{in}, T_{in}, EGR rate, and equivalence ratio (phi) are given in Table 7.2. The EGR valve and VNT positions varied based on the engine load but remained constant for different concentrations of primary fuel; however, less available energy in the exhaust gas yielded progressively lower intake boost pressures with increasing PES. In this first set of tests, the operating points were attained by gradually reducing the pilot quantity and increasing propane concentration while maintaining the desired load. At 5 bar BMEP, a minimum pilot injection duration limited the maximum PES of propane to 86 percent (without changing diesel injection pressure). At 10, 15, and 20 bar BMEPs, a maximum pressure rise rate (MPRR) (greater than 15 bar/CAD) and excessive combustion noise (greater than 94 db) limited the PES of propane to 60, 33, and 25 percent, respectively. Similar trends were observed by Goldsworthy [2012] at high load (BMEP = 17 bar) in a diesel-ignited propane dual fuel engine, where the maximum PES of propane (35%) was limited by extreme MPRR (MPRR = 58 bar/CAD) and knock.

Table 7.1 Experimental Matrix for PES Effects at Different BMEPs

BMEP (bar)	Percent Energy Substitution									
	0%	10%	20%	30%	40%	50%	60%	70%	80%	86%
5	X	X	X	X	X	X	X	X	X	X
10	X	X	X	X	X	X	X	O	O	
15	X	X	X	X	33%					
25	X	X	X	25%						

Note: Data points marked by an "O" indicate that optimization was required

Table 7.2 Inlet Condition Ranges for Constant BMEP Experiments

BMEP (bar)	P_{in} (bar)	T_{in} (°C)	EGR (%)	Phi
5	1.66 – 1.58	44.7 – 40.2	35.5 – 33.9	0.50 – 0.56
10	2.37 – 2.01	32.3 – 31.9	25.5 – 25.4	0.53 – 0.60
15	2.90 – 2.77	34.3 – 32.2	18.9 – 17.5	0.54 – 0.55
20	3.40 – 3.25	37.2 – 28.8	16.8 – 15.2	0.61 – 0.62

7.3.1.1 Combustion Behavior

Heat release rate and cylinder pressure profiles for 5, 10, 15, and 20 bar BMEP conditions are shown in Figure 7.1. Overall, the heat release rate results of conventional diesel-ignited propane dual fuel combustion were similar to previous results obtained with the light-duty VW TDI engine, although much higher BMEPs were possible with the MX10 engine. Certain aspects of the MX10 engine proved advantageous for diesel-ignited propane dual fueling, increasing the achievable PES of propane at low and medium loads. The first major advantage was the lower compression ratio, resulting in lower bulk temperatures near TDC. The second advantage was the added cooled EGR loop, with which varying quantities of EGR could be used to decrease available oxygen in the intake charge, decreasing temperatures and reducing combustion rates. Both of these advantages resulted in increasing the achievable PES of propane at a given load during conventional dual fuel combustion by reducing MPRR.

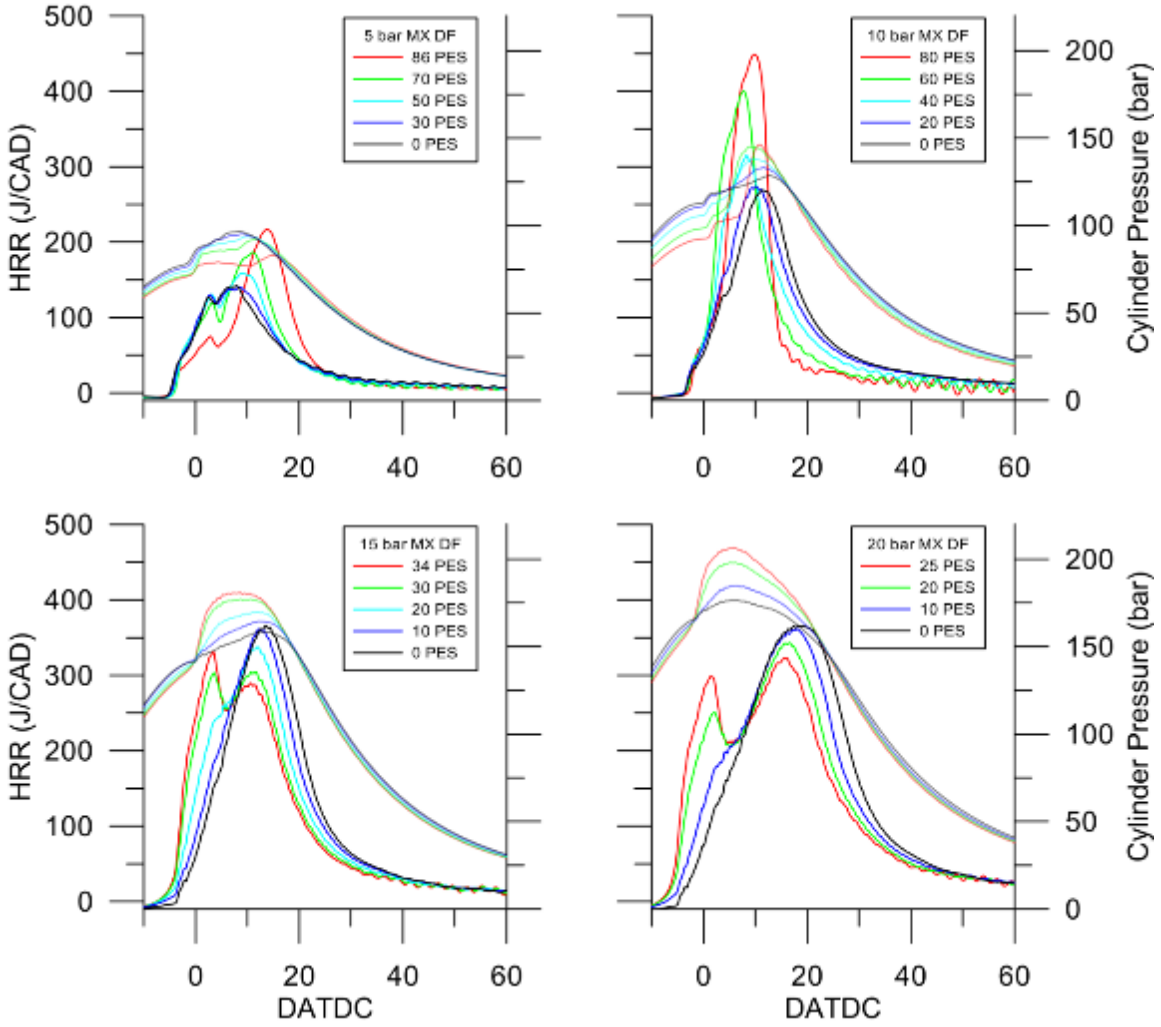

Figure 7.1 Heat release rate vs. crank angle for 5, 10, 15, and 20 bar BMEPs and PES of propane ranging from baseline (diesel only) to maximum

At low load (BMEP = 5 bar), as the PES of propane was increased, the first stage of heat release decreases while the second stage increases in magnitude. This shift from first stage to second stage is accompanied by a retardation of the combustion phasing (CA50) and a decrease in the combustion duration (CA10-90), as shown in Figure 7.2. As the PES of propane was increased, an increasing percentage of fuel was burned by flame propagation, thereby reducing the percentage of heat release early in the cycle.

However, heat release ends at approximately the same engine position, tapering off at approximately 25 DATDC. Therefore, combustion is both retarded and shortened in duration. This behavior results in low temperatures and bulk quenching, contributing significantly to high CO and THC emissions as well as low fuel conversion efficiency at high PES.

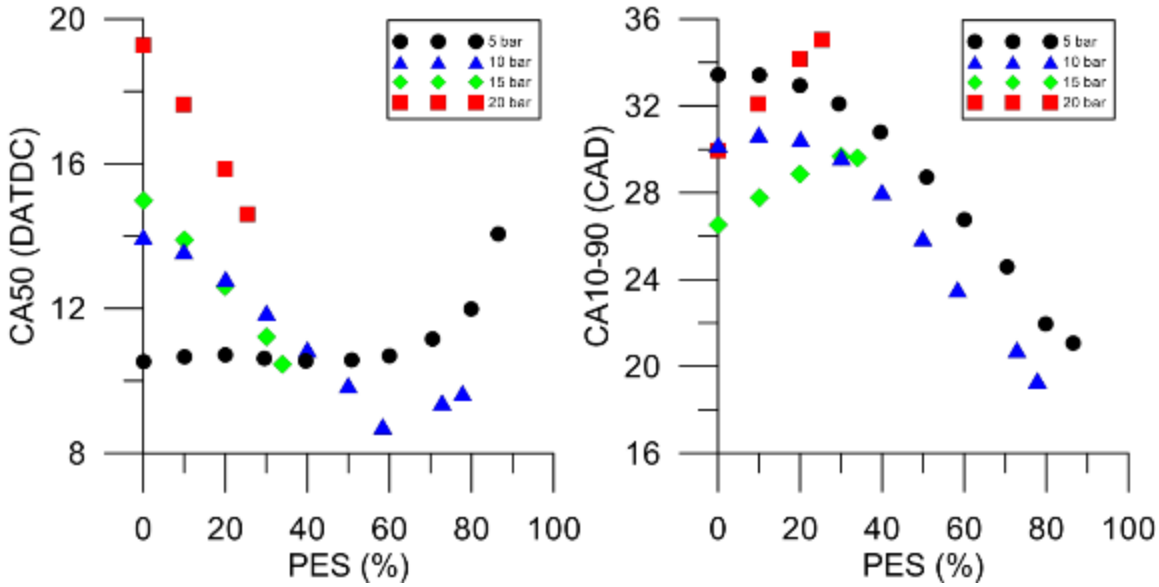

Figure 7.2 Combustion phasing (CA50) and duration (CA10-90) for diesel-ignited propane at 5, 10, 15, and 20 bar BMEP

At medium load (BMEP = 10 bar), a different trend was observed. As opposed to low load, the CA50 was advanced while the CA10-90 decreased. At this load, cylinder pressures were higher, causing increased bulk temperatures. As the PES of propane was increased, a larger portion of fuel was burned early in the cycle. This was caused by increased burn rates in the propane-air mixture due to the relatively high reactivity and laminar burning velocity of propane, resulting in advanced CA50 and decreased CA10-

90. At high PES of propane at 10 bar BMEP (PES > 60), the CA50 began to reverse its trend and retard. As the pilot quantity was reduced sufficiently in size, the initial heat release associated with the diesel-propane mixture retarded, however peak heat release rate continued to increase and CA10-90 continued to decrease.

At high loads (BMEP = 15 and 20 bar), a third trend was observed. As the PES of propane was increased, the CA50 advanced and the CA10-90 increased. At these high loads, bulk temperatures and fast propane burn rates prevented high PES operation due to excessive MPRR. Therefore, most of the heat release was due to diesel combustion. Also, at these loads, bulk temperatures were high enough to facilitate propane auto-ignition. As a result, increased PES of propane advanced the start of combustion while diesel injection regulated the end of combustion, causing CA50 to advance and CA10-90 to be increased.

7.3.1.2 Emissions and Performance

Two significant benefits for dual fuel combustion are improved NO_x and smoke emissions. However, low load conditions can result in increased CO and THC emissions. As shown in Figure 7.3, these trends follow mostly as expected. At almost all conditions, NO_x emissions are decreased or maintained and smoke emissions are reduced with sufficiently high PES of propane, while CO and THC emissions generally increase with PES, though more prominently at lower loads.

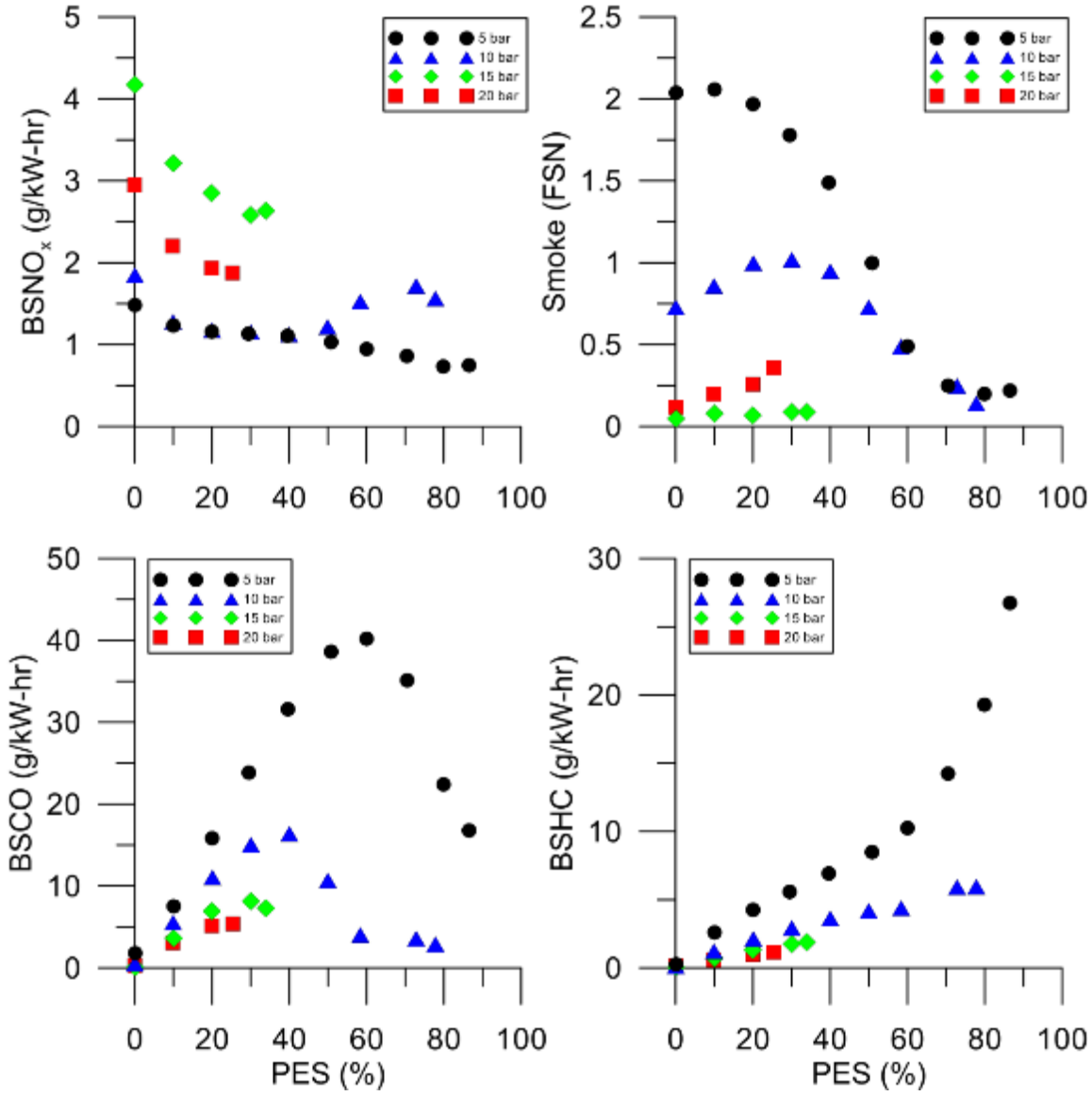

Figure 7.3 Brake-specific NO_x, smoke, brake-specific CO, and brake-specific HC emissions for 5, 10, 15, and 20 bar BMEP and PES ranging from baseline (diesel) to maximum

At 5 bar BMEP, low boost (1.62 to 1.58 bar) and high EGR rates (35%) were the reason for the high smoke associated with straight diesel operation. Oxygen concentration was low enough to inhibit soot oxidation while temperatures were not low enough to prevent its formation. Increasing the PES of propane reduced the size of the

diesel spray, which consequently reduced the size of the soot formation regions (locally rich areas) and smoke to low levels. Both CO and THC emissions initially increased steadily with PES, then CO emissions peaked and decreased while THC emissions increased at a higher rate. This behavior is likely due to both CO and THC competing for oxidation due to the high EGR rate and decreasing intake boost pressure; this behavior was previously noted by Shoemaker *et al.* [2012].

At 10 bar BMEP, trends similar to those at 5 bar BMEP were observed, however CO and THC emissions were considerably lower. At high PES, NO_x emissions increased slightly, however they were still below baseline diesel conditions. The increase in NO_x emissions was likely due to the very high heat release rates resulting in high local temperatures, which facilitated NO_x formation. Similarly, CO emissions decreased at these conditions, as CO oxidation requires high temperatures.

At 15 and 20 bar BMEPs, NO_x emissions are decreased while CO and THC increased less than lower load conditions. As PES is increased, shortened pilot injection duration (and smaller diesel sprays) contributed to the decrease in NO_x while high bulk temperatures kept CO and THC emissions relatively low. At 15 bar BMEP, smoke emissions were unchanged with increasing PES, however at 20 bar BMEP, smoke emissions increased. Due to the relatively long injection duration of pilot fuel at 20 bar, a considerable amount of fuel was injected during the expansion stroke, facilitating high exhaust temperatures and therefore soot oxidation. As the pilot injection duration was decreased, less fuel was injected in the expansion stroke, reducing exhaust temperatures, lowering intake boost pressure, increasing equivalence ratio, and reducing soot oxidation.

Fuel conversion efficiency and combustion efficiency trends are shown in Figure 7.4. The largest factors affecting FCE are the combustion efficiency, CA50, CA10-90, and pumping losses. Increasing PES of propane had the largest effect on combustion efficiency. As PES of propane was increased, lower local equivalence ratios yielded lower local temperatures which resulted in partial oxidation and bulk quenching of the propane-air mixture, and therefore higher CO and THC emissions, respectively. Because the propane fuel is incompletely burned, combustion efficiency suffers. These effects are more prominent at lower loads than higher loads due to lower bulk temperatures. As the load increased, the variable nozzle turbine of the turbocharger allowed for increased turbocharger efficiency, increasing intake boost pressure while minimizing pumping losses which remain relatively constant despite increasing air and fuel flowrates, as shown in Table 7.3. This resulted in an increase in FCE. The FCE also tracked with combustion phasing; as CA50 neared TDC, FCE increased and vice versa. This trend is most noticeable with increasing PES.

Table 7.3 Ranges of gross, pumping, and net IMEPs for constant BMEP conditions

BMEP (bar)	Gross IMEP (bar)	Pumping IMEP (bar)	Net IMEP (bar)
5	7.0 – 7.8	-0.6 – -0.5	6.4 – 7.3
10	12.4 – 12.0	-0.6 – -0.5	11.8 – 11.5
15	17.9 – 17.7	-0.7 – -0.7	17.2 – 17.0
20	23.4 – 23.2	-0.8 – -0.8	22.6 – 22.4

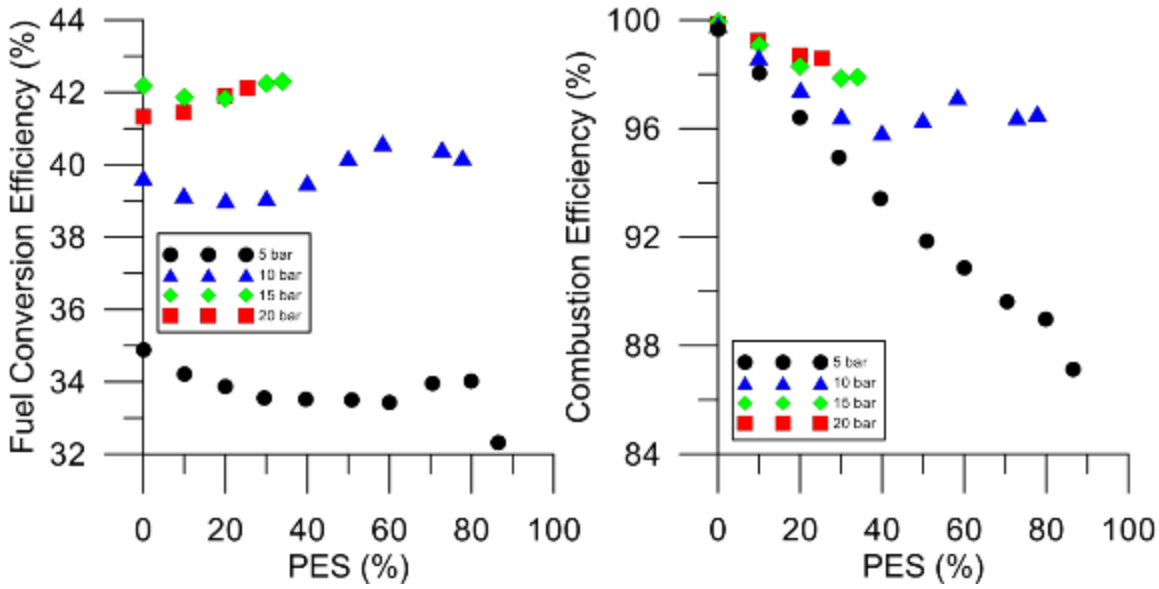

Figure 7.4 Fuel conversion efficiency and combustion efficiency for 5, 10, 15, and 20 bar BMEP and PES ranging from baseline (diesel) to maximum

7.3.1.3 Optimizing for the Maximum PES of Propane

7.3.1.3.1 Fueling Strategy

Based on the MPRR plot from the initial testing, shown in Figure 7.5, it was hypothesized that a higher PES of propane could be achieved at higher loads with a different fueling strategy. At 5 bar BMEP, the MPRR first increased then decreased as the PES of propane was increased. The initial increase in MPRR is due to the first stage of heat release; as the air-fuel mixture surrounding the initial diesel jet becomes more fuel-rich, the rate of heat release increases, causing higher MPRR. As the pilot quantity decreases at high PES, however, the initial heat release diminishes causing lower MPRR. At 10 bar BMEP, the MPRR increased until it exceeded the self-imposed operational limit of 15 bar/CAD as PES increased. The steeper increase in MPRR is related to the second stage of heat release and the relatively high reactivity of propane compared to

diesel. At 30 PES of propane, a shift in MPRR location occurs; at low PES MPRR occurs during the initial heat release while above 30 PES the MPRR occurs during the second stage of heat release. At a BMEP of 10 bar, higher pressures yield higher bulk temperatures, causing a sufficiently fuel-rich propane-air mixture to burn more quickly, yielding higher heat release rates. At 15 and 20 bar BMEPs, the shift in MPRR location from the first to second stage of heat release occurs progressively earlier in terms of increasing PES of propane.

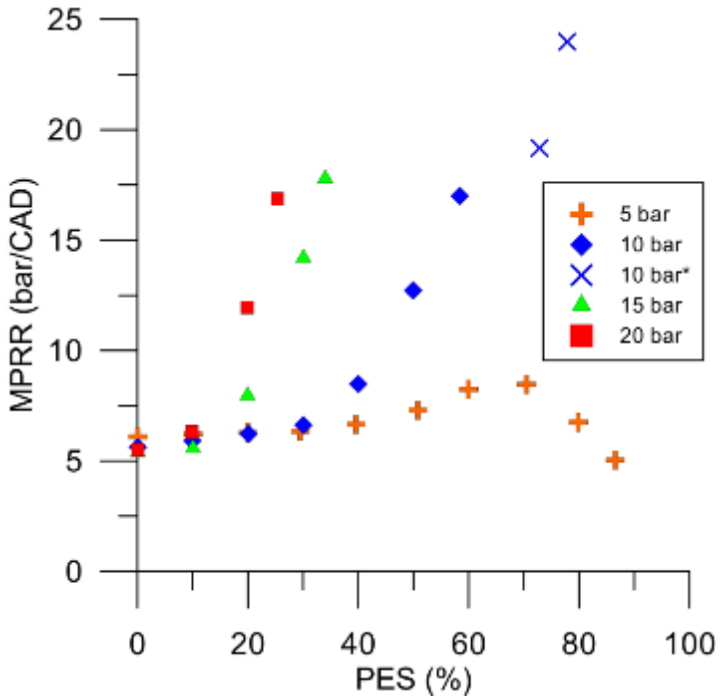

Figure 7.5 MPRR versus PES for 5, 10, 15, and 20 bar BMEPs; 10 bar* represents the operating conditions achieved by optimization

To suppress the high heat release rate at 10 bar BMEP and to increase the PES of propane, optimization of the fueling strategy was required. Instead of gradually

decreasing the pilot and increasing propane concentration while maintaining load at 10 bar BMEP, the operating conditions were achieved by first fixing the desired pilot quantity and then increasing propane fueling to reach the desired load. This strategy was chosen in an effort to reduce the pilot quantity, thereby reducing in-cylinder temperatures during transient operation while achieving the desired steady state operating point. By adopting this strategy, the maximum PES of propane at 10 bar BMEP was increased to 80 percent, as denoted by the "O" data points in Table 7.1. A decreased pilot quantity permitted a higher PES to be achieved, but the rapid rise in MPRR was only delayed. The maximum PES of propane was again limited by a high MPRR and excessive combustion noise due to rapid heat release. This operating condition might be viewed as quasi-steady because slight changes in operating conditions led to significant increases in MPRR during operation.

7.3.1.3.2 Fuel Injection Timing

To reduce the MPRR at 10 bar BMEP and 80 PES of propane, injection timing variations were investigated. Injection timings ranged from the stock timing, 8.6 degrees before top dead center (DBTDC), to 2.6 DBTDC in 1 degree increments. As the injection timing was retarded, the peak pressure reduced in magnitude until 6.6 DBTDC, as shown in Figure 7.6. The MPRR was decreased because MPRR location shifted back to the first stage of heat release; this is due to the second stage of heat release occurring later in the expansion stroke, resulting in lower peak pressures, lower bulk temperatures, and consequently lower fuel conversion efficiencies (FCEs). Retarding the injection timing beyond 6.6 DBTDC led to an increase and slight advance of the peak heat release rate. This trend is initially counter-intuitive, but retarding the injection created more

exhaust energy to be available to the turbocharger, increasing boost pressure and therefore bulk temperatures. Higher bulk temperatures resulted in faster heat release rates during the second stage of combustion associated with flame propagation. Once injection is sufficiently delayed (2.6 DBTDC), high intake boost pressures result in a second stage of heat release similar to that of 8.6 DBTDC. In turn, this results in a significant increase in MPRR because MPRR location is shifted back to the second stage of heat release, causing the "jump" shown in Figure 7.6 and limiting more retarded injection timings. Based on the MPRR / FCE tradeoff, an injection location of 6.6 DBTDC appears to be the optimal choice within this range of injection timings.

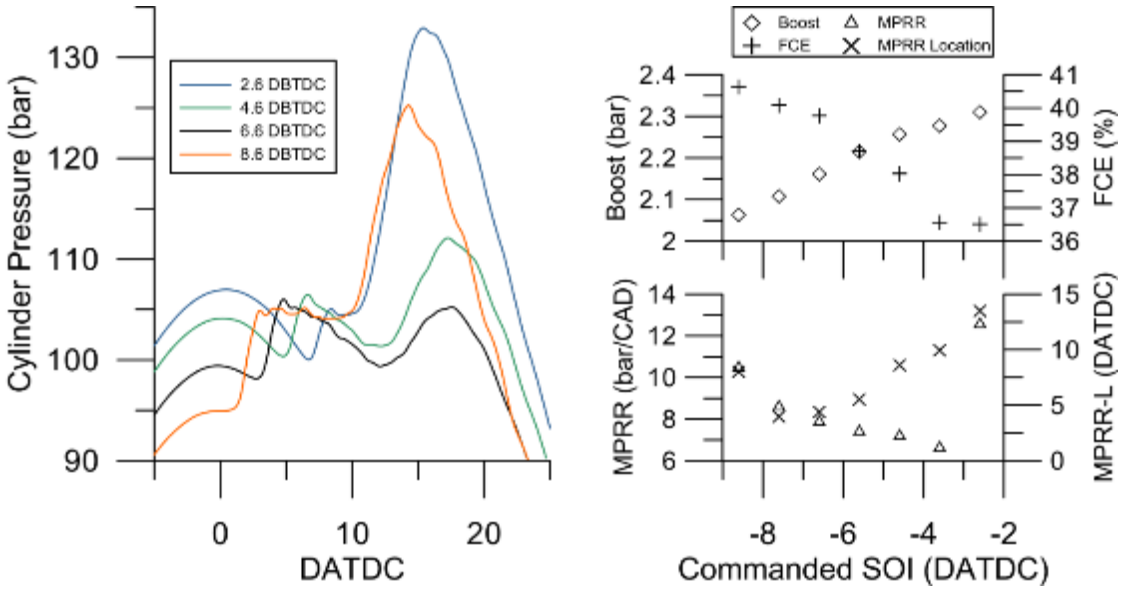

Figure 7.6 Cylinder pressure, MPRR, and FCE for a range of injection timings

BMEP = 10 bar, PES = 80 %, T_{in} = 26.8°C

7.3.2 Dual Fuel LTC Experiments

The second set of experiments targeted dual fuel LTC operation, utilizing early injection strategies similar to those used in ALPING combustion [Srinivasan 2003,

Krishnan 2004]. A schematic of the dual fuel LTC concept is shown in Figure 7.7. In this concept, a lean propane-air mixture is inducted during the intake stroke, during which an early pilot spray (e.g., 50 DBTDC) of diesel is injected. As compression progresses, the diesel fuel becomes spatially dispersed, creating few fuel-rich regions. Near compression TDC, the dispersed diesel pilot auto-ignites, creating distributed ignition centers. Since ignition occurs throughout the cylinder, the air-fuel mixture can burn more completely despite its lean state, providing better fuel conversion efficiencies. Lean combustion prevents the formation of particulate emissions due to a lack of fuel-rich regions and promotes low local temperatures, which in turn reduce NO_x emissions.

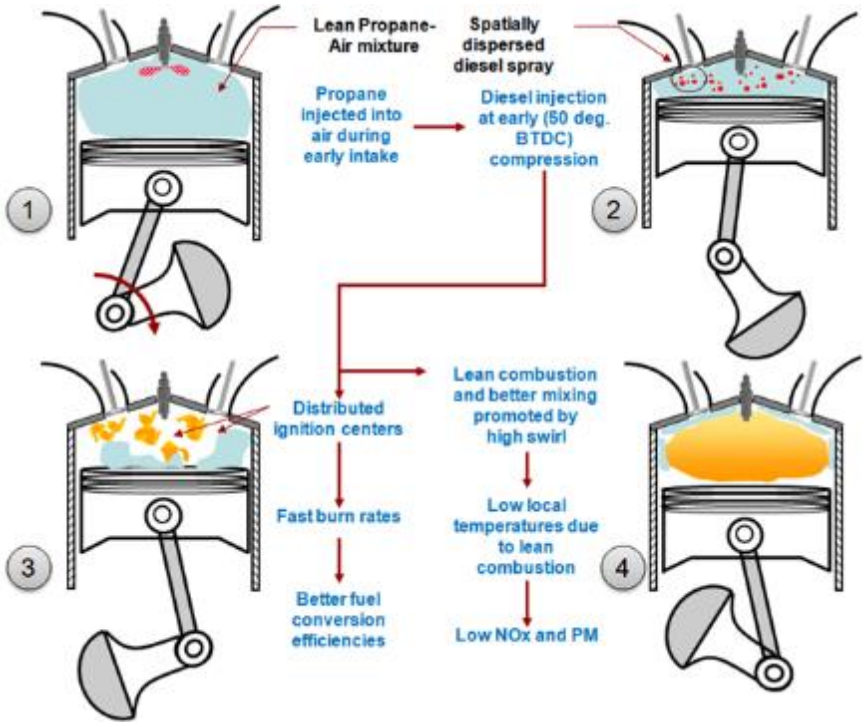

Figure 7.7 A schematic of the diesel-ignited propane dual fuel LTC concept

A full range of injection timings was investigated, extending from 50 DBTDC (earliest achievable with the MX10 engine) to 10 degrees DBTDC. In addition, a range of fueling strategies, i.e. varying the PES of propane, was investigated at 50 DBTDC. Finally, EGR rate and intake boost pressure were manipulated to increase the PES of propane at the injection timing of 50 DBTDC.

7.3.2.1 Dual Fuel LTC - Effects of Injection Timing

Based on the results from conventional dual fueling, a low load (BMEP = 5 bar), high PES (84%) condition was chosen to investigate dual fuel LTC. An injection timing sweep was performed, with the commanded start of injection (SOI) ranging from 50 DBTDC[1] to 10 DBTDC. Intake boost pressure (P_{in} = 1.88 bar), EGR rate (10.6%), and intake mixture temperature (T_{in} = 20.1°C) were kept constant. As shown in Figure 7.8, fuel injection pressure ranges from 100 to 400 bar at an SOI of 50 DBTDC. As SOI is retarded, the injection pressure range increases to approximately 100 to 900 bar at 30 DBTDC and 100 to 1100 bar at 10 DBTDC, requiring the injection duration to be decreased at SOIs of 30 and 50 in order to maintain the same flow of pilot fuel, engine load, and PES of propane. Also shown in Figure 7.8, the heat release rate profiles reveal the difference between the conventional and low temperature dual fuel combustion regimes. At a commanded SOI of 10 DBTDC, a short ignition delay is followed by an initial heat release associated with pilot ignition and then a very high rate of heat release as the remaining propane-air mixture is burned. At 30 DBTDC, the heat release profile

[1] The MX10 engine is equipped with electronic unit pumps (EUPs), which supply the injection fuel pressure. The EUPs are cam driven, and therefore sensitive to engine position. As injection timing is changed, the available fuel pressure also changes. Therefore, the earliest injection timing that was able to sustain pilot injection on the MX10 engine was found to be approximately 50 DBTDC.

resembles that of conventional dual fuel combustion, with two distinct heat release stages. The first stage is associated with the ignition of premixed pilot fuel followed by the propane-air mixture in and around the pilot flame, and the second stage is associated with flame propagation in the propane-air mixture. At an SOI of 50 DBTDC, the heat release rate is nearly sinusoidal, indicating a well-mixed pilot, distributed ignition centers, and uniform combustion.

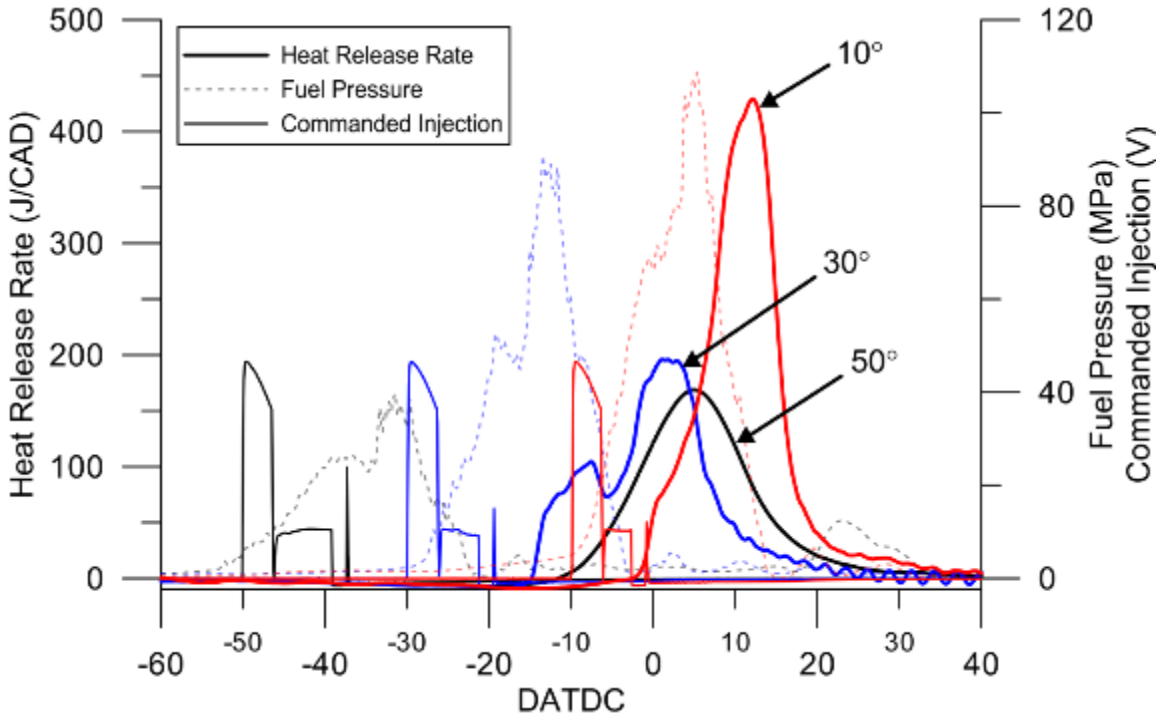

Figure 7.8 Dual fuel heat release rate, fuel pressure, and commanded injection profiles at commanded SOIs of 50, 30, and 10 DBTDC for 84 PES of propane

black: SOI = 50 DBTDC, blue: SOI = 30 DBTDC, red: SOI = 10 DBTDC; BMEP = 5 bar, N = 1500 RPM, EGR = 10.6%, P_{in} = 1.88bar, T_{in} = 20.1°C

The apparent ignition delay (ID_A) is shown along with COV of IMEP, MPRR, and combustion noise in Figure 7.9. As commanded SOI was advanced, ID_A increased, corresponding to a decrease in NO_x emissions with SOIs more advanced than 25

DBTDC. As the ID_A period neared 40 CAD, in-cylinder mixing of the diesel pilot was sufficient to prevent any high local temperatures and significant NO_x formation. At advanced SOIs, CA50 was delayed due to slower burn rates which resulted in increased COV of IMEP. The increase in COV of IMEP can be counteracted by increasing in-cylinder temperatures, thereby increasing burn rates. In this case, intake boost pressures were high enough, increasing in-cylinder pressures (and temperatures) to facilitate relatively low COV of IMEP even at an SOI of 50 DBTDC. As the SOI was advanced, the MPRR decreased considerably. Injection near TDC resulted in short ignition delays, low mixing, high local equivalence ratios, and high local temperatures; as a result, the very reactive propane-air mixture in and around the pilot burned very quickly, yielding very high peak heat release rates, high MPRR, and considerable combustion noise. However, as injection was advanced, ignition centers were increasingly distributed, having lower equivalence ratios and local temperatures. The smooth, nearly sinusoidal heat release peak indicates that the mixture is ignited almost volumetrically. As a result, pressure rise rates were relatively low, yielding little combustion noise.

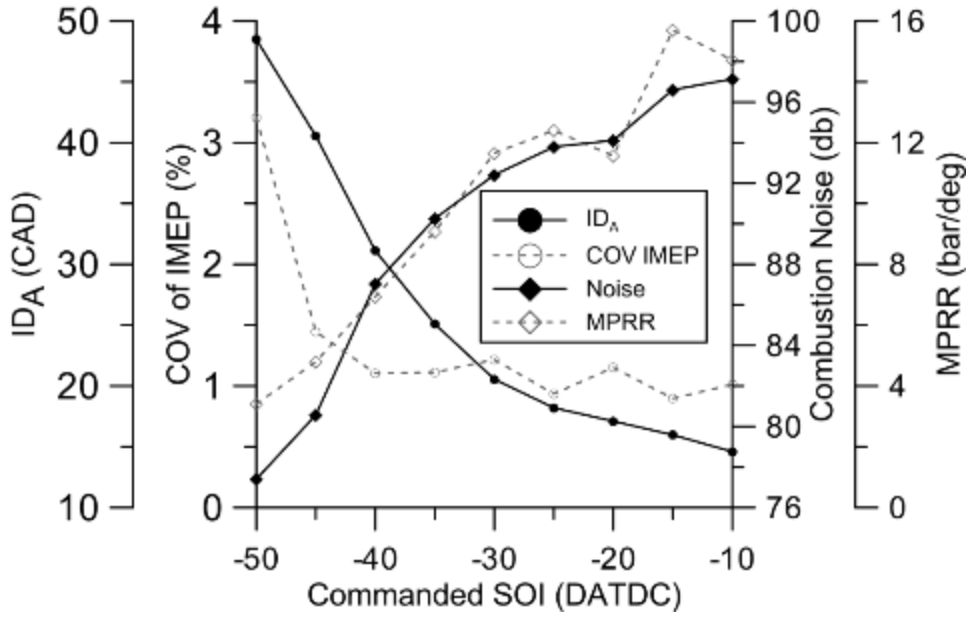

Figure 7.9 Apparent ignition delay, COV of IMEP, combustion noise, and MPRR vs. commanded SOI

BMEP = 5 bar, N = 1500 RPM, EGR = 10.6%, Pin = 1.88 bar, Tin = 20.1°C

To understand whether this combustion process is conventional dual fuel combustion or dual fuel LTC, the NO_x and smoke emissions were examined. All injection timings tested yielded lower NO_x and smoke emissions than the diesel baseline tests, shown in Table 7.4, however the injection timing did have a significant impact on NO_x emissions, as shown in Figure 7.10. At SOIs near TDC (SOI = 10 DBTDC), short ignition delay periods indicate the presence of a conventional diesel pilot spray. Albeit small, the pilot spray facilitated NO_x formation due to the existence of the diffusion flame, where temperatures are highest in conventional diesel combustion. As the SOI was advanced to 35 DBTDC, CA50 was advanced and CA10-90 increased; as CA50 neared TDC temperatures became higher, and longer residence times at higher temperature yielded increased NO_x emissions. However, as the commanded SOI was

advanced beyond 25 DBTDC, NO_x emissions decrease. Advancing the SOI increased the ignition delay period, which facilitates mixing. A sufficiently advanced pilot spray will lack the high local temperature regions necessary to facilitate NO_x formation. At 45 and 50 DBTDC, NO_x emissions drop to near-zero levels, even below the threshold required by the EPA 2010 NO_x restrictions. Despite little change in smoke emissions (as characterized by FSN) throughout the timing sweep, the particle size distribution changes considerably with injection timing, as shown in Figure 7.12. The normalized particle number concentration ($dN/dlogD_p$) is plotted versus particle size.[2] The most noticeable difference in size distribution is between the diesel baseline condition and the dual fuel conditions; the diesel baseline condition produces more particles in both the nucleation and accumulation mode regimes[3], also related by the higher FSN. As injection timing is advanced, the peak particle number concentration decreases. Longer ignition delays provide for better mixing and fewer fuel-rich areas, preventing initial soot formation. This change is likely not indicated by FSN trends because larger particles have a more significant effect on FSN, having a greater chance to be trapped in the filter paper, and the number of larger particles at each injection timing (greater than 100 nm) varies far less than the number of smaller particles. Particles in the nucleation mode remain relatively unchanged in the dual fuel combustion mode, regardless of injection timing but

[2] Because the number of particle sizing bins in a given instrument is finite, the $dN/dlogD_p$ metric is used to normalize the particle concentration in a given bin by the bin size, allowing comparison between different instruments utilizing different numbers of bins [TSI 2012]. For example, if a 64 channel scanning mobility particle sizer (SMPS) was used which spanned the same overall particle size range of the EEPS, a regular distribution would peak at a lower value than the 16 channel EEPS because approximately one quarter of the number of particles would exist in each given bin of the SMPS.

[3] Conventional diesel combustion has been shown to produce soot with a log-normal distribution of 20-300 nm diameter particles in a mixture containing solid and semivolatile fractions [Harris and Maricq 2001], which are referred to as accumulation mode particles. In addition, cooling of the exhaust can cause semivolatile materials to nucleate, producing smaller diameter "nucleation mode" particles.

are significantly fewer in number than the nucleation mode particles resulting from baseline diesel combustion.

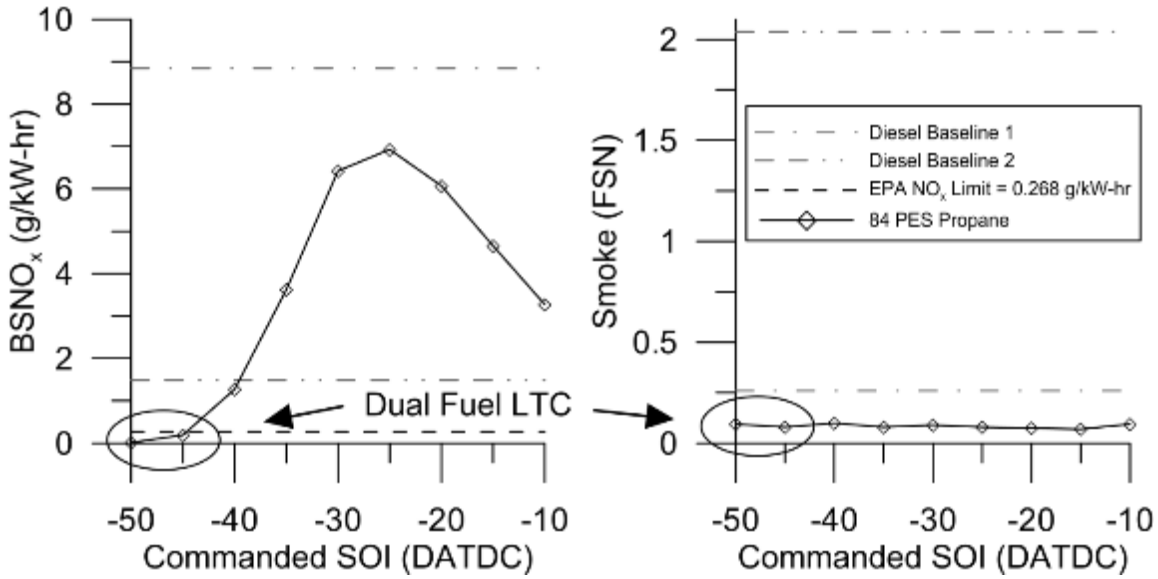

Figure 7.10 Brake-specific NO_x and smoke emissions vs. commanded SOI for 84 PES of propane, diesel baseline 1, and diesel baseline 2

BMEP = 5 bar, N = 1500 RPM, EGR = 10.6%, P_{in} = 1.88 bar, T_{in} = 20.1°C

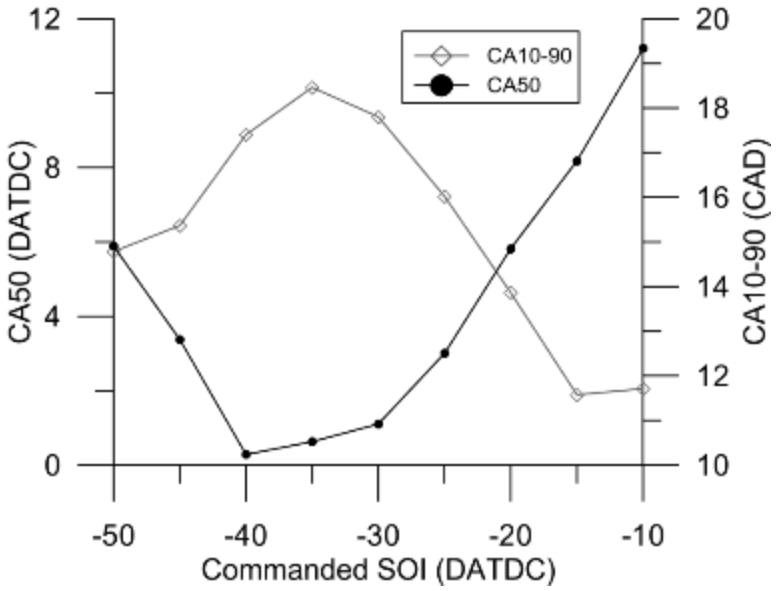

Figure 7.11 Combustion phasing and combustion duration vs. commanded SOI for 84 PES of propane

BMEP = 5 bar, N = 1500 RPM, EGR = 10.6%, P_{in} = 1.88 bar, T_{in} = 20.1°C

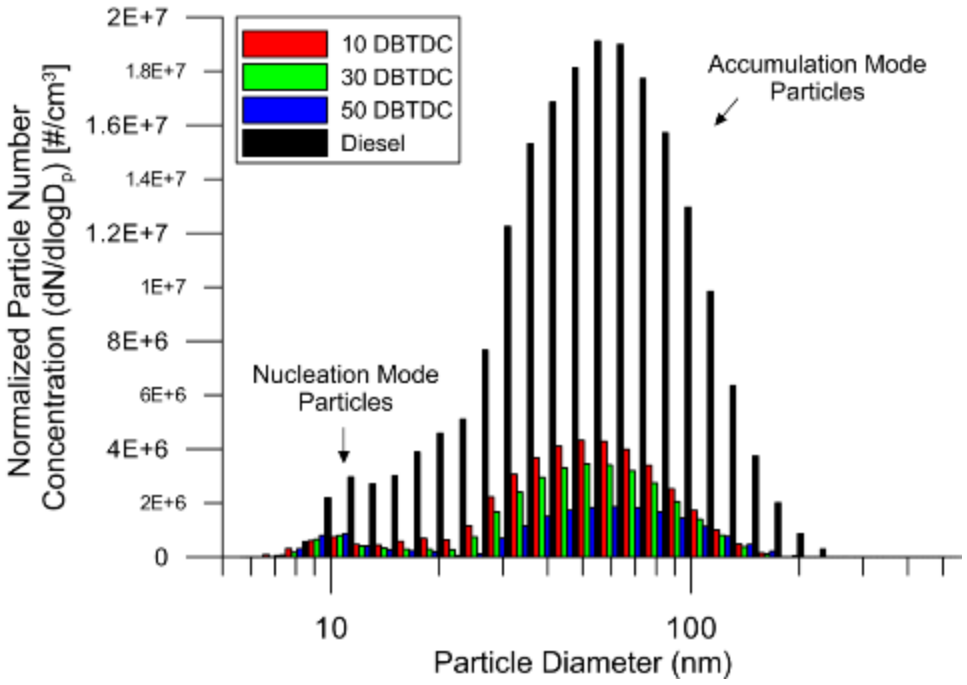

Figure 7.12 Normalized particle number size distribution for 84 PES of propane and diesel baseline

BMEP = 5 bar, N = 1500 RPM, EGR = 10.6%, P_{in} = 1.88 bar, T_{in} = 20.1°C

Table 7.4 Diesel-only baseline conditions 5 bar BMEP

	BMEP (bar)	Intake Boost Pressure (bar)	EGR Rate (%)	$BSNO_x$ (g/kW-hr)	Smoke (FSN)
Baseline 1	5	1.89	10.9	8.84	0.26
Baseline 2	5	1.66	35.5	1.48	2.04

Note: Unlike baseline 1, baseline 2 does not match the intake boost pressure and EGR conditions used for all other points in the injection timing sweep; it is included for completeness in terms of potential baseline diesel operation

Brake-specific hydrocarbon emissions and fuel conversion efficiency both varied considerably with injection timing. Plots of $BSNO_x$-BSHC and $BSNO_x$-FCE tradeoffs are shown in Figure 7.13. The reference baseline diesel condition is also shown in each plot. The $BSNO_x$-BSHC tradeoff shows that hydrocarbons were minimized at an SOI of approximately 35 DBTDC; however, BSHC emissions remained fairly constant from an SOI of 30 DBTDC to 50 DBTDC. The $BSNO_x$-FCE tradeoff shows a similar, though opposite trend with FCE; FCE was maximized at an SOI of approximately 40 DBTDC, but remained fairly constant from an SOI of 30 DBTDC to 50 DBTDC. A similar $BSNO_x$-FCE tradeoff plot is observed by Krishnan *et al.* [2004] for ALPING combustion. These tradeoff trends are likely related; decreasing combustion efficiency at early injection timings yields high THC emissions, leaving potential fuel chemical energy to be expelled in the exhaust, transferring less energy to the piston, and decreasing fuel conversion efficiency. This trend is reinforced by the combustion efficiency, propane, and formaldehyde emissions shown for the range of injection timings in Figure 7.14. As injection timing was advanced, combustion efficiency initially increased, then decreased; similarly, propane (a combustion product) and formaldehyde (an intermediate species known for its toxicity) initially decreased and then increased. Based on these trends, it is

clear that NO_x emissions can be greatly reduced with an advanced pilot injection with little or no compromise in FCE or THC emissions.

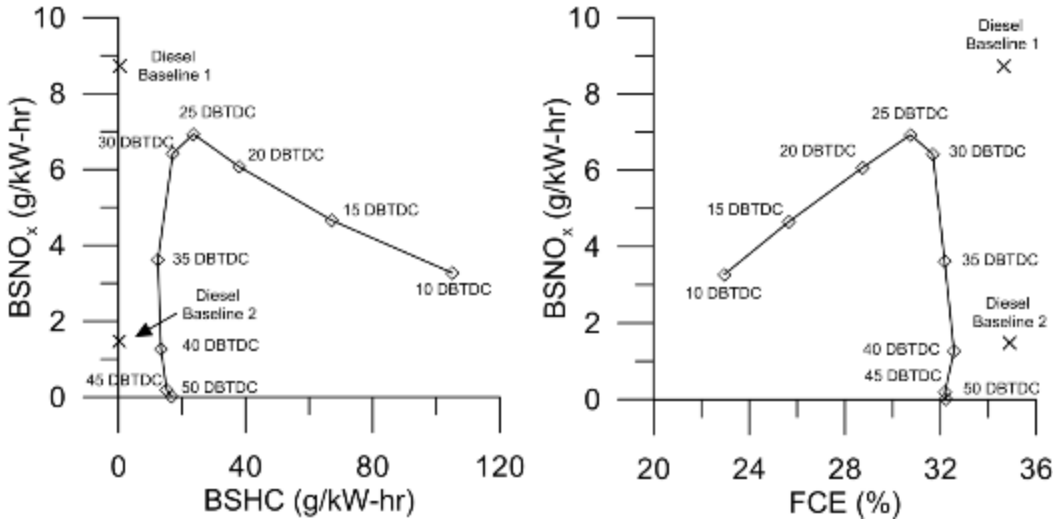

Figure 7.13 Brake-specific NO_x vs. brake-specific HC and fuel conversion efficiency for 84 PES of propane, diesel baseline 1, and diesel baseline 2

BMEP = 5 bar, N = 1500 RPM, EGR = 10.6%, P_{in} = 1.88 bar, T_{in} = 20.1°C

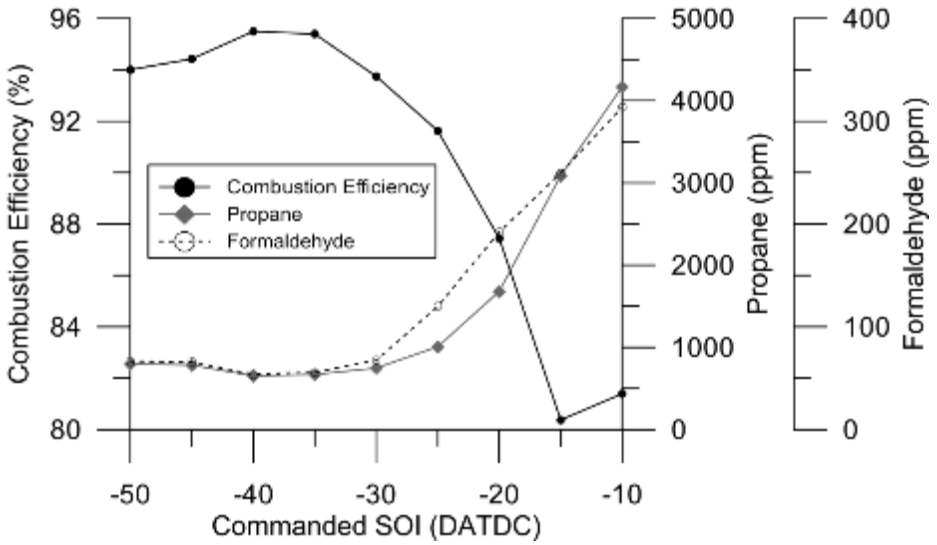

Figure 7.14 Combustion efficiency, propane, and formaldehyde emissions for 84 PES of propane

BMEP = 5 bar, N = 1500 RPM, EGR = 10.6%, P_{in} = 1.88 bar, T_{in} = 20.1°C

7.3.2.2 Dual Fuel LTC - Effects of PES, Intake Boost Pressure, and EGR Rate

A low load (BMEP = 5 bar), early injection timing (SOI = 50 DBTDC) operating condition was chosen to investigate the effects of primary fuel concentration, intake boost pressure, and EGR rate on dual fuel LTC. Three sets of heat release rates and cylinder pressure histories are shown in Figure 7.15. The first (top) set relates a progression in PES of propane from 65 to 84 percent at a constant intake boost pressure (P_{in} = 1.57 bar) and EGR rate (35%). The lowest PES of propane, 65 percent, exhibited signs of incipient knock, related by the high-frequency oscillations in pressure. This is due to the large pilot quantity required for 65 PES conditions, increasing the auto-ignition properties of the well-mixed fuel-air charge, facilitating advanced combustion phasing, even before TDC. The rapid pressure rise results in an apparent acoustic resonance leading to light knock. As PES is increased, the resistance of the air-fuel mixture to auto-ignition is increased, the CA50 is retarded, the MPRR decreases, and knock is diminished. In fact, the MPRR varies almost inversely to CA50, as shown in Figure 7.16. For the first data, the COV of IMEP increased as PES increased to 11.1 percent at 84 PES. The increase in COV of IMEP is a result of combustion phasing retarding with increasing PES of propane. To suppress increasing combustion variability, the intake boost pressure was increased and the EGR was decreased, as shown in the second (middle) set of Figure 7.15 for a PES range of 84 to 89 percent. Because neither boost pressure nor EGR are simulated, the two variables are not independent, limiting analysis of each variable independently. As the EGR valve is closed, more exhaust energy is available to the turbine, increasing boost pressure and vice versa. Changing the VNT position to counteract changes in intake boost pressure alters exhaust manifold pressure, which also

affects the EGR rate. The overall effect of changing intake boost pressure and EGR rate simultaneously is a compounded effect on oxygen availability, so small changes can be significant to the combustion process. As boost is increased and the EGR is decreased, increased bulk temperatures advance combustion phasing, facilitating consistent burn rates and decreasing COV of IMEP. In addition, the COV of IMEP and combustion duration appear to vary somewhat proportionally, indicating that faster burn rates facilitate stability. With the COV of IMEP sufficiently decreased, the PES of propane can be increased but deteriorating FCEs deter PES higher than 93 percent. Heat release rate profiles at the high boost condition are shown in Figure 7.15 (bottom). Fuel conversion efficiencies are low at very high PES due to very lean conditions; as the pilot quantity decreases, flame propagation must take a larger role in order to sustain combustion efficiency. Despite the high bulk temperatures, bulk quenching results from very lean equivalence ratios (ϕ = 0.3), resulting in poor combustion efficiency and poor fuel conversion efficiency. Fuel conversion efficiency is highest at 77 PES when CA50 is phased nearest to TDC and equivalence ratio is sufficiently high to maintain reasonably high combustion efficiencies (96 percent).

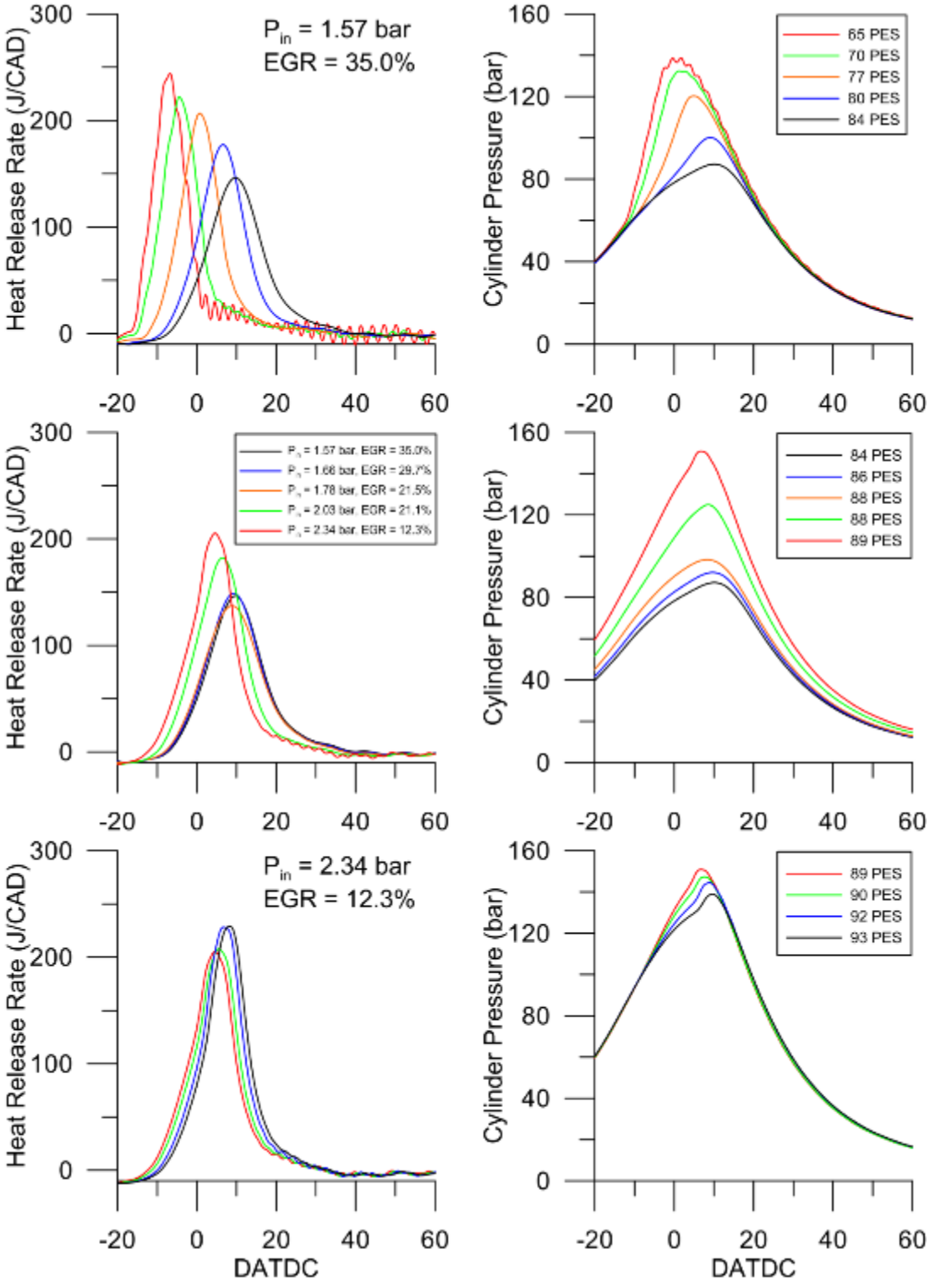

Figure 7.15 Heat release rate and cylinder pressure vs. engine position for a range of PES of propane at a commanded SOI of 50 DBTDC

BMEP = 5 bar, N = 1500 RPM

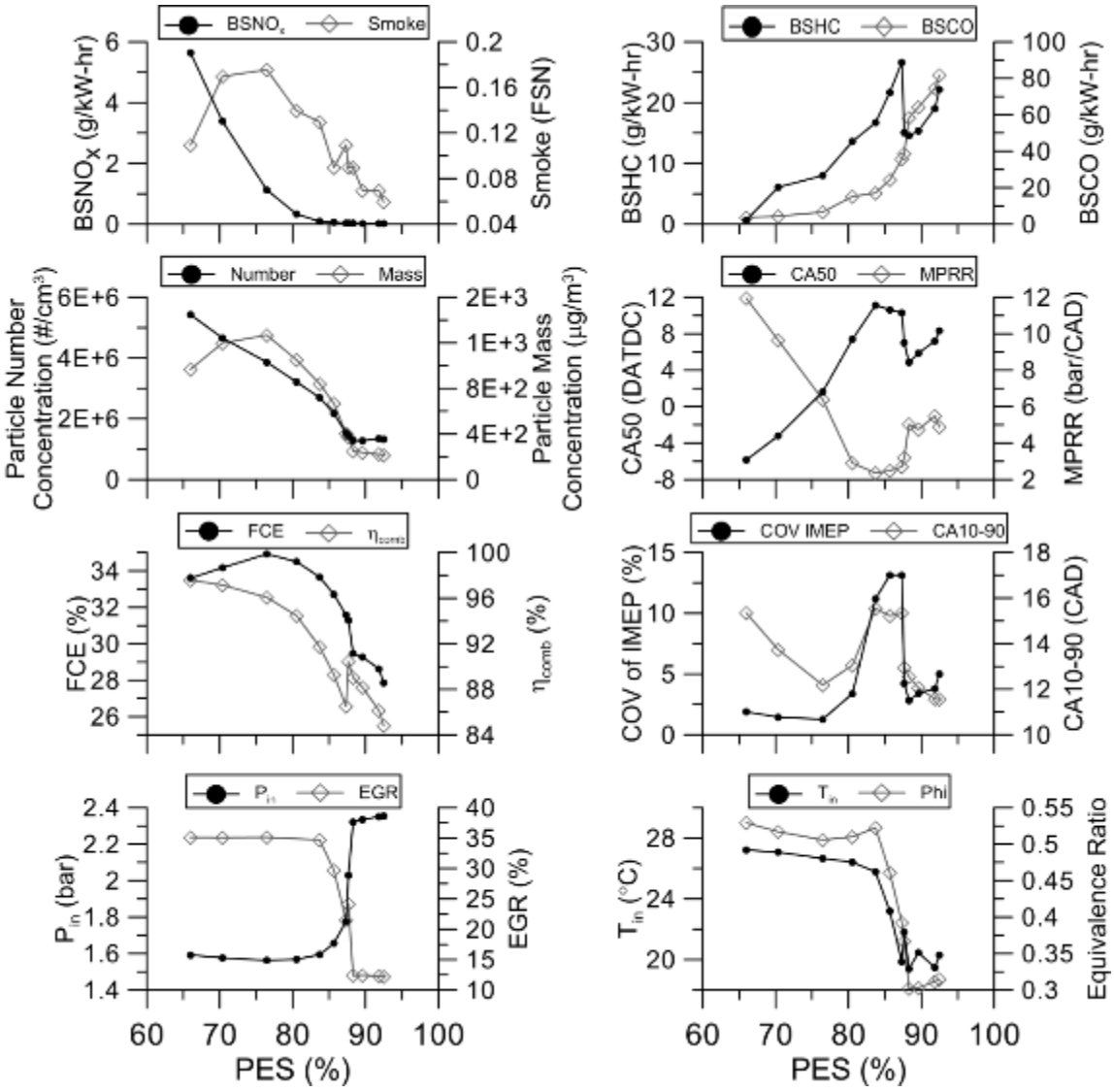

Figure 7.16 Emissions, performance, and combustion metrics for a range of PES of propane at a commanded SOI of 50 DBTDC

BMEP = 5 bar, N = 1500 RPM

As the PES of propane is increased, the pilot quantity decreases resulting in a corresponding decrease in NO_x emissions, reaching near-zero values at 84 PES of propane. Trends for smoke and particulate mass concentration vary similarly; because particles in the nucleation mode are mostly volatile [Kittelson 1998], they do not get trapped in the filter paper, having little effect on FSN. Instead, particles in the

accumulation mode, which are larger and predominantly dictate particle mass, are trapped and increase FSN. Therefore, FSN decreased at very high PES.

Carbon monoxide emissions increase moderately at first, but increase significantly as the intake boost pressure is increased. Unburned hydrocarbon emissions increase steadily until intake boost pressure is increased, where a significant decrease in THC emissions is observed. These trends are related due to an increase in bulk temperatures at higher boost pressures. Increased temperatures facilitate the initial breakdown of more of the hydrocarbon fuel (propane), but bulk temperatures are not high enough to facilitate complete CO oxidation.

7.4 Conclusions

Conventional and low temperature dual fuel combustion was characterized experimentally with two sets of experiments for diesel-ignited propane combustion in a 12.9-liter MX10 heavy duty diesel engine (with open architecture Drivven controller) at a constant engine speed of 1500 rpm. The first set of experiments utilized stock control parameters, varying PES of propane at the constant BMEP conditions of 5, 10, 15, and 20 bar. At 10 bar BMEP, fueling strategy and injection timing were optimized to increase the maximum achievable PES and to limit MPRR. The second set of experiments was performed using early injection LTC strategies. Injection timing and PES sweeps were completed. Analysis of the results obtained led to the following important conclusions:

1. A high PES (86%) of propane at low load, high EGR, low boost operation (BMEP = 5 bar, EGR = 35%, P_{in} = 1.6 bar) yielded significant improvement in smoke emissions. Carbon monoxide and THC emissions increased with PES at a higher rate at low load than high load; a

competition for oxidation was observed between CO and THC emissions at high PES, likely as a result of the low O_2 concentrations due to high EGR rates and low intake boost pressure.

2. At sufficiently high load (BMEP = 15 and 20 bar), the combustion duration (CA10-90) increased with increasing PES due to auto-ignition of the propane-air mixture and sustained injection duration (due to low PES). In addition, CA50 was advanced, yielding very high MPRR which prevented high load operation at PES values higher than 35% at 15 bar BMEP and 25% at 20 bar BMEP.
3. At a load of 10 bar BMEP, the maximum achievable PES of propane was increased by optimizing the fueling strategy. By starting with a low, pre-calculated pilot quantity and increasing the propane flow rate to reach the desired load, high MPRRs were avoided during transient operation. Despite optimizing the fueling strategy, high MPRR (>15 bar/CAD) limited the maximum PES value to 80%. Retarding the injection timing resulted in a minimum MPRR at an SOI of 6.6 DBTDC with minimal FCE loss tradeoff. Further retardation of SOI resulted in increased MPRR and decreased FCE.
4. Diesel-ignited propane dual fuel LTC was achieved at BMEP = 5 bar using an SOI greater than 45 DBTDC and a PES of propane of about 84 percent. At these conditions, NO_x emissions ($BSNO_x$ = 0.019 g/kW-hr) were below EPA 2010 restrictions, and smoke emissions were very low (FSN = 0.09). At a constant PES of 84 percent, fuel conversion efficiency

and THC trends were shown to be fairly insensitive at SOIs greater than 30 DBTDC, but more retarded SOIs yielded poor FCEs and THC emissions. High PES operation was limited by an increasing COV of IMEP due to low bulk temperatures as a result of retarded CA50.

5. Dual fuel LTC was optimized for high PES of propane operation (up to 93 percent) at an SOI of 50 DBTDC and 5 bar BMEP using increased boost and decreased EGR rate to increase bulk temperatures, advance CA50, and decrease the COV of IMEP. Knock was observed at 65 PES due to apparent acoustic resonance caused by excessive pressure rise rate. However, FCE suffers due to poor combustion efficiency at increasing PES of propane; despite high bulk temperatures at increased boost, lean conditions (ϕ = 0.3) facilitate bulk quenching, resulting in very high CO and THC emissions.

CHAPTER VIII

SUMMARY AND RECOMMENDATIONS FOR FURTHER RESEARCH

8.1 Summary

This study has examined conventional and low temperature dual fuel combustion using either propane or methane as primary fuels and diesel as a pilot fuel for potential improvement of engine-out emissions and increased utilization of alternative fuels. Increased emissions regulations have driven the search for improved modes of combustion and dual fuel combustion shows significant potential in this regard. The conventional dual fuel combustion mode requires little engine modification and can simultaneously reduce NO_x and smoke emissions. Increased CO and THC emissions are a potential side effect, but can be treated using cheap oxidation catalysts, given adequate exhaust temperature for light-off. While requiring more control than conventional dual fuel combustion, dual fuel LTC offers improved NO_x emissions and higher percent energy substitution (PES) by primary fuel. The primary goal of implementing, optimizing, and assessing dual fuel LTC was achieved using diesel-ignited propane in the MX10 heavy-duty diesel engine. The following experimental investigations and analyses led to the completion of this goal.

In the first experimental investigation, a light-duty 1.9L Volkswagen TDI engine was used to perform conventional dual fuel experiments using diesel-ignited methane and diesel-ignited propane. The engine had a wastegated turbocharger for intake boost

pressure control and no EGR. Engine-position resolved pressure measurements were obtained and heat release rate analyses were performed. Two sets of experiments were performed; the first experiment utilized constant pilot quantities and varying overall equivalence ratio and the second experiment examined various PES of primary fuel at four different constant-BMEP conditions. In both cases, the PES of primary fuel was limited by engine instability due to cyclic variability in IMEP at low loads and excessive pressure rise rates and the incidence of knock at high loads.

The first analysis concentrated on dual fuel ignition delay behavior for various concentrations of primary fuel. The length of the ignition delay period is important as it determines the amount of fuel-air mixing before ignition occurs which can have a significant effect on the ensuing combustion process, especially in LTC applications. Results indicated that with a constant but large pilot quantity, increasing propane concentration will decrease ignition delay. A sufficiently high overall equivalence ratio may facilitate spontaneous auto-ignition of propane even before diesel injection. A cycle-by-cycle analysis shows that for a constant pilot quantity, cyclic variations in the start of combustion increased as propane concentration increased. A similar analysis of diesel-ignited methane combustion revealed very few cyclic variations of the SOC as methane concentration increased. Different ignition delay trends were observed at low and high constant BMEP conditions with increasing PES of propane; at low BMEPs, the ignition delay increased to a maximum and then decreased as engine instability increased. At high BMEPs, increasing PES of propane shortened the ignition delay period. At low BMEPs, cyclic variability of both diesel-ignited methane and diesel-ignited propane increased with increasing PES.

In the next analysis, diesel-ignited propane and diesel-ignited methane dual fuel combustion in the light-duty Volkswagen engine were characterized based on heat release rate profiles and metrics such as combustion phasing (CA50) and combustion duration (CA10-90), as related to performance and emissions results. At low pilot quantities, it was shown that diesel-ignited propane and diesel-ignited methane combustion behave similarly, although propane exhibits slightly faster combustion, likely due to its higher laminar burning velocity. With a larger fixed pilot quantity, propane addition advanced the combustion phasing and the peak AHRR increased while increased methane concentration resulted in a retarded or constant combustion phasing. It was shown for all fixed-pilot conditions that, as gaseous fuel concentration was increased, NO_x emissions decreased or remained constant while smoke emissions increased. The CO and THC emissions increased with increasing primary fuel concentration at low loads and decreased as pilot quantity was increased. Overall, diesel-ignited propane combustion yielded higher CO, lower THC, and slightly higher FCE than diesel-ignited methane combustion, which is attributed the fuel properties of propane. At high constant BMEP conditions, the same differences were observed in diesel-ignited propane and diesel-ignited methane combustion. As methane concentration was increased, ignition delay increased which is attributed to oxygen displacement and chemical effects present with the high methane fueling rates needed to achieve high PES operation. Increasing concentration of propane decreased ignition delay, transforming the conventional two-peak heat release profile into a single, early AHRR peak of substantially higher magnitude. This behavior of diesel-ignited propane combustion indicates a departure

from the classical interpretation of dual fuel combustion, instead resembling a "diesel-regulated HCCI-like" process.

In the second experimental investigation, a heavy-duty 12.9L MX10 diesel engine was used to perform conventional and low temperature dual fuel experiments using diesel-ignited propane. The engine had a VNT turbocharger for intake boost pressure control and a cooled EGR loop. The MX10 engine was controlled using a Drivven open-architecture controller, which provided much better control of all engine parameters compared to the OE ECM of the VW engine. Engine-position resolved pressure measurements were obtained and heat release rate analyses were performed. Two sets of experiments were performed; the first experiment utilized stock control parameters to examine various PES of propane at four different constant-BMEP conditions and the second experiment utilized very early injection timings and high PES of propane to implement and optimize dual fuel LTC at 5 bar BMEP.

The first analysis examined conventional dual fuel combustion using diesel-ignited propane on the MX10 engine. Results revealed that higher PES of propane operation was possible before knocking conditions were encountered on the MX10 than the VW TDI while at equivalent loading conditions (BMEPs). This is likely a result of a lower geometric compression ratio for the MX10 engine and the presence of a cooled EGR loop. A high PES of propane operation at low load yielded significant improvement in smoke emissions over the stock operation. As with the VW engine, the CO and THC emissions increased with PES, more so at lower loads than at higher loads. A competition for oxidation was observed between CO and THC emissions, likely as a result of low O_2 concentration at 5 bar BMEP. At a sufficiently high load, the

combustion duration increased with increasing PES due to auto-ignition of the propane-air mixture prior to diesel injection. Subsequently, CA50 was advanced yielding very high MPRR and combustion noise, thereby preventing operation at higher PES. Since a high MPRR was the primary limitation of high PES operation, the fueling strategy and injection timings were optimized at 10 bar BMEP which led to an increase from 60 to 80 PES of propane and a decrease in MPRR.

Finally, dual fuel LTC was implemented and examined using very early injection strategies similar to ALPING combustion [Srinivasan 2003] at 5 bar BMEP. At an SOI of 50 DBTDC and PES of 84 percent propane, engine-out NO_x emissions ($BSNO_x$ = 0.019 g/kW-hr) were decreased below the EPA 2010 emissions regulatory limit (0.268 g/kW-hr) without a sacrifice in smoke emissions (smoke = 0.09 FSN). Fuel conversion efficiency was slightly greater than 32 percent at this condition and proved to be relatively insensitive to injection timings until 30 DBTDC. Increasing the PES of propane above 84 percent was limited by an increasing COV of IMEP, which was 11 percent at this condition. Finally, dual fuel LTC was optimized for high PES operation (up to 93 percent) at an SOI of 50 DBTDC and 5 bar BMEP. Increased boost and decreased EGR was used to increase bulk temperatures, advanced CA50, and decrease the COV of IMEP. However, FCE suffered due to poor combustion efficiencies, likely resulting from very lean conditions (ϕ = 0.3). Higher intake mixture temperatures along with higher equivalence ratios may improve the FCE at high PES operation, but high MPRR and knock may be a concern.

8.2 General Recommendations

Based on the present study, it is clear that the dual fuel LTC concept has the potential to drastically reduce engine-out emissions and utilize alternative fuels. In fact, a very wide range of alternative and renewable fuels could be utilized with this concept provided one fuel is a high cetane fuel directly injected into the cylinder and the other is a low cetane fuel. Fueling systems could be adapted to the type(s) of fuel available domestically for a given region, or the needs of a particular application, i.e. automotive vs. stationary engine. Fuel storage is a concern with mobile applications, and volumetrically energy dense fuels such as gasoline and diesel are preferred. As fossil fuel resource concerns become increasingly prominent, renewable alternatives such as ethanol (low cetane) and biodiesel (high cetane) are suitable alternatives. In addition, the fuel properties of these two fuels will likely lend to improved operation of the dual fuel LTC concept. Ethanol has a higher resistance to knock than propane, potentially allowing higher PES operation; biodiesel typically has a higher cetane number than normal diesel, which may improve HC and CO emissions with faster burn rates. It is unlikely that any one (or two) fuels will ever satisfy all power-generation needs; therefore, continued research into many alternative and renewable fuels that meet the criteria necessary for conventional and low temperature dual fuel combustion is recommended.

8.3 Project-Specific Recommendations

8.3.1 Hardware Modifications on the MX10 Engine

There are several hardware modifications that have the potential to improve conventional dual fuel operation using diesel-ignited propane at high PES. Slightly lower

compression ratios (CR = 15) would decrease peak pressures, reducing the potential for knock at high loads while maintaining high efficiency operation. Similarly, a modified valve train utilizing a late intake valve closing time could reduce the effective compression ratio while maintaining good volumetric expansion ratios, characteristic of a high geometric compression ratio. However, both of these recommendations would require extensive engine modification.

The method of propane introduction has room for improvement. As propane was introduced upstream of the turbocharger, the compressor had to do extra work re-compressing propane, reducing turbocharger efficiency. By the same effect, oxygen displacement occurred as the flow rate of propane was increased. Introducing propane after the compressor may be advantageous in this regard. In addition, the potential negative side effects of fumigation during transient operation should be investigated. Since fumigation took place far upstream of the cylinders, a considerable lag may be noticed during transient operation. Port fuel injection (PFI) near the intake valves has the potential to solve both of these issues, but may require some engine modification. Liquid propane PFI or direct injection (DI) are more ambitious injection strategies, but would yield similar improvements as well as potential advantages of their own. Injecting liquid propane in the intake manifold or directly into the cylinder would have a significant charge cooling effect due to evaporation of the propane. Cooler charge temperatures would prevent the onset of knock, allowing higher compression ratio operation. Similar to gasoline direct injection strategies, a propane DI system would also allow for in-cylinder fuel stratification, further preventing the onset of knock and allowing even higher compression ratio operation.

A major limiting factor during dual fuel LTC operation was the diesel injection system. While the EUP system provides many advantages in terms of reliability and rapidly adjustable fuel pressures, it also causes many challenges in terms of early injection timing and separating the injection timing and injection pressure variables. A modern common-rail direct injection fuel system would enable the investigation of injection timing earlier than 50 DBTDC and provide steady fuel injection pressures.

8.3.2 Dual Fuel LTC – Investigate Intake Mixture Temperature Effects

An experimental investigation of the effects of intake mixture temperature could be very beneficial to the improvement of FCEs during high PES dual fuel LTC operation at low loads. If high bulk temperatures can be achieved with sufficiently high equivalence ratios, combustion efficiency might be significantly improved, decreasing CO and THC emission and increasing FCE. Potential negative side effects are high MPRR and knock and potentially higher NO_x emissions; however, these may be avoided through the use of diluents such as EGR. In fact, one mechanism for increasing the intake mixture temperature is uncooled (hot) EGR, however some modification would be required to implement this on the MX10 engine.

8.3.3 Dual Fuel LTC – Utilize Multiple Injections to Control Combustion Phasing

Because the injection and ignition events in dual fuel LTC are separated, there is some control over the combustion event due to the fuel injection itself and the fuel mixture auto-ignition properties. A potential advantage of the EUP fuel system is the ability to have multiple injections during the same combustion cycle at drastically different injection pressures. An early injection could utilize a low injection pressure,

minimizing wall impingement, while a high pressure, late injection event takes place near TDC. Therefore, a strategy utilizing both early and late LTC injection strategies has the potential to significantly reduce emissions while adequately controlling combustion phasing, allowing higher load conditions. A potential challenge with this strategy will be facilitating the necessary mixing after the late injection event to prevent NO_x and soot formation. Typically engines that employ late injection strategies utilize a significant amount of swirl to promote mixing during the ignition delay period, however the MX10 combustion chamber is thought to be relatively quiescent.

8.3.4 Specific Heat Ratio Experiments

When performing the heat release rate analyses for dual fuel combustion, a specific heat ratio, or polytropic coefficient is required. The correlation for the polytropic coefficient of the intake charge used in this work is based on temperature [Brunt 1998], but does not take equivalence ratio into account. Other correlations for lean burn single fuel mixtures also exist [Ceviz and Kaymaz 2005], and should be investigated and implemented in conjunction with the DCAT code for use in future heat release analyses. Similarly, experiments could be performed in order to model a correlation for a specific fuel, such as propane. Pressure data would be taken while motoring the single cylinder research engine in the MSU ACE laboratory with an AC dynamometer fumigated with various propane concentrations but not ignited with diesel. The pressure data would then be analyzed on a logP vs logV plot and the polytropic coefficient (slope of the compression and expansion lines) specific to each condition could be extracted.

REFERENCES

Abd Alla, G. H., Soliman, H. A., Badr, O. A., Abd Raboo, M. F. (2000). Effect of pilot fuel quantity on the performance of a dual fuel engine. Energy Conversion and Management, Vol. 41, pp. 559-572.

Akagawa, H., Miyamoto, A., Harada A., Sasaki, S. *et al.* (1999). Approaches to Solve Problems of the Premixed Lean Diesel Combustion. SAE Paper 1999-01-0183.

Akihama, K., Takatori, Y., Inagaki, K., Sasaki, S. (2001). Mechanism of the Smokeless Rich Diesel Combustion by Reducing Temperature. SAE Technical Paper 2001-01-0655, doi:10.4271/2001-01-0655.

Bade Shrestha, S. O. and Karim, G. A. (2006). "The operational mixture limits in engines fueled with alternative gaseous fuels." ASME J Energy Resources Tech, 128(3).

Badr, O., Karim, G. A., and Liu, B. (1999). An examination of the flame spread limits in a dual fuel engine. Applied Thermal Engineering, Vol 19, pp. 1071-1080.

Bose, P. K. and Banerjee, R. (2012). "An experimental investigation on the role of hydrogen in the emission reduction and performance trade-off studies in an existing diesel engine operating in dual fuel mode under exhaust gas recirculation." ASME J Energy Resources Tech, 134(1).

Brunt, M. F. J., Rai, H., and Emtage, A. L. (1998). The Calculation of Heat Release Energy from Engine Cylinder Pressure Data. SAE Paper 981052.

Ceviz, M. A. and Kaymaz, I. (2005). "Temperature and air-fuel ratio dependent specific heat ratio fucntions for lean burned and unburned mixture." Energy Conversion and Management, 46, pp. 2387-2404.

Dec, J. E. (1997). A Conceptual Model of DI Diesel Combustion Based on Laser-Sheet Imaging. SAE Paper 970873.

Dec, J. E. (2009). Advanced compression-ignition engines - understanding the in-cylinder processes. Proceedings of the Combustion Institute, Vol. 32, Issue 2, pp. 2727-2742.

Dockery, D.W., Pope, C.A., (1994) "Acute Respiratory Effects of Particulate Air Pollution." Annual Review of Public Health, 15, 107-132

Egolfopoulos, F. N., Holley, A. T., and Law, C. K. (2007). An Assessment of the Lean Flammability Limits of CH4/Air and C3H8/Air Mixtures at Engine-Like Conditions. Proceedings of the Combustion Institute, Vol. 31, 3015-3022.

Filippo, D., and Maricq, M. M. (2008). "Diesel Nucleation Mode Particles: Semivolatile or Solid?" Environ. Sci. Technol., Vol. 42, pp. 7957-7962.

Gibson, C. M., Polk, A. C., Shoemaker, N. T., Srinivasan, K. K., and Krishnan, S. R. (2011). Comparison of propane and methane performance and emissions in a turbocharged direct injection dual fuel engine. Trans. ASME: Journal of Engineering for Gas Turbines and Power, Vol. 133, Issue 9, Paper 092806, [DOI: 10.1115/1.4002895].

Goldsworthy, L. (2012). "Combustion Behaviour of a Heavy Duty Common Rail Marine Diesel Engine Fumigated With Propane." Exp. Therm. and Fluid Sci., [http://dx.doi.org/10.1016/j.expthermflusci.2012.04.016].

Gunea, C. Razavi, R. M., and Karim, G. A. (1998). "The effects of pilot fuel quality on dual fuel ignition delay." SAE Paper 982453.

Gurgenci, H., and Aminossadati, S. M. (2009). "Investigating the use of methane as diesel fuel in off-road haul road truck operations." ASME J Energy Resources Tech, 131(3).

Harris, S. J., and Maricq, M. M. (2001). "Signature size distributions for diesel and gasoline engine exhaust particulate matter." J. Aerosol Sci., Vol. 32, pp. 749-764.

Heywood, J. B. (1988). Internal Combustion Engine Fundamentals, McGraw-Hill, Inc.

Hohenberg, G. (1979). "Advanced Approaches for Heat Transfer Correlations." SAE Paper 790825.

Ishiyama, T., Shioji, M., Mitani, S., and Shibata, H. (2000). Improvement of performance and exhaust emissions in a converted dual-fuel natural gas engine. SAE Paper 2000-01-1866.

Iwabuchi, Y., Kawai, K., Shoji, T., and Takeda, Y. (1999). Trial of New Concept Diesel Combustion System – Premixed Compression-Ignited Combustion. SAE Paper 1999-01-0185.

Kalghatgi, G. T., Risberg, P., and Angstrom, H. K. (2006). "Advantages of fuels with high resistance to auto-ignition in late-injection, low-temperature, compression ignition combustion." SAE Paper 2006-01-3385.

Kamimoto, T. and Bae, M. (1988). High Combustion Temperature for the Reduction of Particulate in Diesel Engines. SAE Technical Paper 880423, doi:10.4271/880423.

Karim, G. A. (1987). "The dual fuel engine." In Automotive Engine Alternatives (Ed. R. L. Evans), Plenum Press.

Karim, G. A. (1991). An examination of some measures for improving the performance of gas fuelled diesel engines at light load. SAE Paper 912366.

Karim, G. A. (2003). "Combustion in gas fueled compression-ignition engines of the dual fuel type." ASME J Eng Gas Turb Power, 125(3), pp. 827-836.

Karim, G. A., Jones, W., and Raine, R. R. (1989). "An examination of the ignition delay period in dual fuel engines." SAE Paper 892140.

Karim, G. A., Liu, Z., and Jones, W. (1993). "Exhaust Emissions from Dual Fuel Engines at Light Load." SAE Paper 932822.

Kimura, S., Aoki, O., Kitahara, Y., and Aiyoshizawa, E. (2001). Ultra-Clean Combustion Technology Combining a Low-Temperature and Premixed Combustion Concept for Meeting Future Emission Standards. SAE Paper 201-01-0200.

Kittelson, D. B. (1998). Engines and Nanoparticles: A Review. Journal of Aerosol Science, Vol. 29, No. 5-6, pp. 575-588.

Kokjohn S. L., Hanson, R. M., Splitter, D. A., and Reitz, R. (2009). "Experiments and Modeling of Dual-Fuel HCCI and PCCI Combustion Using In-Cylinder Fuel Blending." SAE Paper 2009-01-2647.

Kook, S., Bae, C., Miles, P., Choi, D. (2005). The Influence of Charge Dilution and Injection Timing on Low-Temperature Diesel Combustion and Emissions. SAE Technical Paper 2005-01-3837, doi:10.4271/2005-01-3837.

Krishnan, S. R., Biruduganti, M., Mo, Y., Bell, S. R., and Midkiff, K. C. (2002). "Performance and heat release analysis of a pilot-ignited natural gas engine." International Journal of Engine Research, 3(3), pp. 171-184.

Krishnan, S. R., Srinivasan, K. K., Singh, S., Bell, S. R., Midkiff, K. C. (2004). "Strategies for Reduced NO_x Emissions in Pilot-Ignited Natural Gas Engines." Trans. ASME: Journal of Engineering for Gas Turbines and Power, Vol. 126, Issue 7, pp. 665-671.

Kubesh, J., and Brehob, D. (1992). Analysis of Knock in a Dual-Fuel Engine. SAE Paper 922367.

Law, C. K. Combustion Physics, Cambridge University Press, 2010.

Liu, H., Yao M., Zhang B., and Zheng Z. (2008). "Effects of Inlet Pressure and Octane Numbers on Combustion and Emissions of a Homogeneous Charge Compression Ignition (HCCI) Engine." Energy and Fuels, 22(4), pp. 2207-2215.

Liu, Z. and Karim, G. A. (1995). "The ignition delay period in dual fuel engines." SAE Paper 950466.

Lu, T., Cheung, C. S., and Huang, Z. (2012). "Effects of engine operating conditions on the size and nanostructure of diesel particles." Journal of Aerosol Science, Vol. 47, pp. 27-38.

Nielson, O. B., Qvale, B., and Sorenson, S. (1987). "Ignition delay in the dual fuel engine." SAE Paper 870589.

Ojeda, W., Zoldak, P., Espinosa, R., and Kumar, R. (2008). Development of a Fuel Injection Strategy for Diesel LTC. SAE Paper 2008-01-0057.

Opat, R., Ra, Y., Gonzalez D., M.A., Krieger, R., Reitz, R.D., Foster, D.E., Siewert, R., and Durrett, R. (2007). "Investigation of Mixing and Temperature Effects on HC/CO Emissions for Highly Dilute Low Temperature Combustion in a Light Duty Diesel Engine." SAE Technical Paper 2007-01-0193.

Papagiannakis, R. G. and Hountalas, D. T. (2003). "Experimental investigation concerning the effect of natural gas percentage on performance and emissions of a DI dual fuel diesel engine." Applied Thermal Engineering, 23, pp. 353–365.

Papagiannakis, R. G. and Hountalas, D. T. (2004). Combustion and exhaust emission characteristics of a dual fuel compression ignition engine operated with pilot diesel fuel and natural gas. Energy Conversion and Management, Vol 45, pp. 2971-2987.

Polk, A. C., Gibson, C. M., Shoemaker, N. T., Srinivasan, K. K., Krishnan, S. R. (2011). "Analysis of Ignition Behavior in a Turbocharged Direct Injection Dual Fuel Engine using Propane and Methane as Primary Fuels." ASME ICEF 2011, October 2-5, Morgantown, West Virginia, also accepted for publication in the ASME J Energy Resources Tech.

Polk, A. C., Gibson, C. M., Shoemaker, N. T., Srinivasan, K. K., Krishnan, S. R. (2013). "Detailed Characterization of Diesel-Ignited Propane and Methane Dual Fuel Combustion in a Turbocharged DI Diesel Engine." Accepted for publication in the Proc. Inst. Mech. Engrs., Part D: Journal of Automobile Engineering.

Poonia, M. P., Ramesh, A., and Gaur, R. R. (1999). "Experimental investigation of the factors affecting the performance of a LPG – diesel dual fuel engine." SAE Paper 1999-01-1123.

Prakash, G., and Ramesh, A. (1999). "An approach for estimation of ignition delay in a dual fuel engine." SAE Paper 1999-01-0232.

Ramadhas, A. S., Jayaraj, S., Muraleedharan., C. (2008). "Dual fuel mode operation in diesel engines using renewable fuels: Rubber seed oil and coir-pith producer gas." Renewable Energy, 33(9), pp. 2077-2083.

Ryan, T., and Callahan, T. (1996). Homogenous Charge Compression Ignition of Diesel Fuel. SAE Paper 961160.

Sequera, A. J., Parthasarathy, R. N., and Golahalli, S. R. (2011). "Effects of fuel injection timing in the combustion of biofuels in a diesel engine at partial loads." ASME J Energy Resources Tech, 133(2).

Shoemaker N. T., Gibson, C. M., Polk, A. C., Krishnan, S. R., and Srinivasan, K. K. (2012). Performance and Emissions Characteristics of Bio-Diesel (B100)-Ignited Methane and Propane Combustion in a Four Cylinder Turbocharged Compression Ignition Engine. Journal of Engineering for Gas Turbines and Power, Vol. 134, Issue 8, [DOI: 10.1115/1.4005993].

Splitter, D., Wissink, M., DelVescovo, D., and Reitz, R. (2013). "RCCI Engine Operation Towards 60% Thermal Efficiency." SAE Paper 2013-01-0279.

Srinivasan, K. K., Krishnan, S. R., Qi, Y., Midkiff, K. C. and Yang, H. (2007). "Analysis of diesel pilot-ignited natural gas low-temperature combustion with hot exhaust gas recirculation." Combustion Science and Technology, 179(9), pp. 1737-1776.

Srinivasan, K. K., Krishnan, S. R., Singh, S., Midkiff, K. C. and Bell S. R. (2003). "The Advanced Low Pilot Ignited Natural Gas Engine – A Low NO_x Alternative to the Diesel Engine." Proceedings of IJPGC 2003, June 16-19, Atlanta, Georgia.

Srinivasan, K. K., Krishnan, S. R., Singh, S., Midkiff, K. C., Bell S. R., Gong, W., Fiveland, S. B., and Willi, M. (2006). "The Advanced Low Pilot Ignited Natural Gas Engine: A Combustion Analysis." Trans. ASME: Journal of Engineering for Gas Turbines and Power, 128(1), pp. 213-218.

Stewart, J., Clarke, A., and Chen, R. (2007). "An experimental study of the dual-fuel performance of a small compression ignition diesel engine operating with three gaseous fuels." Proc. Inst. Mech. Engrs., Part D: Journal of Automobile Engineering, 221(8), pp. 943-956.

Stone, Richard. Introduction to Internal Combustion Engines, 3rd Edition, Society of Automotive Engineers, 1999.

Sun, Y., and Reitz, R.D. (2008). "Adaptive Injection Strategies (AIS) for Ultra-Low Emissions Diesel Engines." SAE paper 2008-01-0058.

Tao, Y., Hodgins, K. B., and Hill, P. G. (1995). "NO_x emissions from a diesel engine fueled with natural gas." ASME J Energy Resources Tech, 117(4).

TSI Incorporated. "Aerosol statistics lognormal distributions and $dN/dlogD_p$." PR-001 Rev. B. 2012.

Walter, B., and Gatallier, B. (2002). Development of the High Power NADI Concept Using Dual Mode Diesel Combustion to Achieve Zero NO_x and Particulate Emissions. SAE Paper 2002-01-1744.

Weaver, C. S., and Turner, S. H. (1994). "Dual fuel natural gas/diesel engines: technology, performance, and emissions." SAE Paper 940548.

Yanagihara, H. (2001). Ignition timing control at Toyota 'UNIBUS' combustion system. Proceedings of IFP International Congress on a New Generation of Engine Combustion Processes for the Fugure, pp. 34-42.

APPENDIX A

LABVIEW DATA ACQUISITION VI – VOLKSWAGEN TDI ENGINE

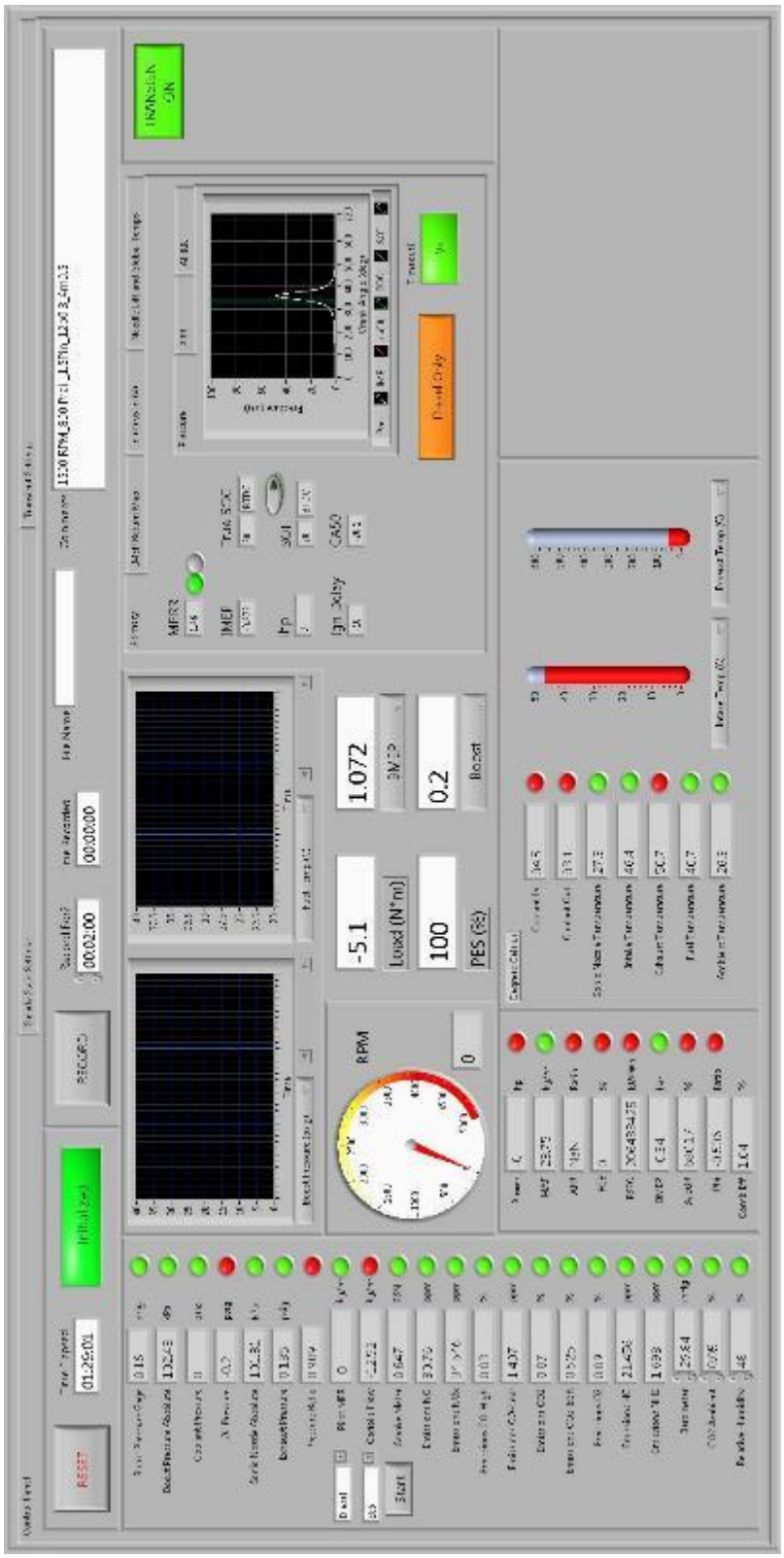

Figure A.1 DAQ VI Front Panel

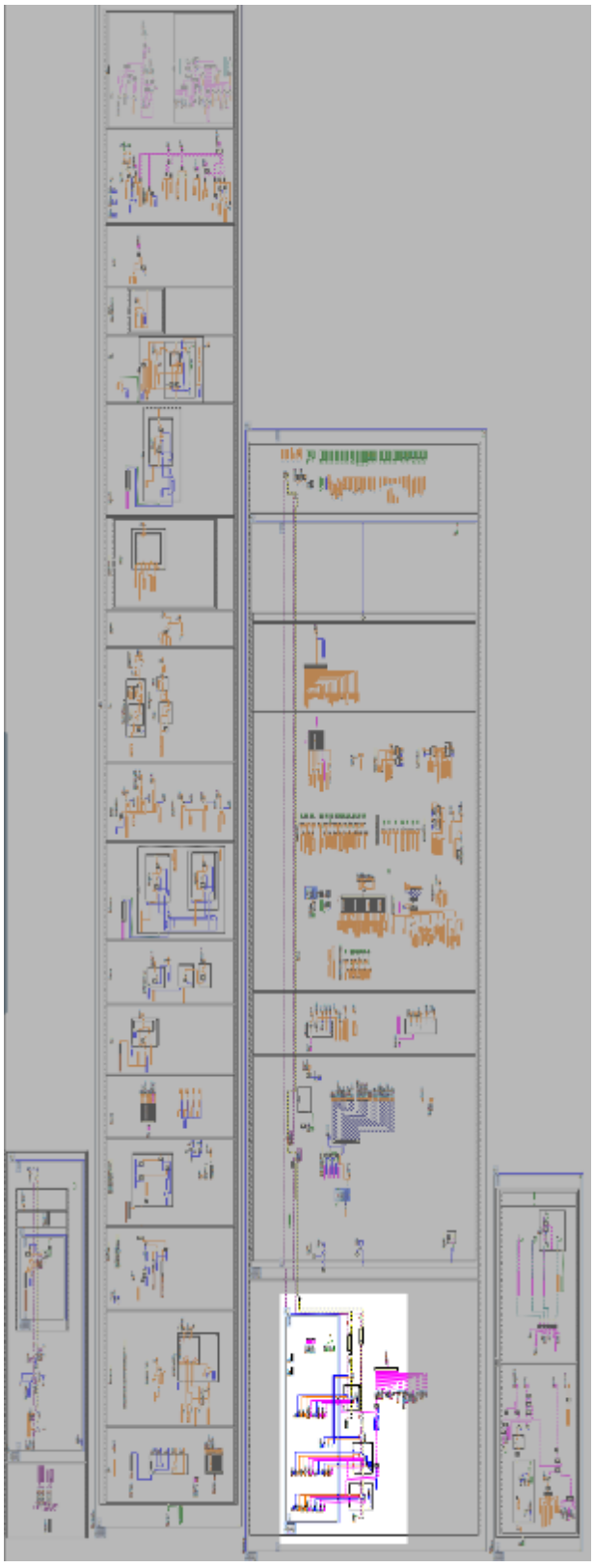

Figure A.2 DAQ VI Block Diagram – Overview

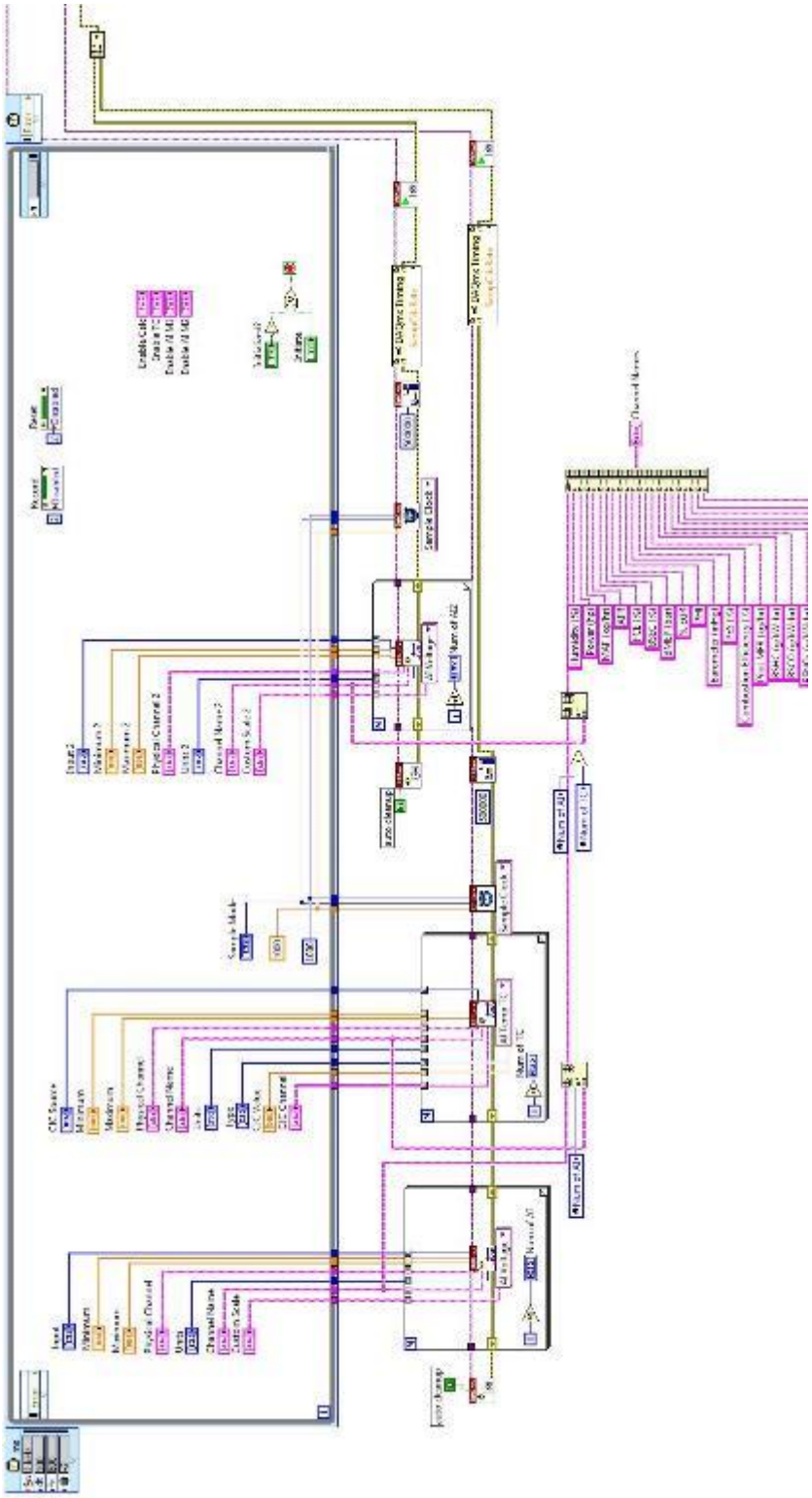

Figure A.3 DAQ VI Block Diagram – Steady State 1

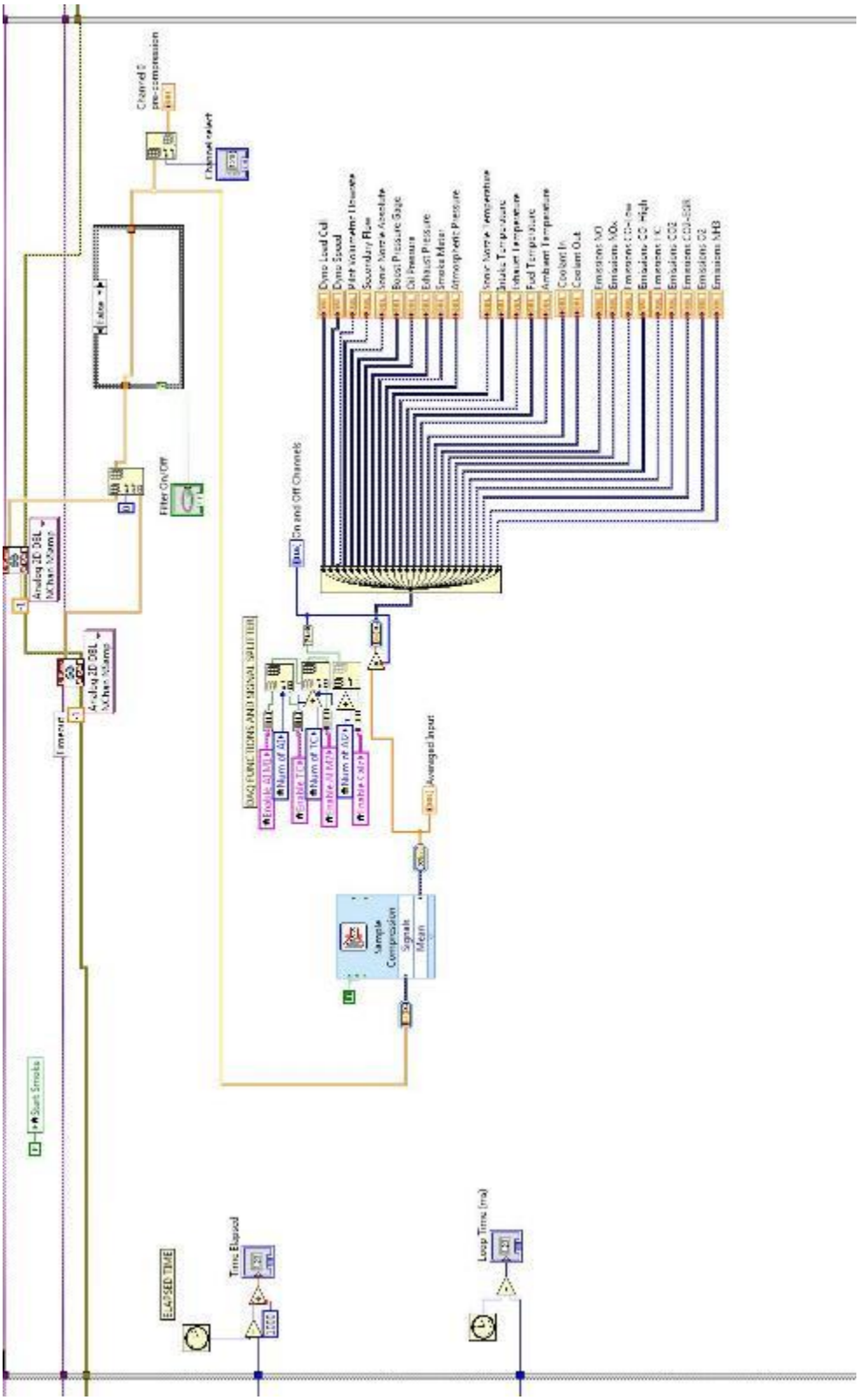

Figure A.4 DAQ VI Block Diagram – Steady State 2

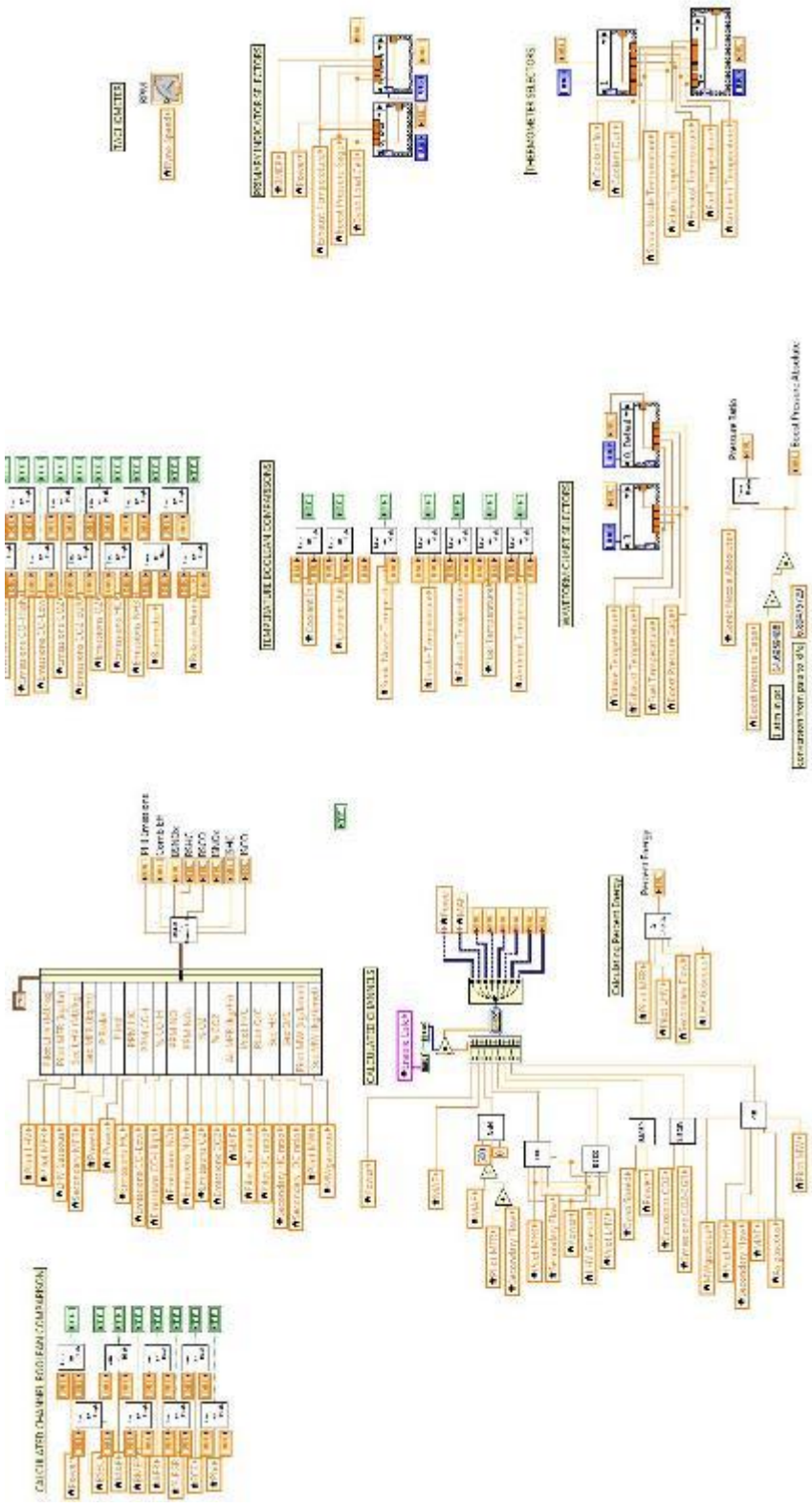

Figure A.5 DAQ VI Block Diagram – Steady State 3

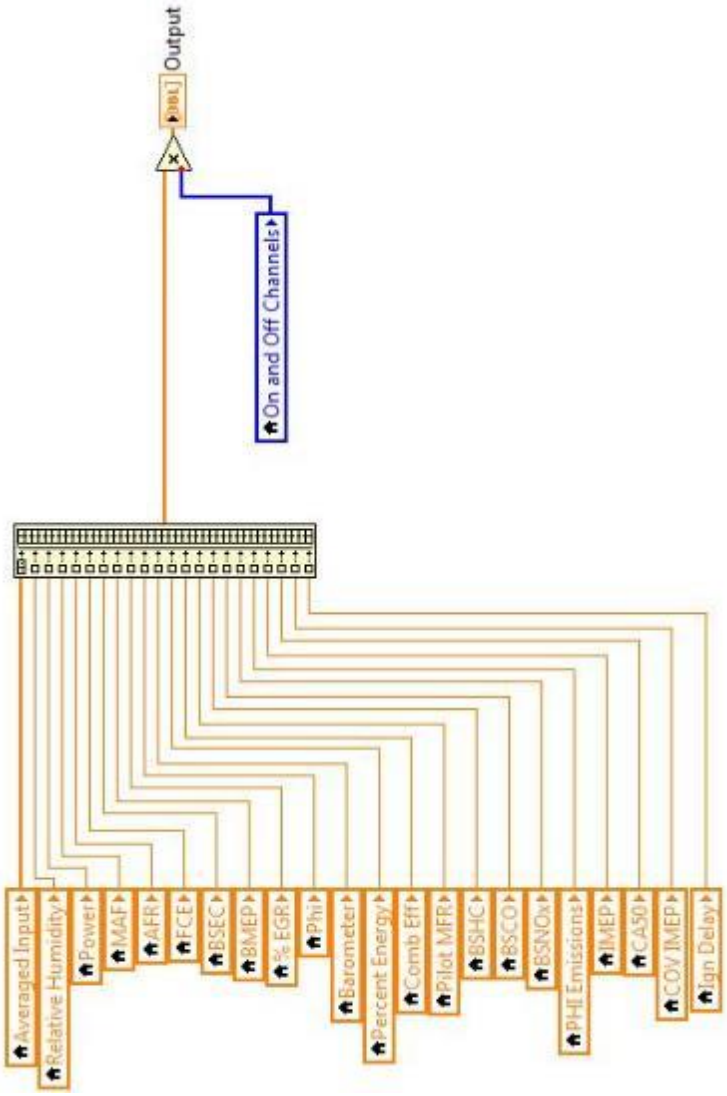

Figure A.6 DAQ VI Block Diagram – Steady State 4

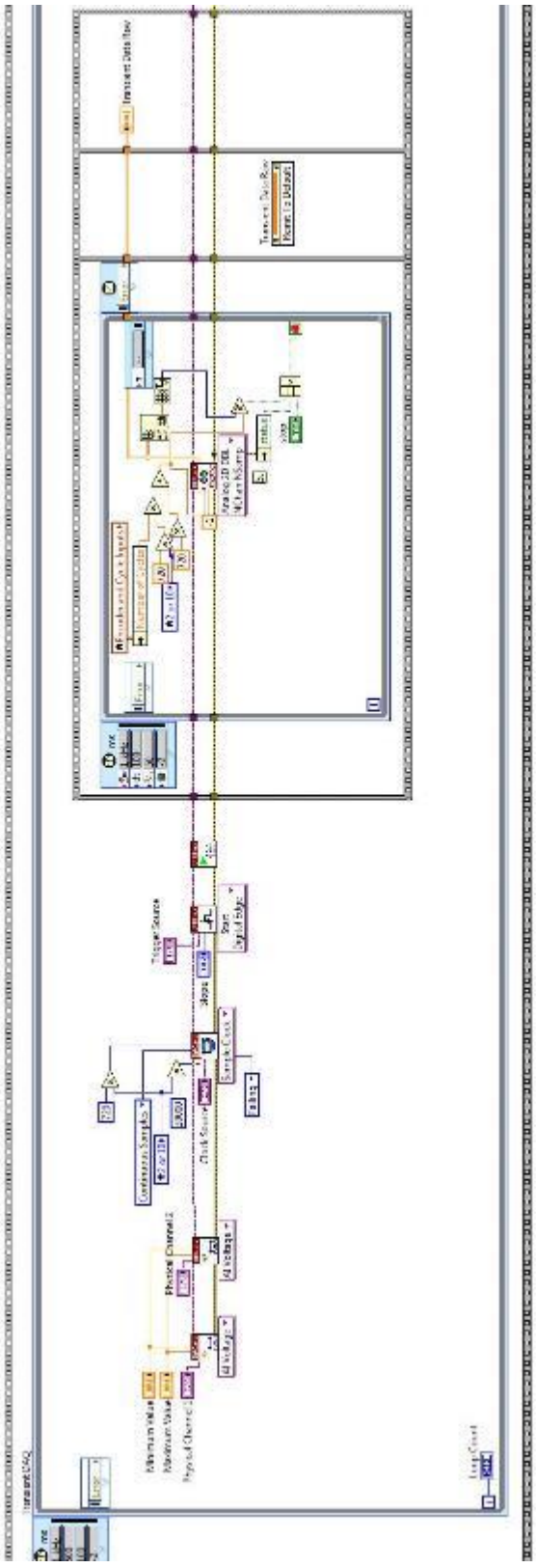

Figure A.7 DAQ VI Block Diagram – Transient DAQ

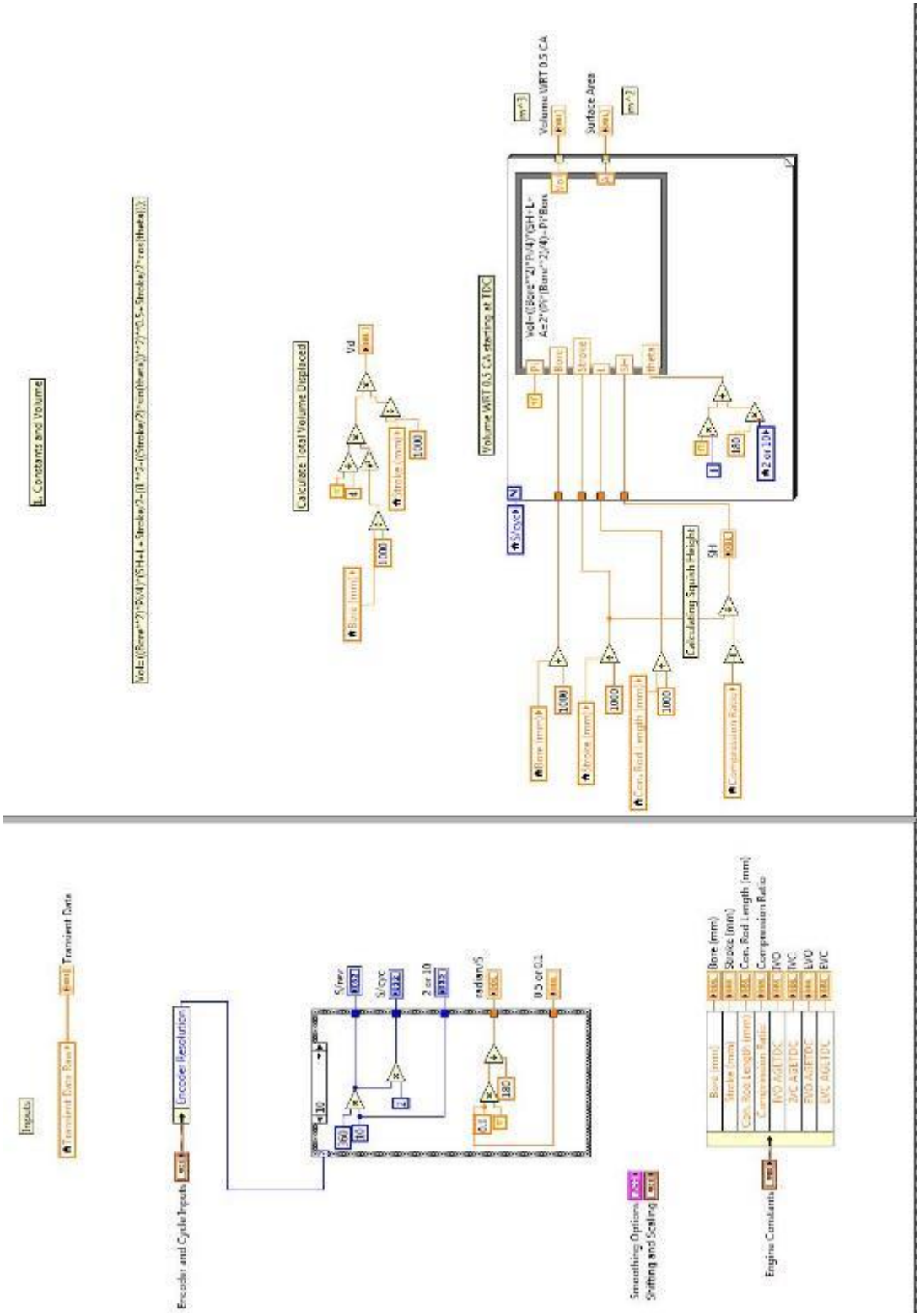

Figure A.8 DAQ VI Block Diagram – Transient Inputs and Constants

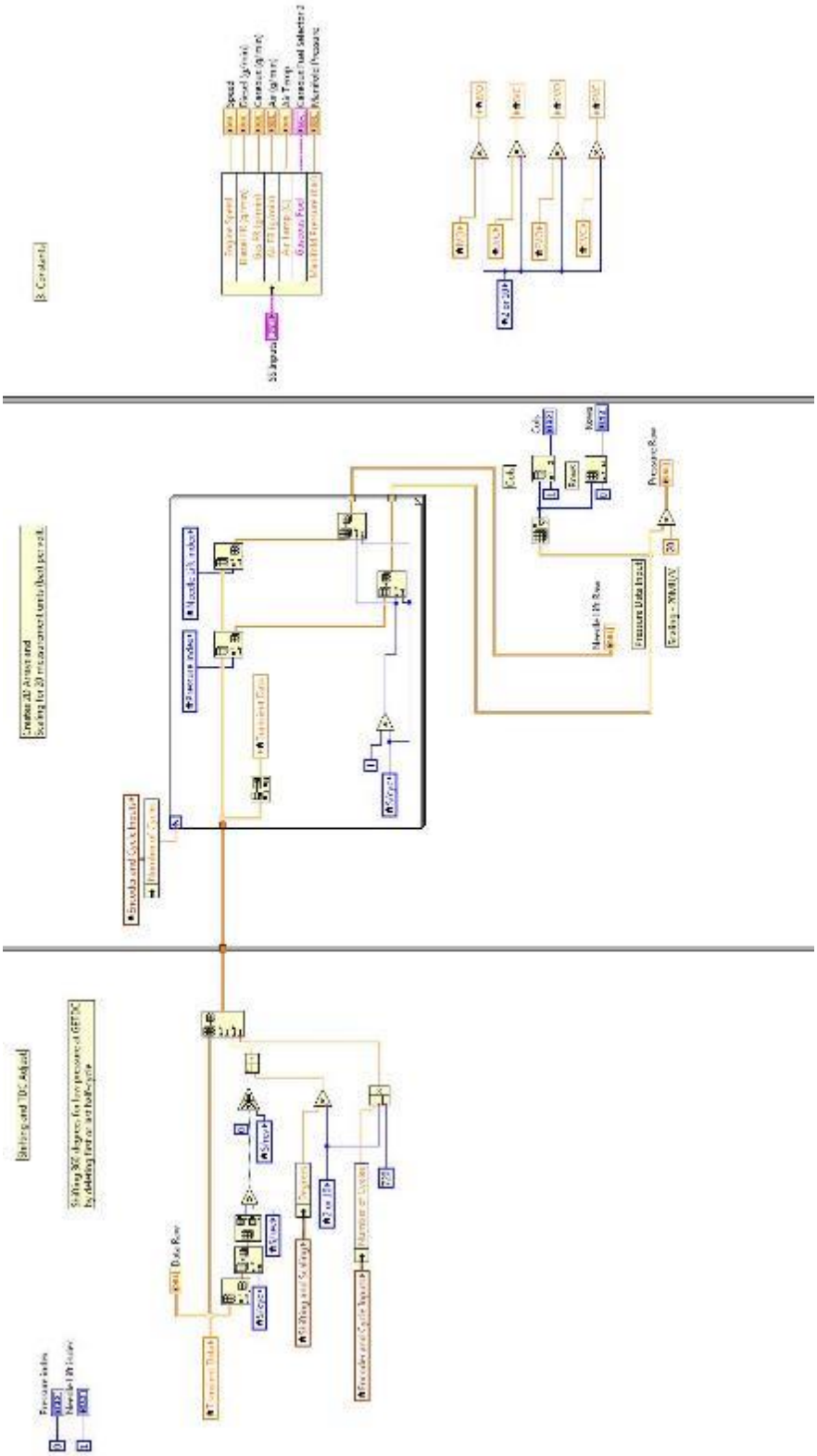

Figure A.9 DAQ VI Block Diagram – Transient Creating Array and Shifting

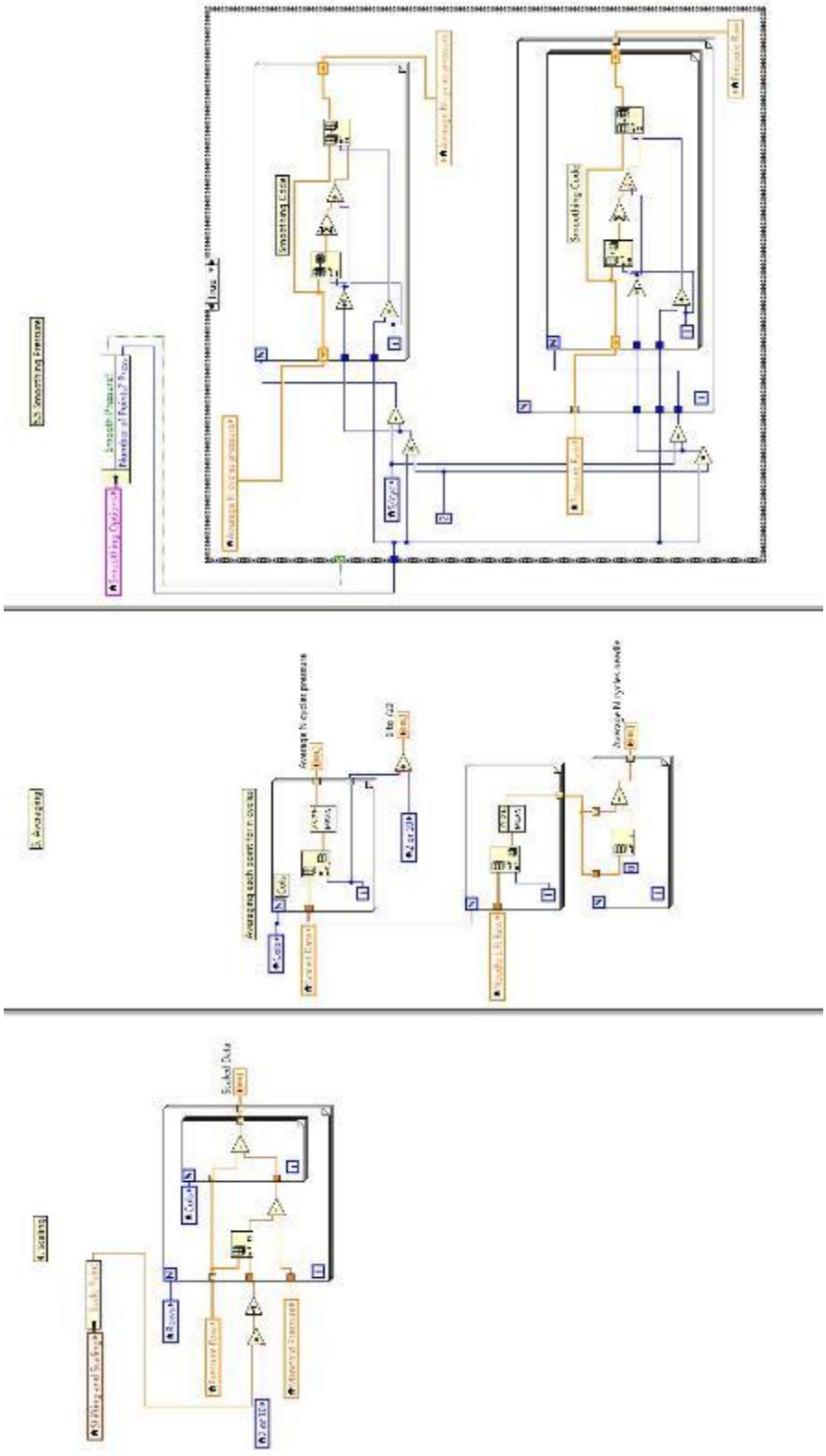

Figure A.10 DAQ VI Block Diagram – Transient Scaling and Smoothing

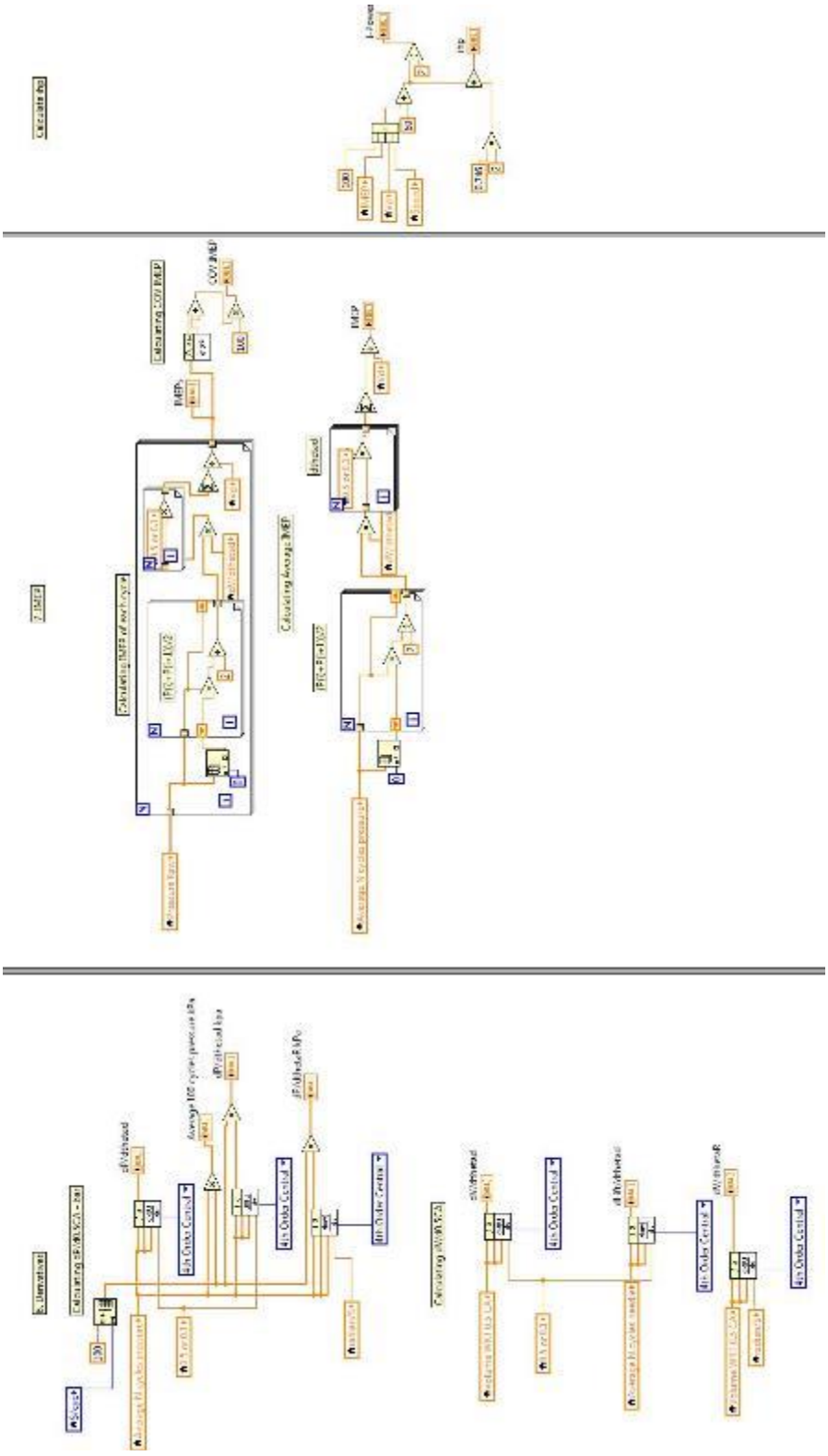

Figure A.11 DAQ VI Block Diagram – Transient Derivatives and IMEP

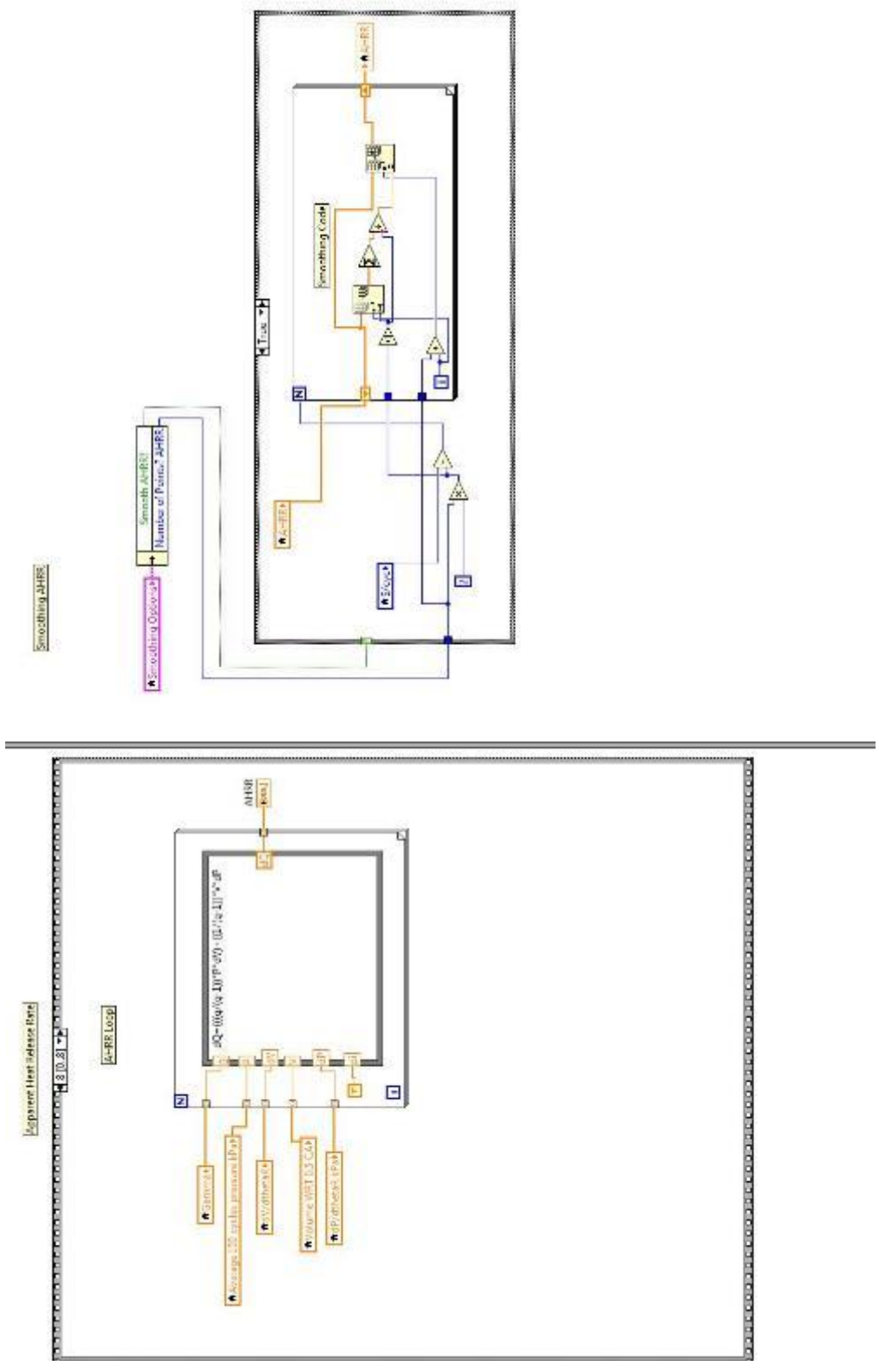

Figure A.12 DAQ VI Block Diagram – Transient Heat Release and AHRR Smoothing

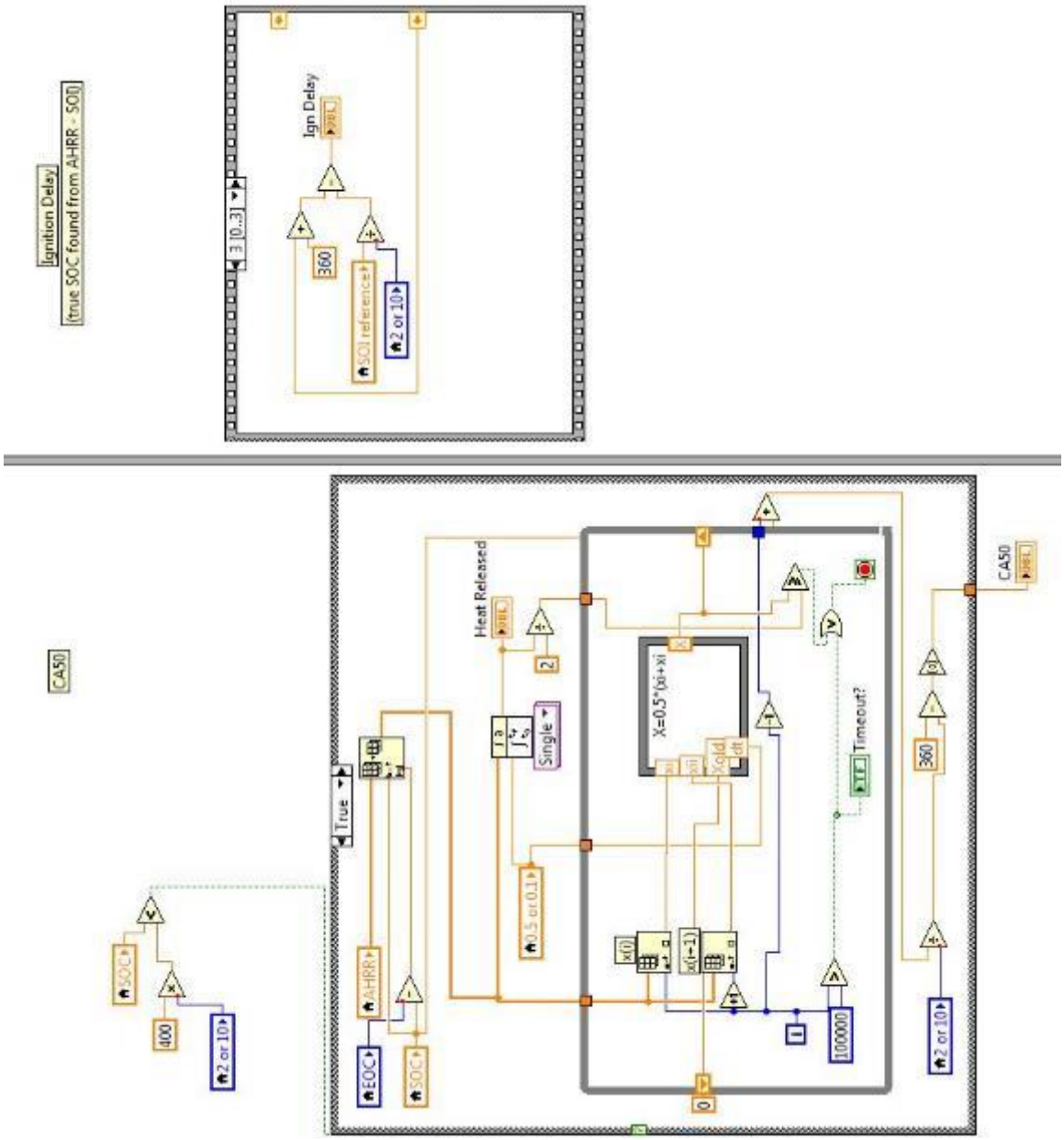

Figure A.13 DAQ VI Block Diagram – Transient CA50 and Ignition Delay

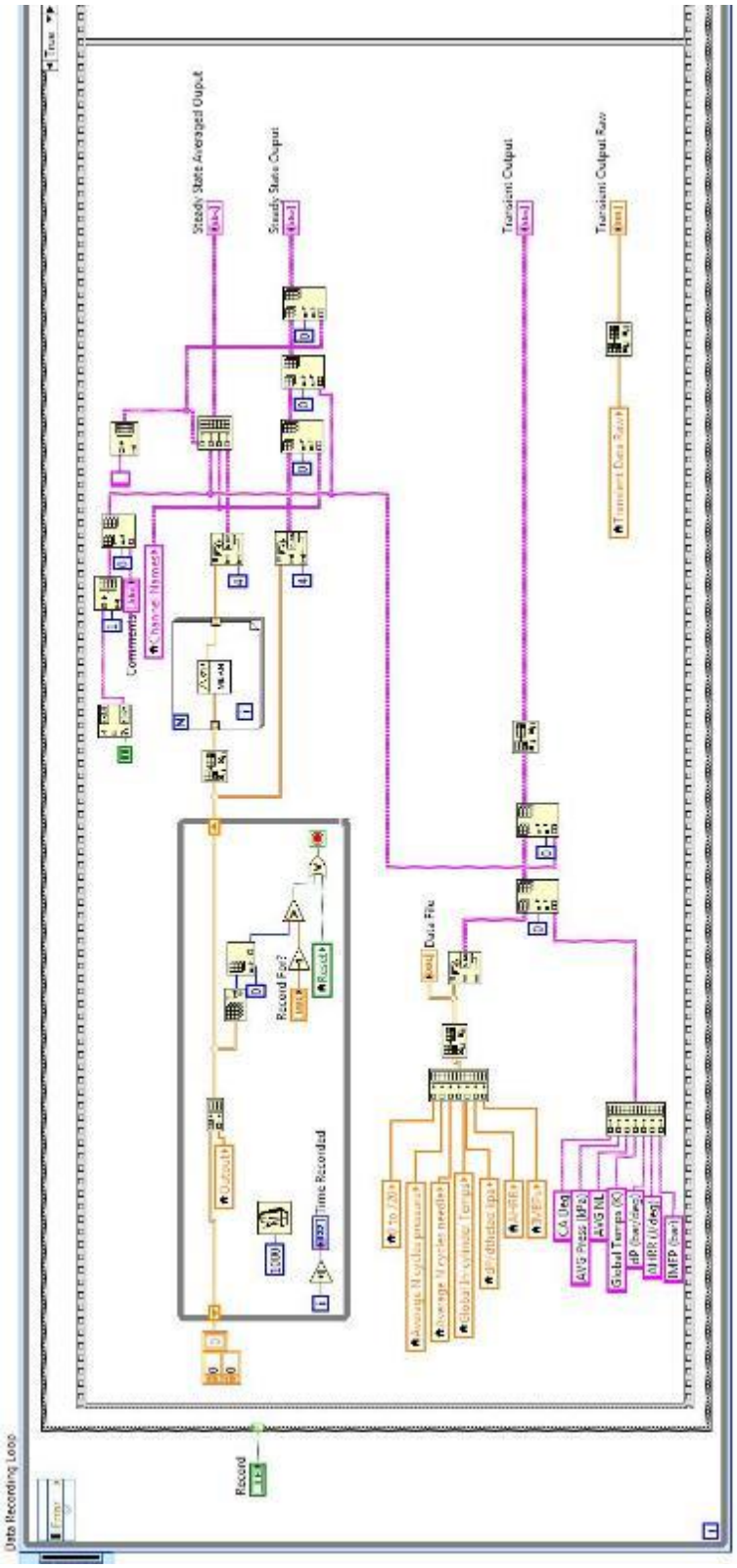

Figure A.14 DAQ VI Block Diagram – Recording 1

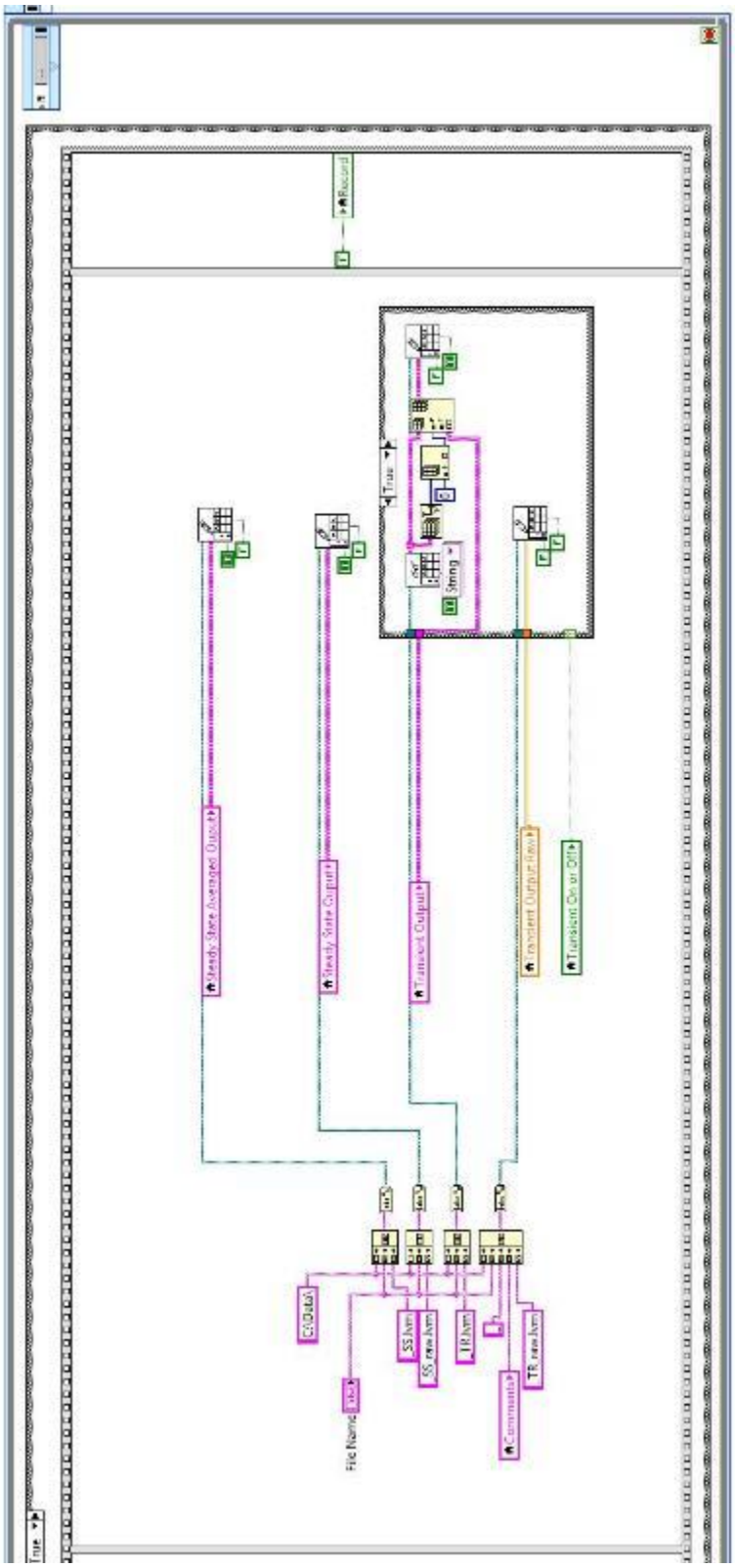

Figure A.15 DAQ VI Block Diagram – Recording 2

APPENDIX B

ADDITIONAL DRAWINGS AND SCHEMATICS: MX10 TEST CELL

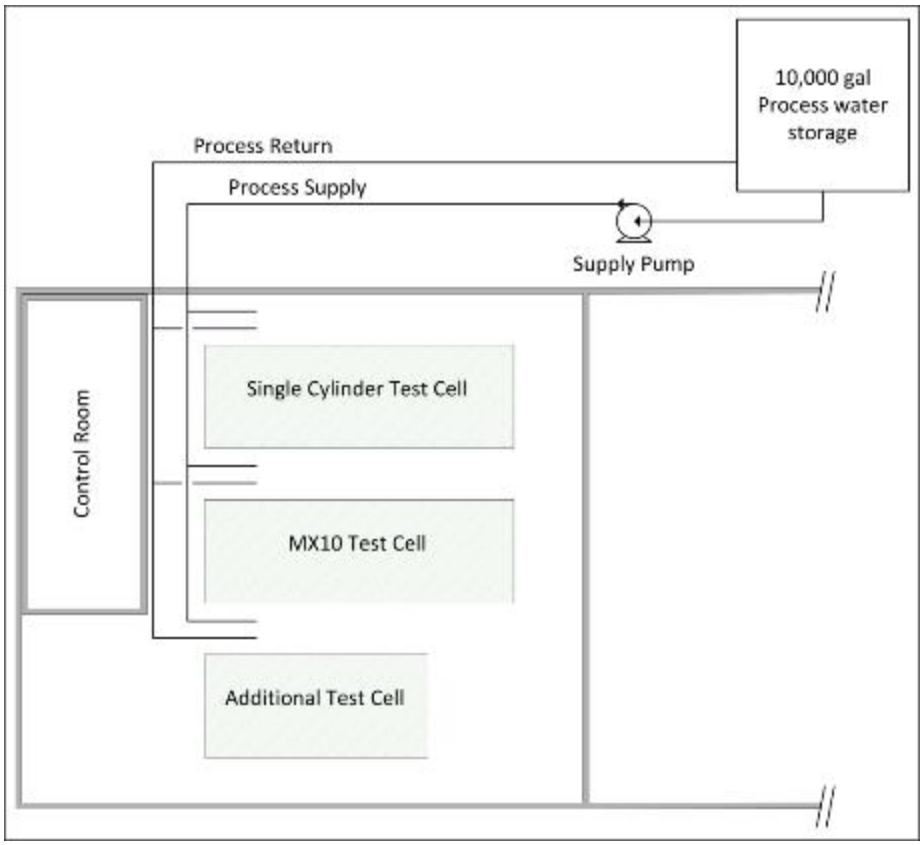

Figure B.1 Facilities process water system

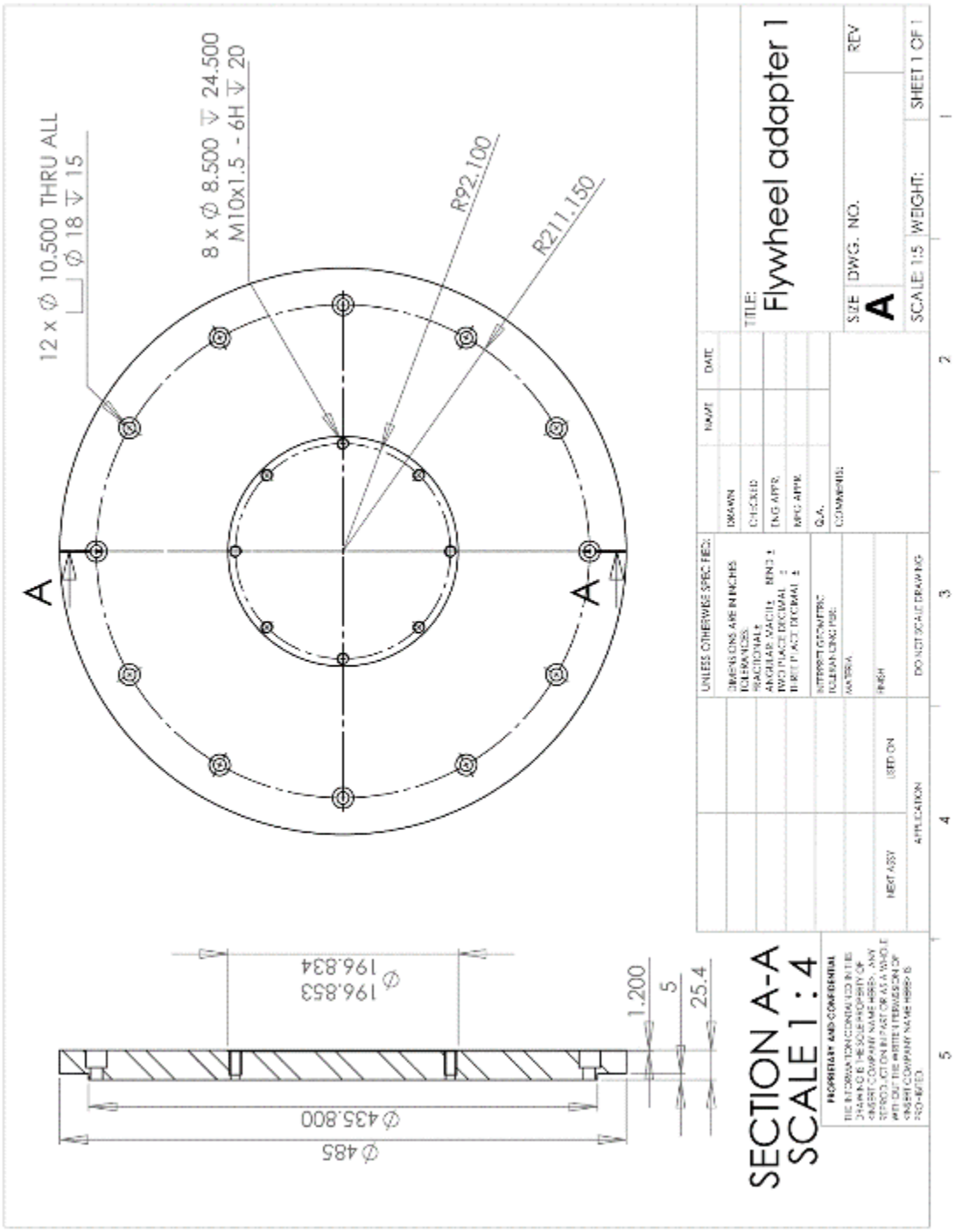

Figure B.2 Flywheel adapter engineering drawing

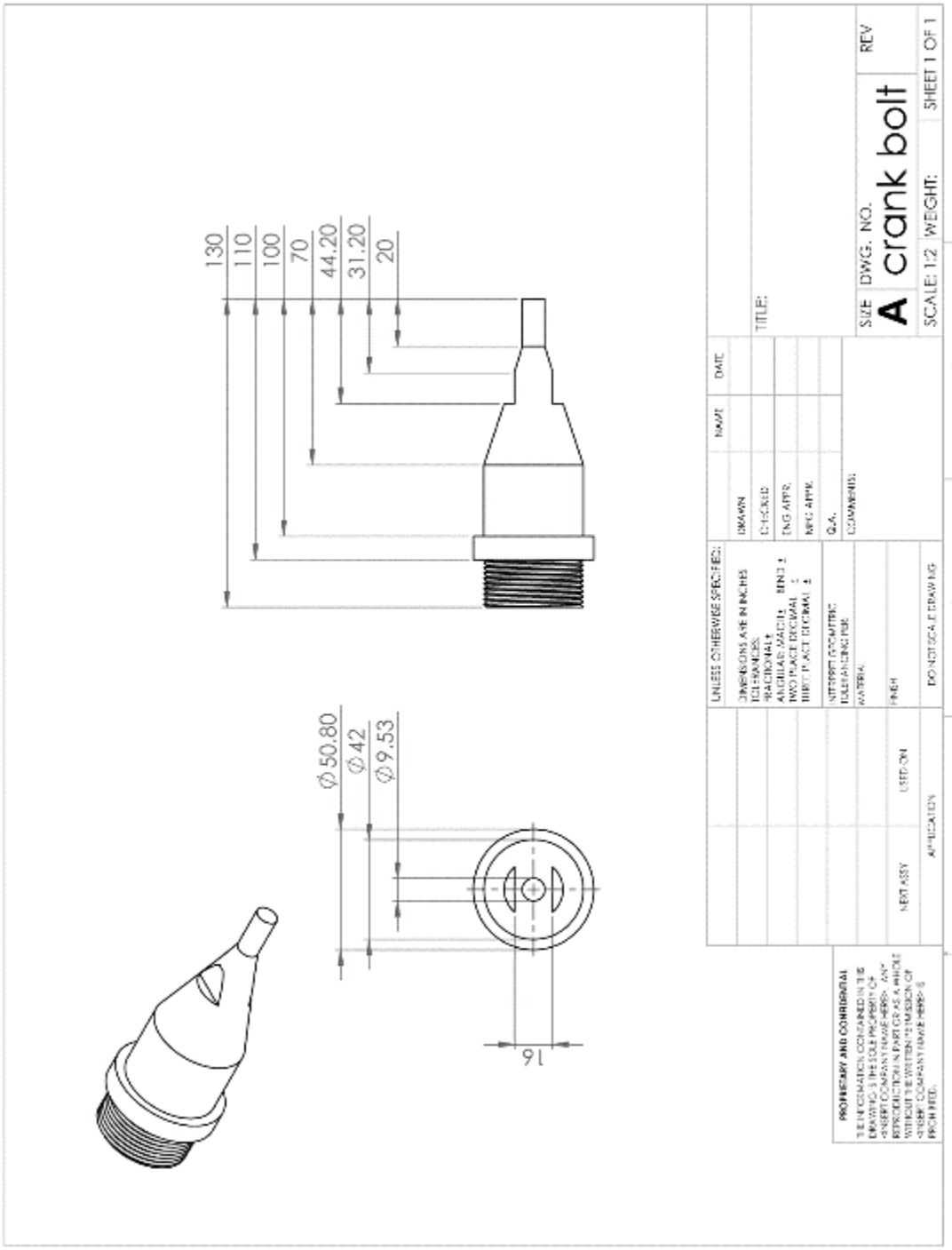

Figure B.3 Crank bolt engineering drawing

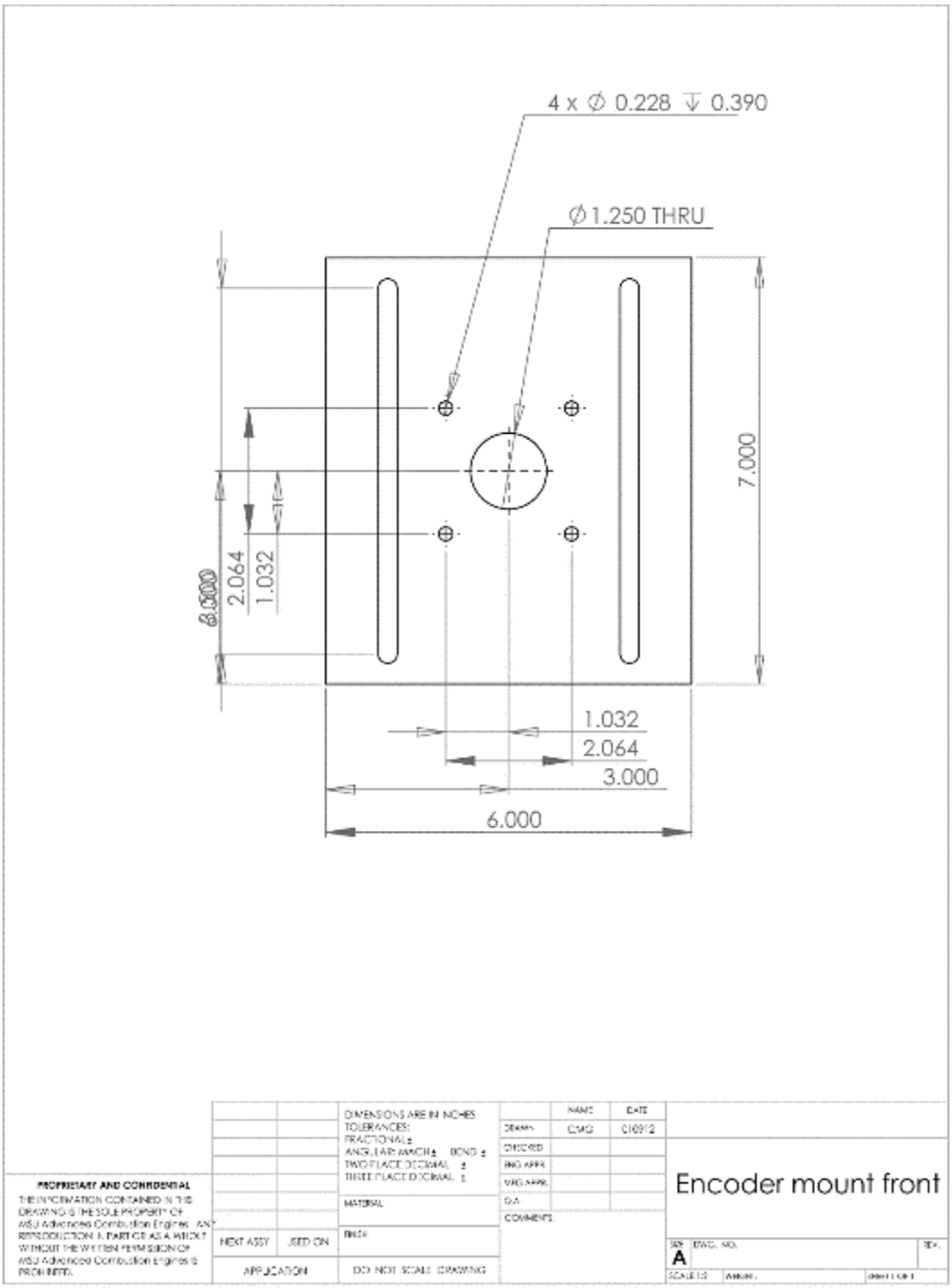

Figure B.4 Encoder mount engineering drawing

APPENDIX C

CAN VI BLOCK DIAGRAMS BASED ON SAE J1939 FOR USE ON MX10 TEST CELL WITH OE ECM

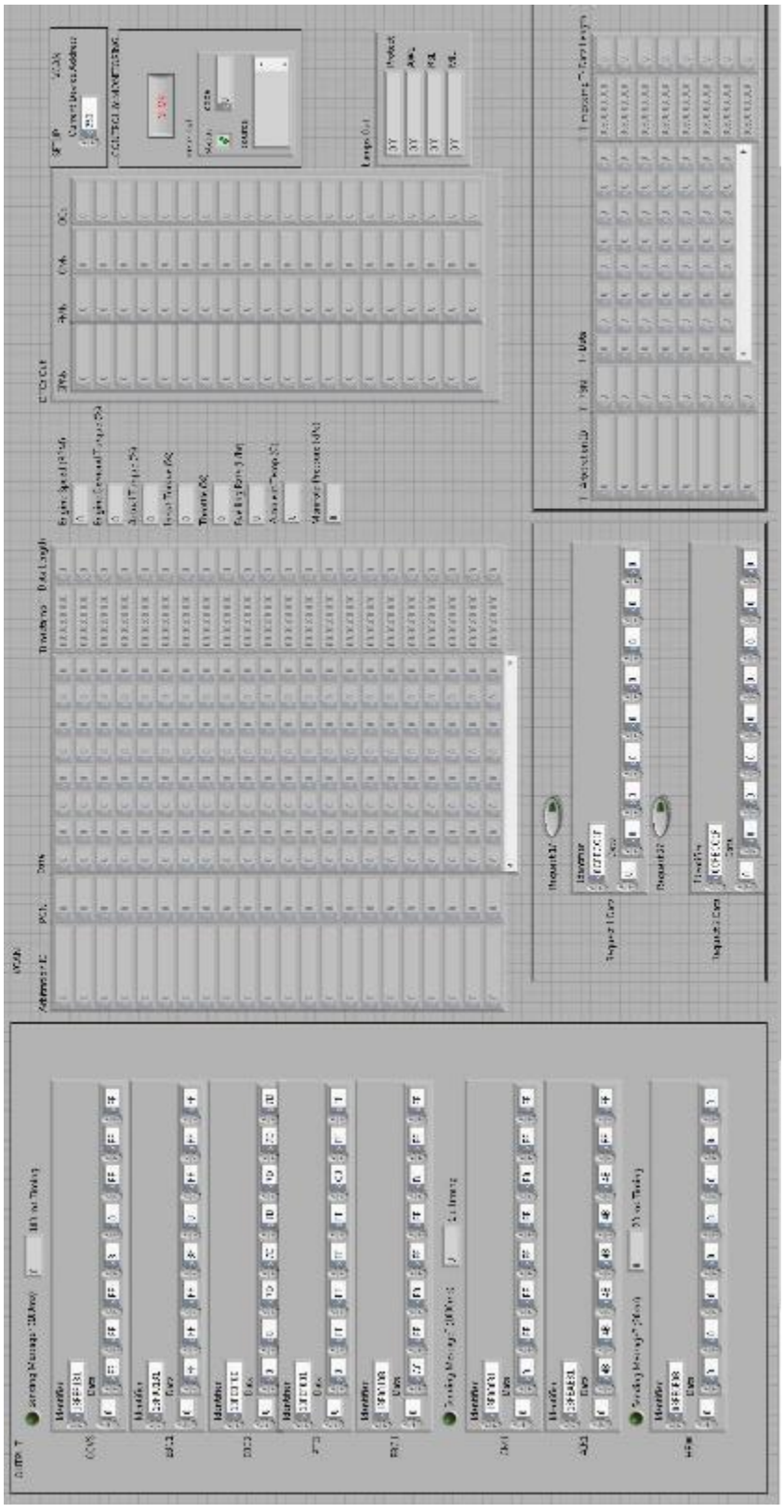

Figure C.1 CAN VI – Front Panel

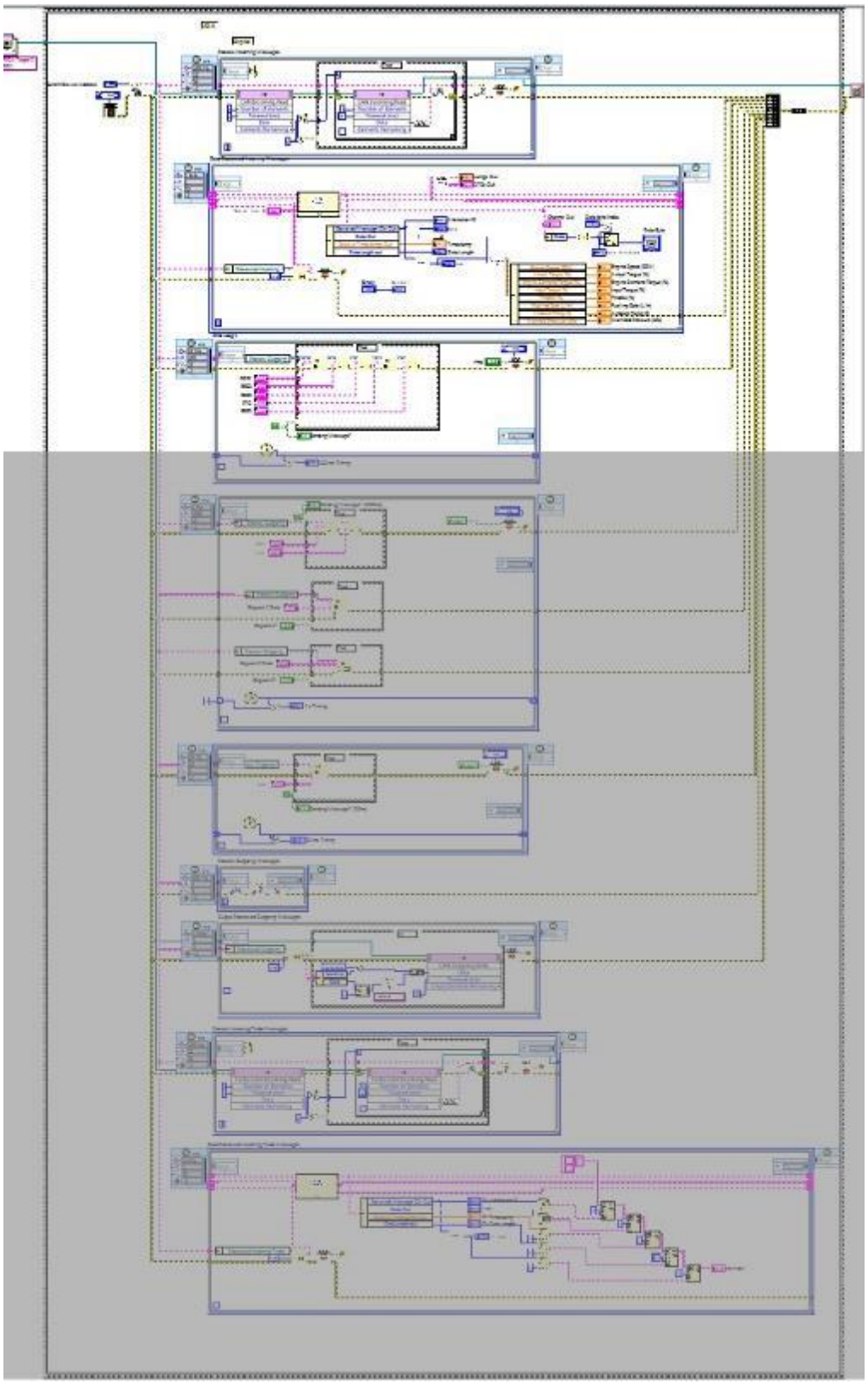

Figure C.2 CAN VI – Block Diagram Overview

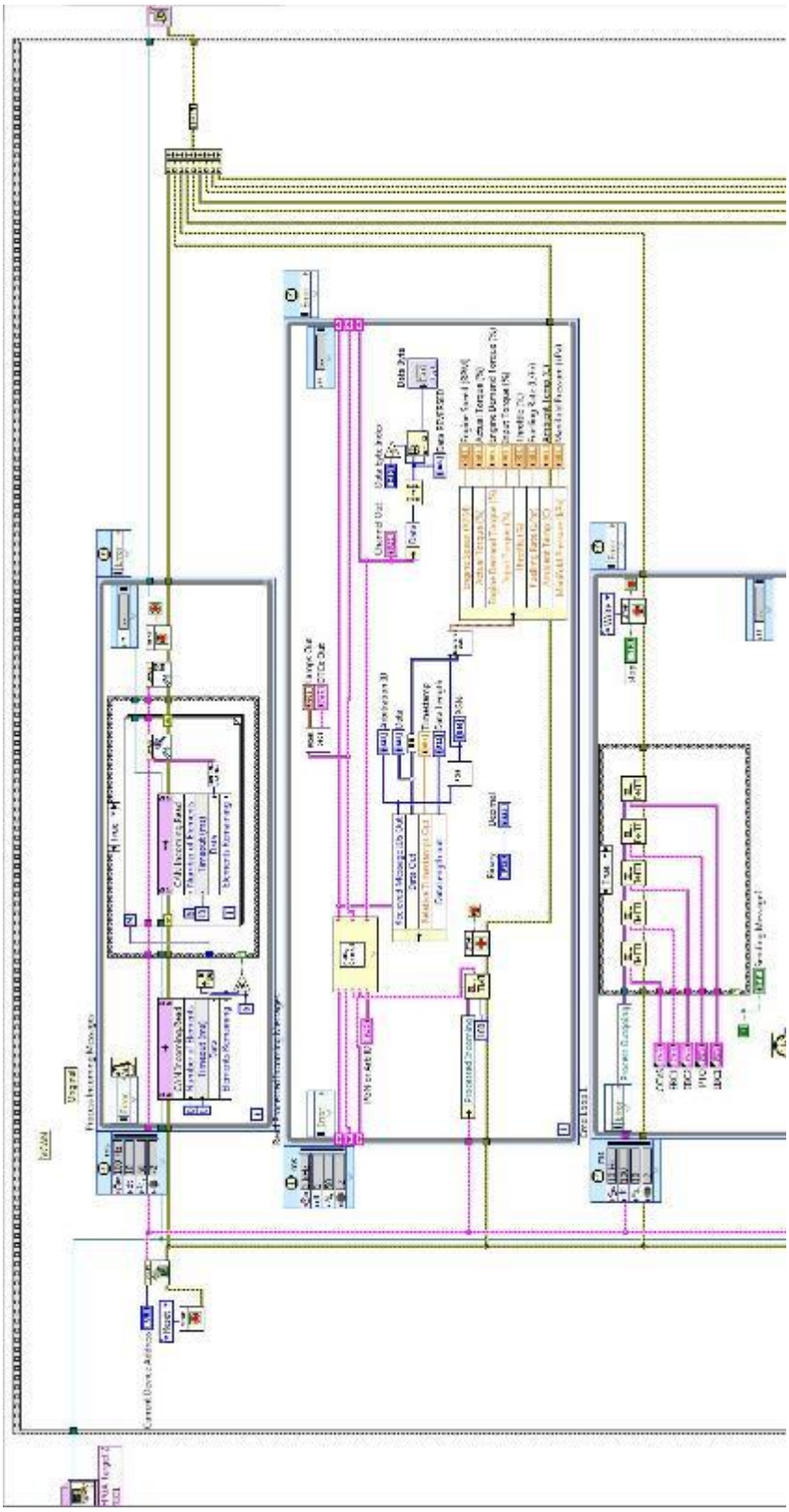

Figure C.3 CAN VI – Block Diagram 1

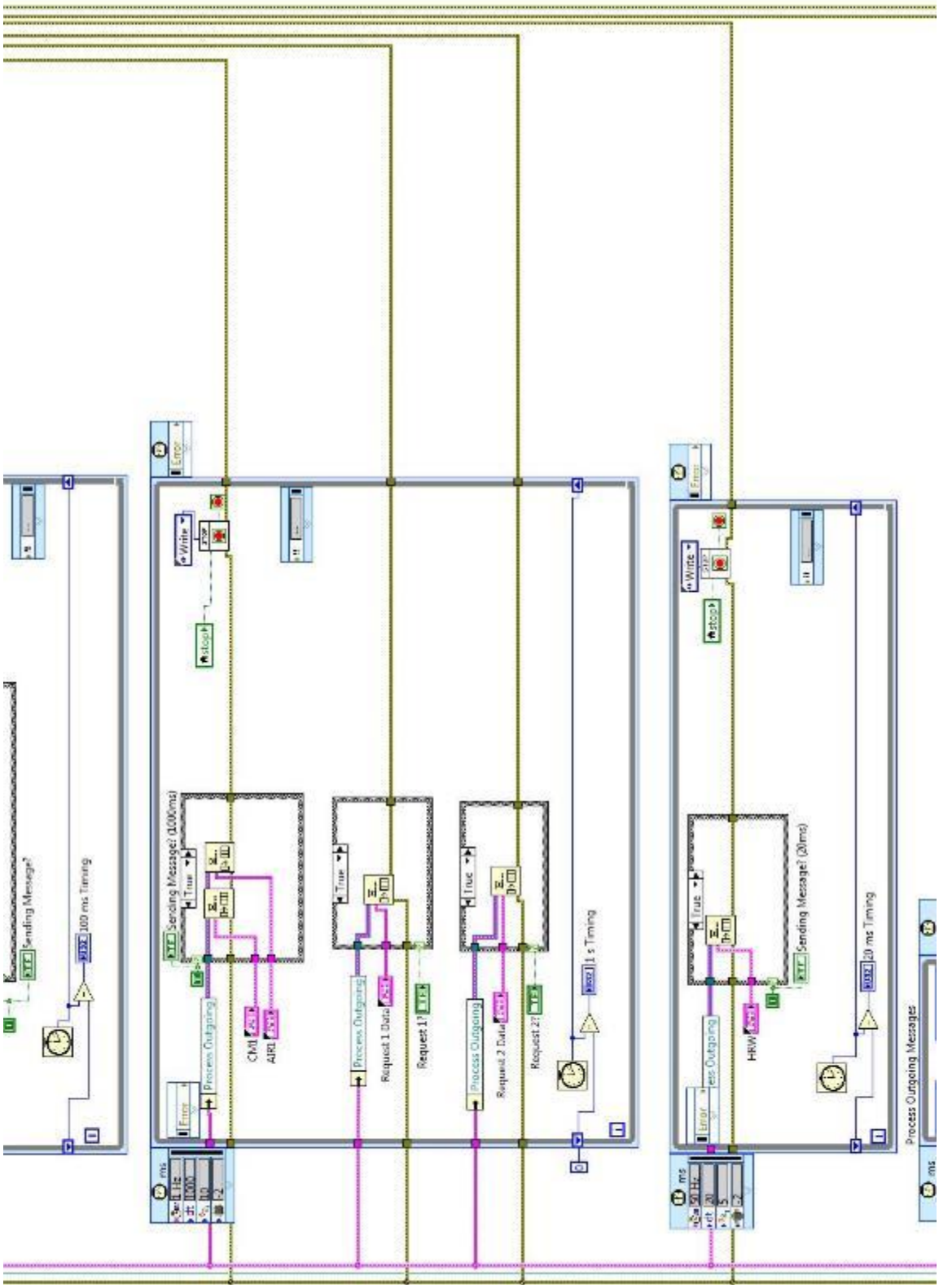

Figure C.4 CAN VI – Block Diagram 2

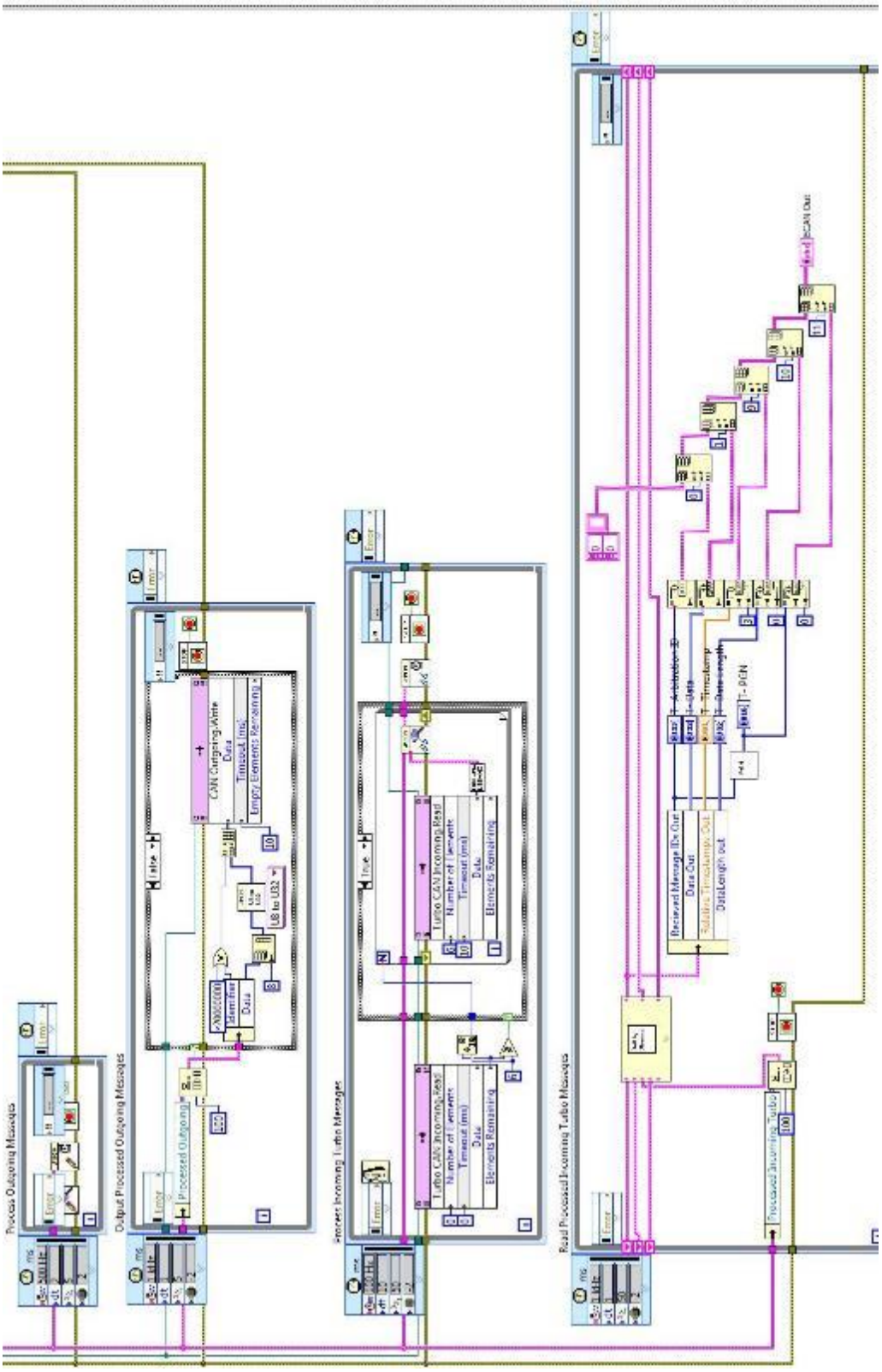

Figure C.5 CAN VI – Block Diagram 3

APPENDIX D

CONTROL AND DAQ VI BLOCK DIAGRAMS BASED ON DRIVVEN HARDWARE AND DCAT FOR USE ON MX10 TEST CELL

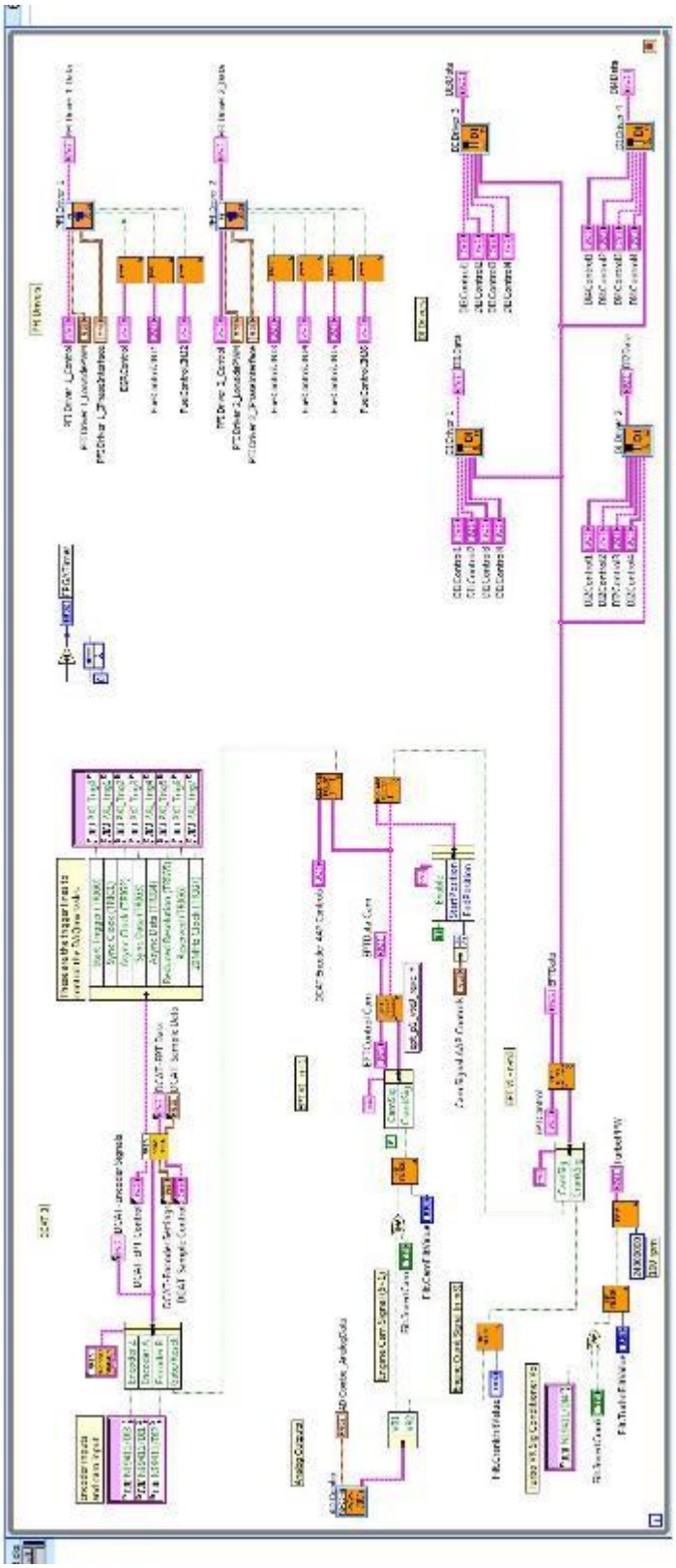

Figure D.1 Drivven Engine Synchronous FPGA – Overview

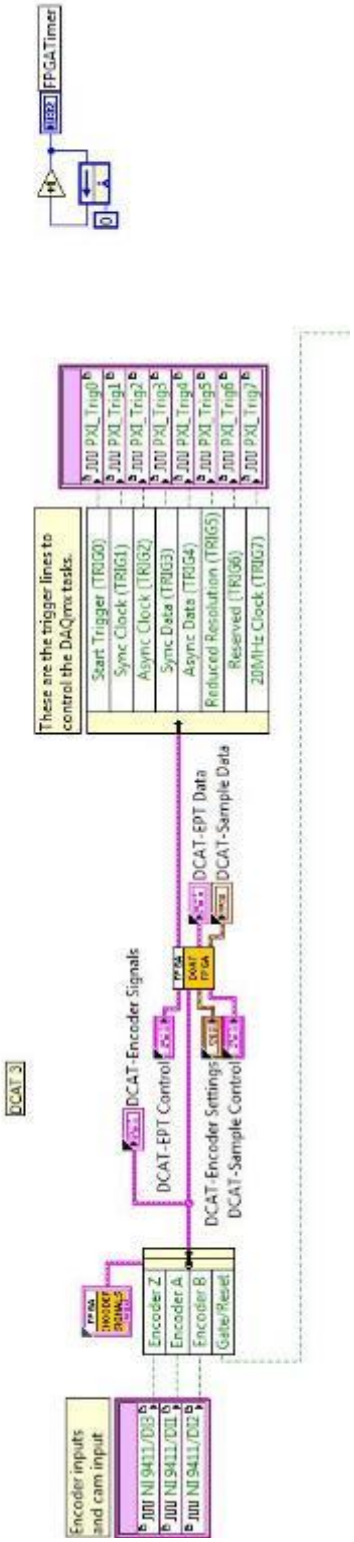

Figure D.2 Drivven Engine Synchronous FPGA – DCAT 3

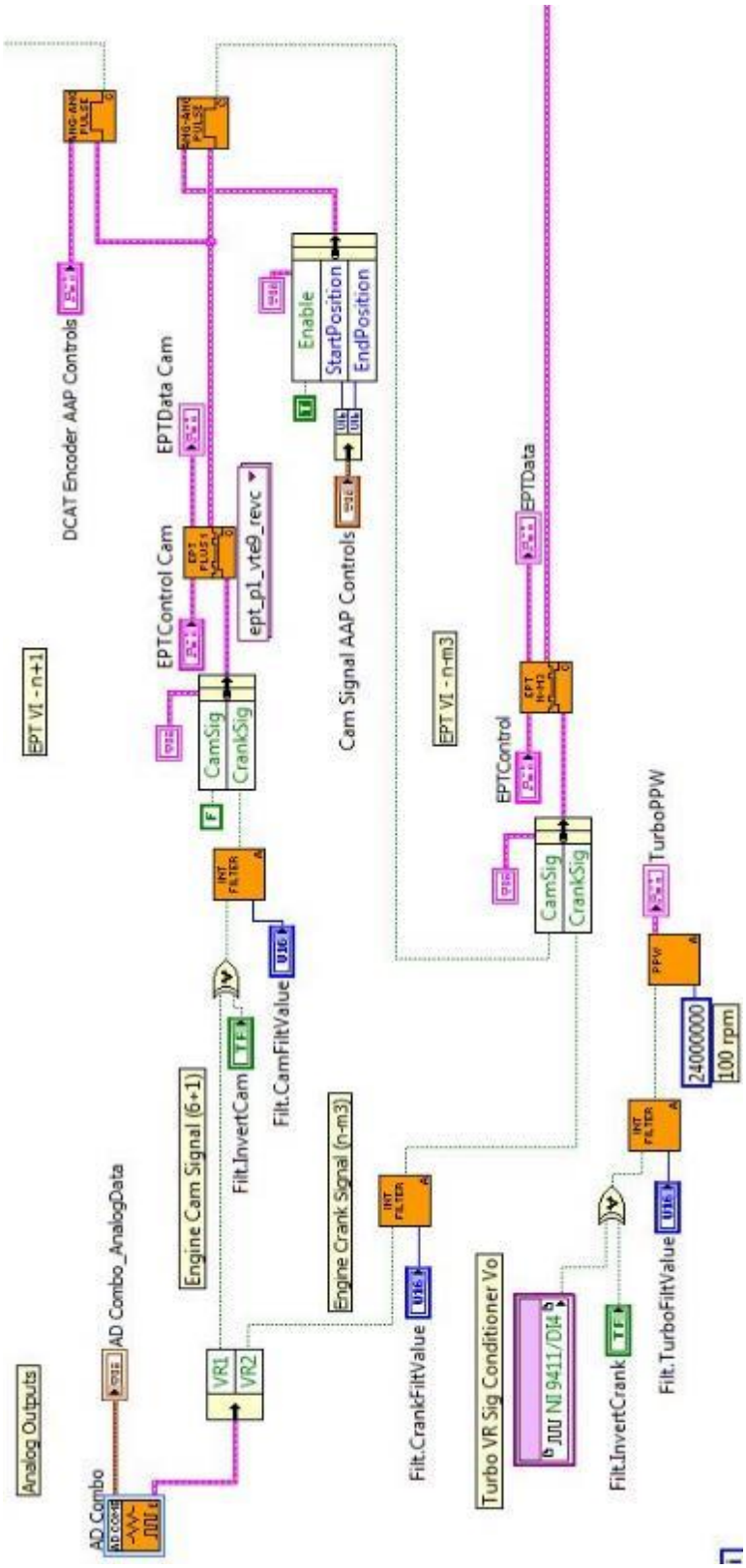

Figure D.3 Drivven Engine Synchronous FPGA – ADCombo inputs and EPT VIs

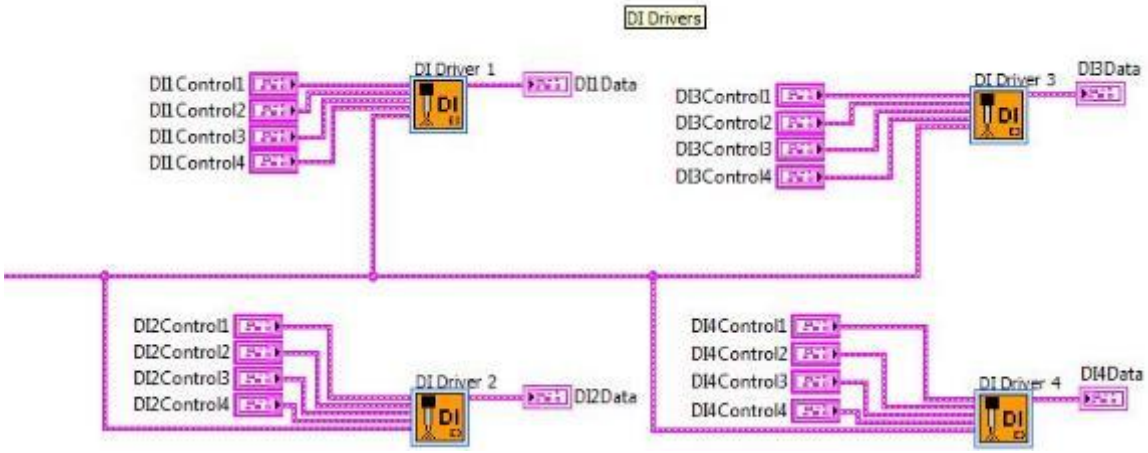

Figure D.4 Drivven Engine Synchronous FPGA – DI Drivers

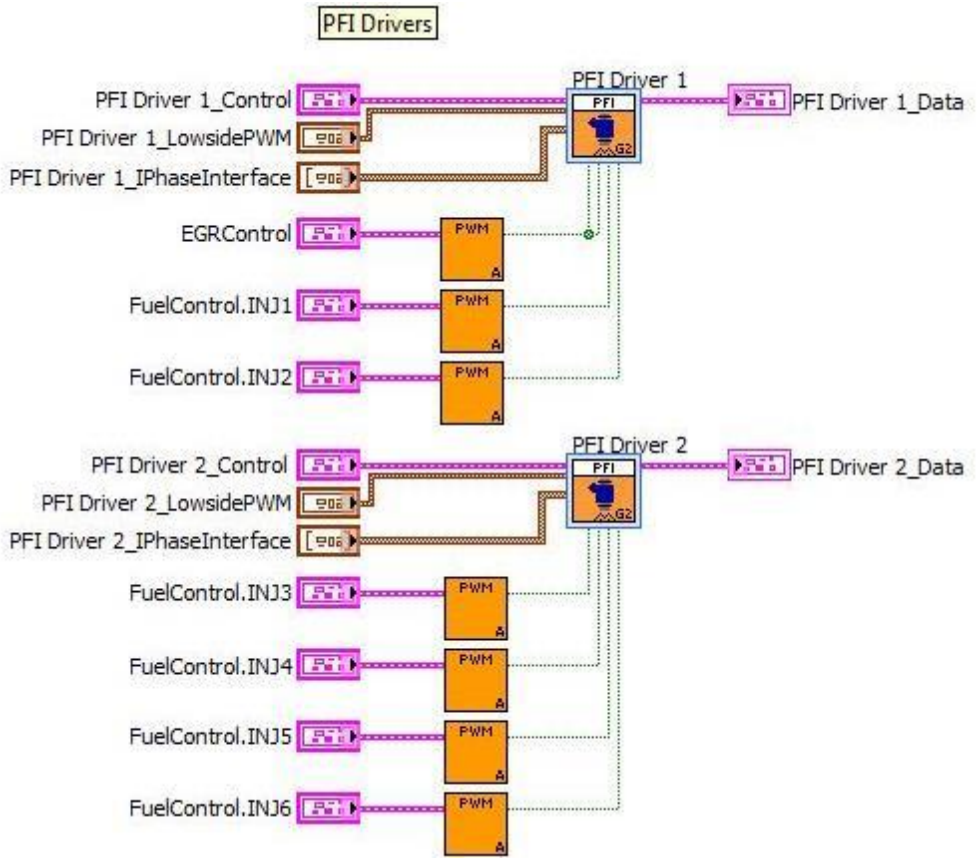

Figure D.5 Drivven Engine Synchronous FPGA – PFI Drivers

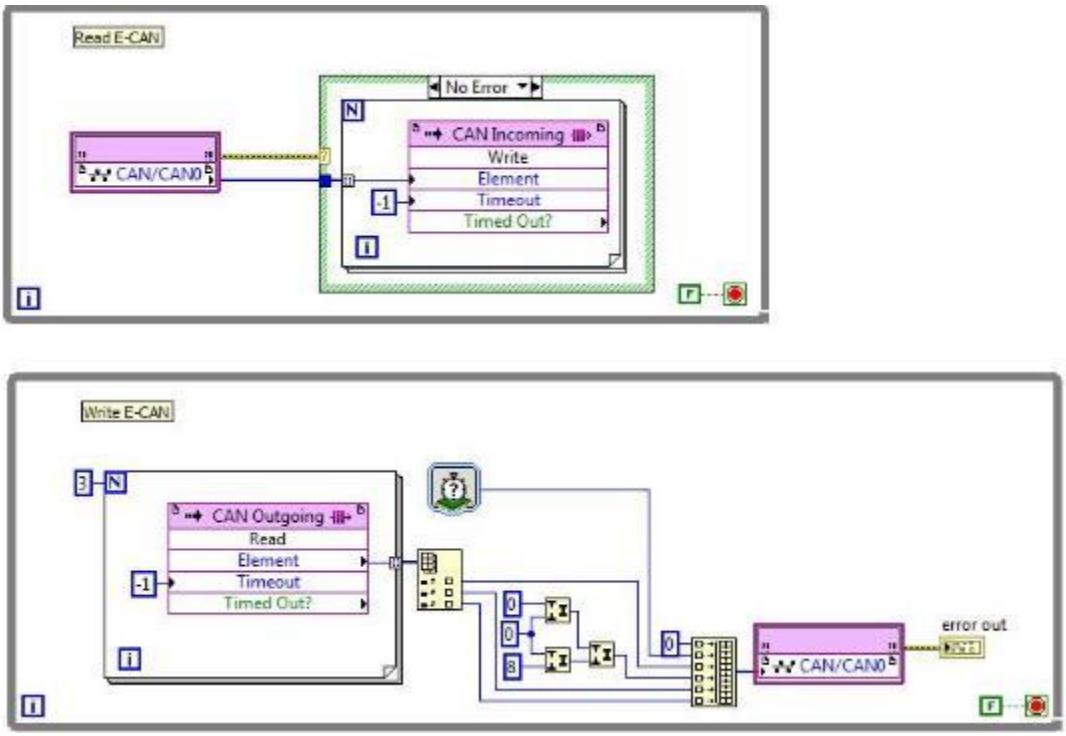

Figure D.6 Drivven Engine Asynchronous FPGA – Overview

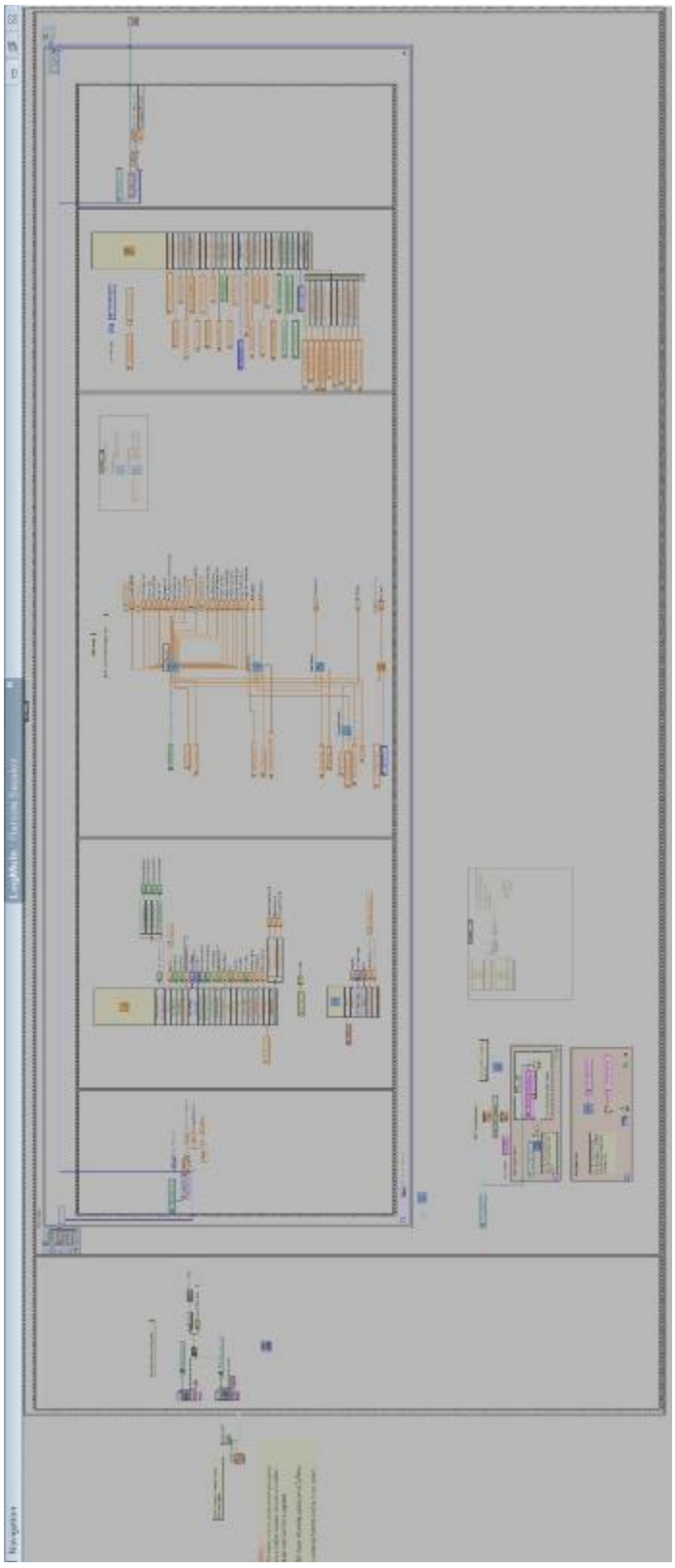

Figure D.7 Drivven Realtime Control – Overview

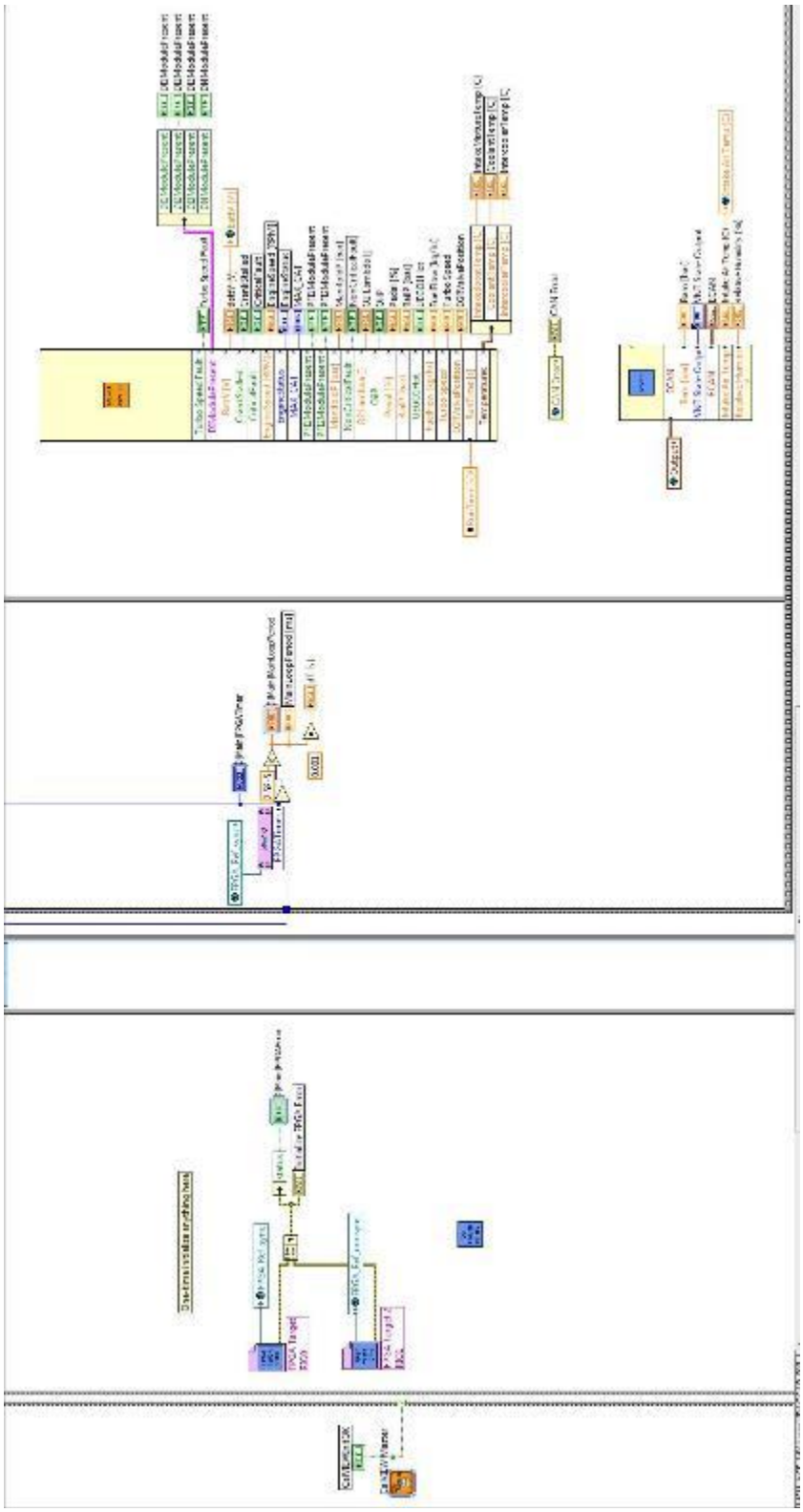

Figure D.8 Drivven Realtime Control – CalVIEW Master, FPGA references, and Read Inputs subVI

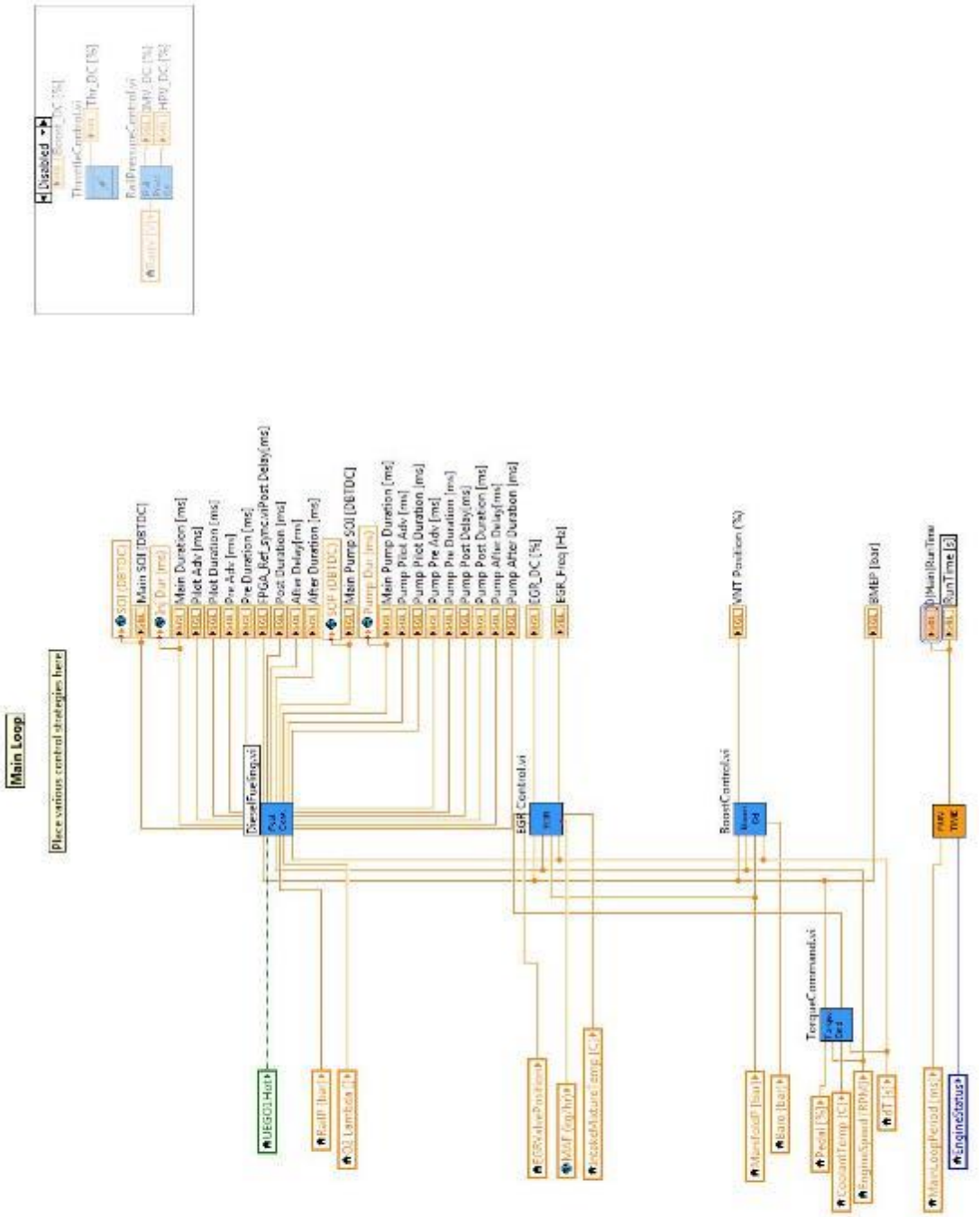

Figure D.9 Drivven Realtime Control – Control algorithms

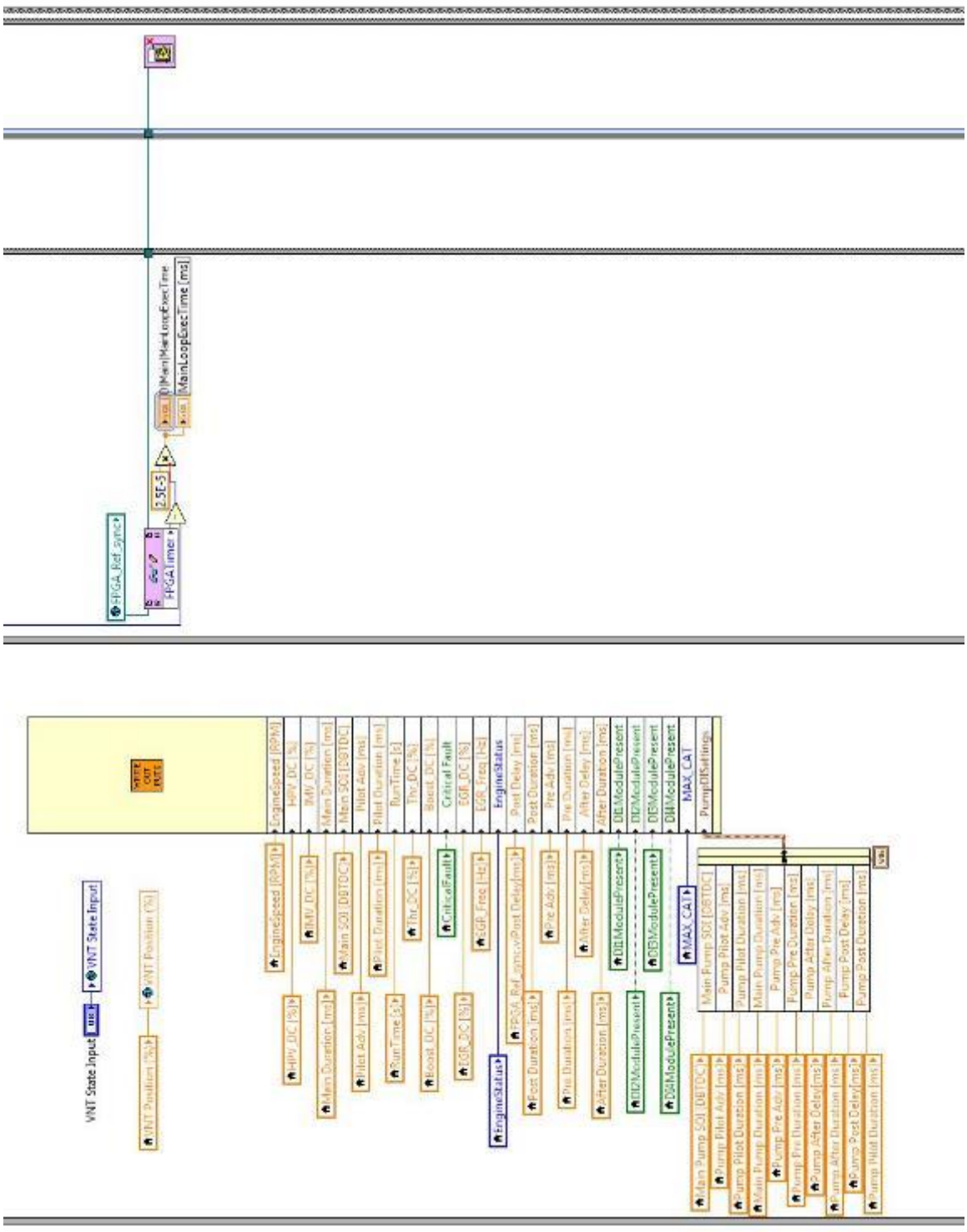

Figure D.10 Drivven Realtime Control – Write Outputs subVI and loop timer

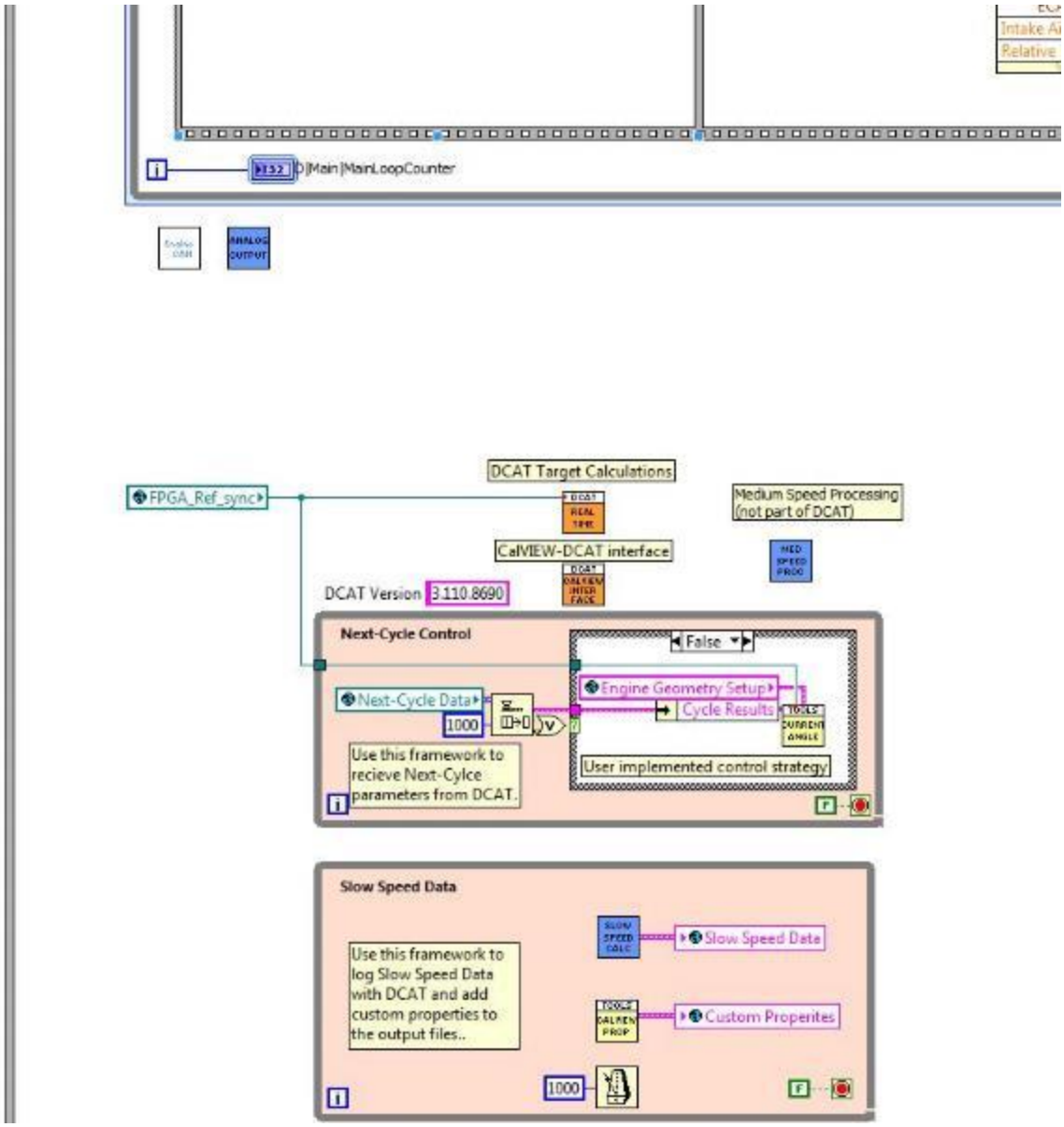

Figure D.11 Drivven Realtime Control – Engine CAN, Analog output, and DCAT 3 subVIs

APPENDIX E

DCAT CONFIGURATION FOR THE PACCAR MX10 DUAL FUEL LTC EXPERIMENTS

The following paragraphs outline the specific options and settings configured for recording data using DCAT on the PACCAR MX10 engine. Values shown in figures indicate the values used while taking data for the PACCAR MX10 dual fuel LTC experiments. Any settings not explicitly mentioned here utilized the default parameters.

E.1 Setup Tab

The following settings must be configured before DCAT can be initialized.

E.1.1 Engine Setup

Engine geometry parameters, valve timing, polytropic exponent source, encoder resolution, extrapolation level, cycle phasing method, and DAQ rates are outlined in the engine setup tab. The cycle phasing method refers to the way in which DCAT determines which rotation is associated with compression in a four stroke cycle. "Gate Z," the cycle phasing method used, requires a once-per-cycle Boolean input at the FPGA level to occur at the same time as the encoder index. In this case, an angle-angle-pulse subVI is used to create the necessary pulse. Other phasing method options are available, such as the 'random Z' method, which does not require a cam signal. The engine setup tab as configured for the MX10 engine is shown in Figure D.1.

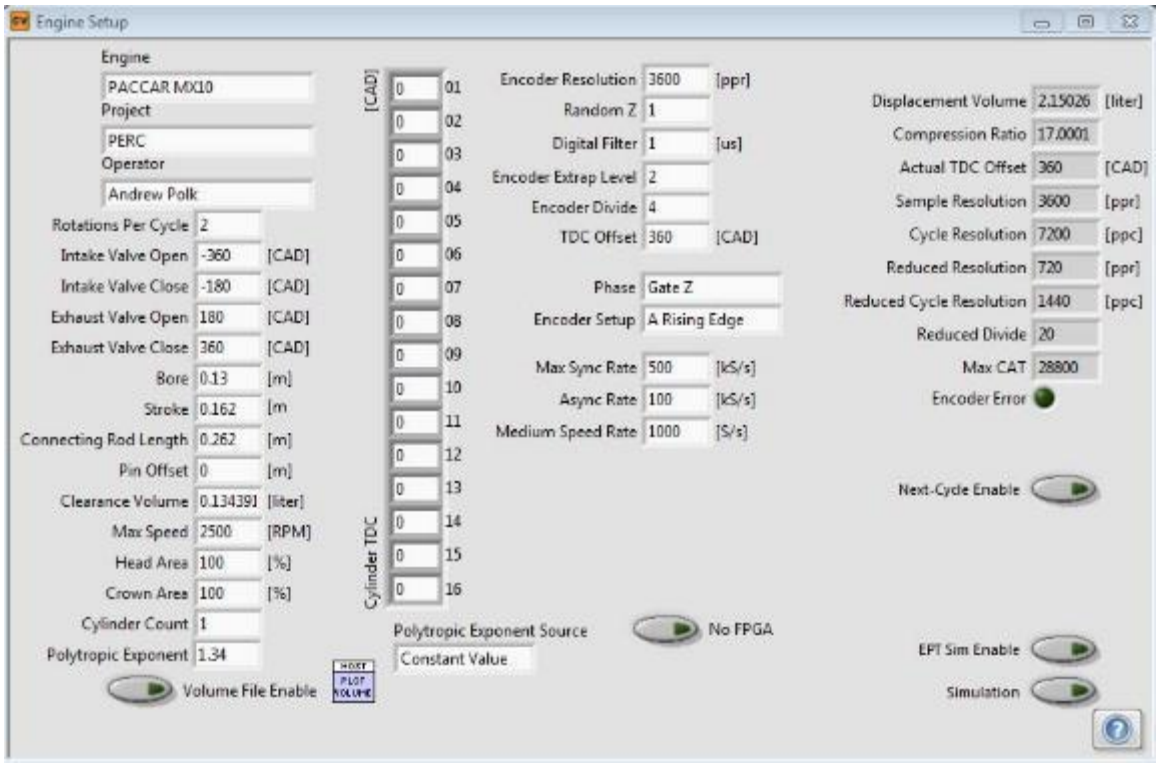

Figure E.1 Engine setup tab in DCAT configured for MX10 test cell

E.1.2 Synchronous Setup

Cylinder pressure, fuel pressure, injector command voltage, and manifold pressure signals are configured on the synchronous setup tab. The name, physical channel, signal type, units, scaling, and filter are specified on this page.

E.1.3 Medium Speed Setup

All steady state analog input signals are configured on the medium speed setup tab. This includes emissions, dyno speed and load, pressures, flow rates, and temperatures. As with the synchronous setup, the name, physical channel, units, and scaling, among others, are configured here.

E.2 Settings Tab

The following settings may be configured either before or after DCAT is initialized.

E.2.1 TDC Offset Settings

While monitoring the cylinder pressure plot during engine motoring (achieved by turning off the injection event only in the cylinder with the pressure sensor), the fine adjust was set to a value which provided a peak pressure location of about 0.5 DBTDC. This setting is verified in the log P vs log V plot by very straight compression and expansion lines with no crossover.

E.2.2 Pegging Settings

Manifold air pressure (MAP) was used to scale, or peg the cylinder pressure signal. Therefore, the "synchronous MAP" setting was used. Manifold air pressure was sampled at a location of 300 DBTDC for a 5 CAD window.

E.2.3 Filter Settings

A boxcar type filter was used on the cylinder pressure signal. A value of 6 was used for "N". This filter is also known as a "moving average."

E.2.4 Heat Release Settings

A "single zone + heat transfer" model was chosen. The heat release curve was smoothed by one percent. The heat transfer calculation employed a Hohenberg correlation [Hohenberg 1979], with the wall temperature profile approximated as a

constant 480 degrees K. For the purpose of calculating the mass fraction burned, the start and end of combustion were set at a constant 60 DBTDC and 60 DATDC, respectively.

E.3 Controls Tab

E.3.1 Calculations

The parameters chosen for calculations include the following: Basic, MEP, Motoring, Gas Temp, Injector, Heat Release, Noise, Misfire, Pump, Knock, and Medium Speed. These options must be selected before DCAT is initialized.

E.3.2 Raw File Save

In most cases, raw files were recorded and later post-processed. Data are initially recorded to the PXI hard disk and must be transferred via FTP to the host computer to be processed. One thousand consecutive cycles were taken unless operating conditions required a shorter duration (e.g. high pressure rise rates or knock).